Representations of Geometry for Computer Graphics

Course 29
Tuesday / Full Day / Advanced

The latest research on the most important computational representations of geometry used in computer graphics. The emphasis is on their strengths and weaknesses and how to build a coherent system that supports multiple representations.

Schedule & Table of Contents

8:30 am: Introduction to Computational Representations of Geometry- Naylor
Course objectives and taxonomy of representations.

8:45 am: Voxels as Computational Representations of Geometry - Kaufman
Volume graphics is an emerging subfield of computer graphics concerned with the synthesis, manipulation, and rendering of volumetric modeled objects, stored as a volume buffer of voxels. Unlike volume visualization which focuses primarily on sampled and computed data sets, volume graphics is concerned primarily with modeled geometric scenes and particularly with those that are represented in a regular volume buffer. Volume graphics has advantages over surface graphics by being viewpoint independent, insensitive to scene and object complexity, and suitable for the representation of sampled and simulated data sets and mixtures thereof with geometric objects. It supports the visualization of internal structures, and lends itself to the realization of block operations, CSG modeling, and hierarchical multi-resolution representations. The problems associated with the volume buffer representation, such as discreteness, memory size, processing time, and loss of geometric representation, echo problems encountered when raster graphics emerged as an alternative technology to vector graphics and can be alleviated in similar ways.

10:00 am: Break

10:15 am: -Specification, Representation, and Construction of Non-Manifolde Geometric Structures - Rossignac
We will discuss boundary/topological representations for characterizing the topological coverages of CAD system, for comparing the data structures they maintain, and for reliably computing boundary models from constructive representations. Creating multi-resolution representation will be addressed.

11:15 am: Modeling with Simplicial Complexes - Edelsbrunner

The main theme of this talk is the idea of using cell decompositions (complexes) to model geometric shapes. The complex is what is often called a grid or mesh. This approach to modeling allows the instantaneous analysis of the created shape. The following specific questions and issues will be addressed.

- What are complexes? (definitions and examples)
- How can the geometric integrity of a complex be guaranteed?
- How can complexes be used to model shape?
- How can complexes be manipulated and maintained?

12:00 noon: Break

1:30 pm: Polynomial Surface-Patch Representations - Bajaj

Algebraic curves and surfaces can be represented in an implicit form, and sometimes also in a parametric form. We will compare the implicit and parametric representations of algebraic surfaces by considering the the parametric form either as a mapping or alternatively, an algebraic variety. In this course, I shall consider specific geometric operations: scattered data fitting and surface display and compare the implicit and parametric forms for their superiority (or lack thereof) in optimizing algorithms for these operations.

3:00 pm: Break

3:15 pm: Binary Space Partitioning Trees - Naylor

Partitioning Trees, a multi-dimensional generalization of binary search trees, provide a computational representation of geometry via recursive subdivision with hyperplanes defined by linear equations. Linearity and recursive subdivision lead to simple algorithms for visibility (hidden surface removal, transparency, shadows) as well as intersections (set operations, collision detection, clipping, ray-tracing). We will present a review of these capabilities as well as present new results on building multi-resolution trees, representing volumetric data, and integrating parametric surfaces into Partitioning Trees to permit local non-linear deformations.

4:15 pm: Building a Whole Geometry System - All

Having presented each of the representational schemes, we will now be in a position to focus exclusively on the relation between the various representations and how one can build a single coherent geometry system that exploits the strengths of each and avoids their weaknesses. We will be able to draw upon the experience of several of the speakers who have built such integrated systems.

Computational Representations of Geometry

Bruce Naylor
Spatial Labs Inc.

Introduction

Computational representations of geometry provide the foundations for all the various areas of computing that involve geometry. These areas currently include Computer Graphics, Computer-Aided Geometric Design, Scientific Visualization, Computational Geometry, Finite Element Analysis, Robotics, Computer Vision and Image Processing. Yet only a few representations of geometry have emerged to date. We believe that the reason for this is that geometric sets are describable in terms of only a few fundamental aspects, e.g. their topology, or set theoretic structure, etc. Many of the representations, in their purest form, describe primarily a single fundamental aspect of geometric sets. Each "pure" representation then is the language for expressing that aspect (it is the syntatic form for which the intended semantic interpretation is direct). For example, the topology of a set is expressed directly and exactly by what we naturally call "a topological representation": a graph with a one-to-one correspondence between graph nodes and topologically connected components, and where graph edges indicate incidence between components. In addition to pure representations, other types of representations may be hybrids, combining multiple aspects simultaneously.

Representatons of geometry have a very strong connection to "traditional" mathematics, both historically, dating back to Classical Greek civilization, and to modern subjects. These include Set Theory, Graph Theory, Algebraic Topology, etc., in addition to the various varieties of Geometry: Projective, Analytic, Algebraic, Differential, and Combinatorial. What is different, as everyone knows, is that computation is "constructive mathematics", and the primary measure of value is not proveability per se (as much as we might want error free programs), but rather performance and accuracy. The pursuit of efficiency has led numerous times to what might initially be considered as a counter-intuitive result: that computing with many simple pieces can be faster than attempting to process fewer but more computationally complicated pieces. This is what we call the verbosity/complexity tradeoff: we trade a relatively small number of complicated operations for many more but simpler operations. This is a very important consideration in geometric computation, and we have given a qualitative picture of this for representations of geometry in Figure 1.

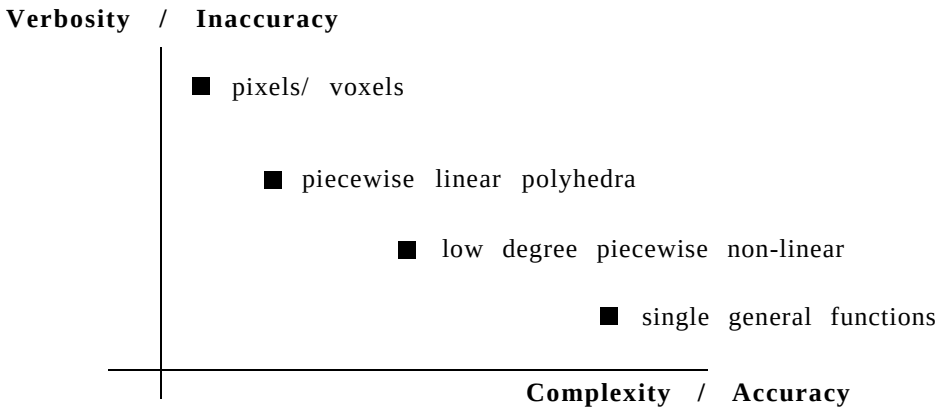

Verbosity / Complexity Tradeoff for Geometric Representations

Additionally, we only need, or can only obtain, the desired answer computed to a limited resolution. If, as in image synthesis, the output of the computation is intended only for direct human perception, then we need to compute the answer only to a limited resolution, because humans have limited perceptual descrimination. But the limit on resolution is even true in the "non-perceptual" realm of manufacturing, where one of the great advances enabling mass production was the recognition that manufactured parts need only be produced within a certain tolerance. This suggests that geometric modeling should only be computing to an analogous tolerance, even if we had unlimited precision for representation numbers. But we do not, and so exactness is difficult to obtain even if we wanted it (although not impossible or even necessarily impractical) due to the finite precision used to represent numbers.

All of this leads us into the realm of approximations, and in particular, to reducing the computational effort by employing approximations of various forms. During the early years of Numerical Analysis, it was quickly recognized that finding the roots of polynomials of modest degree was not only slow, but was often infeasible due to accumulation of numerical error. An importance solution to this problem was provided by Splines, a term we now use to denote the representation of functions (for curves or surfaces) as piecewise polynomials each of low degree. Any arbitrary function, say one continuous for all derivatives, could be approximated arbitrarily well almost everywhere by a set of pieces, each piece being a computationally appealing function. The only places where unbounded continuity is sacrificed is where the pieces met, called "joins". However, the polynomials can be constrained so that the resulting approximation will have any desired but bounded degree of continuity at the joins. The resulting spline representation is then much more attractive computationally than the original complicated function.

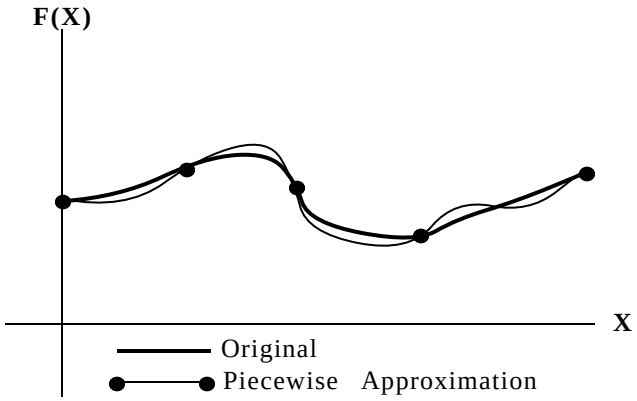

Spline approximation of a continuous function

Splines are a recent example of employing approximations to achieve a verbosity/complexity tradeoff: both accuracy and computational complexity are traded for a simlper and hopefully faster but more verbose and less accurate computation. This idea is not new. For indeed Archimedes used this idea to approximate PI (the originator of the technique is thought to be Apollonius, who was famous for his work on the geometric theory of conics). He knew how to compute the area exactly of certain regular n-sided polygons by, for example, dividing them into triangles. Given a unit circle, he could then use the area of an inscribed n-gon to provide a lower bound on PI, and the area of a circumscribing n-gon to produce an upper bound. By increasing n, he could obtain an answer as accurate as desired, though at greater computational expense. This is a very early example of using piecewise linear approximations of a non-linear set, and more generally, of the complexity vs. verbosity tradeoff in geometric computations.

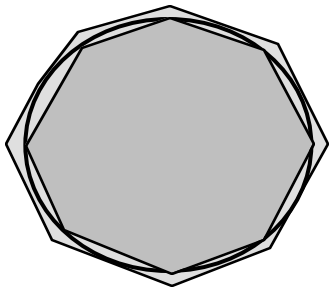

Archimedes/Appollonius piecewise linear approximation of a circle

The simplest and most verbose representation of geometry is the discrete space representation, familiar to us as pixels and voxels. Pixels, while generally thought of as an idea requiring a CRT and a frame-buffer, also have an ancient precursor: mosaics constructed from many small colored tiles (pixels). Indeed, the Sumarians are known to have created mosaics as early as the third millennium B.C. This technique was continued by the Romans, especially in the Byzantine Empire after the ascension of Christianity as the state religion. It is now the basis for all raster graphics.

The verbosity/complexity tradeoff is a central issue in evaluating the various computational representations of geometry. The central question is: Under which circumstances is it best to use which representation, and in particular, when should we trade conciseness and accuracy to gain speed? This is a question that is at the heart of geometric

computations, and one that remains very much open and is unlikely to be resolved any time soon. For example, does the current success of hardware texture mapping of polygons imply that we should also use voxel representations for all 3D geometry? Some people think this could be the case. Or should be retain polygons but dispense with non-linear representations since for example we have fast polygon renderers? A more likely answer is that each principal representation will have its place (its niche) if it describes some essential aspect of geometry. But if so, can we say something now about what these niches will be, and how the representations will be related to one another in a complete system? It is our intention to contribute to this objective by bringing a certain degree of clarity to this important issue.

Taxonomy of Representations of Geometry

In the figure below, we present a partial taxonomy of representations of geometry based on fundamental categories. For each leaf of the classification tree, we have given a representation of geometry that best exemplifies a particular classification. Not all representations in use today are presented, either becasue we have not included all of the possible categories, or because they are hybrids combining various aspects, or because we feel they belong at a higher semantic level than what we are considering here (e.g. CSG). We will discuss some of these later.

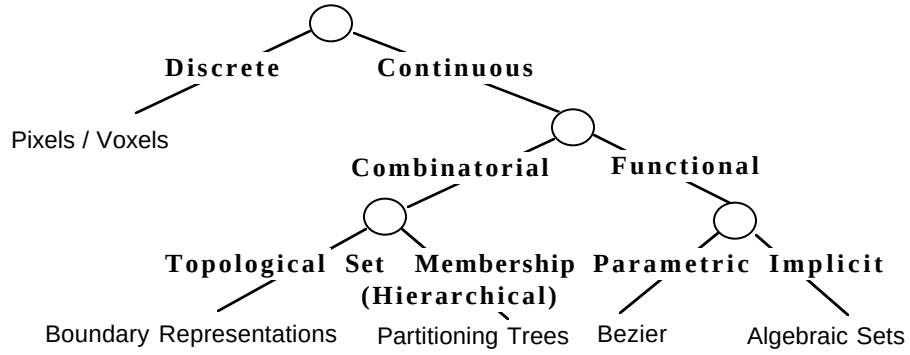

Basic Taxonomy of Representatons of Geometry

It is our thesis that each of each of these primary representations can represent any geometric set and that all geometric operations can be performed using any of them. They are then, at this level of abstraction, equivalent. This is analogous to the fact that the various models of computation that were developed during the 1930's through the 1940's were discovered to be all equivalent in what functions they could compute; in today's vernacular, they were all Turing equivalent. That is, each one of these representations contain enough expressive power to model the semantics of geometric sets.[1]

However, since the character of geometric sets is multi-faceted (especially if they are polyhedra :-), any single representation in its pure form will be limited in the range of operations for which it is ideally suited. Thus, a complete software system for performing geometric computations efficiently must either incorporate multiple representations with conversions between them, or else develop some integrated approach by constructing a

[1] We define geometric sets as subsets of d-dimensional space (Euclidean, Affine and/or Projective). We are most interested in those sets which are comprised of an uncountable (continuous) number of points, as opposed to finite point sets or even countable ones.

hybrid form with sufficient expressive power. If multiple representation are used, then this fact can be hidden from the user by using Object-Oriented Programming. The class "Geometric Set" can be defined, and each operation on that class can decide which representation is best for that operation, maintaining multiple representations simultaneously and/or initiating data-type conversions as needed. If instead, an integrated approach is employed, only a single representation would be needed; but performing each operation may be made more difficult and more expensive by this than if pure forms were used, since more information/properties would need to be maintained during every operation. Irregardless of which methodolgy is used, the best pedagogical approach is to first examine and understand the pure forms; we can then see how hyrids can be constructed and why they may be desireable.

Discrete vs. Continuous

Within the general category of spatial representations, the first distinction is between the discrete vs. continuous. This is the same distinction as between the Integers and the Reals (not finite vs. infinite). As is familiar from grade school, a discrete space representation of a 1-dimensional space is created by discretizing a line into equal intervals marked by integers. A discrete space representation of a d-dimensional space, $d > 1$, is simply a regular lattice of points created by the Cartesian-product of d 1-dimensional spaces, represented computationally as a multi-dimensional array. The coordinates of each point is a d-tuple of integers.

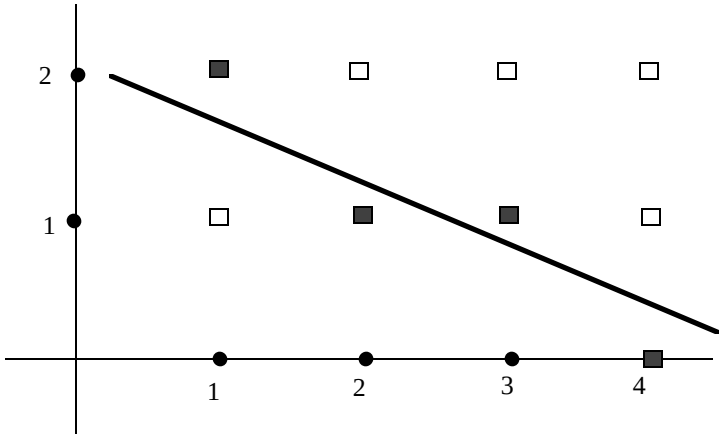

Discrete Space : line segment and its discrete approximation

Discrete space representations, familiar as arrays of pixels or voxels, are at one end of the spectrum in terms of being the simplest representation of geometry, but they are also the most verbose and/or least accurate. They almost seem antithetical to the domain we are dealing with: arbitrary subsets of continuous, not discrete, space. So why is it that we use them? Firstly, it is possible to use discrete space to model continuous space as long as we are willing to accept a limit on the resolution/accuracy of the computations. Since a grid can be made as fine as we wish, we can in principal obtain any level of accuracy we desire. However, the historical entree for discrete space representations was in the context of transducers from the Physical Domain to the Information Domain. Time varying analog signals, such as those produced by a TV camera or by a microphone, where digitized by sampling the signal

at regular intervals using A-to-D converters. The inverse transform could also be produced with D-to-A converters; this is of course the basis for using frame buffers in image synthesis.

Discrete space is computationally trival to represent (a multi-dimensional array), and its simplicity can be put to great advantage when designing special purpose hardware. A good example of this can be found today with graphics hardware for performing texture mapping of polygons in 3-space; texture maps are, after all, nothing more than a discrete space representation of a function mapping a finite domain in 2-space to color values. Texture coordinates at polygonal vertices provide a discrete-to-continuous mapping. However, since texture mapping is performed as part of the scan-conversion process, which is a continuous-to-discrete mapping, it becomes a discrete-to-discrete mapping.

One of the costs of discrete space representations is the error introduced by quantization. This is most apparent to the human eye as aliasing artifacts. It must be compensated for by performing filtering of various kinds, thereby reducing somewhat the original gains due to the simplicity of using discrete space. It is also worth noting that the underlying theory for mapping one image to another using the proper filtering for anti-aliasing is formulated in terms of first reconstructing a continuous signal from samples and then resampling the continuous form to generate the new discrete image. This illustrates quite cleary that when modeling the continuum, it is necessary to retain the semantics of the continuum even when the underlying representation is discrete.

The other most obvious cost in using discrete space represenations is verbosity. While it is true that memory costs continue to decline, memory speeds have not; and even if memory was zero cost, it would still be necessary to spend time processing all elements in the array. So verbosity should in all likelihood remain a consideration, especially for 3D. On more fundamental issues, since space is sampled at a uniform and finite rate, discrete space representations can only represent a finite region of space (within a finite amount of space, i.e. within memory). Finiteness is a natural property of images but not as much so of 3D environments. In addition, the regular grid is completely independent of the contents of space, and so cannot describe any of the structure induced on the space by an image or collection of objects. Computer vision, for example, requires just this structure. Image systhesis begins with this structure and generates a set of pixels from which the human visual system recontructs the structure. And this information is not distributed uniformly throughout 3-space, as is a 3D lattice. More importantly, humans rarely specify objects directly in terms of pixels or voxels, but rather use continuous space representations that correspond to a higher semantic level. So, discrete space representations, while clearly having an important place is geometric computation, are like all other representations in that they do not constitute a complete language for expressing every aspect of geometry.

Continuous Space: Functional vs. Combinatorial

Functional and Combinatoral representations are solving two different problems which, when taken together, give a complete solution for representing geometry. Functional representations use continuous (C^{∞}) functions to specify the continuous sets of points comprising each piece of a geometric set. Combinatorial representations describe how the pieces are related to each other. Functional representations deal with the uncountably infinite, combinatorial with the finite usually and certainly no more than the countably inifinte (cardinality of the integers).

Much of Mathematics, motivated by Physics, has been the study of continuous functions; this characteristic is most evident in the field of Analysis. Despite the wealth of work on

continuous functions, the problem of having humans design objects has resulted in an important contribution to our understanding of how to represent curves and surfaces using polynomials, and how to represent the polynomials themselves. This is most evident in the development of the Bezier/Berstein theory and the closely related B-spline theory. The traditional "power basis" form describes polynomials in terms of a weighted sum of monomials. This turns out to be a direct specification of the behaviour of the polynomial exactly at the origin of the coordinate system in terms of its value and derivatives. The Bezier form instead expresses a polynomial directly as the weighted sum of points (control points) independent of the coordinate system, and its behaviour in the vacintity of these points is understandable in terms of these points. So while any polynomial can be expressed in either the power or the Berstein basis, the latter has proved to be much more attractive computationally.

In contrast to Analysis, Computer Science has been principally the study of the finite, albeit in a computational milieu. This is most evident in the use of combinatorial structures, such as graphs, that provide the basis in computing for data structures. As discussed earlier, a strict devotion to using monolithic but complicated functions for representing objects is much less attractive computationally than using many simpler pieces. It is the problem of representing "the many" that requires the combinatorial component. This can be used to express how the pieces connect to one another or how to organize the pieces hierarchically to significantly improve performance. And once we have a combinatorial structure, it is easy to introduce the discontinuities absent from the standard representations of continuous functions which are C^{∞}. This is most readily perceived if, for example, we interpret a 3D geometric model as a function that maps points in 3-space to some set of attributes, such as color; surfaces then correspond to discontinuities in this function. Analysis has always had difficulty with discontinuites, often resorting to such devices as representing a sample as the limit of an inifinite sequence of continuous functions. This is due to the absence in their language of adequate means for expressing arbitrary discontinuities. The combinatorial component provides us with just such a language.

Functional: Parametrics vs. Implicits

An important distinction for the functional form is between parametrics and implicits. This is nothing more than the difference between whether the set lies in the range or the domain of a function, respectively. The computational impact of this distinction manifest in various geometric operations. Parametrics are naturally suited for generating a finite sampling of points while implicits facilitate computing intersections.

For parametrics, the set lies in the range of a vector valued function $P: T^m \Rightarrow X^n$. For example, if $m = 1$ and $n = 3$, one obtains curves lying in 3-space. In general, the set is m-dimensional lying in an n-dimensional space. Such functions can be specified by n coordinate functions, which are mostly commonly polynomials, each being a scalar valued function of m independent variables: $P_i: T^m \Rightarrow X_i$. The essence of parametric representations is their power to enumerate points in the set. By sampling points in the parameter space T^m, one can generate corresponding points in X^n. This property is commonly used in 3D to generate polygonal approximations of parametrically defined surfaces: the generated points serve as vertices of a polygonal mesh.

In contrast to parametrics, implicit functions are of the form $F(X^n) \Rightarrow Z^1$. We are interested in those functions, $F(X^n) = 0$, which define curves or surfaces. These partition

space into a collection of connected regions such that each region is entirely in $F(X^n) > 0$ or $F(X^n) < 0$. We can then use these to define solids in 3D as those points that satisfy $F(X^n) <= 0$ (or $F(X^n) >= 0$). This gives us a membership function (also called a characteristic function) for the set. A membership function allows us to determine for any point in space whether it is a member of the set by evaluating the function. This is the essential computational characteristic of implicit representations.

Currently, the most popular forms of parametric and implicit functions use polynomials (with rational coefficients). Sets defined in the implicit form by a single polynomial define the class called Algebraic Sets. Surfaces defined parameterically by (rational) polynomial coordinate functions are also algebraic sets; but not all algebraic sets admit such a parameterization. Thus, parametrics are a subset of the implicits when only polynomials are involved. Determining the implicit form of a parametric surface is called implicitization, while determining a parametric form of an implicit is called parameterization. However, neither of these is easy to do in general, requiring techniques from Algebraic Geometry. The one notable exception is when only quadratic polynomials are used, in which case both forms are well known; and quadratic rational parametrics and quadratic implicits define exactly the same class of sets.

The distinction between sets for which one has a membership function, as with implicits, and those for which one has an enumeration function, as with parametrics, lies at the very foundations of the theory of computation. In order for a (countable) set to be characterized as computable, the set must have a computable membership function. Such sets are called Recursive Sets. Those sets for which there exist computable enumerating/generating functions are called Recursively Enumerable Sets. For any recursive set, there exists, in addition to its membership function, a computable generating function for the set, and so the Recursive Sets are also Recursively Enumerable. However, the reverse is not the case, and so the Recursive Sets are a proper subset of the Recursively Enumerable Sets, the later being called semi-computable. This strongly suggests that the distinction between implicits and parametrics corresponds to an important difference in methods of defining sets. (The fact that polynomially define parametrics are a subset of the implicits, rather than the reverse as suggested by recursive sets being a subset of the recursively enumerable, may be an artifact of considering only polynomials.)

The difference in the computational efficacy of the two representations can be largely understood in terms of the difference between membership and enumeration functions. Determining set membership is required for performing any intersection operation (the points of intersection are those which are members of both sets). Such geometric operations include point classification, ray-surface intersection, clipping to a view-volume, collision detection, constructive solid geometry, radiosity, shadows, etc. On the other hand, enumeration is used directly for polygonalization of a curved surface and scan-conversion of polygons. However, the parametric form can be use to compute intersections quite effectively if paired with an implicit. This is commonly done when a parametric representation of a line (ray or edge) is substituted into an implicit equation of a surface. Various values of the parameter are "enumerated" either analytically if the degree is 1 or 2, or numerically by a iterative technique such as Newton iteration.

Combinatorial: Topological vs. Set Membership

Given an object defined by a collection of functionally defined continuous pieces, we must organize them into a whole using combinatorial structures. Currently, combinatorial structures, i.e. graphs, have been used primary to express two fundamental relations between components of a set: the topological structure and the set membership structure.

The topological structure encodes the incidence relations between geometric elements, i.e. which elements "touch" which other elements. These elements may be of the same dimension, such as polyhedral faces which share an edge, or they may be of differing dimensions, as between a polygon and the edges that bound it. This structure is represented by a graph where each node corresponds to an element and graph edges correspond to the incidence relation. It also has a hierarchical structure in which levels of the hierarchy correspond to the various dimensions of the components. Other topological properties, such as number of connected components and genus of each components, can be computed from this graph. The topological form is the basis for the many varieties of boundary representations. As a consequence, for 3D it is most closely associated with surface representations, although volumes be easily included in the schema by adding the appropriate nodes for each 3-dimensional connected region of space (such as F1in the figure below).

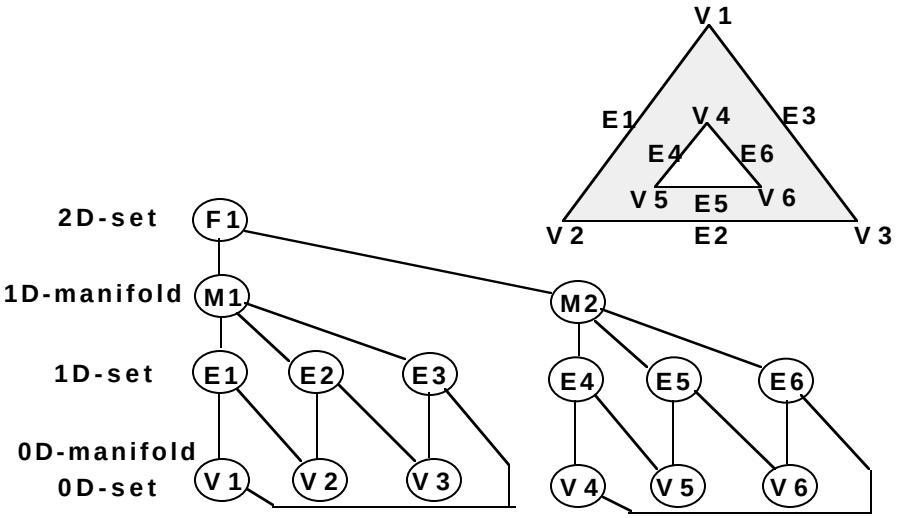

Topological Representation

Representing set membership is more closely identified with volumetric representations than with boundary representations, and the collection of elements are usually not the same as those defined by using the topological properties. Most commonly, the elements are regions of space created as a consequence of forming a hierarchical search structure whose purpose is to accelerate intersection and/or visibility calculations. These include octrees, bounding volume hierarchies, and binary space partitioning trees. They all accelerate intersections using the same prinicpal: the bounding volume principal. If some geometry entity, such as a point, ray or object, does not intersect a region/bounding-volume, then the entity cannot intersect any contents of that region: (B subset of A) & not (C subset of A) $\Rightarrow$ not (B $\cap$ C). Thus the set membership relation confers transitively the non-intersection property. Similarly, if a region has visibility priority over another region, then the set membership relation confers visibility priority transitively.

The idea of a search structure based on the membership relation was first used in symbolic computation involving finite sets, such as lists of names. By organizing a list into a

binary search tree, various operations, such as "find", "insert" and "delete", could be performed in O(log n) rather than O(n) time, and even better when the statistical distribution of the input was known to be other than uniform.

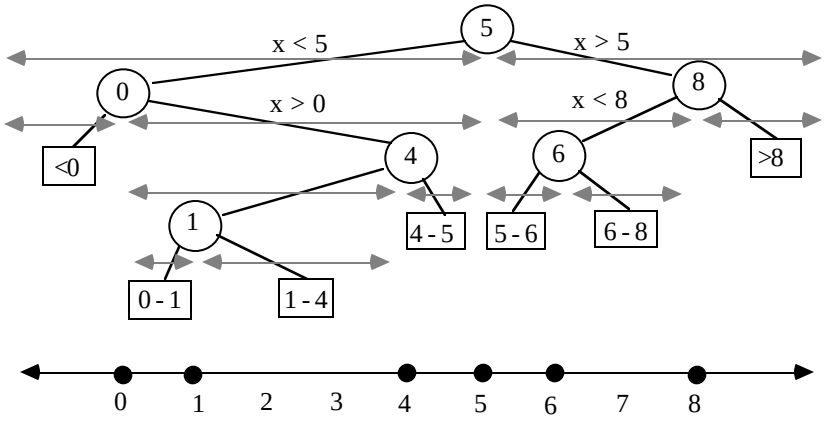

Binary Search Tree for the set { 0,1,4,5,6,8 }

In geometric computation, there can be thousands or millions of pieces, such as polygons. For rendering, we need to determine which of these lie within our view and which ones are hidden from view by other polygons. For physical simulation, of even minimal accuracy, we need to know which objects collide with each other and where the contacts occur. For these and other important operations, a combinatorial structure representing set membership can make an enormous difference. A direct generalization of binary search trees to dimensions greater than 1D is the Binary Space Partitioning Tree depicted below. This structure represents both a hierarchical search of space as well as the contents of the space (e.g. objects).

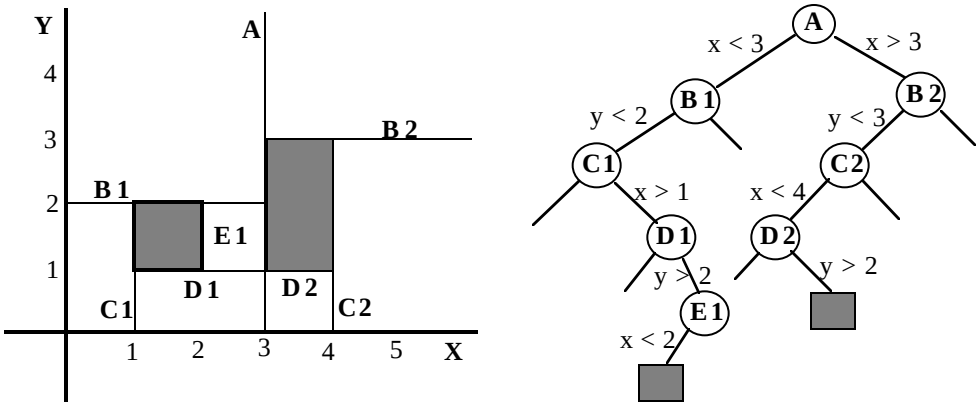

Binary Space Partitioning Tree for two rectangles

Humans perceive connectedness (incidence relation of topology) directly as a primary component of visual cognition, whereas the subset relation is usually perceive only when a physical container is involved (something is "inside" another thing). Yet both relations are important for geometric computation since both are fundamental aspects of geometric sets.

Spatial vs. Frequency

It is somewhat counter-intuitive that "geometry", which is almost synonymous with the term "spatial", can be represented in a non-spatial way, in particular, represented in the frequency domain, as is natural to do for something like sound waves. For indeed most geometric features are non-periodic and local, while sine waves are exactly the opposite, periodic and global (from -inf to +inf). For representing geometry, this incompatibility has required introducing locality into the frequency paradigm to produce something of a hybrid frequency/spatial schema. Initially, this was accomplished by such mechanisms as the "Windowed Fourier Transform".

But more recently, this difficulty has been addresses by the use of "wavelets". This technique replaces sine and cosine, which are the Fourier Transform basis functions and are non-zero over an infinite domain (possessing "infinite support"), with ones that are non-zero over only a finite domain (possessing local support), such as an isolated square pulse. However, local support has a price in the frequency domain: the Fourier Transform of such a function has infinite support in Fourier-space, another form of the uncertainity principle. A wavelet transform begins with a single generating (mother) wavelet, and then it is scaled, often by 2^{-n}, $n > 0$, and translated to create a collection of basis functions. In the typical case, this scaling and translating of a function with local support results in a hierarchical spatial subdivision analogous to a quadtree (in 2D). Thus, achieving a truely effective use of the frequency concept for representing geometry has led to the introduction of an increasingly geometric character. Given the success of frequency domain based operations for image/video compression and the emerging wavelet theory, we would expect such frequency/spatial hybrid schemes to become much more widely used for geometric computation in the future.

Voxels as a Computational Representation of Geometry

Arie E. Kaufman

Computer Science Department
State University of New York at Stony Brook
Stony Brook, NY 11794-4400
ari@cs.sunysb.edu
http://www.cs.sunysb.edu

Abstract

This paper is a survey of volume visualization, volume graphics, and volume rendering techniques. It focuses specifically on the use of the voxel representation and volumetric techniques for geometric applications.

1. Introduction

Volume data are 3D entities that may have information inside them, might not consist of surfaces and edges, or might be too voluminous to be represented geometrically . *Volume visualization* is a method of extracting meaningful information from volumetric data using interactive graphics and imaging, and it is concerned with volume data representation, modeling, manipulation, and rendering [49]. Volume data are obtained by sampling, simulation, or modeling techniques. For example, a sequence of 2D slices obtained from Magnetic Resonance Imaging (MRI) or Computed Tomography (CT) is 3D reconstructed into a volume model and visualized for diagnostic purposes or for planning of treatment or surgery. The same technology is often used with industrial CT for non-destructive inspection of composite materials or mechanical parts. Similarly, confocal microscopes produce data which is visualized to study the morphology of biological structures. In many computational fields, such as in computational fluid dynamics, the results of simulation typically running on a supercomputer are often visualized as volume data for analysis and verification. Recently, many traditional geometric computer graphics applications, such as CAD and simulation, have been exploiting the advantages of volume techniques called *volume graphics* for modeling, manipulation, and visualization.

Over the years many techniques have been developed to visualize 3D data. Since methods for displaying geometric primitives were already well-established, most of the early methods involve approximating a surface contained within the data using geometric primitives. When volumetric data are visualized using a surface rendering technique, a dimension of information is essentially lost. In response to this, volume rendering techniques were developed that attempt to capture the entire 3D data in a single 2D image. Volume rendering convey more information than surface rendering images, but at the cost of increased algorithm complexity, and consequently increased rendering times. To improve interactivity in volume rendering, many optimization methods as well as several special-purpose volume rendering machines have been developed.

We begin with an introduction to volumetric data. Section 3 covers briefly surface rendering techniques for volume data. Section 4 discusses in details volume rendering techniques, including image-order, object-order, and domain techniques. Optimization methods for volume rendering are discussed in Section 5, and special-purpose volume rendering hardware is described in Section 6. Section 7 introduces global illumination of volumetric data, including volumetric ray tracing and volumetric radiosity. Irregular grid rendering is briefly discussed in Section 8. Volume graphics is introduced in

Section 9, including several volume modeling techniques, such as voxelization, texture mapping, amorphous phenomena, block operations, constructive solid modeling, and volume sculpting.

2. Volumetric Data

Volumetric data is typically a set S of samples (x, y, z, v), representing the value v of some property of the data, at a 3D location (x, y, z). If the value is simply a 0 or a 1, with a value of 0 indicating background and a value of 1 indicating the object, then the data is referred to as binary data. The data may instead be multivalued, with the value representing some measurable property of the data, including, for example, color, density, heat or pressure. The value v may even be a vector, representing, for example, velocity at each location.

In general, the samples may be taken at purely random locations in space, but in most cases the set S is isotropic containing samples taken at regularly spaced intervals along three orthogonal axes. When the spacing between samples along each axis is a constant, but there may be three different spacing constants for the three axes the set S is anisotropic. Since the set of samples is defined on a regular grid, a 3D array (called also *volume buffer, cubic frame buffer, 3D raster*) is typically used to store the values, with the element location indicating position of the sample on the grid. For this reason, the set S will be referred to as the array of values $S(x, y, z)$, which is defined only at grid locations. Alternatively, either rectilinear, curvilinear (structured), or unstructured grids, are employed (e.g., [94]). In a *rectilinear* grid the cells are axis-aligned, but grid spacings along the axes are arbitrary. When such a grid has been non-linearly transformed while preserving the grid topology, the grid becomes *curvilinear*. Usually, the rectilinear grid defining the logical organization is called *computational space*, and the curvilinear grid is called *physical space*. Otherwise the grid is called *unstructured* or *irregular*. An unstructured or irregular volume data is a collection of cells whose connectivity has to be specified explicitly. These cells can be of an arbitrary shape such as tetrahedra, hexahedra, or prisms.

The array S only defines the value of some measured property of the data at discrete locations in space. A function $f(x, y, z)$ may be defined over R^3 in order to describe the value at any continuous location. The function $f(x, y, z) = S(x, y, z)$ if (x, y, z) is a grid location, otherwise $f(x, y, z)$ approximates the sample value at a location (x, y, z) by applying some interpolation function to S. There are many possible interpolation functions. The simplest interpolation function is known as *zero-order interpolation*, which is actually just a nearest-neighbor function. The value at any location in R^3 is simply the value of the closest sample to that location. With this interpolation method there is a region of constant value around each sample in S. Since the samples in S are regularly spaced, each region is of uniform size and shape. The region of constant value that surrounds each sample is known as a *voxel* with each voxel being a rectangular cuboid having six faces, twelve edges, and eight corners.

Higher-order interpolation functions can also be used to define $f(x, y, z)$ between sample points. One common interpolation function is a piecewise function known as *first-order interpolation*, or *trilinear interpolation*. With this interpolation function, the value is assumed to vary linearly along directions parallel to one of the major axes. Let the point P lie at location (x_p, y_p, z_p) within the regular hexahedron, known as a *cell*, defined by samples A through H. For simplicity, let the distance between samples in all three directions be 1, with sample A at $(0, 0, 0)$ with a value of v_A, and sample H at $(1, 1, 1)$ with a value of v_H. The value v_P, according to trilinear interpolation, is then:

$$v_P = v_A\,(1 - x_p)(1 - y_p)(1 - z_p) + v_E\,(1 - x_p)(1 - y_p)\,z_p\ + \qquad (1)$$

$$v_B\ \ x_p\ (1-y_p)(1-z_p) + v_F\ x_p\ (1-y_p)\ z_p\ +$$

$$v_C\ (1-x_p)\ y_p\ (1-z_p) + v_G\ (1-x_p)\ y_p\ \ z_p\ +$$

$$v_D\ x_p\ y_p\ (1-z_p) + v_H\ x_p\ y_p\ \ z_p$$

In general, A will be at some location (x_A, y_A, z_A), and H will be at $(x_{H,} y_{H,} z_H)$. In this case, x_p in Equation 1 would be replaced by $\frac{(x_p - x_A)}{(x_H - x_A)}$, with similar substitutions made for y_p and z_p.

3. Surface Rendering Techniques

Several surface rendering techniques have been developed which approximate a surface contained within volumetric data using geometric primitives, which can be rendered using conventional graphics accelerator hardware. A surface can be defined by applying a binary segmentation function $B(v)$ to the volumetric data. $B(v)$ evaluates to 1 if the value v is considered part of the object, and evaluates to 0 if the value v is part of the background. The surface is then the region where $B(v)$ changes from 0 to 1. If a zero-order interpolation function is being used, then the surface is simply the set of faces which are shared by voxels with differing values of $B(v)$. If a higher-order interpolation function is being used, then the surface passes between sample points according to the interpolation function.

For zero-order interpolation functions, the natural choice for a geometric primitive is the 3D rectangular cuboid, since the surface is a set of faces, and each face is a rectangle. An early algorithm for displaying human organs from computed tomograms [35] uses the square as the geometric primitive. To simplify the projection calculation and decrease rendering times, the assumption is made that the sample spacing in all three directions is the same. A software Z-buffer algorithm is then used to project the shaded squares onto the image plane to create the final image.

With continuous interpolation functions, a surface, known as an *iso-valued surface* or an *iso-surface*, may be defined by a single value. Several methods for extracting and rendering iso-surfaces have been developed, a few are briefly described here. The Marching Cubes algorithm [63] was developed to approximate an iso-valued surface with a triangle mesh. The algorithm breaks down the ways in which a surface can pass through a cell into 256 cases, reduces by symmetry to only 15 topologies. For each of these 15 cases, a generic set of triangles representing the surface is stored in a look-up table. Each cell through which a surface passes maps to one of the 15 cases, with the actual triangle vertex locations being determined using linear interpolation on the cell vertices. A normal value is estimated for each triangle vertex, and standard graphics hardware can be utilized to project the triangles, resulting in a smooth shaded image of the iso-valued surface.

When rendering a sufficiently large data set with the Marching Cubes algorithm, millions of triangles may be generated many of them map to a single pixel when projected onto the image plane. This fact led to the development of surface rendering algorithms that use 3D points as the geometric primitive. One such algorithm is Dividing Cubes [8], which subdivides each cell through which a surface passes into subcells. The number of divisions is selected such that the subcells project onto a single pixel on the image plane. Another algorithm which uses 3D points as the geometric primitive is the Trimmed Voxel Lists method [91]. Instead of subdividing, this method uses only one 3D point per visible surface cell, projecting that point on up to three pixels of the image plane to insure coverage in the image.

4. Volume Rendering Techniques

Representing a surface contained within a volumetric data set using geometric primitives can be useful in many applications, however there are several main drawbacks to this approach. First, geometric primitives can only approximate surfaces contained within the original data. Adequate approximations may require an excessive amount of geometric primitives. Therefore, a trade-off must be made between accuracy and space requirements. Second, since only a surface representation is used, much of the information contained within the data is lost during the rendering process. For example, in CT scanned data useful information is contained not only on the surfaces, but within the data as well. Also, amorphous phenomena, such as clouds, fog, and fire cannot be adequately represented using surfaces, and therefore must have a volumetric representation, and must be displayed using volume rendering techniques.

In the next subsections various volume rendering techniques are explored. *Volume rendering* is the process of creating a 2D image directly from 3D volumetric data. Although several of the methods described in these subsections render surfaces contained within volumetric data, these methods operate on the actual data samples, without the intermediate geometric primitive representations used by the algorithms in Section 3.

Volume rendering can be achieved using an *object-order*, an *image-order*, or a *domain-based* technique. Object-order volume rendering techniques use a *forward mapping* scheme where the volume data is mapped onto the image plane. In image-order algorithms, a *backward mapping* scheme is used where rays are cast from each pixel in the image plane through the volume data to determine the final pixel value. In a domain-based technique the spatial volume data is first transformed into an alternative domain, such as compression frequency, and wavelet, and then a projection is generated directly from that domain.

4.1. Object-Order Techniques

Object-order techniques involve mapping the data samples on to the image plane. One way to accomplish a projection of a surface contained within the volume is to loop through the data samples, projecting each sample which is part of the object onto the image plane. For this algorithm, the data samples are binary voxels, with a value of 0 indicating background and a value of 1 indicating the object. Also, the data samples are on a grid with uniform spacing in all three directions.

If an image is produced by projecting all voxels with a value of 1 to the image plane in an arbitrary order, we are not guaranteed a correct image. If two voxels project to the same pixel on the image plane, the one that was projected later will prevail, even if it is farther from the image plane than the earlier projected voxel. This problem can be solved by traversing the data samples in a *back-to-front* order. For this algorithm, the strict definition of back-to-front can be relaxed to require that if two voxels project to the same pixel on the image plane, the first processed voxel must be farther away from the image plane than the second one. This can be accomplished by traversing the data plane-by-plane, and row-by-row inside each plane. For arbitrary orientations of the data in relation to the image plane, some axes may be traversed in an increasing order, while others may be considered in a decreasing order. The traversal can be accomplished with three nested loops, indexing on x, y, and z. Although the relative orientations of the data and the image plane specify whether each axis should be traversed in an increasing or decreasing manner, the ordering of the axes in the traversal is arbitrary.

An alternative to back-to-front projection is a *front-to-back* method in which the voxels are traversed in the order of increasing distance from the image plane. Although a back-to-front method is easier to implement, a front-to-back method has the advantage that once a voxel is projected onto a pixel, other voxels which project to the same pixel are ignored, since they would be hidden by the first voxel. Another advantage of front-to-back projection methods is that if the axis which is most parallel to the viewing direction is chosen to be the outermost loop of the data traversal, meaningful partial image results can be displayed to the user. This allows the user to better interact with the data and terminate the image generation if, for example, an incorrect view direction was selected. Partial image results can be displayed to the user during a back-to-front method also, but the value of a pixel may change many times during image generation. With a front-to-back method, once a pixel value is set, its value remains unchanged.

Clipping planes orthogonal to the three major axes, and clipping planes parallel to the view plane are easy to implement using either a back-to-front or a front-to-back algorithm. For orthogonal clipping planes, the traversal of the data is limited to a smaller rectangular region within the full data set. To implement clipping planes parallel to the image plane, data samples whose distance to the image plane is less than the distance between the cut plane and the image plane are ignored. This ability to explore the whole data set is a major difference between volume rendering techniques and the surface rendering techniques described in Section 3. In surface rendering techniques, the geometric primitive representation of the object need to be changed in order to implement cut planes, which could be a time-consuming process. In a back-to-front method, cut planes can be achieved by simply modifying the bounds of the data traversal, and utilizing a condition when placing depth values in the image plane pixels.

For each voxel, its distance to the image plane could be stored in the pixel to which it maps along with the voxel value. At the end of a data traversal a 2D array of depth values, called a Z-buffer, is created, where the value. at each pixel in the Z-buffer is the distance to the closest non-empty voxel. A 2D discrete shading technique can then be applied to the image, resulting in a shaded image suitable for display. The 2D discrete shading techniques described here take as input a 2D array of depth values and a 2D array of projected voxel values, and produce as output a 2D image of intensity values. The simplest 2D discrete shading method is known as depth shading, or *depth-only shading* [36, 103], where only the Z-buffer is used and the intensity value stored in each pixel of the output image is inversely proportional to the depth of the corresponding input pixel. This produces images where features far from the image plane appear dark, while close feature are bright. Since surface orientation is not considered in this shading method, most details such as surface discontinuities and object boundaries are lost.

A more accurately shaded image can be obtained by passing the 2D depth image to a gradient-shader [29] which can take into account the object surface orientation and the distance from the light at each pixel to produce a shaded image. This method evaluates the gradient at each (x, y) pixel location in the input image by

$$\nabla z = \left(\frac{\delta z}{\delta x}, \frac{\delta z}{\delta y}, -1 \right) \tag{2}$$

where $z = D(x, y)$ is the depth stored in the Z-buffer associated with pixel (x, y). The estimated gradient vector at each pixel is then used as a normal vector for shading purposes.

The value $\frac{\delta z}{\delta x}$ can be approximated using a backward difference $D(x, y) - D(x-1, y)$, a forward

difference $D(x+1, y) - D(x, y)$, or a central difference $\frac{1}{2}(D(x+1, y) - D(x-1, y))$. Similar equations are used for approximating $\frac{\delta z}{\delta y}$. In general, the central difference is a better approximation of the derivative, but along object edges where, for example, pixels (x, y) and $(x+1, y)$ belong to two different objects, a backward difference would provide a better approximation. A context sensitive normal estimation method [120] was developed to provide more accurate normal estimations by detecting image discontinuities. In this method, two pixels are considered to be in the same ''context'' if their depth values, and the first derivative of the depth at these locations do not greatly differ. The gradient vector at some pixel p is then estimated by considering only those pixels which lie within a user-defined neighborhood, and belong to the same context as p. This ensures that sharp object edges, and slope changes are not smoothed out in the final image.

The previous rendering methods consider only binary data samples where a value of 1 indicates the object and a value of 0 indicates the background. Many forms of data acquisition (e.g., CT) produce data samples with 8, 12, or even more bits of data per sample. If these data samples represent the values at some sample points, and the value vary according to some convolution applied to the data samples which can reconstruct the original 3D signal, then a scalar field which approximates the original 3D signal has been defined.

One way to reconstruct the original signal is, as described previously, to define a function $f(x, y, z)$ which determines the value at any location in space. This technique is typically employed by backward-mapping (image-order) algorithms. In forward mapping algorithms, the original signal is reconstructed by spreading the value at a data sample into space. Westover describes a splatting algorithm [111] for approximating smooth object-ordered volume rendering, in which the value of the data samples represents a density. Each data sample $s = (x_s, y_s, z_s, \rho(s))$, $s \in S$, has a function C defining its contribution to every point (x, y, z) in the space:

$$C_s(x, y, z) = h_v(x - x_s, y - y_s, z - z_s)\rho(s) \tag{3}$$

where h_v is the volume reconstruction kernel and $\rho(s)$ is the density of sample s which is located at (x_s, y_s, z_s). The contribution of a sample s to an image plane pixel (x, y) can then be computed by integration:

$$C_s(x, y) = \rho(s) \int_{-\infty}^{\infty} h_v(x - x_s, y - y_s, u)du \tag{4}$$

where the u coordinate axis is parallel to the view ray. Since this integral is independent of the sample density, and depends only on its (x, y) projected location, a footprint function F can be defined as follows:

$$F(x, y) = \int_{-\infty}^{\infty} h_v(x, y, u)du \tag{5}$$

where (x, y) is the displacement of an image sample from the center of the sample's image plane projection. The weight w at each pixel can then be expressed as:

$$w(x, y)_s = F(x - x_s, y - y_s) \tag{6}$$

where (x, y) is the pixel location, and (x_s, y_s) is the image plane location of the sample s.

A footprint table can be generated by evaluating the integral in Equation 5 on a grid with a resolution much higher than the image plane resolution. All table values lying outside of the footprint table extent

have zero weight and therefore need not be considered when generating an image. A footprint table for a data sample s, can be centered on the projected image plane location of s, and be sampled in order to determine the weight of the contribution of s to each pixel on the image plane. Multiplying this weight by $\rho(s)$ then gives the contribution of s to each pixel.

Computing a footprint table can be difficult due to the integration required. Discrete integration methods can be used to approximate the continuous integral, but generating a footprint table is still a costly operation. Luckily, for orthographic projections, the footprint of each sample is the same except for an image plane offset. Therefore, only one footprint table needs to be calculated per view. Since this still would require too much computation time, only one generic footprint table is built for the kernel. For each view, a view-transformed footprint table is created from the generic footprint table. The generic footprint table can be precomputed, therefore, it does not matter how long the computation takes.

Generating a view-transformed footprint table from the generic footprint table can be accomplished in three steps. First, the image plane extent of the projection of the reconstruction kernel is determined. Next a mapping is computed between this extent and the extent that surrounds the generic footprint table. Finally, the value for each entry in the view-transformed footprint table is determined by mapping the location of the entry to the generic footprint table, and sampling. The extent of the reconstruction kernel is either a sphere, or is bounded by a sphere, so the extent of the generic footprint table is always a circle. If the grid spacing of the data samples is uniform along all three axes, then the reconstruction kernel is a sphere and the image plane extent of the reconstruction kernel will be a circle. The mapping from this extent to the extent of the generic footprint table is simply a scaling operation. If the grid spacing differs along the three axes, then the reconstruction kernel is an ellipsoid and the image plane extent of the reconstruction kernel will be an ellipse. In this case, a mapping from this ellipse to the circular extent of the generic footprint table must be computed.

There are three modifiable parameters in this algorithm which can greatly affect image quality. First, the size of the footprint table can be varied. Small footprint tables produce blocky images, while large footprint tables may smooth out details and require more space. Second, different sampling methods can be used when generating the view-transformed footprint table from the generic footprint table. Using a nearest-neighbor approach is fast, but may produce aliasing artifacts. On the other hand, using bilinear interpolation produces smoother images at the expense of longer rendering times. The third parameter which can be modified is the reconstruction kernel itself. The choice of, for example, a cone function, Gaussian function, sync function or bilinear function affects the final image.

Drebin, Carpenter, and Hanrahan [16] developed a technique for rendering volumes that contain mixtures of materials, such as CT data containing bone, muscle and flesh. In this method, various assumptions about the volume data are made. First, it is assumed that the scalar field was sampled above the Nyquist frequency, or a low-pass filter was used to remove high frequencies before sampling. The volume contains either several scalar fields, or one scalar field representing the composition of several materials. If the latter is the case, it is assumed that material can be differentiated either by the scalar value at each point, or by additional information about the composition of each volume element.

The first step in this rendering algorithm is to create new scalar fields from the input data, known as material percentage volumes. Each material percentage volume is a scalar field representing only one material. Color and opacity are then associated with each material, with composite color and opacity obtained by linearly combining the color and opacity for each material percentage volume. A matte volume, that is, a scalar field on the volume with values ranging between 0 and 1, is used to slice the

volume or perform other spatial set operations. Actual rendering of the final composite scalar field is obtained by transforming the volume so that one axis is perpendicular to the image plane. The data is then projected plane by plane in a back-to-front manner and composited to form the final image.

4.2. Image-Order Techniques

Image-order volume rendering techniques are fundamentally different from object-order rendering techniques. Instead of determining how a data sample affects the pixels on the image plane, in an image-order technique we determine for each pixel on the image plane, the data samples contribute to it are determined.

One of the first image-order volume rendering techniques, which may be called *binary ray casting* [101], was developed to generate images of surfaces contained within binary volumetric data without the need to explicitly perform boundary detection and hidden-surface removal. For each pixel on the image plane, a ray is cast from that pixel to determine if it intersects the surface contained within the data. For parallel projections, all rays are parallel to the view direction, where as for perspective projections, rays are cast from the eye point according to the view direction and the field of view. If an intersection does occur, shading is performed at the intersection point, and the resulting color is placed in the pixel. In order to determine the first intersection along the ray a stepping technique is used where the value is determined at regular intervals along the ray until the object is intersected. Data samples with a value of 0 are considered to be the background while those with a value of 1 are considered to be part of the object. A zero-order interpolation technique is used, so the value at a location along the ray is 0 if that location is not in any voxel of the data, otherwise it is the value of the closest data sample. For a step size d, the i^{th} point sample p_i would be taken at a distance $i \times d$ along the ray. For a given ray, either all point samples along the ray have a value of 0 (the ray missed the object entirely), or there is some sample p_i taken at a distance $i \times d$ along the ray, such that all samples p_j, $j < i$, have a value of 0, and sample p_i has a value of 1. Point sample p_i is then considered to be the first intersection along the ray. In this algorithm, the step size d must be chosen carefully. If d is too large, small features in the data may not be detected. On the other hand, if d is small, the intersection point is more accurately estimated at the cost of higher computation time.

There are several optimizations which can be made to this algorithms. First, the number of steps which must be made along each ray can be reduced by traversing only the part of the ray contained within the bounding box of the data. A second optimization involves the representation of the data in memory. This algorithm was originally developed on a machine with only 32K of RAM, so data compression was a critical issue. Instead of simply storing the data as a binary array of 0's and 1's, a scan-line representation can be used. For each scan-line in the data, a list of end points can be stored which represent the segments belonging to the object. This representation is compact, yet does not add too much time to the intersection calculation.

The previous algorithm deals with the display of surfaces within binary data. A more general algorithm can be used to generate surface and composite projections of multivalued data. Instead of traversing a continuous ray and determining the closest data sample for each step with a zero-order interpolation function, a discrete representation of the ray could be traversed. This discrete ray is generated using a 3D Bresenham-like algorithm or a 3D line scan-conversion (voxelization) algorithm [43, 49] (see Section 9.1). As in the previous algorithms, for each pixel in the image plane, the data samples contribute to it need to be determined. This could be done by casting a ray from each pixel in the direction of the viewing ray. This ray would be discretized (voxelized), and the contribution from each

voxel along the path is considered when producing the final pixel value. This technique is referred to as *discrete ray casting* [122].

In order to generate a 3D discrete ray using a voxelization algorithm, the 3D discrete topology of 3D paths has to be understood. There are three types of connected paths: 6-connected, 18-connected, and 26-connected, which are based upon the three adjacency relationships between consecutive voxels along the path. An example of these three types of connected paths is given in Figure 1. Assuming a voxel is represented as a box centered at the grid point, two voxels are said to be 6-connected if they share a face, they are 18-connected if they share a face or an edge, and they are 26-connected if they share a face, an edge, or a vertex. A 6-connected path is a sequence of voxels, v_1, v_2, ... v_N, where for each pair of voxels v_i, v_{i+1} $(1 \leq i < N)$, v_i and v_{i+1} are 6-connected. Similar definitions exist for 18- and 26-connected paths.

In discrete ray casting, a ray is discretized into a 6-, 18-, or 26-connected path, and only the voxels along this path are considered when determining the final pixel value. If a surface projection is required, the path is traversed until the first voxel which is part of the object is encountered. This voxel is then shaded and the resulting color value is stored in the pixel. 6-connected paths contain almost twice as many voxels as 26-connected paths, so an image created using 26-connected paths would require less computation, but a 26-connected path may miss an intersection that would be detected using a 6-connected path.

To produce a shaded image, the distance to the closest intersection is stored at each pixel in the image, and, then this image is passed to a 2D discrete shader, such as those described previously. However, better results can be obtained by performing a 3D discrete shading operation at the intersection point. One 3D discrete shading method, known as *normal-based contextual shading* [5], can be employed to estimate the normal when zero-order interpolation is used. The normal for a face of a voxel that is on the surface of the object is determined by examining the orientation of that face, and the orientation of the four faces on the surface that are edge connected to that face. Since a face of a voxel can have only six possible orientations, the error in the approximated normal can be significant. More accurate results can be obtained using a technique known as *gray-level shading* [4, 8, 38, 97, 98]. If the intersection occurs at location (x, y, z) in the data, then the gray-level gradient at that location can be approximated with a central difference:

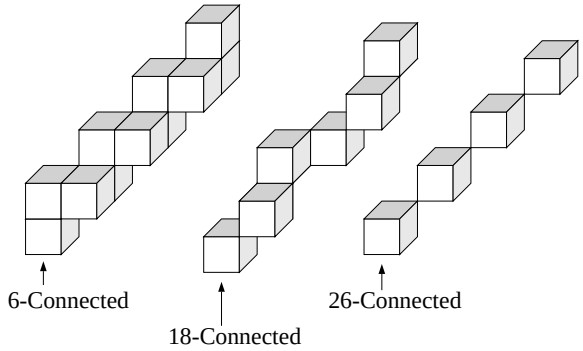

Figure 1: 6-, 18-, and 26-connected paths

$$G_x = \frac{f(x+1,y,z) - f(x-1,y,z)}{2D_x},$$

$$G_y = \frac{f(x,y+1,z) - f(x,y-1,z)}{2D_y}, \tag{7}$$

$$G_z = \frac{f(x,y,z+1) - f(x,y,z-1)}{2D_z},$$

where (G_x, G_y, G_z) is the gradient vector, and D_x, D_y, and D_z are the distances between neighboring samples in the x, y, and z directions, respectively. The gradient vector is used as a normal vector for shading calculation, and the intensity value obtained from shading is stored in the image. A normal estimation can be performed at point sample p_i, and this information, along with the light direction, and the distance $i \times d$ can be used to shade p_i.

Actually, stopping at the first opaque voxel and shading there is only one of many operations which can be performed on the voxels along a discrete path or continuous ray. Instead, the whole ray could be traversed, storing in the image plane pixel the maximum value encountered along the ray. Figure 2 (a) is a first opaque, or surface, projection of a bullfrog sympathetic ganglion cell, which was reconstructed from confocal microscope data, while Figure 2 (b) is a maximum projection of the same cell. Figure 2 was generated using the PARC algorithm, which is described in Section 5. As opposed to a surface projection, a maximum projection is capable of revealing some internal parts of the data. Another option is to store the sum (simulating X-rays) or average of all values along the ray. More complex techniques, which are described below, may involve defining an opacity and color for each scalar value, and then accumulating intensity along the ray according to some compositing function, revealing 3D structure information and 3D internal features (see Figure 2(c)).

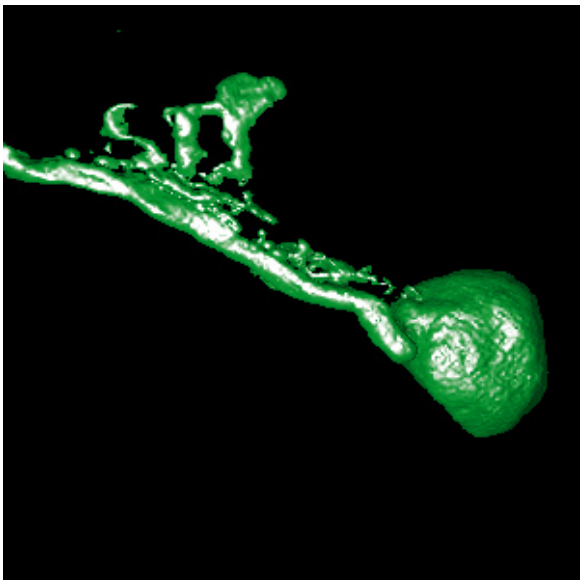

Figure 2(a): A surface projection of a nerve cell.

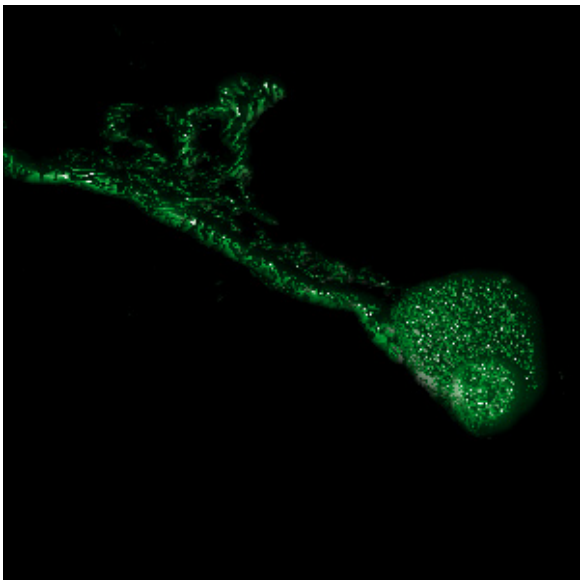

Figure 2(b): A maximum projection of a nerve cell.

The previous two rendering techniques, binary ray casting and discrete ray casting, use zero-order interpolation in order to define the scalar value at any location in R^3. One advantage to using zero-order interpolation is simplicity and speed, since many of the calculations required can be done using integer arithmetic. One disadvantage though is the aliasing effects in the image. Higher-order interpolation functions can be used to create a more accurate image, but generally at the cost of algorithm complexity and computation time. The next three algorithms described in this section all use higher-order interpolation functions.

When creating a composite projection of a data set, there are two important parameters, the color at a sample point, and the opacity at that location. An image-order volume rendering algorithm developed by Levoy [60] states that given an array of data samples S, two new arrays S_c and S_α, which define the color and opacity at each grid location can be generated using preprocessing techniques. The interpolation functions $f(x, y, z)$, $f_c(x, y, z)$, and $f_\alpha(x, y, z)$, which specify the sample value, color, and opacity at any location in R^3, are then defined. f_c and *fsunx* are often referred to as transfer functions.

Generating the array S_c of color values involves performing a shading operation, such as gray-level shading, at each data sample in the original array S. For this purpose, the Phong illumination model, for example, could be used. The normal at each data sample is the unit gradient vector at that location. The gradient vector at any location can be computed by partially differentiating the interpolation function with respect to *x, y,* and *z* to get each component of the gradient. If the interpolation function is not first derivative continuous, aliasing artifacts will occur in the image due to the discontinuous normal vector. A smoother set of gradient vectors can be obtained using a central differencing method similar to the one described earlier in this section.

Calculating the array S_α is essentially a surface classification operation. There are different ways to classify surfaces within a scalar field, and each way requires a new mapping from $S(x, y, z)$ to $S_\alpha(x, y, z)$. When an iso-surface at some constant value v with an opacity α_v ought to be viewed,

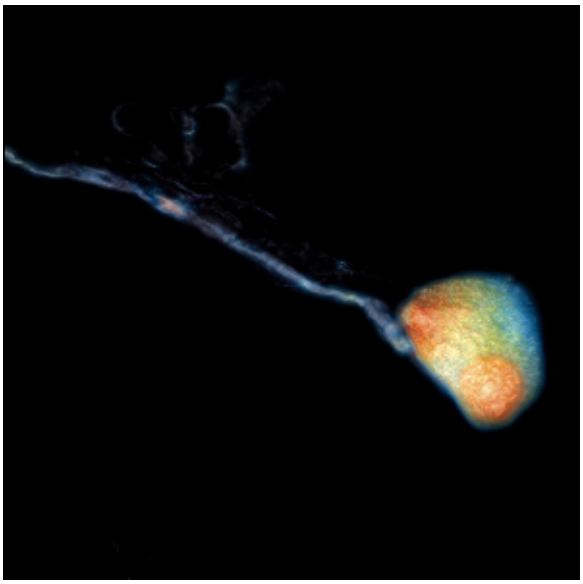

Figure 2(c): A composited projection of a nerve cell.

$S_\alpha(x, y, z)$ is simply assigned to α_v if $S(x, y, z)$ is v, otherwise $S_\alpha(x, y, z) = 0$. This would produce aliasing artifacts, which can be reduced by setting $S_\alpha(x, y, z)$ close to α_v if $S(x, y, z)$ is close to v. The best results are obtained when the thickness of the transition region is constant throughout the volume. This can be approximated by having the opacity fall off at a rate inversely proportional to the magnitude of the local gradient vector. Multiple iso-surfaces can be displayed in a single image by separately applying the classification mappings, then combining the opacities.

Once the $S_c(x, y, z)$ and $S_\alpha(x, y, z)$ arrays have been determined, rays are cast from the pixels, through these two arrays, sampling at evenly spaced locations. To determine the value at a location, the trilinear interpolation functions f_c and f_α are used. Once these point samples along the ray have been computed, a fully opaque background is added in, and then the values in a back-to-front order are composited to produce a single color that is placed in the pixel.

Two rendering techniques for displaying volumetric data, known as the V-Buffer method, were developed by Upson and Keeler [102]. One of the methods for visualizing the scalar field is an image-order ray-casting technique. In this method, rays are cast from each pixel on the image plane into the volume. For each cell in the volume along the path of this ray, the scalar value is determined at the point where the ray first intersects the cell. The ray is then stepped along until it traverses the entire cell, with calculations for scalar values, shading, opacity, texture mapping, and depth cuing performed at each stepping point. This process is repeated for each cell along the ray, accumulating color and opacity, until the ray exits the volume, or the accumulated opacity reaches unity. At this point, the accumulated color and opacity for that pixel are stored, and the next ray is cast.

The goal of this method is not to produce a realistic image, but instead to provide a representation of the volumetric data which can be interpreted by a scientist or an engineer. For this purpose, the user is given the ability to modify certain parameters in the shading equations which will lead to an informative, rather than physically accurate shaded image. A simplified shading equation is used where the perceived intensity as a function of wavelength, $I(\lambda)$ is define as:

$$I(\lambda) = K_a(\lambda)I_a + K_d(\lambda)\sum_j[(N \cdot L_j)I_j] \tag{8}$$

In this equation, K_a is the ambient coefficient, I_a is the ambient intensity, K_d is the diffuse coefficient, N is the normal approximated by the local gradient, L_j is the vector to the j^{th} light source, and I_j is the intensity of the j^{th} light source. In order to highlight certain features in the final image, the diffuse coefficient can be defined as a function of not only wavelength, but also scalar value and solid texture:

$$K_d(\lambda, S, M) = K(\lambda)\ T_d(\lambda, S(x, y, z)\ M(\lambda, x, y, z)), \tag{9}$$

where K is the actual diffuse coefficient, T_d is the color transfer function, S is the sample array, and M is the solid texture map. The color transfer function is defined for red, green, and blue, and maps scalar value to intensity. In this method the following intensity integral is approximated when accumulating along the ray:

$$I(\lambda) = \int_w \left[\tau(d)O(s)\left[K_a(\lambda)I_a + K_d(\lambda, S, M)\sum\left[(N \cdot L_j)I_j\right]\right] + (1 - \tau(d)bc(\lambda))\right]du \tag{10}$$

where $\tau\ (d)$ represents atmospheric attenuation as a function of distance d, $O\ (s)$ is the opacity transfer function, bc is the background color, and u is a vector in the direction of the view ray. The opacity transfer function is similar to the color transfer function in that it defines opacity as a function of scalar value. Different color and opacity transfer functions can be defined to highlight different features in the volume.

The second method for visualizing the scalar field is a cell-by-cell processing technique [Upston Keeler 1988.], where within each cell an image-order ray-casting technique is used, thus making this a hybrid technique. In this method, each cell in the volume is processed in a front-to-back order. Processing begins on the plane closest to the viewpoint, and progresses in a plane-by-plane manner. Within each plane, processing begins with the cell closest to the viewpoint, then continues in order of increasing distance from the viewpoint. Each cell is processed by first determining for each scan line in the image plane, which pixels are affected by the cell. Then, for each pixel an integration volume is determined. Within the bounds of the integration volume, an intensity calculation similar to Equation 10 is performed according to:

$$I(\lambda) = \int_x \int_y \int_z \left[\tau(d)O(s)\left[K_a(\lambda)I_a + K_d(\lambda, S, M)\sum\left[(N \cdot L_j)I_j\right]\right] + (1 - \tau(d)bc(\lambda))\right]dxdydz \tag{11}$$

This process continues in a front-to-back order, until all cells have been processed, with intensity accumulated into pixel values. Once a pixel opacity reaches unity, a flag is set and this pixel is not processed further. Due to the front-to-back nature of this algorithm, incremental display of the image is possible.

In order to simulate light coming from translucent objects, volumetric data with data samples representing density values can be considered as a field of density emitters [84]. A density emitter is a tiny particle that both emits and scatters light. The amount of density emitters in any small region within the volume is proportional to the scalar value in that region. These density emitters are used to correctly model the occlusion of deeper parts of the volume by closer parts, but both shadowing and color variation due to differences in scattering at different wavelengths are ignored. These effects are ignored because it is believed that they would complicate the image, detracting from the perception of density variation. Similar to the V-Buffer method, rays are cast from the eye point, through each pixel on the image plane, and into the volume. The intensity I of light for a given pixel is calculated according to:

$$I = \int_{t_1}^{t_2} e^{-\tau \int_{t_1}^{t} \rho^{\gamma}(\lambda) d\lambda} \rho^{\gamma}(t) dt \tag{12}$$

In this equation, the ray is traversed from t_1 to t_2, accumulating at each location t the density $\rho^{\gamma}(t)$ at that location attenuated by the probability $e^{-\tau \int_{t_1}^{t} \rho^{\gamma}(\lambda) d\lambda}$ that this light will be scattered before reaching the eye. The parameter τ is modifiable, and controls the attenuation, with higher values of τ specifying a medium which darkens more rapidly. The parameter γ is also modifiable, and controls the spread of density values. Low γ values produce a diffuse cloud appearance, while higher γ values highlight dense portions of the data. For each ray, three values in addition to I maybe computed. The maximum value encountered along the ray, the distance at which that maximum occurred, and the center of gravity of density emitters along the ray. By mapping these values to different color parameters (such as hue, saturation and lightness), interesting effects can be achieved. Krueger [55] showed that the various existing volume rendering models can be described as special cases of an underlying transport theory model of the transfer of particles in inhomogeneous media. The basic idea is that a beam of ''virtual'' particles is sent through the volume, with the user selecting the particle properties and the laws of interaction between the particles and the data. The image plane then contains the ''scattered'' virtual particles, and information about the data is obtained from the scattering pattern. If, for example, the virtual particles are chosen to have the properties of photons, and the laws of interaction are governed by optical laws, then this model essentially becomes a generalized ray tracer. Other virtual particles and interaction laws can be used, for example, to identify periodicities and similar hidden symmetries of the data.

Using Krueger's transport theory model, the intensity of light I at a pixel can be described as a path integral along the view ray:

$$I = \int_{p_{near}}^{p_{far}} Q(p) e^{-\int_{p_{near}}^{p} \sigma_a(p') + \sigma_{pc}(p') dp'} dp \tag{13}$$

The emission at each point p along the ray is scaled by the optical depth to the eye to produce the final intensity value for a pixel. The optical depth is a function of the total extinction coefficient, which is composed of the absorption coefficient σ_a, and the scattering coefficient σ_{sc}. The generalized source $Q(p)$ is defined as:

$$Q(p) = q(p) + \sigma_{sc(p)} \int \rho_{sc}(\vec{\omega}' \rightarrow \vec{\omega}) I(S, \vec{\omega}') d\vec{\omega}' \tag{14}$$

This generalized source consists of the emission at a given point $q(p)$, and the incoming intensity along all directions scaled by the scattering phase ρ_{sc}. Typically, a low albedo approximation is used to simplify the calculations, reducing the integral in Equation 15 to a sum over all light sources.

4.3. Domain Volume Rendering

In domain rendering the spatial 3D data is first transformed into another domain, such as compression, frequency, and wavelet domain, and then a projection is generated directly from that domain or with the help of information from that domain. The frequency domain rendering applies the Fourier slice projection theorem, which states that a projection of the 3D data volume from a certain view direction can be obtained by extracting a 2D slice perpendicular to that view direction out of the 3D Fourier

spectrum and then inverse Fourier transforming it. This approach obtains the 3D volume projection directly from the 3D spectrum of the data, and therefore reduces the computational complexity for volume rendering from $O(N^3)$ to $O(N^2 \log N)$ [18, 62, 64, 65]. A major problem of frequency domain volume rendering is the fact that the resulting projection is a line integral along the view direction which does not exhibit any occlusion and attenuation effects. Totsuka and Levoy [99] proposed a linear approximation to the exponential attenuation [84] and an alternative shading model to fit the computation within the frequency-domain rendering framework.

The compression domain rendering performs volume rendering from compressed scalar data without decompressing the entire data set, and therefore reduces the storage, computation and transmission overhead of otherwise large volume data. For example, Ning and Hesselink [73, 74] first applied vector quantization in the spatial domain to compress the volume and, then directly rendered the quantized blocks using regular spatial domain volume rendering algorithms. Fowler and Yagel [22] combined differential pulse-code modulation and Huffman coding, and developed a lossless volume compression algorithm, but their algorithm is not coupled with rendering. Yeo and Liu [123] applied discrete cosine transform based compression technique on overlapping blocks of the data. Chiueh et al. [6] applied 3D Hartley transform to extend the JPEG still image compression algorithm [105] for the compression of subcubes of the volume, and performed frequency domain rendering on the subcubes before compositing the resulting sub-images in the spatial domain. Each of the 3D Fourier coefficients in each subcube is then quantized, linearly sequenced through a 3D zig-zag order, and then entropy encoded. In this way, they alleviated the problem of lack of attenuation and occlusion in frequency domain rendering while achieving high compression ratios, fast rendering speed compared to spatial volume rendering, and improved image quality over conventional frequency domain rendering techniques. Figure 3 shows a CT scan of a lobster that was rendered out of the compressed frequency domain.

Rooted in time-frequency analysis, wavelet theory [7, 15] has gained popularity in the recent years. A

Figure 3: Compression domain volume rendering of a CT scan of a lobster.

wavelet is a fast decaying function with zero averaging. The nice features of wavelets are that they have local property in both spatial and frequency domain, and can be used to fully represent the volumes with small number of wavelet coefficients. Muraki [71] first applied wavelet transform to volumetric data sets, Gross et al. [30] found an approximate solution for the volume rendering equation using orthonormal wavelet functions, and Westermann [110] combined volume rendering with wavelet-based compression. However, all of these algorithms have not focused on the acceleration of volume rendering using wavelets. The greater potential of wavelet domain, based on the elegant multiresolution hierarchy provided by the wavelet transform, is still far from fully utilized for volume rendering. A possible research and development is to exploit the local frequency variance provided by wavelet transform and accelerate the volume rendering in homogeneous area.

5. Volume Rendering Optimizations

Volume rendering can produce informative images that can be useful in data analysis, but a major drawback of the techniques described above is the time required to generate a high-quality image. In this section, several volume rendering optimizations are described that decrease rendering times, and therefore increase interactivity and productivity. Other optimizations have been discussed briefly earlier in the paper, along with the original algorithms. Another way to speed up volume rendering is to employ special-purpose hardware accelerators for volume rendering, which are described in Section 6.

Object-order volume rendering typically loops through the data, calculating the contribution of each volume sample to pixels on the image plane. This is a costly operation for moderate to large sized data sets (e.g., 128M bytes for a 512^3 sample data set, with one byte per sample), leading to rendering times that are non-interactive. Viewing the intermediate results in the image plane may be useful, but these partial image results are not always representatives of the final image. For the purpose of interaction, it is useful to be able to generate a lower quality image in a shorter amount of time. For data sets with binary sample values, bits could be packed into bytes such that each byte represents a 2×2×2 portion of the data [101]. The data would be processed bit by bit to generate the full resolution image, but lower resolution image could be generated by processing the data byte by byte. If more than four bits of the byte are set, the byte is considered to represent an element of the object, otherwise it represents the background. This will produce an image with one-half the linear resolution in approximately one-eighth the time.

A more general method for decreasing data resolution is to build a pyramid data structure, which for an original data set of N^3 data samples, consists of a sequence of $\log N$ volumes. The first volume is the original data set, while the second volume is created by averaging each 2×2×2 group of samples of the original data set to create a volume of one-eight the resolution. The third volume is created from the second volume in a similar fashion, with this process continuing until all $\log N$ volumes have been created. An efficient implementation of the splatting algorithm, called hierarchical splatting [58], uses such a pyramid data structure. According to the desired image quality, this algorithm scans the appropriate level of the pyramid in a back-to-front order. Each element is splatted onto the image plane using the appropriate sized splat. The splats themselves are approximated by polygons which can efficiently be rendered by graphics hardware.

Image-order volume rendering involves casting rays from the image plane into the data, and sampling along the ray in order to determine pixel values. The idea of pyramid can also be used here. Actually, Wang and Kaufman [108] have proposed the use of multi-resolution hierarchy at arbitrary resolutions.

In discrete ray casting, the ray would be discretized, and the contribution from each voxel along the path is considered when producing the final pixel value. It would be quite computationally expensive to discretize every ray cast from the image plane. Fortunately, this is unnecessary for parallel projections. Since all the rays are parallel, one ray can be discretized into a 26-connected line and used as a ‘‘template’’ for all other rays. This technique, developed by Yagel and Kaufman [119], is called *template-based volume viewing*. If this template were used to cast a ray from each pixel in the image plane, some voxels in the data may contribute to the image twice while others may not be considered at all. To solve this problem, the rays are cast instead from a *baseplane*, that is, the plane of the volume buffer most parallel to the image plane. This ensures that each data sample can contribute at most once to the final image, and all data samples could potentially contribute. Once all the rays have been cast from the base plane, a simple final step of resampling is needed, which uses bilinear interpolation to determine the pixel values on the image plane from the ray values that have been calculated on the base plane.

An extension can be made to this template-based ray casting to allow higher-order interpolation [121]. The template for higher-order interpolation consists of connected cells, as opposed to the connected voxel template used for zero-order interpolation. Since the value varies within a cell, it is desirable to take multiple samples along the continuous ray inside of each cell. Since these samples are taken at regular intervals, and the same template is used for every ray, there is only a finite number of 3D locations (relative to a cell) at which sampling occurs. This fact allows us to precompute part of the interpolation function and store it in a table, allowing for faster rendering times.

Another extension to template-based ray casting allows for screen space supersampling to improve image quality [118]. This is accomplished by allowing rays to originate at sub-pixel locations. A finite number of sub-pixel locations from which a ray can originate is selected, and a template is created for each. When a ray is cast, its sub-pixel location determines which template is used. For example, to accomplish a 2×2 uniform supersampling, four rays would be cast per pixel, and therefore four sub-pixel locations are possible. Stochastic supersampling can also be supported by limiting the possible ray origins to a finite number of sub-pixel locations, and precomputing a template for each.

Lacroute and Levoy [56] extended the previous ideas in an algorithm called shear-warp factorization. It is based on algorithm that factors the viewing transformation into a 3D shear parallel to the data-slices, a projection to form an intermediate but distorted image, and a 2D warp to form an undistorted final image. The algorithm is extended in three ways. First, a fast object-order rendering algorithm based on the factorization algorithms with pre-processing and some loss of image quality, has been developed. Shear-warp factorization has the property that rows of voxels in the volume are aligned with rows of pixels in the intermediate image. Consequently, a scanline-based algorithm has been constructed that traverses the volume and the intermediate image in synchrony, taking advantage of the spatial coherence present in both. Spatial data structures based on run-length encoding for both the volume and the intermediate image are used. An implementation running on an SGI Indigo workstation renders a 256^3 voxel data set in one second. The second extension is shear-warp factorization for perspective viewing transformations. Third, a data structure for encoding spatial coherence in unclassified volumes (i.e., scalar fields with no precomputed opacity) has been introduced. When combined with the shear-warp rendering algorithm this data structure supports classification and rendering a 256^3 voxel volume in three seconds. The method extends to support mixed volumes and geometry and is parallelizable [57].

One obvious optimization for both discrete and continuous ray casting which has already been discussed is to limit the sampling to the segment of the ray which intersects the data, since samples outside of the data evaluate to 0 and do not contribute to the pixel value. If the data itself contains many zero-valued

data samples, or a segmentation function is applied to the data that evaluates to 0 for many samples, the efficiency of ray casting can be greatly enhanced by further limiting the segment of the ray in which samples are taken. One algorithm of this sort is known as *polygon assisted ray casting*, or *PARC* [1]. This algorithm approximates objects contained within a volume using a crude polyhedral representation. The polyhedral representation is created so that it completely contains the objects. Using conventional graphics hardware, the polygons are projected twice to create two Z-buffers. The first Z-buffer is the standard closest-distance Z-buffer, while the second is a farthest-distance Z-buffer. Since the object is completely contained within the representation, the two Z-buffer values for a given image plane pixel can be used as the starting and ending points of a ray segment on which samples are taken.

The PARC algorithm is part of the *VolVis* volume visualization system [1, 2], which provides a multi-algorithm progressive refinement approach for interactivity. By using available graphics hardware, the user is given the ability to interactively manipulate a polyhedral representation of the data. When the user is satisfied with the placement of the data, light sources, and view, the Z-buffer information is passed to the PARC algorithm, which produces a ray-cast image. In a final step, this image is further refined by continuing to follow the PARC rays which intersected the data according to a volumetric ray tracing algorithm [92] in order to generate shadows, reflections, and transparency (See Section 7.1). The ray tracing algorithm uses various optimization techniques, including uniform space subdivision and bounding boxes, to increase the efficiency of the secondary rays. Surface rendering, as well as transparency with color and opacity transfer functions, are incorporated within a global illumination model.

6. Special-Purpose Volume Rendering Hardware

The high computational cost of direct volume rendering makes it difficult for sequential implementations and general-purpose computers to deliver the targeted level of performance. This situation is aggravated by the continuing trend towards higher and higher resolution datasets. For example, to render a dataset of 1024^3 16-bit voxels at 30 frames per second requires 2 GBytes of storage, a memory transfer rate of 60 GBytes per second and approximately 300 billion instructions per second, assuming 10 instructions per voxel per projection. To address this challenge, researchers have tried to achieve interactive display rates on supercomputers and massively parallel architectures [70, 86, 104, 124]. However, most algorithms require very little repeated computation on each voxel and data movement actually accounts for a significant portion of the overall performance overhead. Todays commercial supercomputer memory systems don’t have and will not have in the near future adequate latency and memory bandwidth for efficiently transferring the required large amounts of data. Furthermore, supercomputers seldom contain frame buffers and, due to their high cost, are frequently shared by many users.

The same way as the special requirements of traditional computer graphics lead to high-performance graphics engines, volume visualization naturally lends itself to special-purpose volume renderers that separate real-time image generation from general-purpose processing. This allows for stand-alone visualization environments that help scientists to interactively view their data on a single user workstation, either augmented by a volume rendering accelerator or connected to a dedicated visualization server. Furthermore, a volume rendering engine integrated in a graphics workstation is a natural extension of raster based systems into 3D volume visualization.

Several researchers have proposed special-purpose volume rendering architectures [49, Chapter 6] [27,

41, 47, 68, 76, 95, 96, 116]. Most recent research focuses on accelerators for ray-casting of regular datasets. Ray-casting offers room for algorithmic improvements while still allowing for high image quality. Recent architectures [37] include VOGUE, VIRIM, and Cube.

VOGUE [54], a modular add-on accelerator, is estimated to achieve 2.5 frames per second for 256^3 datasets. For each pixel a ray is defined by the host computer and sent to the accelerator. The VOGUE module autonomously processes the complete ray, consisting of evenly spaced resampling locations, and returns the final pixel color of that ray to the host. Several VOGUE modules can be combined to yield higher performance implementations. For example, to achieve 20 projections per second of 512^3 datasets requires 64 boards and a 5.2 GB per second ring-connected cubic network.

VIRIM [31] is a flexible and programmable ray-casting engine. The hardware consists of two separate units, the first being responsible for 3D resampling of the volume using lookup tables to implement different interpolation schemes. The second unit performs the ray-casting through the resampled dataset according to user programmable lighting and viewing parameters. The underlying ray-casting model allows for arbitrary parallel and perspective projections and shadows. An existing hardware implementation for the visualization of $256 \times 256 \times 128$ datasets at 10 frames per second requires 16 processing boards.

The Cube project aims at the realization of high-performance volume rendering systems for large datasets and pioneered several hardware architectures. Cube-1, a first generation hardware prototype, was based on a specially interleaved memory organization [46], which has also been used in all subsequent generations of the Cube architecture. This interleaving of the n^3 voxel enables conflict-free access to any ray parallel to a main axis of n voxels. A fully operational printed circuit board (PCB) implementation of Cube-1 is capable of generating orthographic projections of 16^3 datasets from a finite number of predetermined directions in real-time. Cube-2 was a single-chip VLSI implementation of this prototype [3].

To achieve higher performance and to further reduce the critical memory access bottleneck, Cube-3 introduced several new concepts [78-80]. A high-speed global communication network aligns and distributes voxels from the memory to several parallel processing units and a circular cross-linked binary tree of voxel combination units composites all samples into the final pixel color. Estimated performance for arbitrary parallel and perspective projections is 30 frames per second for 512^3 datasets. Cube-4 [81] has only simple and local interconnections, thereby allowing for easy scalability of performance. Instead of processing individual rays, Cube-4 manipulates a group of rays at a time. As a result, the rendering pipeline is directly connected to the memory. Accumulating compositors replace the binary compositing tree. A pixel-bus collects and aligns the pixel output from the compositors. Cube-4 is easily scalable to very high resolution of 1024^3 16-bit voxels and true real-time performance implementations of 30 frames per second.

The choice of whether one adopts a general-purpose or a special-purpose solution to volume rendering depends upon the circumstances. If maximum flexibility is required, general-purpose appears to be the best way to proceed. However, an important feature of graphics accelerators is that they are integrated into a much larger environment where software can shape the form of input and output data, thereby providing the additional flexibility that is needed. A good example is the relationship between the needs of conventional computer graphics and special-purpose graphics hardware. Nobody would dispute the necessity for polygon graphics acceleration despite its obvious limitations. The exact same argument can be made for special-purpose volume rendering architectures.

7. Volumetric Global Illumination

Speed and accuracy of the final image are both important, yet often conflicting aspects of the rendering process. For this reason, a comprehensive volume rendering system, such as *VolVis*, includes a rang of rendering algorithms from the fast, rough approximation of the final image, to the comparatively slow, accurate rendering within a global illumination model. Also, every rendering algorithm should support several levels of accuracy, giving the user an even greater amount of control over the speed and accuracy of the final image.

Standard volume rendering techniques typically employ only a local illumination model for shading, and therefore produce images without global effects. Including a global illumination model within a visualization system has several advantages. First, global effects are often desirable in scientific applications. For example, by placing mirrors in the scene, a single image can show several views of an object in a natural, intuitive manner leading to a better understanding of the 3D nature of the scene. Also, complex geometric surfaces are often easier to render when represented volumetrically than when represented by high-order functions or geometric primitives, and global effects using ray tracing or radiosity are desirable for such applications called volume graphics applications (see Section 9). Volumetric ray tracing is described in Section 7.1 and volumetric radiosity is discussed in Section 7.2.

7.1. Volumetric Ray Tracing

A 3D raster ray tracing (RRT) method, developed by Yagel, Cohen and Kaufman [117, 122], produces realistic images of volumetric data using a global illumination model. The RRT algorithm is a discrete ray-tracing algorithm similar to the discrete ray-casting algorithm described in Section 4.2. Discrete primary rays are cast from the image plane, through the data to determine pixel values. Secondary rays are recursively spawned when a ray encounters a voxel belonging to an object in the data. To save time, the view-independent parts of the illumination equation can be precomputed and added to the voxel color, thereby avoiding the calculation of this quantity during the ray tracing. Also, two bits per light source per voxel can be precomputed, indicating whether the light is definitely visible, possibly visible, or definitely invisible from that voxel. Shadow rays need only be cast during the ray tracing if the bits indicate that the light is possibly visible through a translucent object. Actually, all view-independent attributes (including normal, texture, and antialiasing) can be precomputed and stored with each voxel.

There are several advantages to using RRT instead of conventional ray tracing. One such advantage is that sampled or computed data, possibly intermixed with voxelized geometric data, can be ray traced directly without having to approximate the sampled data using geometric primitives. Another advantage is that there is only one primitive to deal with − the voxel, which greatly simplifies ray-object intersection calculations. Unlike conventional ray tracing that computes expensive continuous ray-object intersections, RRT traverses discrete rays through discrete data and therefore it is basically insensitive to scene complexity and object complexity. RRT is also very effective for ray tracing voxelized geometric models, such as constructive solid geometry (CSG) models. This is an example for the emerging field of volume graphics [51] in which geometric scenes are modeled using voxelized objects and efficiently rendered using a volume rendering algorithm such as RRT. Volume graphics is discussed in Section 9.

A volumetric ray tracer [92] is intended to produce much more accurate, informative images. In classical ray tracing, the rendering algorithm is designed to generate images that are accurate according to the laws of optics. A volumetric ray tracer should handle volumetric data as well as classical

geometric objects, and strict adherence to the laws of optics is not always desirable. For example, a user may wish to generate an image with no shadows or to view the maximum value along the segment of a ray passing through a volume, instead of the optically-correct composited value. Figure 4 illustrates the importance of including global effects in a maximum-value projection of a hippocampal pyramidal neuron data set which was obtained using a laser-scanning confocal microscope. Since maximum-value projections do not give depth information, a floor is placed below the cell, and a light source above the cell. This results in a shadow of the cell on the floor, adding back depth information lost by the maximum value projection.

In order to incorporate both volumetric and geometric objects into one scene, the standard ray tracing intensity equation must be expanded. Since the illumination equation in classical ray tracing is evaluated only at surface locations, volumetric data cannot be incorporated into the scene. This problem can be solved by extending the standard illumination equation to include volumetric effects. The intensity of light, $I_\lambda(x, \vec{\omega})$, for a given wavelength λ, arriving at a position x, from the direction $\vec{\omega}$, can be computed by:

$$I_\lambda(x, \vec{\omega}) = I_{v\lambda}(x, x') + \tau_\lambda(x, x') I_{s\lambda}(x', \vec{\omega}). \tag{16}$$

where x' is the first surface intersection point encountered along the ray $\vec{\omega}$ originating at x. $I_{s\lambda}(x', \vec{\omega})$ is the intensity of light at this surface location, and can be computed with a standard ray tracing illumination equation [112]. $I_{v\lambda}(x, x')$ is the volumetric contribution to the intensity along the ray from x to x', and $\tau_\lambda(x, x')$ is the attenuation of $I_{s\lambda}(x', \vec{\omega})$ by any intervening volumes. These values are determined using volume rendering techniques, based on a transport theory model of light propagation [55]. The basic idea is similar to classical ray tracing, in that rays are cast from the eye into the scene, and surface shading is performed on the closest surface intersection point. The difference is that shading must be performed for all volumetric data that are encountered along the ray while traveling to

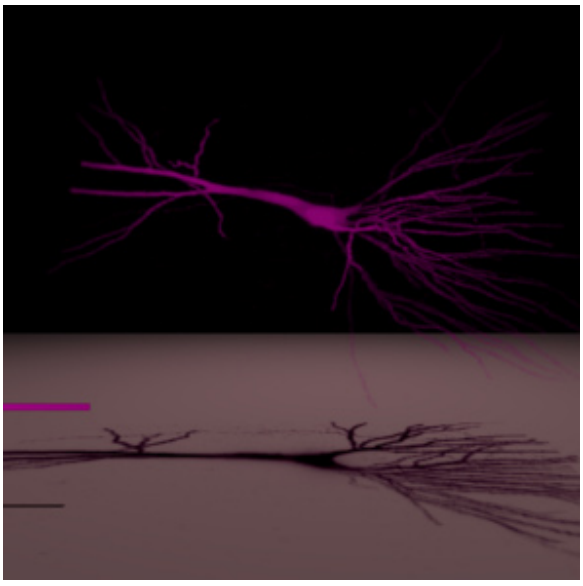

Figure 4: A maximum-value projection of a cell casting a shadow on the floor using the *VolVis* volumetric ray tracer.

the closest surface intersection point.

For photo-realistic rendering, the user typically wants to include the maximum amount of shading effects that can be calculated within a given time limit. For visualization, however, the user may find it necessary to view volumetric data with no shading effects, such as when using a maximum-value projection. For example, in Figure 4 no shading effects were included for the maximum-value projection of the cell, while all parts of the illumination equation were considered when shading the geometric polygon. In another example, the user may place a mirror behind a volumetric object in a scene in order to capture two views in one image, but may not want the volumetric object to cast a shadow on the mirror. This can be accomplished easily by ‘‘turning off’’ the shadowing calculations for the mirror, as shown in Figure 5. The head data was obtained using magnetic resonance imaging, with the brain segmented from the same dataset. The mirror is a voxelized polygon, which was created using the non-binary voxelization technique described in Section 9.4

7.2. Volumetric Radiosity

The ray tracing algorithm described in the previous section can be used to capture specular interactions between objects in a scene. In reality, most scenes are dominated by diffuse interactions, which are not accounted for in the standard ray tracing illumination model, but accounted for by a radiosity algorithm for volumetric data [93]. In volumetric radiosity, the basic ‘‘patch’’ element of classical radiosity is replaced by a ‘‘voxel’’. As opposed to previous methods that use participating media to augment geometric scenes [40, 83], this method moves the radiosity equations into volumetric space, and renders

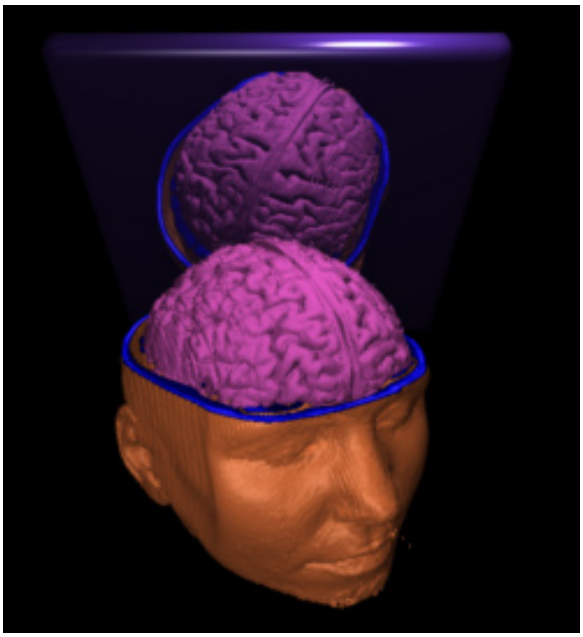

Figure 5: A ray traced image of a human head. Shadowing effects were not included in this image in order to produce a clear reflection in the mirror.

scenes consisting solely of volumetric data. Each voxel can emit, absorb, scatter, reflect, and transmit light. Both isotropic and diffuse emission of light are allowed, where ‘‘isotropic’’ implies directional independence, and ‘‘diffuse’’ implies Lambertian reflection (i.e., dependent on normal or gradient). Light is scattered isotropically, and is reflected diffusely by a voxel. Light entering a voxel that is not absorbed, scattered, or reflected by the voxel is transmitted unchanged.

In order to cope with the high number of voxel interactions required, a hierarchical technique similar to [32] can be used. The basic hierarchical concept is that the radiosity contribution from some voxel v_i to another voxel v_j is similar to the radiosity contribution from v_i to v_k if the distance between v_j and v_k is small, and the distance between v_i and v_j is large. For each volume, a hierarchical radiosity structure is built by combining each subvolume of eight voxels at one level to form one voxel at the next higher level. An iterative algorithm [9] is then used to shoot voxel radiosities, where several factors govern the highest level in the hierarchy at which two voxels can interact. These factors include the distance between the two voxels, the radiosity of the shooting voxel, and the reflectance and scattering coefficients of the voxel receiving the radiosity. This hierarchical technique can reduce the number of interactions required to converge on a solution by more than four orders of magnitude.

After the view-independent radiosities have been calculated, a view-dependent image is generated using a ray casting technique, where the final pixel value is determined by compositing radiosity values along the ray. Figure 6 shows a scene containing a volumetric sphere, polygon, and light source. The light source is isotropically emitting light, and both the sphere and the polygon are diffusely reflecting light. The light source is above the sphere, and therefore the top half of the sphere is directly illuminated. The bottom half of the sphere is indirectly illuminated by light diffusely reflected from the red polygon.

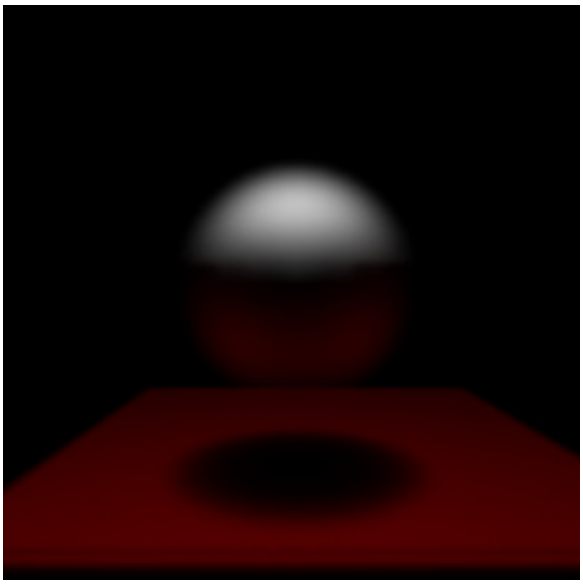

Figure 6: A volumetric radiosity projection of a voxelized sphere and polygon.

8. Irregular Grid Rendering

All the algorithms discussed above handle only regular gridded data. Irregular gridded data comes in a large variety [94], including curvilinear data or unstructured (scattered) data, where no explicit connectivity is defined between cells (one can even be given a scattered collection of points that can be turned into an irregular grid by interpolation [66, 72]). For rendering purposes, manifold (locally homeomorphic to R^3) grids composed of convex cells are usually necessary. In general, the most convenient grids for rendering purposes are tetrahedral grids and hexahedral grids. One disadvantage of hexahedral grids is that the four points on the side of a cell may not necessarily lie on a plane forcing the rendering algorithm to approximate the cells by convex ones during rendering. Tetrahedral grids have several advantages, including easier interpolation, simple representation (specially for connectivity information because the degree of the connectivity graph is bounded, allowing for compact data structure representation), and the fact that any other grid can be interpolated to a tetrahedral one (with the possible introduction of Steiner points). Among their disadvantages is the fact that the size of the datasets tend to grow as cells are decomposed into tetrahedra. In the case of curvilinear grids, an accurate (and naive) decomposition will make the cell complex contain five times as many cells.

As compared to regular grids, operations for irregular grids are more complicated and the effective visualization methods are more sophisticated in all fronts. Shading, interpolation, point location, etc., are all harder (and some even not well defined) for irregular grids. One notable exception is isosurface generation [63], that even in the case of irregular grids is fairly simple to compute given suitable interpolation functions. Slicing operations are also simple [94].

Volume rendering irregular grids is a hard operation and there are several different approaches to this problem. The simplest and most inefficient is to resample the irregular grid to a regular grid. In order to achieve the necessary accuracy, a high enough sampling rate has to be used what in most cases will make the resulting regular grid volume too large for storage and rendering purposes, not mentioning the time to perform the re-sampling.

Extending the simple volumetric point sampling ray tracing to irregular grids is a challenge. For ray tracing, it is necessary to depth-sort samples along ray emanating from each screen pixel. In the case of irregular grids, it is not trivial to perform this sorting operation. Garrity [24] proposed a scheme where the cells are convex and connectivity information is available. He proposed to pre-process the grid finding the external cells to help locating the boundary elements during ray tracing, and using the connectivity information for cell skipping. The actual resampling and shading, that is simple in the regular grid, is not trivial here and has to be carefully considered, usually taking into account the specific application at hand (actually the development of accurate illumination models for volume rendering has irregular grid rendering as one of its main uses [67]). Simple ray casting is too inefficient, as there is a large amount of inter-pixel and inter-scanline coherency in ray casting. Giertsen [25] proposed a sweep-plane approach to ray casting that uses different forms of "caching" to speed up ray casting irregular grids.

Another approach for rendering irregular grids is the use of feed-forward (or projection) methods, where the cells are projected onto the screen one by one accumulating their contributions incrementally to the final image [66, 89, 113, 114]. One major advantage of these methods is the ability to use the graphics hardware on graphics workstations to compute the volumetric lighting models (usually simplified) in order to speed up rendering. Another advantage is that the user can see the rendering as it progresses. One problem with this method is generating the ordering for the cell projections. In general, such ordering does not even exist and cells have to be partitioned into multiple cells for projection. The

partitioning is (in general) view dependent, but some types of irregular grids (like delaunay triangulations in space) are acyclic and do not need any partitioning.

9. Volume Graphics

The 3D raster representation seems to be more natural for empirical imagery then for geometric objects, due to its ability to represent interiors and digital samples. Nonetheless, the advantages of this representation are also attracting traditional surface-based applications that deal with the modeling and rendering of synthetic scenes made out of geometric models. The geometric model is *voxelized (3D scan-converted)* into a set of voxels that ''best'' approximate the model. Each of these voxels is then stored in the volume buffer together with the voxel pre-computed view-independent attributes. The voxelized model can be either binary (see [10, 43-45]) or volume sampled [106] which generates alias-free density voxelization of the model. Some surface-based application examples are the rendering of fractals [75], hyper textures [77], fur [42], gases [20], and other complex models [90] including CAD models and terrain models for flight simulators [11, 51, 115]. Furthermore, in many applications involving sampled data, such as medial imaging, the data need to be visualized along with synthetic objects that may not be available in digital form, such as scalpels, prosthetic devices, injection needles, radiation beams, and isodose surfaces. These geometric objects can be voxelized and intermixed with the sampled organ in the voxel buffer [48].

Volume graphics [51], which is an emerging subfield of computer graphics, is concerned with the synthesis, modeling, manipulation, and rendering of volumetric geometric objects, stored in a volume buffer of voxels. Unlike volume visualization which focuses primarily on sampled and computed datasets, volume graphics is concerned primarily with modeled geometric scenes and commonly with those that are represented in a regular volume buffer. As an approach, volume graphics has the potential to greatly advance the field of 3D graphics by offering a comprehensive alternative to traditional surface graphics.

In the next sub-sections we describe the volumetric approach to several common volume graphics modeling techniques. We describe the generation of object primitives (voxelization), 3D antialiasing, texture and photo mapping, solid-texturing, modeling of amorphous phenomena, modeling by block operations, constructive solid modeling, and volume sculpting. Then, volume graphics is contrasted with surface graphics, and the corresponding advantages are discussed.

9.1. Voxelization

An indispensable stage in volume graphics is the synthesis of voxel-represented objects from their geometric representation. This stage, which is called *voxelization*, is concerned with converting geometric objects from their continuous geometric representation into a set of voxels that ''best'' approximates the continuous object. As this process mimics the scan-conversion process that pixelizes (rasterizes) 2D geometric objects, it is also referred to as *3D scan-conversion*. In 2D rasterization the pixels are directly drawn onto the screen to be visualized and filtering is applied to reduce the aliasing artifacts. However, the voxelization process does not render the voxels but merely generates a database of the discrete digitization of the continuous object.

Intuitively, one would assume that a proper voxelization simply ''selects'' all voxels which are met (if

only partially) by the object body. Although this approach could be satisfactory in some cases, the objects it generates are commonly too coarse and include more voxels than are necessary. For example, when a 2D curve is rasterized into a connected sequence of pixels, the discrete curve does not ''cover'' the entire continuous curve, but it is connected and concisely and successfully ''separates'' both ''sides'' of the curve [12].

One practical meaning of separation is apparent when a voxelized scene is rendered by casting discrete rays from the image plane to the scene. The penetration of the background voxels (which simulate the discrete ray traversal) through the voxelized surface causes the appearance of a hole in the final image of the rendered surface. Another type of error might occur when a 3D flooding algorithm is employed either to fill an object or to measure its volume, surface area, or other properties. In this case the nonseparability of the surface causes a leakage of the flood through the discrete surface.

Unfortunately, the extension of the 2D definition of separation to the third dimension and to voxel surfaces is not straightforward since voxelized surfaces cannot be defined as an ordered sequence of voxels and a voxel on the surface does not have a specific number of adjacent surface voxels. Furthermore, there are important topological issues, such as the separation of both sides of a surface, which cannot be well-defined by employing 2D terminology. The theory that deals with these topological issues is called *3D discrete topology*. We sketch below some basic notions and informal definitions used in this field.

9.2. Fundamentals of 3D Discrete Topology

The 3D discrete space is a set of integral grid points in 3D Euclidean space defined by their Cartesian coordinates (x, y, z). A voxel is the unit cubic volume centered at the integral grid point. The voxel value is mapped onto {0,1}: the voxels assigned ''1'' are called the ''black'' voxels representing opaque objects, and those assigned ''0'' are the ''white'' voxels representing the transparent background. In Section 9.4 we describe non-binary approaches where the voxel value is mapped onto the interval [0,1] representing either partial coverage, variable densities, or graded opacities. Due to its larger dynamic range of values, this approach supports 3D antialiasing and thus supports higher quality rendering.

Two voxels are *26-adjacent* if they share either a vertex, an edge, or a face (see Figure 1). Every voxel has 26 such adjacent voxels: eight share a vertex (corner) with the center voxel, twelve share an edge, and six share a face. Accordingly, face-sharing voxels are defined as *6-adjacent*, and edge-sharing and face-sharing voxels are defined as *18-adjacent*. The prefix N is used to define the adjacency relation, where $N = 6, 18,$ or 26. A sequence of voxels having the same value (e.g., ''black'') is called an *N-path* if all consecutive pairs are N-adjacent. A set of voxels W is *N-connected* if there is an N-path between every pair of voxels in W. An *N-connected component* is a maximal N-connected set.

Given a 2D discrete 8-connected black curve, there are sequences of 8-connected white pixels (8-component) that pass from one side of the black component to its other side without intersecting it. This phenomenon is a discrete disagreement with the continuous case where there is no way of penetrating a closed curve without intersecting it. To avoid such a scenario, it has been the convention to define ''opposite'' types of connectivity for the white and black sets. ''Opposite'' types in 2D space are 4 and 8, while in 3D space 6 is ''opposite'' to 26 or to 18.

Assume that a voxel space, denoted by Σ, includes one subset of ''black'' voxels S. If $\Sigma - S$ is not N-connected, that is, $\Sigma - S$ consists of at least two white N-connected components, then S is said to be N-

separating in Σ. Loosely speaking, in 2D, an 8-connected black path that divides the white pixels into two groups is 4-separating and a 4-connected black path that divides the white pixels into two groups is 8-separating. There are no analogous results in 3D space.

Let W be an N-separating surface. A voxel $p \in W$ is said to be an *N-simple voxel* if $W - p$ is still N-separating. An N-separating surface is called *N-minimal* if it does not contain any N-simple voxel. A *cover* of a continuous surface is a set of voxels such that every point of the continuous surface lies in a voxel of the cover. A cover is said to be a *minimal cover* if none of its subsets is also a cover. The cover property is essential in applications that employ space subdivision for fast ray tracing [26]. The subspaces (voxels) which contain objects have to be identified along the traced ray. Note that a cover is not necessarily separating, while on the other hand, as mentioned above, it may include simple voxels. In fact, even a minimal cover is not necessarily N-minimal for any N [12].

9.3. Binary Voxelization

An early technique for the digitization of solids was spatial enumeration which employs point or cell classification methods in either an exhaustive fashion or by recursive subdivision [59]. However, subdivision techniques for model decomposition into rectangular subspaces are computationally expensive and thus inappropriate for medium or high resolution grids. Instead, objects should be directly voxelized, preferably generating an N-separating, N-minimal, and covering set, where N is application dependent. The voxelization algorithms should follow the same paradigm as the 2D scan-conversion algorithms; they should be incremental, accurate, use simple arithmetic (preferably integer only), and have a complexity that is not more than linear with the number of voxels generated.

The literature of 3D scan-conversion is relatively small. Danielsson [14] and Mokrzycki [69] developed independently similar 3D curve algorithms where the curve is defined by the intersection of two implicit surfaces. Voxelization algorithms have been developed for 3D lines, 3D circles, and a variety of surfaces and solids, including polygons, polyhedra, and quadric objects [43]. Efficient algorithms have been developed for voxelizing polygons using an integer-based decision mechanism embedded within a scan-line filling algorithm [44], for parametric curves, surfaces, and volumes using an integer-based forward differencing technique [45], and for quadric objects such as cylinders, spheres, and cones using ‘‘weaving’’ algorithms by which a discrete circle/line sweeps along a discrete circle/line [10]. Figure 7 consists of a variety of objects (polygons, boxes, cylinders) voxelized using these methods. These pioneering attempts should now be followed by enhanced voxelization algorithms that, in addition to being efficient and accurate, will also adhere to the topological requirements of separation, coverage, and minimality.

9.4. 3D Antialiasing

The previous sub-section discussed binary voxelization, which generate topologically and geometrically consistent models, but exhibit object space aliasing. These algorithms have used a straightforward method of sampling in space, called *point sampling*. In point sampling, the continuous object is evaluated at the voxel center, and the value of 0 or 1 is assigned to the voxel. Because of this binary classification of the voxels, the resolution of the 3D raster ultimately determines the precision of the discrete model. Imprecise modeling results in jagged surfaces, known as *object space aliasing* (see Figure 7). In this section, a 3D object-space antialiasing technique is presented. It performs antialiasing once, on a 3D view-independent representation, as part of the modeling stage. Unlike antialiasing of 2D

Figure 7: A volumetric model of terrain enhanced with photo mapping of satellite images. The buildings are synthetic voxel models raised on top of the terrain. The voxelized terrain has been mapped with aerial photos during the voxelization stage.

scan-converted graphics, where the main focus is on generating aesthetically pleasing displays, the emphasis in antialiased 3D voxelization is on producing alias-free 3D models that are stored in the view-independent volume buffer for various volume graphics manipulations, including but not limited to the generation of aesthetically pleasing displays.

To reduce object space aliasing, a *volume sampling* technique have been developed [106], which estimates the density contribution of the geometric objects to the voxels. The density of a voxel is attenuated by a filter weight function which is proportional to the distance between the center of the voxel and the geometric primitive. To improve performance, precomputed lookup tables of densities for a predefined set of geometric primitives can be used to select the density value of each voxel. For each voxel visited by the binary voxelization algorithm, the distance to the predefined primitive is used as an index into a lookup table of densities.

Since the voxelized geometric objects are represented as volume rasters of density values, they can essentially be treated as sampled or simulated volume datasets, such as 3D medical imaging datasets, and one of many volume rendering techniques for image generation can be employed. One primary advantage of this approach is that volume rendering or volumetric global illumination carries the smoothness of the volume-sampled objects from object space over into its 2D projection in image space [107]. Hence, the silhouette of the objects, reflections, and shadows are smooth. Furthermore, by not performing any geometric ray-object intersections or geometric surface normal calculations, the bulk of the rendering time is saved. In addition, CSG operations between two volume-sampled geometric models are accomplished at the voxel level after voxelization, thereby reducing the original problem of evaluating a CSG tree of such operations down to a fuzzy Boolean operation between pairs of non-binary voxels [108] (see Section 9.7). Volume-sampled models are also suitable for intermixing with sampled or simulated datasets, since they can be treated uniformly as one common data representation. Furthermore, volume-sampled models lend themselves to alias-free multi-resolution hierarchy

construction [108].

9.5. Texture Mapping

One type of object complexity involves objects that are enhanced with texture mapping, photo mapping, environment mapping, or solid texturing. Texture mapping is commonly implemented during the last stage of the rendering pipeline, and its complexity is proportional to the object complexity. In volume graphics, however, texture mapping is performed during the voxelization stage, and the texture color is stored in each voxel in the volume buffer.

In photo mapping six orthogonal photographs of the real object are projected back onto the voxelized object. Once this mapping is applied, it is stored with the voxels themselves during the voxelization stage, and therefore does not degrade the rendering performance. Texture and photo mapping are also viewpoint independent attributes implying that once the texture is stored as part of the voxel value, texture mapping need not be repeated. This important feature is exploited, for example, by voxel-based flight simulators (see Figure 7) and in CAD systems (see Figure 8).

A central feature of volumetric representation is that, unlike surface representation, it is capable of representing inner structures of objects, which can be revealed and explored with appropriate manipulation and rendering techniques. This capability is essential for the exploration of sampled or computed objects. Synthetic objects are also likely to be solid rather than hollow. One method for modeling various solid types is solid texturing, in which a function or a 3D map models the color of the objects in 3D (see Figure 8). During the voxelization phase each voxel belonging to the objects is assigned a value by the texturing function or the 3D map. This value is then stored as part of the voxel information. Again, since this value is view independent, it does not have to be recomputed for every change in the rendering parameters.

9.6. Amorphous Phenomena

While translucent objects can be represented by surface methods, these methods cannot efficiently support the modeling and rendering of amorphous phenomena (e.g., clouds, fire, smoke) that are volumetric in nature and lack any tangible surfaces. A common modeling and rendering approach is based on a function that, for any input point in 3D, calculates some object features such as density, reflectivity, or color. These functions can then be rendered by ray casting, which casts a ray from each pixel into the function domain. Along the passage of the ray, at constant intervals the function is evaluated to yield a sample. All samples along each ray are combined to form the pixel color. Some examples for the use of this or similar techniques are the rendering of fractals [33], hypertextures [77], fur [42], and gases [20].

The process of function evaluation at each sample point in 3D has to be repeated for each image generated. In contrast, the volumetric approach allows the pre-computation of these functions at each grid point of the volume buffer. The resulting volumetric dataset can then be rendered from multiple viewpoints without recomputing the modeling function. As in other volume graphics techniques, accuracy is traded for speed, due to the resolution limit. Instead of accurately computing the function at each sample point, some type of interpolation from the precomputed grid values is employed.

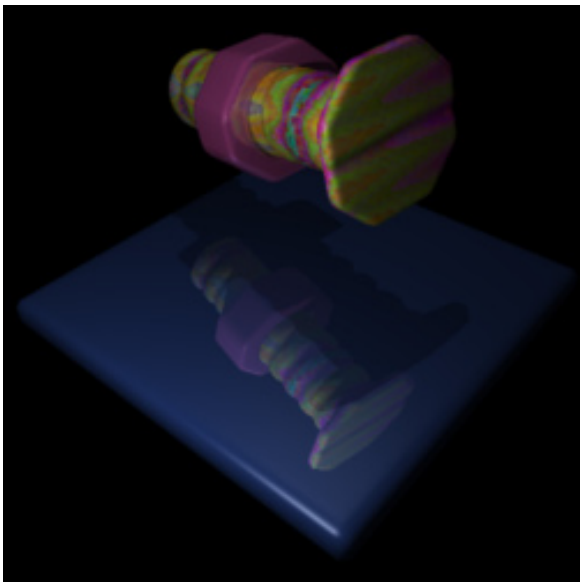

Figure 8: Volume-sampled bolt and nut generated by a sequence of CSG operations on hexagonal, cylindrical, and helix primitives, reflected on a volume-sampled mirror.

9.7. Block Operations and Constructive Solid Modeling

The presortedness of the volume buffer naturally lends itself to grouping operations that can be exploited in various ways. For example, by generating multi-resolution volume hierarchy that can support time critical and space critical volume graphics applications can be better supported. The basic idea is similar to that of level-of-detail surface rendering which has proliferated recently [21, 39, 82, 87, 100], in which the perceptual importance of a given object in the scene determines its appropriate level-of-detail representation. One simple approach is the 3D "mip-map" approach [61, 85], where every level of the hierarchy is formed by averaging several voxels from the previous level. A better approach is based on sampling theory, in which an object is modeled with a sequence of alias-free volume buffers at different resolutions using the volume-sampled voxelization approach [34]. To accomplish this, high frequencies that exceed the Nyquist frequency of the corresponding volume buffer are filtered out by applying an ideal low-pass filter (*sinc*) with infinite support. In practice, the ideal filter is approximated by filters with finite support. Low sampling resolution of the volume buffer corresponds to a lower Nyquist frequency, and therefore requires a low-pass filter with wider support for good approximation. As one moves up the hierarchy, low-pass filters with wider and wider support are applied. Compared to the level-of-detail hierarchy in surface graphics, the multi-resolution volume buffers are easy to generate and to spatially correspond neighboring levels, and are free of object space aliasing. Furthermore, arbitrary resolutions can be generated, and errors caused by a non-ideal filter do not propagate and accumulate from level to level. Depending on the required speed and accuracy, a variety of low-pass filters (zero order, cubic, Gaussian) can be applied.

An intrinsic characteristic of the volume buffer is that adjacent objects in the scene are also represented by neighboring memory cells. Therefore, rasters lend themselves to various meaningful grouping-based operations, such as *bitblt* in 2D, or *voxblt* in 3D [50]. These include transfer of volume buffer rectangular blocks (cuboids) while supporting voxel-by-voxel operations between source and

destination blocks. Block operations add a variety of modeling capabilities which aid in the task of image synthesis and form the basis for the efficient implementation of a 3D ‘‘room manager’’, which is the extension of window management to the third dimension.

Since the volume buffer lends itself to Boolean operations that can be performed on a voxel-by-voxel basis during the voxelization stage, it is advantageous to use CSG as the modeling paradigm. Subtraction, union, and intersection operations between two voxelized objects are accomplished at the voxel level, thereby reducing the original problem of evaluating a CSG tree during rendering time down to a 1D Boolean operation between pairs of voxels during a preprocessing stage.

For two point-sampled binary objects the Boolean operations of CSG or *voxblt* are trivially defined. However, the Boolean operations applied to volume-sampled models are analogous to those of fuzzy set theory (cf. [17]). The volume-sampled model is a density function $d(x)$ over R^3, where d is 1 inside the object, 0 outside the object, and $0 < d < 1$ within the "soft" region of the filtered surface. Some of the common operations, intersection, complement, difference, and union, between two objects A and B are defined as follows:

$$d_{A \bigcap B}(x) \equiv \min (d_A(x), d_B(x)) \tag{17}$$

$$d_{\bar{A}}(x) \equiv 1 - d_A(x) \tag{18}$$

$$d_{A-B}(x) \equiv \min (d_A(x), 1 - d_B(x)) \tag{19}$$

$$d_{A \bigcup B}(x) \equiv \max (d_A(x), d_B(x)) \tag{20}$$

The only law of set theory that is no longer true is the excluded-middle law (i.e., $A \bigcap \bar{A} \neq \phi$ and $A \bigcup \bar{A} \neq Universe$). The use of the min and max functions causes discontinuity at the region where the soft regions of the two objects meet, since the density value at each location in the region is determined solely by one of the two overlapping objects.

Complex geometric models can be generated by performing the CSG operations in Equations 17-20 between volume-sampled primitives. Volume-sampled models can also function as matte volumes [16] for various matting operations, such as performing cut-aways and merging multiple volumes into a single volume using the union operation. However, in order to preserve continuity on the cut-away boundaries between the material and the empty space, one should use an alternative set of Boolean operators based on algebraic sum and algebraic product [17, 28] :

$$d_{A \bigcap B}(x) \equiv d_A(x)\ d_B(x) \tag{21}$$

$$d_{\bar{A}}(x) \equiv 1 - d_A(x) \tag{22}$$

$$d_{A-B}(x) \equiv d_A(x) - d_A(x)\ d_B(x) \tag{23}$$

$$d_{A \bigcup B}(x) \equiv d_A(x) + d_B(x) - d_A(x)\ d_B(x) \tag{24}$$

Unlike the min and max operators, algebraic sum and product operators result in $A \bigcup A \neq A$, which is undesirable. A consequence, for example, is that during modeling via sweeping, the resulting model is sensitive to the sampling rate of the swept path [108].

Once a CSG model has been constructed in voxel representation, it is rendered in the same way any other volume buffer is. This makes, for example, volumetric ray tracing of constructive solid models straightforward [92] (see Figure 8).

9.8. Volume Sculpting

Surface-based sculpting has been studied extensively (e.g., [13, 88]), while volume sculpting has been recently introduced for clay or wax-like sculptures [23] and for comprehensive detailed sculpting [109]. The latter approach is a free-form interactive modeling technique based on the metaphor of sculpting and painting a voxel-based solid material, such as a block of marble or wood. There are two motivations for this approach. First, modeling topologically complex and highly-detailed objects are still difficult in most CAD systems. Second, sculpting has shown to be useful in volumetric applications. For example, scientists and physicians often need to explore the inner structures of their simulated or sampled datasets by gradually removing material.

Real-time human interaction could be achieved in this approach, since the actions of sculpting (e.g., carving, sawing) and painting are localized in the volume buffer, a localized rendering can be employed to reproject only those pixels that are affected. Carving is the process of taking a pre-existing volume-sampled tool to chip or chisel the object bit by bit. Since both the object and the tool are represented as independent volume buffers, the process of sculpting involves positioning the tool with respect to the object and performing a Boolean subtraction between the two volumes. Sawing is the process of removing a whole chunk of material at once, much like a carpenter sawing off a portion of a wood piece. Unlike carving, sawing requires generating the volume-sampled tool on-the-fly, using a user interface. To prevent object space aliasing and to achieve interactive speed, 3D splatting is employed.

9.9. Surface Graphics vs. Volume Graphics

Contemporary 3D graphics has been employing an object-based approach at the expense of maintaining and manipulating a display list of geometric objects and regenerating the frame-buffer after every change in the scene or viewing parameters. This approach, termed *surface graphics*, is supported by powerful geometry engines, which have flourished in the past decade, making surface graphics the state-of-the-art in 3D graphics.

Surface graphics strikingly resembles vector graphics that prevailed in the sixties and seventies, and employed vector drawing devices. Like vector graphics, surface graphics represents the scene as a set of geometric primitives kept in a display list. In surface graphics, these primitives are transformed, mapped to screen coordinates, and converted by scan-conversion algorithms into a discrete set of pixels. Any change to the scene, viewing parameters, or shading parameters requires the image generation system to repeat this process. Like vector graphics that did not support painting the interior of 2D objects, surface graphics generates merely the surfaces of 3D objects and does not support the rendering of their interior.

Instead of a list of geometric objects maintained by surface graphics, volume graphics employs a 3D volume buffer as a medium for the representation and manipulation of 3D scenes. A 3D scene is discretized earlier in the image generation sequence, and the resulting 3D discrete form is used as a database of the scene for manipulation and rendering purposes, which in effect decouples discretization from rendering. Furthermore, all objects are converted into one uniform meta-object − the voxel. Each voxel is atomic and represents the information about at most one object that resides in that voxel.

Volume graphics offers similar benefits to surface graphics, with several advantages that are due to the decoupling, uniformity, and atomicity features. The rendering phase is viewpoint independent and insensitive to scene complexity and object complexity. It supports Boolean and block operations and

constructive solid modeling. When 3D sampled or simulated data are used, such as that generated by medical scanners (e.g., CT, MRI) or scientific simulations (e.g., CFD), volume graphic is suitable for their representation too. It is capable of representing amorphous phenomena and both the interior and exterior of 3D objects. These features of volume graphics as compared with surface graphics are discussed in detail in Section 9.10. Several weaknesses of volume graphics are related to the discrete nature of the representation, for instance, transformations and shading are performed in discrete space. In addition, this approach requires substantial amounts of storage space and specialized processing. These weaknesses are discussed in detail in Section 9.11.

Table 1 contrasts vector graphics with raster graphics. A primary appeal of raster graphics is that it decouples image generation from screen refresh, thus making the refresh task insensitive to the scene and object complexities. In addition, the raster representation lends itself to block operations, such as *bitblt* and quadttree. Raster graphics is also suitable for displaying 2D sampled digital images, and thus provides the ideal environment for mixing digital images with synthetic graphic. Unlike vector graphics, raster graphics provides the capability to present shaded and textured surfaces, as well as line drawings. These advantages, coupled with advances in hardware and the development of antialiasing methods, have led raster graphics to supersede vector graphics as the primary technology for computer graphics. The main weaknesses of raster graphics are the large memory and processing power it requires for the frame buffer, and the discrete nature of the image. These difficulties delayed the full acceptance of raster graphics until the late seventies when the technology was able to provide cheaper and faster memory and hardware to support the demands of the raster approach. In addition, the discrete nature of rasters makes them less suitable for geometric operations such as transformations and accurate measurements, and once discretized the notion of objects is lost.

The same appeal that drove the evolution of the computer graphics world from vector graphics to raster graphics, once the memory and processing power became available, is driving a variety of applications from a surface-based approach to a volume-based approach. Naturally, this trend first appeared in

Table 1: Comparison between vector graphics and raster graphics and between surface graphics and volume graphics.

2D	Vector Graphics	Raster Graphics
Scene/object complexity	−	+
Block operations	−	+
Sampled data	−	+
Interior	−	+
Memory and processing	+	−
Aliasing	+	−
Transformations	+	−
Objects	+	−
3D	Surface Graphics	Volume Graphics

applications involving sampled or computed 3D data, such as 3D medical imaging and scientific visualization, in which the datasets are in volumetric form. This diverse empirical applications of volume visualization still provide a major driving force for advances in volume graphics.

The comparison in Table 1 between vector graphics and raster graphics strikingly resembles a comparison between surface graphics and volume graphics. Actually Table 1 itself is used also to contrast surface graphics and volume graphics. Section 9.10 discusses the features of volume graphics while Section 9.11 discusses the weaknesses of volume graphics relative to surface graphics.

9.10. Volume Graphics Features

One of the most appealing attributes of volume graphics is its insensitivity to the complexity of the scene, since all objects have been pre-converted into a finite size volume buffer. Although the performance of the pre-processing voxelization phase is influenced by the scene complexity [10, 43-45], rendering performance depends mainly on the constant resolution of the volume buffer and not on the number of objects in the scene. Insensitivity to the scene complexity makes the volumetric approach especially attractive for scenes consisting of a large number of objects.

In volume graphics, rendering is decoupled from voxelization and all objects are first converted into one meta object, the voxel, which makes the rendering process insensitive to the complexity of the objects. Thus, volume graphics is particularly attractive for objects that are hard to render using conventional graphics systems. Examples of such objects include curved surfaces of high order and fractals which require the expensive computation of an iterative function for each volume unit [75]. Constructive solid models are also hard to render by conventional methods, but are straightforward to render in volumetric representation (see below).

Anti-aliasing and texture mapping are commonly implemented during the last stage of the conventional rendering pipeline, and their complexity is proportional to object complexity. Solid texturing, which employs a 3D texture image, has also a high complexity proportional to object complexity. In volume graphics, however, anti-aliasing, texture mapping, and solid texturing are performed only once, during the voxelization stage, where the color is calculated and stored in each voxel. The texture can also be stored as a separate volumetric entity which is rendered together with the volumetric object, as in the *VolVis* software system for volume visualization [1].

The textured objects in Figures 7 and 8 have been assigned texture during the voxelization stage by mapping each voxel back to the corresponding value on a texture map or solid. Once this mapping is applied, it is stored with the voxels themselves during the voxelization stage, which does not degrade the rendering performance. In addition, texture mapping and photo mapping are also viewpoint independent attributes, implying that once the texture is stored as part of the voxel value, texture mapping need not be repeated.

In anticipation of repeated access to the volume buffer (such as in animation), all viewpoint independent attributes can be precomputed during the voxelization stage, stored with the voxel, and be readily accessible for speeding up the rendering. The voxelization algorithm can generate for each object voxel its color, its texture color, its normal vector (for visible voxels), antialiasing information [106], and information concerning the visibility of the light sources from that voxel. Actually, the viewpoint independent parts of the illumination equation, can also be precomputed and stored as part of the voxel value.

Once a volume buffer with precomputed view-independent attributes is available, a rendering algorithm such as a discrete ray tracing or a volumetric ray tracing algorithm can be engaged. Either ray tracing approach is especially attractive for complex surface scenes and constructive solid models, as well as 3D sampled or computed datasets (see below). Figures 4, 5 and 8 show examples of objects that were ray traced in discrete voxel space. In spite of the complexity of these scenes, volumetric ray tracing time was approximately the same as for much simpler scenes and significantly faster than traditional space-subdivision ray tracing methods. Moreover, in spite of the discrete nature of the volume buffer representation, images indistinguishable from the ones produced by conventional surface-based ray tracing can be generated by employing, accurate ray tracing, auxiliary object information, or screen supersampling techniques.

Sampled datasets, such as in 3D medical imaging (see Figures 5 and 9), volume microscopy (see Figures 2 and 4), and geology, and simulated datasets, such as in computational fluid dynamics, chemistry, and materials simulation are often reconstructed from the acquired sampled or simulated points into a regular grid of voxels and stored in a volume buffer. Such datasets provide for the majority of applications using the volumetric approach. Unlike surface graphics, volume graphics naturally and directly supports the representation, manipulation, and rendering of such datasets, as well as provides the volume buffer medium for intermixing sampled or simulated datasets with geometric objects [48], as can be seen in Figures 4-6 and 8-9. For compatibility between the sampled/computed data and the voxelized geometric object, the object can be volume sampled [106] with the same, but not necessarily the same, density frequency as the acquired or simulated datasets. In volume sampling the continuous object is filtered during the voxelization stage generating alias-free 3D density primitives. Volume graphics also naturally supports the rendering of translucent volumetric datasets (see Figure 9).

A central feature of volumetric representation is that, unlike surface representation, it is capable of representing inner structures of objects, which can be revealed and explored with the appropriate

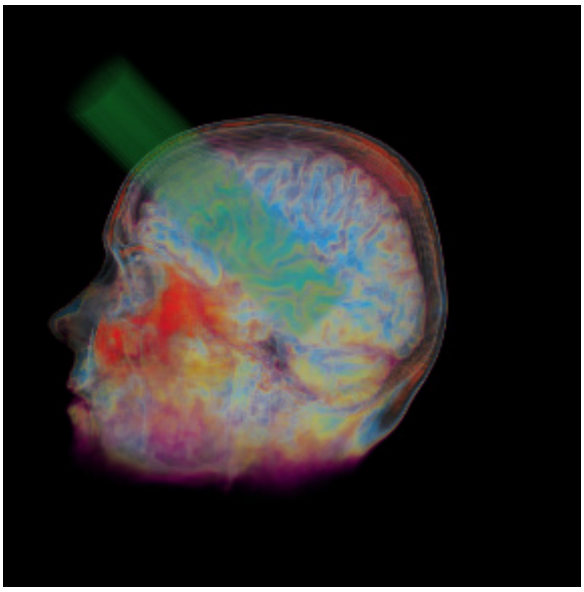

Figure 9: Intermixing of a volume-sampled cylinder with an MRI head using a union operation.

volumetric manipulation and rendering techniques. Natural objects as well as synthetic objects are likely to be solid rather than hollow. The inner structure is easily explored using volume graphics and cannot be supported by surface graphics (see Figures 2(b), 2(c), 3-6 and 9). Moreover, while translucent objects can be represented by surface methods, these methods cannot efficiently support the translucent rendering of volumetric objects, or the modeling and rendering of amorphous phenomena (e.g., clouds, fire, smoke) that are volumetric in nature and do not contain any tangible surfaces [20, 42, 77].

An intrinsic characteristic of rasters is that adjacent objects in the scene are also represented by neighboring voxels. Therefore, rasters lend themselves to various meaningful block-based operations which can be performed during the voxelization stage. For example, the 3D counterpart of the *bitblt* operations, termed *voxblt* (voxel block-transfer), can support transfer of cuboidal voxel blocks with a variety of voxel-by-voxel operations between source and destination blocks [50]. This property is very useful for *voxblt* and CSG. Once a CSG model has been constructed in voxel representation, it is rendered like any other volume buffer. This makes rendering of constructive solid models straightforward.

The spatial presortedness of the volume buffer voxels lends itself to other types of grouping or aggregation of neighboring voxels. For example, the terrain image shown in Figure 7 was generated by the voxel-based Hughes Aircraft Co. flight simulator [115]. It simulates a flight over voxel-represented terrain enhanced with satellite or aerial photo mapping with additional synthetic raised objects, such as buildings, trees, vehicles, aircraft, clouds and the like. Since the information below the terrain surface is invisible, terrain voxels can be actually represented as tall cuboids extending from sea level to the terrain height. The raised and moving objects, however, have to be represented in a more conventional voxel-based form.

Similarly, voxels can be aggregated into super-voxels in a pyramid-like hierarchy. For example, in a voxel-based flight simulator, the best resolution can be used for takeoff and landing. As the aircraft ascends, fewer and fewer details need to be processed and visualized, and a lower resolution suffices. Furthermore, even in the same view, parts of the terrain close to the observer are rendered at high resolution which deceases towards the horizon. A hierarchical volume buffer can be prepared in advance or on-the-fly by subsampling or averaging the appropriate size neighborhoods of voxels (see also [34]).

9.11. Weaknesses of Volume Graphics

A typical volume buffer occupies a large amount of memory. For example, for a medium resolution of 512^3, two bytes per voxel, the volume buffer consists of 256M bytes. However, since computer memories are significantly decreasing in price and increasing in their compactness and speed, such large memories are becoming common place. This argument echoes a similar discussion when raster graphics emerged as a technology in the mid-seventies. With the rapid progress in memory price and compactness, it is safe to predict that, as in the case of raster graphics, the memory will soon cease to be a stumbling block for volume graphics.

The extremely large throughput that has to be handled requires a special architecture and processing attention (see [49] Chapter 6). *Volume engines*, analogous to the currently available geometry (polygon) engines, are emerging. Because of the presortedness of the volume buffer and the fact that only a simple single type of object has to be handled, volume engines are conceptually simpler to implement than current geometry engines (see Section 6). We predict that, consequently, volume engines will materialize in the near future, with capabilities to synthesize, load, store, manipulate, and render

volumetric scenes in real time (e.g., 30 frames/sec), configured possibly as accelerators or co-systems to existing geometry engines.

Unlike surface graphics, in volume graphics the 3D scene is represented in discrete form. This is the cause of many of the problems of voxel-based graphics, which are similar to those of 2D rasters [19]. The finite resolution of the raster poses a limit on the accuracy of some operations, such as volume and area measurements, that are based on voxel counting.

Since the discrete data is sampled during rendering, a low resolution volume yields high aliasing artifacts. This becomes especially apparent when zooming in on the 3D raster. When naive rendering algorithms are used, holes may appear "between" voxels. Nevertheless, this can be alleviated in ways similar to those adopted by 2D raster graphics, such as employing either reconstruction techniques, a higher-resolution volume buffer, or volume sampling.

Manipulation and transformation of the discrete volume are difficult to achieve without degrading the image quality or losing some information. Rotation of rasters by angles other than 90 degrees is especially problematic since a sequence of consecutive rotations will distort the image. Again, these can be alleviated in ways similar to the 2D raster techniques.

Once an object has been voxelized, the voxels comprising the discrete object do not retain any geometric information regarding the geometric definition of the object. Thus, it is advantageous, when exact measurements are required (e.g., distance, area), to employ conventional modeling where the geometric definition of the object is available. A voxel-based object is only a discrete approximation of the original continuous object where the volume buffer resolution determines the precision of such measurements. On the other hand, several measurement types are more easily computed in voxel space (e.g., mass property, adjacency detection, and volume computation).

The lack of geometric information in the voxel may inflict other difficulties, such as surface normal computation. In voxel-based models, a discrete shading method is commonly employed to estimate the normal from a context of voxels. A variety of image-based and object-based methods for normal estimation from volumetric data has been devised (see [120], [49, Chapter 4]) and some have been discussed above. Most methods are based on fitting some type of a surface primitive to a small neighborhood of voxels.

A partial integration between surface and volume graphics is conceivable as part of an object-based approach in which an auxiliary object table, consisting of the geometric definition and global attributes of each object, is maintained in addition to the volume buffer. Each voxel consists of an index to the object table. This allows exact calculation of normal, exact measurements, and intersection verification for discrete ray tracing [122]. The auxiliary geometric information might be useful also for re-voxelizing the scene in case of a change in the scene itself.

10. Conclusions

Many of the important concepts and computational methods of volume visualization have been presented. Surface rendering algorithms for volume data were briefly described in which an intermediate representation of the data is used to generate an image of a surface contained within the data. Object order, image order, and domain volume rendering techniques were presented for generating images of surfaces within the data, as well as volume rendered images that attempt to capture

all three dimensions of information in the 2D image. Several optimization techniques that aim at decreasing the rendering time for volume visualization as well as realistic global illumination rendering were also described.

Although volumetric representations and visualization techniques seem more natural for sampled or computed data sets, their advantages are also attracting traditional geometric-based applications. This trend implies an expanding role for volume visualization, and it has thus the potential to revolutionize the field of computer graphics, by providing an alternative to surface graphics, called volume graphics. We have introduced recent trends in volume visualization that brought about the emergence of volume graphics. As summarized in Table 1, volume graphics has advantages over surface graphics by being viewpoint independent, insensitive to scene and object complexity, and it lends itself to the realization of block operations, CSG modeling, and hierarchical representation. It is suitable for the representation of sampled or simulated datasets and their intermixing with geometric objects, and it supports the visualization of internal structures. The problems associated with the volume buffer representation, such as memory size, processing time, aliasing, and lack of geometric representation, echo problems encountered when raster graphics emerged as an alternative technology to vector graphics and can be alleviated in similar ways.

The progress so far in volume graphics, in computer hardware, and memory systems, coupled with the desire to reveal the inner structures of volumetric objects, suggests that volume visualization and volume graphics may develop into major trends in computer graphics. Just as raster graphics in the seventies superseded vector graphics for visualizing surfaces, volume graphics has the potential to supersede surface graphics for handling and visualizing volumes as well as for modeling and rendering synthetic scenes composed of surfaces.

Acknowledgments

Special thanks are due to Lisa Sobierajski, Rick Avila, Roni Yagel, Dany Cohen, Sid Wang, Taosong He, Hanspeter Pfister, and Lichan Hong who contributed to this paper, co-authored with me related papers [2, 51-53], and helped with the *VolVis* software. (*VolVis* can be obtained by sending email to: volvis@cs.sunysb.edu.) This work has been supported by the National Science Foundation under grants CCR-9205047 and MIP-9527694, and a grant from the Department of Energy under PICS grant. The MRI head data in Figures 4 and 9 is courtesy of Siemens Medical Systems, Inc., Iselin, NJ. Figure 7 is courtesy of Hughes Aircraft Company, Long Beach, CA. This image has been voxelized using voxelization algorithms, a voxel-based modeler, and a photo-mapper developed at Stony Brook Visualization Lab. The confocal microscope data in Figures 2 and 4 are courtesy of Howard Hughes Medical Institute at Stony Brook, NY. The CT lobster data in Figure 5 is courtesy of AVS, Waltham, MA.

11. References

1. Avila, R., Sobierajski, L. and Kaufman, A., ‘‘Towards a Comprehensive Volume Visualization System’’, *Visualization ’92 Proceedings*, October 1992, 13-20.
2. Avila, R., He, T., Hong, L., Kaufman, A., Pfister, H., Silva, C., Sobierajski, L. and Wang, S., ‘‘VolVis: A Diversified Volume Visualization System’’, *Visualization ’94 Proceedings*, Washington, DC, October 1994, 31-38.
3. Bakalash, R., Kaufman, A., Pacheco, R. and Pfister, H., ‘‘An Extended Volume Visualization System for Arbitrary Parallel Projection’’, *Proceedings of the 1992 Eurographics Workshop on*

Graphics Hardware, Cambridge, UK, September 1992.

4. Barillot, C., Gibaud, B., Luo, L. M. and Scarabin, I. M., ‘‘3D Representation of Anatomic Structures From CT Examinations’’, *Proceedings SPIE*, **602**, (1985), 307-314.
5. Chen, L. S., Herman, G. T., Reynolds, R. A. and Udupa, J. K., ‘‘Surface Shading in the Cuberille Environment’’, *IEEE Computer Graphics & Applications*, **5**, 12 (December 1985), 33-43.
6. Chiueh, T., He, T., Kaufman, A. and Pfister, H., ‘‘Compression Domain Volume Rendering’’, Technical Report 94.01.04, Computer Science, SUNY at Stony Brook, January 1994.
7. Chui, C., *An Introduction to Wavelets*, Academic Press, 1992.
8. Cline, H. E., Lorensen, W. E., Ludke, S., Crawford, C. R. and Teeter, B. C., ‘‘Two Algorithms for the Three-Dimensional Reconstruction of Tomograms’’, *Medical Physics*, **15**, 3 (May/June 1988), 320-327.
9. Cohen, M. F., Chen, S. E., Wallace, J. R. and Greenberg, D. P., ‘‘A Progressive Refinement Approach to Fast Radiosity Image Generation’’, *Computer Graphics (Proc SIGGRAPH)*, 1988, 75-84.
10. Cohen, D. and Kaufman, A., ‘‘Scan Conversion Algorithms for Linear and Quadratic Objects’’, in *Volume Visualization*, A. Kaufman, (ed.), IEEE Computer Society Press, Los Alamitos, CA, 1991, 280-301.
11. Cohen, D. and Shaked, A., ‘‘Photo-Realistic Imaging of Digital Terrain’’, *Computer Graphics Forum*, **12**, 3 (September 1993), 363-374.
12. Cohen-Or, D. and Kaufman, A., ‘‘Fundamentals of Surface Voxelization’’, *CVGIP: Graphics Models and Image Processing*, **56**, 6 (November 1995), 453-461.
13. Coquillart, S., ‘‘Extended Free-Form Deformation: A Sculpturing Tool for 3D Geometric Modeling’’, *Computer Graphics*, **24**, 4 (August 1990), 187-196.
14. Danielsson, P. E., ‘‘Incremental Curve Generation’’, *IEEE Transactions on Computers*, **C-19**, (1970), 783-793.
15. Daubechies, I., *Ten Lectures on Wavelets, CBMS-NSF Regional Conference Series in Applied Mathematics*, SIAM, 1992.
16. Drebin, R. A., Carpenter, L. and Hanrahan, P., ‘‘Volume Rendering’’, *Computer Graphics (Proc. SIGGRAPH)*, **22**, 4 (August 1988), 65-74.
17. Dubois, D. and Prade, H., *Fuzzy Sets and Systems: Theory and Applications*, Academic Press, 1980.
18. Dunne, S., Napel, S. and Rutt, B., ‘‘Fast Reprojection of Volume Data’’, *Proceedings of the 1st Conference on Visualization in Biomedical Computing*, Atlanta, GA, 1990, 11-18.
19. Eastman, C. M., ‘‘Vector versus Raster: A Functional Comarison of Drawing Technologies’’, *IEEE Computer Graphics & Applications*, **10**, 5 (September 1990), 68-80.
20. Ebert, D. S. and Parent, R. E., ‘‘Rendering and Animation of Gaseous Phenomena by Combining Fast Volume and Scanline A-buffer Techniques’’, *Computer Graphics*, **24**, 4 (August 1990), 357-366.
21. Eck, M., DeRose, T., Duchamp, T., Hoppe, H., Lounsbery, M. and Stuetzle, W., ‘‘Multiresolution Analysis of Arbitrary Meshes’’, *SIGGRAPH’95 Conference Proceedings*, August 1995, 173-182.
22. Fowler, J. and Yagel, R., ‘‘Lossless Compression of Volume Data’’, *Proceedings Symposium on Volume Visualization*, Washington, DC, October 1994, 43-50.

23. Galyean, T. A. and Hughes, J. F., ‘‘Sculpting: An Interactive Volumetric Medeling Technique’’, *Computer Graphics*, **25**, 4 (July 1991), 267-274.

24. Garrity, M. P., ‘‘Raytracing Irregular Volume Data’’, *Computer Graphics*, **24**, 5 (November 1990), 35-40.

25. Giertsen, C., ‘‘Volume Visualization of Sparse Irregular Meshes’’, *IEEE Computer Graphics & Applications*, **12**, 2 (March 1992), 40-48.

26. Glassner, A. S., ‘‘Space Subdivision for Fast Ray Tracing’’, *IEEE Computer Graphics and Applications*, **4**, 10 (October 1984), 15-22.

27. Goldwasser, S. M., Reynolds, R. A., Bapty, T., Baraff, D., Summers, J., Talton, D. A. and Walsh, E., ‘‘Physician’s Workstation with Real-Time Performance’’, *IEEE Computer Graphics & Applications*, **5**, 12 (December 1985), 44-57.

28. Goodman, J. R. and Sequin, C. H., ‘‘Hypertree: A Multiprocessor Interconnection Topology’’, *IEEE Transactions on Computers*, **C-30**, 12 (December 1981), 923-933.

29. Gordon, D. and Reynolds, R. A., ‘‘Image Space Shading of 3-Dimensional Objects’’, *Computer Vision, Graphics and Image Processing*, **29**, (1985), 361-376.

30. Gross, M. H., Koch, R., Lippert, L. and Dreger, A., ‘‘A New Method to Approximate the Volume Rendering Equation using Wavelet Bases and Piecewise Polynomials’’, *Computers & Graphics*, **19**, 1 (1995), 47-62.

31. Guenther, T., Poliwoda, C., Reinhard, C., Hesser, J., Maenner, R., Meinzer, H. and Baur, H., ‘‘VIRIM: A Mssivealy Parallel Processor for Real-Time Volume Visualization in Medicine’’, *Proceedings of the 9th Eurographics Hardware Workshop*, Oslo, Norway, September 1994, 103-108.

32. Hanrahan, P., Salzman, D. and Aupperle, L., ‘‘A Rapid Hierarchical Radiosity Algorithm’’, *Computer Graphics*, **25**, 4 (July 1991), 197-206.

33. Hart, J. C., Sandin, D. J. and Kauffman, L. H., ‘‘Ray Tracing Deterministic 3-D Fractals’’, *Computer Graphics*, **23**, 3 (July 1989), 289-296.

34. He, T., Hong, L., Kaufman, A., Varshney, A. and Wang, S., ‘‘Voxel-Based Object Simplification’’, *IEEE Visualization ’95 Proceedings*, Los Alamitos, CA, October 1995, 296-303.

35. Herman, G. T. and Liu, H. K., ‘‘Three-Dimensional Display of Human Organs from Computed Tomograms’’, *Computer Graphics and Image Processing*, **9**, (January 1979), 1-21.

36. Herman, G. T. and Udupa, J. K., ‘‘Display of Three Dimensional Discrete Surfaces’’, *Proceedings SPIE*, **283**, (1981), 90-97.

37. Hesser, J., Maenner, R., Knittel, G., Strasser, W., Pfister, H. and Kaufman, A., ‘‘Three Architectures for Volume Rendering’’, *Computer Graphics Forum*, **14**, 3 (August 1995), 111-122.

38. Hoehne, K. H. and Bernstein, R., ‘‘Shading 3D-Images from CT Using Gray-Level Gradients’’, *IEEE Transactions on Medical Imaging*, **MI-5**, 1 (March 1986), 45-47.

39. Hoppe, H., DeRose, T., Duchamp, T., McDonald, J. and Stuetzle, W., ‘‘Mesh Optimization’’, *Computer Graphics (SIGGRAPH ’93 Proceedings)*, **27**, (August 1993), 19-26.

40. Hottel, H. C. and Sarofim, A. D., *Radiative Transfer*, McGraw-Hill, New York, New York, 1967.

41. Jackel, D., ‘‘The Graphics PARCUM System: A 3D Memory Based Computer Architecture for Processing and Display of Solid Models’’, *Computer Graphics Forum*, **4**, (1985), 21-32.

42. Kajiya, J. T. and Kay, T. L., ‘‘Rendering Fur with Three Dimensional Textures’’, *Computer Graphics*, **23**, 3 (July 1989), 271-280.

43. Kaufman, A. and Shimony, E., ‘‘3D Scan-Conversion Algorithms for Voxel-Based Graphics’’, *Proc. ACM Workshop on Interactive 3D Graphics*, Chapel Hill, NC, October 1986, 45-76.

44. Kaufman, A., ‘‘An Algorithm for 3D Scan-Conversion of Polygons’’, *Proc. EUROGRAPHICS’87*, Amsterdam, Netherlands, August 1987, 197-208.

45. Kaufman, A., ‘‘Efficient Algorithms for 3D Scan-Conversion of Parametric Curves, Surfaces, and Volumes’’, *Computer Graphics*, **21**, 4 (July 1987), 171-179.

46. Kaufman, A. and Bakalash, R., ‘‘Memory and Processing Architecture for 3-D Voxel-Based Imagery’’, *IEEE Computer Graphics & Applications*, **8**, 6 (November 1988), 10-23. Also in Japanese, *Nikkei Computer Graphics*, 3, 30, March 1989, pp. 148-160.

47. Kaufman, A. and Bakalash, R., ‘‘CUBE - An Architecture Based on a 3-D Voxel Map’’, in *Theoretical Foundations of Computer Graphics and CAD*, R. A. Earnshaw, (ed.), Springer-Verlag, 1988, 689-701.

48. Kaufman, A., Yagel, R. and Cohen, D., ‘‘Intermixing Surface and Volume Rendering’’, in *3D Imaging in Medicine: Algorithms, Systems, Applications*, K. H. Hoehne, H. Fuchs and S. M. Pizer, (eds.), June 1990, 217-227.

49. Kaufman, A., *Volume Visualization*, IEEE Computer Society Press Tutorial, Los Alamitos, CA, 1991.

50. Kaufman, A., ‘‘The *voxblt* Engine: A Voxel Frame Buffer Processor’’, in *Advances in Graphics Hardware III*, A. A. M. Kuijk, (ed.), Springer-Verlag, Berlin, 1992, 85-102.

51. Kaufman, A., Cohen, D. and Yagel, R., ‘‘Volume Graphics’’, *IEEE Computer*, **26**, 7 (July 1993), 51-64. Also in Japanese, *Nikkei Computer Graphics*, 1, No. 88, 148-155 & 2, No. 89, 130-137, 1994.

52. Kaufman, A., Yagel, R. and Cohen, D., ‘‘Modeling in Volume Graphics’’, in *Modeling in Computer Graphics*, B. Falcidieno and T. L. Kunii, (eds.), Springer-Verlag, June 1993, 441-454.

53. Kaufman, A. and Sobierajski, L., ‘‘Continuum Volume Display’’, in *Computer Visualization*, R. S. Gallagher, (ed.), CRC Press, Boca Raton, FL, 1994, 171-202.

54. Knittel, G. and Strasser, W., ‘‘A Compact Volume Rendering Accelerator’’, *Volume Visualization Symposium Proceedings*, Washington, DC, October 1994, 67-74.

55. Kruger, W., ‘‘The Application of Transport Theory to Visualization of 3-D Scalar Data Fields’’, *Computers in Physics*, July/August 1991, 397-406.

56. Lacroute, P. and Levoy, M., ‘‘Fast Volume Rendering using a Shear-Warp Factorization of the Viewing Transformation’’, *Computer Graphics*, **28**, 3 (July 1994), 451-458.

57. Lacroute, P., ‘‘Real-Time Volume Rendering on Shared Memory Multiprocessors Using the Shear-Warp Factorization’’, *1995 Parallel Rendering Symposium*, October 1995, 15-21.

58. Laur, D. and Hanrahan, P., ‘‘Hierarchical Splatting: A Progressive Refinement Algorithm for Volume Renderi ng’’, *Computer Graphics*, **25**, 4 (July 1991), 285-288.

59. Lee, Y. T. and Requicha, A. A. G., ‘‘Algorithms for Computing the Volume and Other Integral Properties of Solids: I-Known Methods and Open Issues; II-A Family of Algorithms Based on Representation Conversion and Cellular Approximation’’, *Communications of the ACM*, **25**, 9 (September 1982), 635-650.

60. Levoy, M., ‘‘Display of Surfaces from Volume Data’’, *Computer Graphics and Applications*, **8**, 5 (May 1988), 29-37.

61. Levoy, M. and Whitaker, R., ‘‘Gaze-Directed Volume Rendering’’, *Computer Graphics (Proc. 1990 Symposium on Interactive 3D Graphics)*, **24**, 2 (March 1990), 217-223.

62. Levoy, M., ‘‘Volume Rendering using the Fourier Projection-Slice Theorem’’, *Graphics Interface ’92*, 1992, 61-69.

63. Lorensen, W. E. and Cline, H. E., ‘‘Marching Cubes: A High Resolution 3D Surface Construction Algorithm’’, *Computer Graphics*, **21**, 4 (July 1987), 163-170.

64. Malzbender, T. and Kitson, F., ‘‘A Fourier Technique for Volume Rendering’’, *Focus on Scientific Visualization*, 1991, 305-316.

65. Malzbender, T., ‘‘Fourier Volume Rendering’’, *ACM Transactions of Graphics*, **12**, 3 (July 1993), 233-250.

66. Max, N., Hanrahan, P. and Crawfis, R., ‘‘Area and Volume Coherence for Efficient Visualization of 3D Scalar Functions’’, *Computer Graphics*, **24**, 5 (November 1990), 27-34.

67. Max, N., ‘‘Optical Models for Direct Volume Rendering’’, *IEEE Transations on Visualization and Computer Graphics*, **1**, 2 (June 1995), 99-108.

68. Meagher, D. J., ‘‘Applying Solids Processing Methods to Medical Planning’’, *Proceedings NCGA’85*, Dallas, TX, April 1985, 101-109.

69. Mokrzycki, W., ‘‘Algorithms of Discretization of Algebraic Spatial Curves on Homogeneous Cubical Grids’’, *Computers & Graphics*, **12**, 3/4 (1988), 477-487.

70. Molnar, S., Eyles, J. and Poulton, J., ‘‘PixelFlow: High-Speed Rendering Using Image Composition’’, *Computer Graphics*, **26**, 2 (July 1992), 231-240.

71. Muraki, S., ‘‘Volume Data and Wavelet Transform’’, *IEEE Computer Graphics & Applications*, **13**, 4 (July 1993), 50-56.

72. Nielson, G. M., ‘‘Scattered Data Modeling’’, *IEEE Computer Graphics & Applications*, **13**, 1 (January 1993), 60-70.

73. Ning, P. and Hesselink, L., ‘‘Vector Quantization for Volume Rendering’’, *Workshop on Volume Visualization*, Boston, MA, October 1992, 69-74.

74. Ning, P. and Hesselink, L., ‘‘Fast Volume Rendering of Compressed Data’’, *Visualization ’93 Proceedings*, October 1993, 11-18.

75. Norton, V. A., ‘‘Generation and Rendering of Geometric Fractals in 3-D’’, *Computer Graphics*, **16**, 3 (1982), 61-67.

76. Ohashi, T., Uchiki, T. and Tokoro, M., ‘‘A Three-Dimensional Shaded Display Method for Voxel-Based Representation’’, *Proceedings EUROGRAPHICS ’85*, Nice, France, September 1985, 221-232.

77. Perlin, K. and Hoffert, E. M., ‘‘Hypertexture’’, *Computer Graphics*, **23**, 3 (July 1989), 253-262.

78. Pfister, H., Kaufman, A. and Chiueh, T., ‘‘Cube-3: A Real-Time Architecture for High-resolution Volume Visualization’’, *Volume Visualization Symposium Proceedings*, Washington, DC, October 1994, 75-82.

79. Pfister, H., Wessels, F. and Kaufman, A., ‘‘Sheared Interpolation and Gradient Estimation for Real-Time Volume Rendering’’, *9th Eurographics Workshop on Graphics Hardware Proceedings*, Oslo, Norway, September 1994.

80. Pfister, H., Wessels, F. and Kaufman, A., ‘‘Sheared Interpolation and Gradient Estimation for Real-Time Volume Rendering’’, *Computers & Graphics*, **19**, 5 (September 1995), 667-677.

81. Pfister, H., Kaufman, A. and Wessels, F., ‘‘Towards a Scalable Architecture for Real-Time Volume Rendering’’, *10th Eurographics Workshop on Graphics Hardware Proceedings*, Maastricht, The Netherlands, August 1995.

82. Rossignac, J. and Borrel, P., ‘‘Multi-Resolution 3D Approximations for Rendering Complex Scenes’’, in *Modeling in Computer Graphics*, B. Falcidieno and T. L. Kunni, (eds.), Springer-Verlag, 1993, 455-465.

83. Rushmeier, H. E. and Torrance, K. E., ‘‘The Zonal Method for Calculating Light Intensities in the Presence of a Participating Medium’’, *Computer Graphics*, **21**, 4 (July 1987), 293-302.

84. Sabella, P., ‘‘A Rendering Algorithm for Visualizing 3D Scalar Fields’’, *Computer Graphics (Proc. SIGGRAPH)*, **22**, 4 (August 1988), 160-165.

85. Sakas, G. and Hartig, J., ‘‘Interactive Visualization of Large Scalar Voxel Fields’’, *Proceedings Visualization ’92*, Boston, MA, October 1992, 29-36.

86. Schroder, P. and Stoll, G., ‘‘Data Parallel Volume Rendering as Line Drawing’’, *Workshop on Volume Visualization*, Boston, MA, October 1992, 25-32.

87. Schroeder, W. J., Zarge, J. A. and Lorensen, W. E., ‘‘Decimation of Triangle Meshes’’, *Computer Graphics*, **26**, 2 (July 26-31 1992), 65-70.

88. Sederberg, T. W. and Parry, S. R., ‘‘Free-Form Deformation of Solid Geometry Models’’, *Computer Graphics*, **20**, 4 (August 1986), 151-160.

89. Shirley, P. and Neeman, H., ‘‘Volume Visualization at the Center for Supercomputing Research and Development’’, in *Proceedings of the Workshop on Volume Visualization*, C. Upson, (ed.), Chapel Hill, NC, May 1989, 17-20.

90. Snyder, J. M. and Barr, A. H., ‘‘Ray Tracing Complex Models Containing Surface Tessellations’’, *Computer Graphics*, **21**, 4 (July 1987), 119-128.

91. Sobierajski, L., Cohen, D., Kaufman, A., Yagel, R. and Acker, D., ‘‘A Fast Display Method for Volumemtric Data’’, *The Visual Computer*, **10**, 2 (1993), 116-124.

92. Sobierajski, L. and Kaufman, A., ‘‘Volumetric Ray Tracing’’, *Volume Visualization Symposium Proceedings*, Washington, DC, October 1994, 11-18.

93. Sobierajski, L. and Kaufman, A., ‘‘Volumetric Radiosity’’, Technical Report 94.01.05, Computer Science, SUNY Stony Brook, January 1994.

94. Speray, D. and Kennon, S., ‘‘Volume Probes: Interactive Data Exploration on Arbitrary Grids’’, *Computer Graphics*, **24**, 5 (November 1990), 5-12.

95. Stytz, M. R. and Frieder, O., ‘‘Computer Systems for Three-Dimensional Diagnostic Imaging: An Examination of the State of the Art’’, *Critical Reviews in Biomedical Engineering*, August 1991, 1-46.

96. Stytz, M. R., Frieder, G. and Frieder, O., ‘‘Three-Dimensional Medical Imaging: Algorithms and Computer Systems’’, *ACM Computing Surveys*, December 1991, 421-499.

97. Tiede, U., Hoehne, K. H. and Riemer, M., ‘‘Comparison of Surface Rendering Techniques for 3D Tomographics Objects’’, *Proceedings NCGA ’88 Conference*, Berlin Heidelberg New York, 1987, 599-610.

98. Tiede, U., Riemer, M., Bomans, M. and Hoehne, K. H., ‘‘Display Techniques for 3-D Tomographic Volume Data’’, *Proceedings of NCGA’88 Conference*, **III**, (March 1988), 188-197, National Computer Graphics Association.

99. Totsuka, T. and Levoy, M., ‘‘Frequency Domain Volume Rendering’’, *Computer Graphics (Proc. SIGGRAPH)*, 1993, 271-278.

100. Turk, G., ‘‘Re-Tiling Polygonal Surfaces’’, *Computer Graphics*, **26**, 2 (July 26-31 1992), 55-64.

101. Tuy, H. K. and Tuy, L. T., ‘‘Direct 2-D Display of 3-D Objects’’, *IEEE Computer Graphics & Applications*, **4**, 10 (November 1984), 29-33.

102. Upson, C. and Keeler, M., ‘‘V-BUFFER: Visible Volume Rendering’’, *Computer Graphics (Proc. SIGGRAPH)*, 1988, 59-64.

103. Vannier, M. W., Marsh, J. L. and Warren, J. O., ‘‘Three-Dimensional Computer Graphics for Craniofacial Surgical Planning and Evaluation’’, *Computer Graphics*, **17**, 3 (July 1983), 263-273.

104. Vezina, G., Fletcher, P. A. and Robertson, P. K., ‘‘Volume Rendering on the MasPar MP-1’’, *Workshop on Volume Visualization*, Boston, MA, October 1992, 3-8.

105. Wallace, G. K., ‘‘The JPEG Still Picture Compression Standard’’, *Communications of the ACM*, **34**, 4 (April 1991), 30-44.

106. Wang, S. and Kaufman, A., ‘‘Volume Sampled Voxelization of Geometric Primitives’’, *Visualization ’93 Proceedings*, San Jose, CA, October 1993, 78-84.

107. Wang, S. and Kaufman, A., ‘‘3D Antialiasing’’, Technical Report 94.01.03, Computer Science, SUNY Stony Brook, January 1994.

108. Wang, S. and Kaufman, A., ‘‘Volume-Sampled 3D Modeling’’, *IEEE Computer Graphics & Applications*, **14**, 5 (September 1994), 26-32.

109. Wang, S. and Kaufman, A., ‘‘Volume Sculpting’’, *ACM Symposium on Interactive 3D Graphics*, Monterey, CA, April 1995, 151-156.

110. Westermann, R., ‘‘A Multiresolution Framework for Volume Rendering’’, *1994 Symposium on Volume Visualization*, Washington, D.C., October 1994, 51-58.

111. Westover, L., ‘‘Footprint Evaluation for Volume Rendering’’, *Computer Graphics (Proc. SIGGRAPH)*, **24**, 4 (August 1990), 144-153.

112. Whitted, T., ‘‘An Improved Illumination Model for Shaded Display’’, *Communications of the ACM*, **23**, 6 (June 1980), 343-349.

113. Wilhems, J. and vanGelder, A., ‘‘A coherent projection approach for direct volume rendering’’, *Computer Graphics (SIGGRAPH ’91 Proceedings)*, **25**, (July 1991), 275-284.

114. Williams, P. L., ‘‘Interactive Splatting of Nonrectilinear Volumes’’, *Proceedings Visualization ’92*, October 1992, 37-44.

115. Wright, J. and Hsieh, J., ‘‘A Voxel-Based, Forward Projection Algorithm for Rendering Surface and Volumetric Data’’, *Proceedings Visualization ’92*, Boston, MA, October 1992, 340-348.

116. Yagel, R. and Kaufman, A., ‘‘The Flipping Cube Architecture’’, Tech. Rep. 91.07.26, Computer Science, SUNY at Stony Brook, July 1991.

117. Yagel, R., Kaufman, A. and Zhang, Q., ‘‘Realistic Volume Imaging’’, *Proceedings Visualization ’90*, San Diego, CA, October 1991, 226-231.

118. Yagel, R., ‘‘Efficient Methods for Computer Graphics’’, PhD Dissertation, SUNY at Stony Brook, December 1991.

119. Yagel, R. and Kaufman, A., ‘‘Template-Based Volume Viewing’’, *Computer Graphics Forum*, **11**, 3 (September 1992), 153-167.

120. Yagel, R., Cohen, D. and Kaufman, A., ‘‘Normal Estimation in 3D Discrete Space’’, *The Visual Computer*, June 1992, 278-291.

121. Yagel, R., ‘‘High Quality Template-Based Volume Viewing’’, *OSU-CISRC-10/92-TR28*, Department of Computer and Information Science, The Ohio State University, October 1992.

122. Yagel, R., Cohen, D. and Kaufman, A., ‘‘Discrete Ray Tracing’’, *IEEE Computer Graphics & Applications*, **12**, 5 (September 1992), 19-28.

123. Yeo, B. and Liu, B., ‘‘Volume Rendering of DCT-Based Compressed 3D Scalar Data’’, *IEEE Transactions on Visualization and Computer Graphics*, **1**, 1 (March 1995), 29-43.

124. Yoo, T. S., Neumann, U., Fuchs, H., Pizer, S. M., Cullip, T., Rhoades, J. and Whitaker, R., ‘‘Direct Visualization of Volume Data’’, *IEEE Computer Graphics & Applications*, **12**, 4 (July 1992), 63-71.

Specification, representation, and construction of non-manifold geometric structures

May 3rd, 1996

Jarek R. Rossignac

IBM, T.J. Watson Research Center
Yorktown Heights, New York 10598

Siggraph 96 course: Computational Representations of Geometry

Abstract

Geometric modelling is central to many applications. Representation schemes that are specialized for a particular application may impose topological and geometric limitations on the domain and thus considerably restrict future extensions. Selective Geometric Complexes (SGCs) provide a practical yet general framework for representing general objects of mixed dimensionality having internal structures and incomplete boundaries. SGCs and their decomposition into regions (i.e., features of interests for a particular applications) may be specified and edited in terms of Constructive Non-Regularized Geometry (CNRG) trees, which define how primitive shapes should be combined through a variety of set-theoretic and topological operators. CNRG operators preserve the structure imposed by their arguments on the underlying set. The combination of CNRG specification and of SGC representation and the associated conversion/evaluation algorithms provide a generalized environment for non-manifold modeling in any dimension. These notes focus on the topological concepts, on the representation and specification schemes, and on the associated algorithms for non-manifold structures, independently of any particular geometric domain (i.e., restriction on the shapes or surfaces) and of the dimension of the underlying space.

Table of Contents

1.0 FORWARD

Computerized models of three-dimensional shapes are central to many applications: manufacturing, geoscience, entertainment, architecture, and medicine are obvious examples. Natural or man-made shapes may be modeled electronically in a variety of ways and with different degrees of accuracy. The choice of a particular modeling scheme and of the associated data-structures often depends on the data acquisition process, on requirements imposed by the application, and of course on the skills, number, ambitions, and preoccupations of the developers.

Four types of representations interplay in many geometric modeling scenarios.

In Computer-Aided Design systems, an intentional model may be used to capture, in an unevaluated form, some of the functional requirements of a product or the designer's intent. One may use a procedural model (programming language, Constructive Solid Geometry, or more general creation history graphs which include Boolean, blending, and deformation operators) or a declarative form (geometric constraints, shape grammars, construction rules). Such models may in general be easily edited or parameterized.

Real or computed shapes may be captured in a sample model derived from physical measurements (seismic data, slices of a medical scan, depth maps from a range finder) or from the results of numeric simulations. Sample models provide shape information only over a set of discrete sample points placed either on the surfaces of the model or distributed in space. Shape between the samples is not well defined and various algorithmic techniques have been proposed to construct continuous interpolations between samples and to decide which neighboring samples should be used for evaluating a given point.

A continuous extensional (i.e. evaluated) model is typically derived algorithmically from an intentional model, a sample model, or both. For example, an operator may design a multi-surface object using crude approximations for each surface and subsequently force each surface to pass through or near a set of sample points measured off a real object or computed via numeric optimization. Most representation schemes for extensional models are enumerative in nature. The most popular representations are dimensionally homogeneous partition of space (voxels, octrees, 3D meshes, BSP trees) or recursive boundary formulations (BReps), where volumes are defined in terms of their bounding faces and where faces are defined in terms of their supporting surfaces and bounding edges.

An abstraction model provides mechanisms for selecting, identifying, or iconifying those subsets of the extensional model's interior or boundary that are appropriate for a particular operation or relevant to a particular annotation. Typical examples include surface features for machining, entities used in the definition of geometric constraints stored in intentional models, or tumors in a segmented 3D medical dataset. Abstraction models may impose an internal structure on the point set of the model.

This lecture focuses on the extension of traditional intentional models (Constructive Solid Geometry) and continuous extensional models (Boundary Representations) to arbitrary topological domains and to pointsets with internal structure. The theoretical underpinnings supporting these extensions are independent of the particular choice of a representation for the individual geometric entities, and hence of the geometric coverage of the modeler. The algorithms developed for constructing and for processing such representation assume however the reliable support of a small set of geometric queries, such as the intersection and ordering of geometric entities.

2.0 INTRODUCTION

The primary schemes for representing three-dimensional geometric objects may be grouped into three broad categories: constructive, boundary, and enumerative representations. By storing a recipe (process) for creating a model from primitive entities and operations, constructive representations capture the designers' intent and provide a powerful design model that is easy to edit and to parameterize. Enumerative representations represent or approximate the desired regions as a collection of primitive entities that are simpler to represent. Enumerative schemes may require that the primitives be mutually disjoint (or at least that their relative interiors be disjoint) and often restrict the primitives to be regularly spaced. Most popular schemes use cubical cells (called voxels), parallelepipeds of uniform cross-section (Ray representations [12]), or constant-thickness slices (cross-sections). These representations may be constructed directly from physical measures or from simulation results or evaluated from other representations. Although often approximate, they have recently gained popularity, because their simplicity is well suited for parallel hardware implementation (see papers in [20]). Boundary representations exploit the fact that a simple enumeration of the bounding (hyper)faces of a bounded region suffices to unambiguously distinguish it from its complement. Most boundary models, however, store additional connectivity information between the geometric boundary elements (vertices, edges, and faces) and exploit it to speed up the boundary traversal parts of fundamental algorithms that build the model from a constructive representation, display it, or extract its topological or geometric properties.

Practitioners often distinguish between the topology and the geometry of a model. While a geometric representation captures the precise shape of each face, or curve of an object, a topological representation focuses on properties that are invariant under continuous deformations, i.e. that are independent of the precise shape of the geometric components. This lecture notes address precise representations of continuous three-dimensional geometric models, because these are important for precise design, visualization, and analysis. Therefore we focus primarily on the topological, representational, and computational aspects of constructive and boundary representation that are independent of any particular geometric domain (i.e. of the nature of the surfaces represented or even of the dimensionality of the problem). Enumerative representations are addressed elsewhere in this course.

Geometric modelling is central to many design, simulation, visualization, analysis, and manufacturing applications. Different applications deal with different geometric and topological entities and thus require different geometric and topological coverages. The geometric coverage of a modeler is characterized by the nature of the geometric entities (such as points, curves, surfaces) it supports and by the ways in which these entities may be created, combined, and manipulated. Topological limitations of a modeler are more subtle to assess. For example, the solid modeling technology is based on a precise definition of solids leading to a complete and unambiguous representation that permits to distinguish between the interior, the boundary, and the exterior of the represented solid [29]. This definition played an essential role in the development of correct algorithms for Boolean operations on solids [30], but has somewhat confined the domain of applications. Indeed, until recently, solid modelers did not explicitly support internal structures nor lower-dimensional (dangling) entities. Surfaces have been extensively used for car body design and are required for representing regions of contacts between solids. Interior faces are used to decompose solids into finite elements or into subsets exhibiting different physical properties. They may also represent cracks in three dimensional sets. Curves may be used as design aides. Although solids, curves, and surfaces can be grouped (overlayed) in the same model and moved or displayed together as a single entity, Boolean and other operations on such groupings have not been implemented, nor even formally defined.

Selective Geometric Complexes (abbreviated SGC) introduced by Rossignac and O'Connor [33] provide a common framework for representing objects of mixed dimensionality possibly having internal structures and incomplete boundaries. SGCs are composed of finite collections of mutually disjoint cells. A cell is an open connected subset of some n-dimensional manifold. The concept of a cell generalizes the concepts of edges, faces, and vertices used in most solid modelers. The connectivity between the cells of an SGC is captured in a very simple incidence graph, whose links indicate boundary-of relations between cells. By choosing which cells of an object are active one can associate various pointsets with a single collection

of cells. These pointsets need not be homogeneous in dimension, nor even be closed or bounded. Although most geometric manipulations that are necessary to support SGCs (at least in three dimensions) are available in many existing geometric modellers, data structures and high-level operations provided with these modellers are not designed to represent and process such complex objects. Therefore, to support useful operations on SGCs, Boolean and other set-theoretic operations (closure, interior, boundary) have been decomposed into combinations of three fundamental steps for which we have developed dimension-independent algorithms: a subdivision step, which makes two objects compatible by subdividing the cells of each object at their intersections with cells of the other object, a selection step, which defines active cells, and a simplification step, which, by deleting or merging certain cells, reduces the complexity of an object's representation without changing the represented pointset and without destroying useful structural information. Furthermore, combinations of these steps may produce a variety of special-purpose operations, whose effect is controlled by simple predicates, or filters, for cell selection.

Solids may be conveniently specified in CSG (Constructive Solid Geometry) by a construction tree that has solid primitives as leaves and rigid body motions or regularized Boolean operations as internal nodes. Algorithms for classifying sets with respect to CSG trees and for evaluating the boundaries of the corresponding solids are known, at least for simple geometric domains. Emerging CAD applications require that we extend the CSG simplification to support more general and more structured geometric objects. The concept of a Constructive Non-Regularized Geometry (abbreviated CNRG) was introduced by Rossignac and Requicha [34] to support a convenient specification of dimensionally non-homogeneous, non-closed pointsets with internal structures. These cover non-manifold structures possibly composed of several mixed-dimensional regions with dangling or missing boundary elements. CNRG trees extend the domain of CSG by supporting non-regularized primitive shapes as leaves and by providing more general set-theoretic and topological operators at interior nodes. Filtering operations construct CNRG objects from aggregates of selected regions of other CNRG objects. The resulting structures may be evaluated and represented in terms of SGC, where references to individual cells are grouped into CNRG regions.

The combination of CNRG specification and of SGC representation and the associated conversion/evaluation algorithms provide a generalized environment for non-manifold modeling in any dimension. However, most of the concepts are introduced using two or three dimensional instantiations for sake of clarity.

These notes are organized as follows. Section 2 introduces the concepts of topological domains and representation validity through the case study of 2-D polygons. It argues that the correct rephrasing of the question “What is a valid polygon?” leads to a precise definition of a polygon and to a natural canonical representation scheme. Section 3 introduces the fundamental concepts of non-manifold modeling and the diversity of topological domains that fall under this imprecise denomination. The discussion starts with an introduction of a decomposition of space into a collection of disjoint cells induced by a given set of primitives (for example, surfaces and curves). Then it discusses the identification of particular cell in such a decomposition. A variety of topological domains may be obtained by restricting which cells of a decompositions should be active (i.e. contributing to the pointset). Section 4 reviews boundary modeling schemes. It introduces the fundamental entities and the topological and ordering relations between these entities. It overviews several popular data structures, including SGCs. Section 5 reviews the main CNRG concepts and the semantics of CNRG operators for specifying and computing non-manifold sets with structures. The appendix contains a short (informal) review of the topological concepts used elsewhere in these notes.

3.0 WHAT IS A VALID POLYGON?

The naive question: “What is a valid polygon?” should lead to a mathematical definition of validity for polygonal representations accepted, processed, or produced by a particular application or algorithm. Numerous definitions have been published in research papers or user manuals. The reader may be puzzled

by the diversity of such definitions and struggle when asked to establish if two definitions are equivalent, if a particular definition is complete, or even if a specific case satisfies a particular definition.

It is helpful to decompose this questions as follows:

1. "What is a polygon?"
2. "What representation scheme (abstract data structure) are we using?"
3. "How do we semantically interpret the representation (for example when testing whether a point lies inside the represented polygon?"
4. "When is a model expressed using that representation scheme valid (i.e., corresponds to a polygon according to the chosen definition)?"

For the sake of elegance, we propose here a definition that is restrictive, but leads naturally to a simple and canonical (i.e. unique) representation scheme.

A polygon is a connected and bounded s-regular subset of E^2 having for boundary a finite union of mutually disjoint cells. Cells are either **crossings:** (i.e., non-manifold points), **vertices:** (i.e. non-smooth manifold points), or **edges:** (i.e., relatively open connected line segments free of crossings).

A set is s-regular if it is equal to the interior of its closure. Such a set is open and thus does not contain its boundary (i.e. its edges, vertices, or crossings).

According to this definition the following statements hold.

A polygon is open (does not contain its boundary) and connected. It may have holes but no islands.

A polygon has no dangling edges, isolated vertices, interior cracks or missing points.

The boundary of a polygon needs not be manifold. Its vertices, crossings, and edges of a polygon are pairwise disjoint. The vertices, crossings, and edges of any given polygon are always unambiguously defined.

Each edge of a polygon separates the inside of the polygon from the outside. The orientation of each edge (following the convention that the inside is on the left) is thus well defined. Each edge is incident on exactly two points (vertices or crossings) and its orientation defines which is the start point and which is the end point.

Each vertex is the start point of exactly one edge and the end point of exactly one other edge. Each crossing has 2k (k positive integer) edges incident on it. It is the start point of exactly k of these.

The successor of an edge E having vertex V as its end point is defined as the only edge having V as its start point. The successor of an edge E having crossing C as its end point is defined as the first edge that has C as its start point as we circle C clockwise in its immediate vicinity starting from E. The successor of an edge is uniquely defined

A loop is defined as a maximally connected subset of the boundary of a polygon. The loops of a polygon are uniquely defined and pairwise disjoint.

Each edge and each vertex or crossing belong to exactly one loop. The successor of an edge belongs to the same loop.

The successor operator (which returns the successor of the argument edge) induces a unique cyclic ordering for all the edges in a loop.

Edges may be uniquely defined by the references to their start and end points. Since the end point of an edge is equal to the start point of its successor, one reference per edge in a loop suffices for defining the

edges. Thus, a loop is completely represented by an ordered circular list of references to the start points of its edges

Each loop has at least 3 references to different points. The starting points of two consecutive edges in a loop are always different (i.e. consecutive point-references in a loop must be different).

These properties lead to a simple and canonical representation:

A polygon may be represented by the set of its points (vertices and crossings) and the set of its loops. Each point is represented by its coordinates. Each loop is represented by a circularly ordered list of references to its points.

Note that given any polygon (i.e. a pointset that meets the proposed definition), its representation in the above scheme (data structure) is unique. (We do not take into account the possible permutations and various representations for sets and list, which can be addresses by imposing the appropriate lexicographic orderings.) For processing convenience, one could also require that the outer loop (which is also always well defined in the plane and the holes (all other loops) be explicitly identified in the data structure.

The opposite assumption is unfortunately not true. A dataset organized in the above data-structure (sets of points and loops) does not necessarily correspond to a valid polygon. Validity violations may be of different nature: geometric, ordering, or topological. Geometric violations correspond to the wrong choice of point coordinates (for example, a point may coincide with another point or with an edge, or two edges may intersect). Ordering violations may simply correspond to the wrong orientation of the edges in a loop or to the wrong branch taken at a crossing (inconsistent with the definition of a successor). Topological violations may correspond to empty edges (two consecutive references to the same point), to degenerate loops (less than three point references), or to loops with non-manifold parts (for example, the multiple use of an edge).

Imposing additional constraints on the representation further restricts the set of representable polygons. For example, if each vertex is used only once in a loop, the polygon has a manifold boundary. If the polygon has a single loop, it is simply connected.

A number of other schemes for representing polygons are popular in CAD and graphics systems. They include:

- Decompositions into simpler disjoint regions (triangles, trapezoids)
- CSG or BSP trees,
- Possibly overlapping trimming loops

These do not easily lead to canonical representations.

4.0 TOPOLOGICAL BACKGROUND

Any set of geometric primitives may be used to impose a decomposition of the underlying three-dimensional Euclidean space into cells of an SGC structure from which one can select a subset of interest (the “active” cells). We describe here informally several ways of defining such a decompositions.

A single primitive decomposes space into three disjoint parts:

- the primitive's interior
- its boundary
- the interior of its complement

These sets may be recursively decomposed into dimensionally homogeneous subsets (i.e. fully three-dimensional volumes, isolated points, dangling curves, and dangling faces). From each subset, one may extract singular points (cusps and self-crossings where some geometric continuity or topological manifold

properties of the supporting geometry vanish) and boundary points (vertices bounding edge segments and edges bounding dangling faces). The sets of singular points may be further (recursively) decomposed in this manner into singularity-free, dimensionally homogeneous sets. Finally, the maximally connected components. of this decomposition may be identified. For example, a cone primitive may decompose space into: the complement of the cone, the three-dimensional interior of the cone, the circular edge at the base, the disk-like base-face (without its bounding circular edge), the apex (tip of the cone), and the conical face (without the bounding edge nor the apex).

The atomic entities defined by this decomposition process correspond to the cells of a geometric complex. They are connected relatively open subsets of some n-dimensional manifold (the 3-D space or a smooth portion of a surface or of a curve). Any two different cells of such a decomposition are mutually disjoint. The boundary of the set of a cell C lying in a manifold M is the union of other cells in the decomposition, which are either entirely in the manifold M, or entirely out if it. For example the boundary of the conical face of a cone primitive is composed of a circular curve (part of the manifold surface supporting the face) and of the apex (singular point, not in the manifold supporting the face).

When several primitives overlap, the space decompositions induced by each primitive must be combined into a single (finer) decomposition. An algorithm for performing such a merging operation is called subdivision (or refinement) and is outlined in [33]. It basically requires that intersections of each cell of one decomposition with each other cell of each other decomposition be computed and further decomposed into dimensionally homogeneous singularity-free connected components.

The space partition induced by a set of planes is a simple example of decomposition. It cells are: points where three or more planes cross, relatively open (and possibly unbounded) line segments where two or more planes cross, relatively open convex polygonal faces induced on each plane by all other non-coincident planes, and the open convex polyhedra (maximally connected components of the complement of the union of all the planes).

4.1 Identifiable sets of cells

A set of primitives used to induce a decomposition of space provides the means for characterizing specific subsets of these cells. Any cell of such a linear partition may be expressed using a Boolean formula which combines the half-spaces bounded by the original planes and involves only set theoretic intersection and complement operators. Yet, the characterization of the union of several cells may be more conveniently expressed in terms of a filter operator. The filters may use the geometric or topological properties of a cell's set or the relation of a cell to any particular primitive. Filters may be categorized as follows.

- Boolean combinations of primitives half-spaces through set theoretic union, intersection, difference, and complement operators are the most popular filters.
- Dimensionality, adjacency, and incidence may also be used for discriminating cells. For example, given a sphere and its center point, the complement of the sphere may be characterized (among many other ways) as the only 3-cell that is not adjacent to a 0-cell.
- Topological operators, such as relative closure, interior, boundary, may be applied to sets of cells and are unambiguously defined in terms of the union of the point-sets represented by the cells [34].
- Geometric filters, which for example extract the one-dimensional singularities, are also important.

These filters and operators may be composed into expressions that may uniquely identify specific sets of cells. However, they may be insufficient for differentiating between specific pairs of cells: the connected components of the result of filtering expressions. A simple example is an infinite line subdivided by a point. It is impossible to distinguish the two half-lines using only combinations of the above operators. The orientation notions discussed in the next section may help in some cases, but the problem remains unsolved in general, and leads to serious complications for picking faces and defining features in parametric models.

Note that arbitrary subsets of the cells of a decomposition do not necessarily correspond to a geometric complex (the boundaries of some cells may be missing). Therefore, to represent the result of a selection (filtering) process, one should construct a Selective Geometric Complex that includes not only the selected cells, but also all the cells in the closure of the desired set. The added boundary cells will simply be inactive.

Since the above decomposition process often introduces unnecessary subdivisions of the desired set, it may be desirable to simplify the representation, i.e. to produce a simpler SGC representing the same set. A systematic simplification process which preserves the validity of the SGC is described in [33]. The simplification process visits each cell only once (by order of decreasing dimensionality) and applies, if appropriate, one of the following three operations: (1) remove inactive cells that are not bounding other active cells, (2) remove active cells that separate two active cells in the same manifold and are not bounding any other cell, and (3) remove active cells that are interior boundaries of only one active cell. The simplification of [33] provides the means of generating a unique SGC for a given set. That is, if two SGCs, A and B, represent the same sets, their simplifications will be identical SGCs.

4.2 Topological characterization

Developers of geometric modeling systems have often restricted the topological domains in various ways. We characterize such restrictions using topological concepts, regardless of the geometric domain or associated data structures, which are discussed in the following section. The characterization is based on the topological properties of the sets (or collections of sets) that can be represented. We use 2-D terminology to and examples illustrate the differences.

- R-set with manifold boundary: Each vertex is adjacent to exactly two edges.
- R-set with non-manifold boundary: A vertex may bound more than two edges, but the set is equal to the closure of its interior. (Note that regions whose interior are disjoint may share common vertices, but not common edges.)
- S-sets: Open-regularized regions composed of open subsets that are disjoint, but whose boundaries need not be disjoint. Edges bounding two subsets are called “interior”. However, each region is equal to the interior of its closure (i.e. does not contain dangling edges nor cracks).
- Non-regular open sets: Extensions of s-sets that may contain non-separating interior boundary elements, but no dangling lower dimensional entities.
- Inhomogeneous closed sets: Extensions of r-sets with non-manifold to possibly include dangling edges or isolated vertices.
- One-dimensional non-manifold set: Union of edges and vertices that may separate its complement into more than two connected cells. (Such sets are typically called “non-manifold boundaries”, although there does not necessarily exist a bounded and closed or open 2-D region having such a set for boundary.)
- Partially closed sets: Extensions of non-regular open sets to include subsets of their boundaries.
- Disconnected non-regularized set: Extensions of partially closed sets to include dangling edges and vertices. Interior edges are not part of the set.
- Closed non-manifold structures: Subdivisions of closed non-manifold sets into distinguishable subsets. (The boundary of each cell is included in the set.)
- Selective Geometric Complex: Combinations of closed non-manifold structures and disconnected regularized sets. (Interior edges need not be in the set.) SGCs are collections of disjoint relatively open cells—here, 2-cells, edges, and vertices.

Another important characterization addresses restrictions that force the decomposition of natural topological entities into collections of simpler ones. SGCs require that each cell be connected. Thus, the volumes, faces, and edges of a model represented as an SGC must be broken into connected components, each represented by a separate cell.

Restrictions on faces imposed by representations inspired by CW-complexes require that faces with holes be artificially converted into simply connected faces by adding “bridges” (i.e. pairs of edges with opposite orientations that join loops) to merge the various loops into a single loop. Similarly, closed curves and

surfaces that are not homeomorphic to a disk (2-ball) must be artificially split by adding “cuts” (i.e. vertices or edges). Faces are often assumed to be regular (i.e. equal to the interior of their closure). Such a restriction avoids internal face-boundaries, but makes it impossible to represent correctly certain non-manifold r-sets. Restrictions on the face-bounding loops may require that loops be mutually disjoint and 1-manifold. They also lead to serious limitations.

5.0 BOUNDARY REPRESENTATION SCHEMES

We briefly review in this section the most popular data structures for boundary models. A more detailed analysis may be found in [1, 4, 22, 31, 32, 39].

5.1 Fundamental entities

Schemes discussed here use standard data structures, such as a doubly linked list, to store lists of **primary entities** corresponding to cells and organized by dimension (list of vertices, lists of edges...). The geometric information describing the supporting manifolds, such as the equation of a surface that supports a face or of a curve that supports an edge, are accessible from these primary entities.

Grouping entities (such as loops, shells, vertex cones) are sometimes introduced for grouping and ordering primary entities. These grouping entities improve the performance of application algorithms by facilitating the traversal of the cells. For example, certain commands in standard graphics libraries require that polygonal faces be represented a sorted list of vertices along a single loop.

Incidence entities are also used to combine incidence and ordering information in a more compact and regular data structure. Incidence entities are associations of two or three cells of consecutive dimension and having an incidence relation. For example, loops of edges may be represented by associating with each edge-face pair a “next edge” pointer. Because an edge is bounding two faces in manifold models, such a combined entity is sometimes referred to as “half-edge”.

5.2 Incidence orientation and neighborhoods

A great circle splits a spherical surface into two 2-cells (the two connected components of the difference between the sphere and the curve). Given an **orientation** of the circular curve and an orientation of the “outer” normal to the surface, we can define a **“left”** and a **“right”** side to the curve within the surface. Each one of the 2-cells (faces) is adjacent to a different side of the curve. Such a relative orientation is often used to dissociate connected components of a decomposition. We can for example speak of the face that lies “on the left” of the circle (provided that the orientations of the curve and surface are well defined). The relative orientation between a (k+1)-cell (for example a face) and one of its bounding a k-cells (for example a curve) is called a **neighborhood** in [33] and takes three possible values: “left”, “right”, or “both”. The latter value is used for internal boundaries, such as a small disk inside a large ball or a bridge-edge connecting two loops of a face. If the face-edge neighborhood between a face F and an edge E is “left” we will say that “F is incident on E from the left”.

When the boundary cell is not in the manifold containing the higher-dimensional cell, the orientation of the manifold cannot be used to define a relative left and right orientation, and it may not always be possible to define a neighborhood. For instance, consider a self-intersecting surface that exhibits a singular edge where four branches of the surface meet. There is no easily defined “left” of the edge, even if the curve supporting the edge is oriented and if the surface is oriented everywhere except at the self-intersection edge.

Branch numbers could be used to distinguish the surface branches in the neighborhood of the edge. The branches may be defined as the connected components of the portion of the surface (without the self-

intersection curve) that lies inside a sufficiently small tube along the edge. However, the identification of these branches may prove extremely difficult, even for implicit surfaces.

5.3 Circular ordering of incident geometries

Several types of topological ordering relations may be established between cells.

Points on a curve are implicitly ordered by the orientation of the curve. For closed curves, this ordering is cyclic, unless an artificial singularity is introduced (for example the starting and ending point of a parameterization of the curve or a vertex), which permits to treat closed curves as if they were open. (Here the terms “closed” and “open” are not used with the topological meaning defined above, but simply to distinguish curves that form a “closed” loop from curves that do not.) By extension, such an ordering is used for the vertices and edges in a loop bounding a face. A loop is a alternating succession of edges and vertices. The ordering may in fact be used to represent the loop, especially for polyhedral models, where the edges are implicitly defined in terms of their end-vertices.

In the plane or on a manifold surface, edges may be ordered around their common vertex. To be more precise, when the vertex is the starting and ending point of the same edge, the two branches of the edge leaving the vertex appear as distinct entries in the ordering

Consider a sufficiently small circle around the vertex and assume that each edge lies on an oriented curve. We can induce an ordering of the curves around their common vertex by storing the cyclic sequence in which the small circle cuts the curves and, for each curve entry in this sequence, storing a binary flag indicating whether the curve was oriented left-to-right or right-to-left, as seen by an observer traveling on the circle. (The terms left and right may be precisely defined by an orientation of the supporting manifold surface. The circle must be sufficiently small such that there is only one point of contact between the curves in the disc enclosed by the circle.)

The geometric calculations involved in the computation of this ordering may prove very complex and numerically instable. For instance, ordering conic sections around a common point may require computing higher order derivatives, because tangent and curvature values at the contact point are insufficient. (An ellipse and a circle may be tangent to each other and exhibit the same curvature at the contact point.)

The order of faces around an edge, sometimes used to established what is called the “edge neighborhood” is very similar in nature to the order of edges around a vertex. However, the ordering of surfaces around a common intersection curve may change as one travels along the curve. The points where such an ordering changes correspond to zero-dimensional singularities which split the curve into cells (edges) of constant surface-ordering. Except for simple geometries, such as planar surfaces, the numeric computation of the ordering of surface branches around an edge-cell is far more delicate than ordering edges around a vertex.

5.4 Inclusion ordering

A sets of lower-dimensional cells may separate a manifold into two components. For example, a **loop** of edges and vertices may separate a plane into two parts (the interior and the exterior). Similarly, a **shell** of faces, edges, and vertices may separate the Euclidean 3-space into an interior and and exterior parts. Finally, a **vertex cone** of faces and edges may separate the neighborhood of a vertex into two parts. (The neighborhood of a vertex may be viewed as a sufficiently small ball around the vertex, not including the vertex itself.)

A set of nested loops separates a surface into several faces (connected open cells). Each one of these faces is incident on one or more loops and each loop separates exactly two adjacent faces incident upon the loop. A **face-adjacency graph** whose nodes correspond to faces and whose arcs correspond to loops separating adjacent faces is sufficient for capturing the nesting. When the graph is acyclic (i.e. when loops are

mutually disjoint), the graph may be represented as a **face-adjacency tree** by simply picking a root face and by propagating arc orientations away from the root.

In the plane, when loops are bounded, each loop separates the plane into a bounded interior and an unbounded exterior. The loops may then be ordered by saying that a loop A lies inside a loop B if A is contained in the interior side of B. The ordering may be captured in a **loop nesting tree** having the outer loop as root (i.e. the loop that is not contained inside any other loop). Nodes of the nesting tree are loops. The children of a loop L are all the other loops bounding the interior face of L. The nesting tree may be directly derived from the face-adjacency tree when the root face has only one bounding loop.

On a closed surface (a sphere for example), there is no a priori outer loop and in fact any face may be chosen as the root, yielding a different tree each time. It is thus preferable to use the face adjacency graph for capturing the acyclic nature of the partial ordering of loops.

Sets of shells and sets of vertex cones may be ordered in the same way as loops by replacing the nodes of the face adjacency graph by volume nodes that refer to 3-D cells (for ordering shells) or by solid cones of a vertex neighborhood (for ordering vertex cones).

Lower-dimensional elements (isolated vertices in the boundary of a face; dangling faces, edges, or vertices in the boundary of a volume; and dangling edges emanating from a vertex) may also be ordered using the face adjacency graph, the solid adjacency graph, or the vertex cone adjacency graph.

Note that since the connected components of a surface may be represented as genuine cells, the corresponding face adjacency graph is readily imbedded in the more general face-edge-vertex incidence graph, as discussed in the next section. Similarly, the shell nesting is directly available from the general volume-face-edge-vertex incidence graph. On the other hand, the vertex-cone nesting is not explicitly stored in a general adjacency graph since there may not be a unique cell corresponding to each vertex-cone.

5.5 Notation

We use the symbols V, E, F, and R to denote the (vertex, edge, face, and solid region) types of primary entity nodes in the incidence graph. The additional grouping entities for loops and shells are denoted L and S. Incidence types will be written using the concatenation of the letters of the basic types in lower case listed in decreasing order of dimension. For example, the type fe denotes all the associations between faces and their bounding edges.

Arrows indicate incidence relations (or their inverse) and may carry their cardinality (i.e. the number of referenced elements). Simple arrows denote variable number of incident elements. For example, $F \rightarrow E$ implies that faces point to a variable number of edges. A superscript over the arrow indicates the number of these references when it is constant. For example, $E \overset{2}{\rightarrow} V$ indicates that each edge points to exactly two vertices.

Sometimes, incidence references are organized by couples. For example, a face may have one reference to its bounding face-edge couples. We indicate such coupling with parentheses, as in $F \rightarrow (E,V)$.

Many data structures associate to each node of a particular type one or several pointers to other adjacent nodes of the same type. For example, consider pointers from an edge E to a subset of its neighboring edges. The number of such pointers is in general not constant. If we need only one such pointer per face, we can use the notation: $E \overset{F}{\rightarrow} E$. Extending the superscript notation even further, $E \overset{F \times V}{\rightarrow} E$, indicates that from each edge E there are pointers to other edges, one for each face-vertex pair such that the vertex is bounding E and the face is bounded by E.

When the multiple arcs emanating from a node are ordered (possibly in cyclic fashion), we use a double arrow "$\Rightarrow$" instead of "$\rightarrow$". For example, $F \Rightarrow V$ indicates that to each face is associated a list of links to

vertices that are ordered in a circular fashion around the face. (This ordering is often used for simply-connected faces.) For a face with several loops, we write: $F \rightarrow L \Rightarrow V$, ignoring, for simplicity, the fact that nested loops may also be partially ordered.

A entire graph will be described by a syntax that first lists all the node-types used in the graph and then all the types of arcs between these nodes. It is illustrated by the following example:

$$\{R, F, L, V \ : \ R \rightarrow F \rightarrow L \Rightarrow (F,V)\},$$

which indicates that the graph has nodes of type R, F, L, and V, and has a variable number of links from R to F and from F to L. It also has a variable number of link-pairs from L to V and to F that are ordered. (Regions are defined by a variable number of faces; each face is defined by a variable number of loops; each entry in the loop is a double reference to a vertex and to another face.)

5.6 Manifold models

We describe in this sub-section several data-structures for representing manifold models of polyhedra and of curved solids.

5.6.1 Face-vertex structure

For polyhedral models with simply connected faces, the edges are defined implicitly in terms of vertices and are thus not necessary (provided that vertices be ordered along loops). For faces without holes we may use an incidence graph based on face-vertex adjacency:

$$\{R,F,V \ : \ R \rightarrow F \Rightarrow V\},$$

and for multiply connected faces:

$$\{R,F,L,V \ : \ R \rightarrow F \rightarrow L \Rightarrow V\}.$$

5.6.2 Delta

The face-vertex structure may be enhanced with vertex-edge and edge-face back pointers to improve boundary traversal at a small storage cost [1]:

$$\Delta = \{R,V,E,F \ : \ R \rightarrow F \rightarrow V \rightarrow E \overset{2}{\rightarrow} F\} \quad \text{or} \quad \text{reverse-}\Delta = \{V,E,F \ : \ F \rightarrow E \overset{2}{\rightarrow} V \rightarrow F\},$$

and further extended for representing 3D triangulations:

$$\text{3D-}\Delta = \{V,E,F,R \ : \ R \overset{4}{\rightarrow} F \overset{3}{\rightarrow} E \overset{2}{\rightarrow} V \rightarrow R\}.$$

5.6.3 Edge-centered structure

Using edges as the stem of the representation, [40] proposes a different structure targeted at an optimal compromise between space and time efficiency:

$$\{F,E,V \ : \ V \Rightarrow E \overset{2}{\Rightarrow} (V,F) \ , \ F \Rightarrow E\}$$

Each edge points to a next edge around each abutting face. A face points to an ordered list of edges. This data structure only captures manifold topologies with simply-connected faces.

5.6.4 Winged-edge

The pioneering winged-edge representation developed by Baumgart [5, 6] is a bi-directional incidence graph to which ordering information is added as links between edges. The graph can only represent orientable manifold shells. Each edge-node points to four other edge-nodes that share with it a vertex and a face.

$$\text{winged-edge} = \{F,E,V : F \rightarrow E \overset{2}{\Rightarrow} V,\ E \overset{4}{\Rightarrow} E,\ V \rightarrow E \overset{2}{\Rightarrow} (F, E)\}.$$

The winged-edge data structure was extended by adding loops and shells ordering information [11]. In the late seventies a version of it was used by Braid, Eastman, Weiler, and Henrion in the development of GLIDE and another by Braid, Hillyard and Stroud in Cambridge, UK, in the development of BUILD, which later evolved into the ROMULUS system. A comparative analysis of the space and time costs associated with the different data structures for these extensions may be found in [1, 39].

5.6.5 FAHs

A FAH (Face-Adjacency Hypergraph) was used for modeling two-manifold boundaries [2]. The arcs of a FAH define face-face adjacency and simply correspond to edges. Hyperarcs are connecting a vertex to all of its edges. Thus, using E as a symbol for an arc, we have:

$$\text{FAH} = \{F,E,L,V : F \rightarrow L \Rightarrow (E,V),\ E \overset{2}{\Rightarrow} F,\ V \Rightarrow E\}$$

FAH's were subsequently extended for modeling objects at multiple levels of details, reflecting an iterative design process of incrementally adding features and details [14].

5.6.6 Half-edge

Since, in manifold shells, an edge is bounding two faces, it may be convenient to use two fe-nodes to represent each edge. To each fe-node corresponds a different orientation of the edge and is associated one of the two vertices that bound the edge. These fe-nodes have been used in many data structures and have been called “split-edges”, “half-edges”, “edge-uses”, and so on. These half-edges are usually linked to each other half-edges, either directly or through an edge-node so as to capture face-face adjacency [19, 24].

As shown in [1] half-edge data structures correspond to:

$$\text{Half-edge} = \{R,F,L,fe,E,V : R \rightarrow F \rightarrow L \rightarrow fe \overset{1}{\rightarrow} (V,E),\ E \overset{2}{\rightarrow} fe,\ V \overset{1}{\rightarrow} fe \overset{1}{\rightarrow} L \overset{1}{\rightarrow} F \overset{1}{\rightarrow} R\},$$

plus redundant pointers from R to all the L, V, E, and S nodes. The half-edge structure was used by Mäntylä and Sulonen in the GWB system.

5.6.7 Quad-edges

The winged-edge representation was extended by Guibas and Stolfi to subdivisions of orientable surfaces using a quad-edge data structure [15]. Simple primitive operators were provided to move from edge to edge around face loops and around vertices. Each edge refers to four of its neighbors.

5.6.8 Cell-tuples and V-maps

Brisson [7, 8] uses cell-tuples to extend the face-edge data structure [10, 21] and the quad-edge data structures [15] to higher dimensions. A cell-tuple is a combination of cells of all the dimensions, such that each cell (except the full-dimensional one) is in the boundary of the cell of the next dimension in the cell-tuple. For example, in 3D a cell tuple is defined by selecting a region, one of its faces, one of the

edges bounding the face, and a vertex bounding that edge. The switch(k) operator parameterized by the dimension k produces the other tuple that has the same elements, except for the element of dimension k, which is uniquely defined. For example, switch(0) exchanges the two vertices of the edge and switch(1) exchanges the two edges that bound the face and share the vertex. switch is its own inverse. A permutation of switch operators for dimension k and k+1. may be used to order k-cells and (k+1)-cells around (k—1)-cells on a (k+2)-cells. For example, an alternation of switch(1) and switch(2) may be used to visit the edges and faces of the cone of a shell formed around a vertex. Independently, Lienhardt [22, 23] defines n-dimensional generalized maps. For manifold objects, both Lienhardt's and Brisson's representations are equivalent.

5.7 Non-manifold structures

A technique for extending boundary graphs to non-manifold cases, where the solids have internal structures is based on the use of 3D region nodes, R_i, in the delimitation graphs. Each 3D regions is associated with a well defined subset of the boundary that forms a valid shell, or set of shells. (Typically, for simplicity, the solids are restricted to be connected, although not necessarily simply connected. More than one shell may be needed when the solids have internal holes.)

5.7.1 Edge-Less Adjacency Graph

The lack of face-face adjacency information in the simple face-vertex structure may be overcome by extending it into an ELAG (Edge-Less Adjacency Graph) for polyhedra.

In an ELAG, each pair of consecutive vertices in a loop define an edge. (The loop implies a circular ordering and thus the last vertex is followed by the first one. If the loop is non-manifold, several entries in the loop may refer to the same vertex.) We can arbitrarily associate this edge with the first one of the two vertex-entries, in the order of their appearance in the loop. Thus each vertex in a loop implicitly defines a face-edge pair, i.e. an element of type fe. Given a face F and an edge E in the boundary of a solid region R, the pair fe unambiguously defines at most two faces F_1 and F_2, that have E in their boundary and that are adjacent to F in the circular ordering around E of all the faces of R bounded by E. Thus, one can associate two face-pointers with each vertex-entry in each loop. We obtain the following specification:

$$\text{ELAG} = \{R,F,L,V \ : \ R \rightarrow F \rightarrow L \Rightarrow (V, 2F)\},$$

where the notation “$L \Rightarrow (V, 2F)$” indicates that each loop has a variable number of entries, each pointing to one vertex and two faces.

Given the orientations of the faces and of the edges and their neighborhood information with respect to R, we can add to the loop-face links neighborhood information that will enable us to traverse the boundary of a region R by walking from one face to the next in such a manner that the sector specified by these two faces in the vicinity of the edge is inside R and is not intersected by any other face adjacent to E.

Note that for manifold boundaries $F_1 = F_2$, and only one pointer is necessary:

$$\text{Manifold ELAG} = \{R,F,L,V \ : \ R \rightarrow F \rightarrow L \Rightarrow (V, F)\}.$$

When, in addition, faces are simply connected, we can merge the face-nodes with the loop-nodes altogether:

$$\text{Manifold ELAG with simply connected faces} = \{R,F,L,V \ : \ R \rightarrow F \Rightarrow (V, F)\}.$$

When restricted to manifolds shells, the ELAG concept was used in [26] for representing 2D triangulations by associating with each triangular face three pointer-pairs:

$$\text{Triangulation} = \{F,E : F \overset{3}{\Rightarrow} (V,F)\}.$$

The concept was further extended in [9, 13] to higher dimensional triangulations.

5.7.2 Facet-edges

Dobkin and Laszlo extend the approach of [15] to a subdivision of E^3. They define a facet-edge data structure [10, 21] in which each face F points to other adjacent faces that bound the two regions bounded by F.

The two-cycle requirement for shells of regularized solids, does not allow the use of “non-manifold” boundaries in the larger sense of the word, i.e., boundaries that are not two-cycles, because they have dangling faces or edges or because they define a partitioning of the solid into several connected regions. Internal structures may be specified by superimposing on the solid the internal dangling faces and edges.

5.7.3 Half-edges and hybrid-edges

Mantyla's Half-Edge and Kalay's Hybrid-Edge [19, 24] data structures may be used to represent dangling faces together with shells of 3D regions, and are thus useful for extending the topological domain beyond dimensionally homogeneous sets, and even to a limited class of non-manifold boundaries.

5.7.4 Radial-edge

In the winged-edge representation, to each face-edge-vertex and each edge-vertex incidence link is associated a link to a face. Thus, the winged-edge data structure has implicit $ev \overset{1}{\rightarrow} E$ and $fe \overset{1}{\rightarrow} E$ links. Using these auxiliary fe and ev entities as nodes in the graph, Weiler has defined the vertex-edge and the face-edge data structures [37], leading to the radial-edge data structure [38].

5.7.5 Vertex-based structure

The radial-edge data structure explicitly captures how faces are ordered around an edge and how edges are ordered around a face. It does not however provide any information on the vertex-cone nesting, which is important for a consistent traversal of the object's boundary at non-manifold vertices and is addressed in the NOODLES system by Gursoz, Choi, and Prinz [16, 17].

5.7.6 SGCs with NAILs

In a Selective Geometric Complex, introduced by Rossignac and O'Connor, each cell points to all of its bounding and incident cells. When the dimension of two incident cells differs by exactly one, and the lower-dimensional cell is in the manifold supporting the higher-dimensional one, the link is augmented with the (left, right, or both) neighborhood. Cells are tagged as active or inactive.

In addition to the incidence graph used for SGCs, to each edge and to each face node one can associate a two-dimensional table called “NAIL” (for Next cell Around a cell In a cell List). For an edge e, the table is indexed by a reference to a vertex v bounding e and by a reference to a face f incident upon the edge. The corresponding entry e.NAIL(v,f) in the table contains a reference to the next edge around v in f. Where “around” is defined with respect to the orientation of the surface supporting f. For a face f, the table is indexed by a reference to an edge e bounding f and by a reference to a 3-cell r incident upon f. The corresponding entry f.NAIL(e,r) in the table contains a reference to the next face around e bounding r.

6.0 CONSTRUCTIVE NON-REGULARIZED REPRESENTATIONS

A Constructive Solid Geometry (CSG) representation defines a recipe for a solid as a selection of 3-D cells from a decomposition of space induced by the CSG primitives (half-spaces or volume primitives). The operations used to control the selection are the regularized Boolean union, intersection, and difference. A regularized operation returns the closure of the interior of its set theoretic counterpart [27, 28, 36]. Note that, if the arguments are regular, then the result of a set-theoretic union is identical to the result of the regularized union. Furthermore, if the primitives are regular, then the result of an expression involving regularized Booleans is identical to the closure of the interior of the same expression composed of the corresponding set-theoretic operators.

Using this recipe as a fundamental representation instead of a boundary representation has many advantages. The non-evaluated (CSG) representation is always valid and can be easily parameterized. Editing a non-evaluated representation is simple and very efficient; it suffices to change the expression. Non-evaluated representations are less verbose than their evaluated counterparts and lead to considerable storage savings. Finally, many solid modeling algorithms work directly on CSG representations through divide-and-conquer and are numerically more reliable than their counterparts that work on evaluated boundary representations. We discuss in this section several variations of the traditional CSG representation models.

A representation scheme that covers a rich set of inhomogeneous geometric objects and operations was proposed in [34]. It is called Constructive Non-Regularized Geometry (CNRG). CNRG trees represent objects that are aggregates (i.e., unions) of mutually disjoint regions. Each region is a set in $\mathbf{R}^n$ and needs not be connected, regular, or even dimensionally homogeneous. The leaves of a CNRG tree correspond to parameterized primitive shapes such as volumes, faces, curve segments, or points. Internal nodes correspond to intermediate CNRG objects and are associated with topological and Boolean operations.

SGCs provide a model for representing non-regularized internally-segmented sets as a collection of connected open cells defined recursively in terms of their boundaries. CNRG trees yield an alternate representation for these sets as a collection of regions defined in terms of original primitive sets. Regions of CNRG objects need not be open nor connected and typically correspond to unions of SGC cells of various dimensions. CNRG models should be viewed as a primary model for user interaction because they support a high level vocabulary for expressing operations and regions, and because the CNRG trees are, similarly to CSG trees, easy to edit and archive. SGC models should be automatically derived from CNRG representations, as boundary representations are derived from CSG trees.

The scheme proposed in [34] extends CSG in several ways:

1. It uses standard (non-regularized) Boolean operations and topological operations—boundary, closure and interior. The regularized Boolean operations can be implemented in this scheme as three-operator sequences: standard Boolean, followed by interior and closure.
2. It admits as primitives non-solid objects such as points, curves, or surfaces, and higher-dimensional objects.
3. It introduces a new operator, called aggregation, which constructs structured objects composed of several regions. The aggregation operator is a formally-defined and more sophisticated version of the “assembly” operator provided by modelers such as PADL-2. Structured objects are not sets. They are collections of sets, much like the cell complexes of algebraic topology [29]. Structured objects, also called CNRG objects, or simply objects, also have underlying sets, as cell complexes do. The underlying set of a CNRG object is the union of all the regions of the object, and therefore it is a set with no structure or “internal boundaries”.
4. It defines Boolean and topological operations on structured objects.

6.1 Semantics of CNRG operators

A CNRG object is a set of pairwise disjoint possibly non-regular or disconnected sets, called **regions.**

The **set,** pA, of a CNRG object, A, is the union of the sets of its regions.

A CNRG tree is a rooted directed acyclic graph that represents a CNRG object. Leaves of the tree are CNRG primitives, which may be composed of more than one region. For simplicity, we assume that each primitive is given in its absolute position, although in practice, rigid body transformation nodes may be used. Internal nodes represent intermediate CNRG objects obtained by applying Boolean, topological, simplification, or filtering operators to the CNRG objects represented by their child-nodes.

To simplify the following discussion, we use "|" to denote a "gluing" or aggregation binary operator that takes two disjoint regions, aggregates of regions (all of which are pairwise disjoint), or disjoint CNRG objects and produces a CNRG object that aggregates all the regions. Note that expressions involving only aggregate operators are order-independent.

An uppercase letter denotes a CNRG object, and each of the object's regions is denoted by the same letter with a subscript. For example, A_1 and A_2 are two regions of the same CNRG object, A. If A is composed of only these two regions, we write, $A = \{A_1|A_2\}$. By definition, A_i and A_j are disjoint for $i \neq j$. A single-region object, A, is considered distinct from its region A_1. We write $A = \{A_1\}$. Note that $A_1 = pA$ for single region objects.

In the following, we assume that S, A, B, C and D are CNRG objects. Furthermore, we often use C or S to denote the objects produced by applying to A (and to B) a Boolean or topological CNRG operator.

A and B are **disjoint,** if and only if the intersection of their sets, pA and pB, is empty.

Given two regions, A_i and B_j, $A_i \cap B_j$ denotes their intersection and $A_i - B_j$ their difference in the standard set-theoretical sense. Note that $A_i \cap B_j$ and $A_i - B_j$ are single regions that may be empty, disconnected, dimensionally inhomogeneous, and not closed.

A region is said to be **contained** in an object if it is contained in the set of the object. It need not correspond to the union of any subset of the object's regions.

Given n disjoint sets, A_i, the **aggregation** operation, denoted "|", creates the corresponding CNRG object: $A = \{A_1 | A_2 | \ldots | A_n\}$.

The **simplification,** sA, of A is a CNRG object with a single region: the set pA. Thus, $sA = \{pA\}$.

The **complement,** cA, of A is an object composed of a single region that is the set complement of pA. Hence, $cA = \{\overline{pA}\}$.

The **union,** A + B, is an aggregate of regions of the following three types: $A_i \cap B_j$, $A_i - pB$, and $B_j - pA$, for all combinations of regions, A_i, of A and regions, B_j, of B. Potentially each region of A is split into two sets: the part in B and the part outside of B. The second set is a single region. The first set may be decomposed according to the decomposition of B into regions. Union produces a subdivision of $(pA) \cap (pB)$ that is compatible with the decomposition of A and B into regions. We call it "union" because the set p(A + B) equals the set theoretic union, $pA \cup pB$.

The **intersection,** A*B, of A and B is the aggregate of all regions of the type $A_i \cap B_j$. A region, A_i, of A is truncated to $A_i \cap pB$, and is subdivided according to the subdivision of B into regions. Consequently, $p(A*B) = (pA) \cap (pB)$, which justifies the name for this operator.

The **difference,** A\B, is the aggregate of all regions of the type $A_i - pB$. Clearly, $p(A\backslash B) = (pA) - (pB)$. It follows from the definition of union, intersection, and difference that $A + B = \{(A\backslash B) | (A*B) | (B\backslash A)\}$.

The topological **interior,** iA, of A in $\mathbf{R}^n$ is the aggregate of regions, $A_i \cap$ interior(pA), that are the intersection of the regions of A with the topological interior of A in $\mathbf{R}^n$. Note that, although iA is always full-dimensional, regions of iA need not be full-dimensional. Thus the *interior* operator returns a subset of the original object and preserves its internal decomposition into regions. The set, piA, of the interior of A equals the topological interior of pA.

The **closure,** kA, of A, is the aggregate composed of all the regions of A plus a single new region defined as the difference between the topological closure of pA and pA itself. Thus, we can write: $k\{A_1, ..., A_n\} = \{A_1, ..., A_n, | (closure(pA) - pA)\}$, and pkA equals the topological closure of pA.

The topological **boundary,** ∂A, of A is defined as: ∂A = kA\iA. The boundary operator does not necessarily return a single-region object. Note that p(∂A) equals the topological boundary of pA.

The **regularized** version, rA, of A is defined as kiA. The set, prA, spanned by rA corresponds to a regularized solid as defined in [27] and equals rpA. Note that regularization does not imply simplification (i.e., a regularized object may be composed of many non-regularized regions). However, taking the boundary, C, of a regularized object, A, will produce a lower-dimensional object whose set, pC, is the topological boundary of the set of the regularized object, prA.

6.2 Evaluation

CNRG graphs may be evaluated directly or converted into an expanded SGC form, where SGC cells are grouped to form sets that represent CNRG regions.

Point inclusion test for a particular CNRG region may be carried out using an extension of the divide-and-conquer techniques popular with CSG trees (see [34] for details). On the other hand, it may be advantageous to compute and store the SGC representation of the non-manifold structure defined by a CNRG expression. The computation may be simply carried out as an incremental (bottom-up) execution of the CNRG operations.

Each one of these operations may be constructed from combinations of the primitive SGC operations:

- Subdivision, which takes two SGCs and adds to the boundary of each cell of each SGC its lower-dimensional intersections with cells of the other SGC. This addition may result in splitting the cell into separate connected components.
- Selection, which activates or deactivates cells based logical predicated involving topological, geometric, connectivity filters and inclusion in specific regions, and which also assigns cells to the regions of the resulting SGC.
- Simplification, which simplifies the representation of each region by deleting or merging its cells.

The algorithms for these operations have been described in more detail in [33] without limitations to any particular geometric domain.

7.0 CONCLUSION

These notes present the key concepts for analyzing the topological limitations of geometric representation schemes independently of the geometric domain. They also overview a number popular data structures for manifold and non-manifold boundary representations and an extension of CSG representations to non-regularized sets. They promote CNRG expressions for designing and editing non-manifold geometric structures and SGC representations and associated algorithms for computing and storing a boundary representation of these structures.

8.0 APPENDIX: REVIEW OF KEY TOPOLOGICAL CONCEPTS

This appendix provides an informal summary of the key topological notions relevant to this notes. Formal and complete definitions may be found in many textbooks on Algebraic and Combinatorial Topology ([18, 25, 35]).

A **topological space** is a set W with a choice of a class of subsets of W (its **open sets**), each of which is called a **neighborhood** of its points, such that every point of W is in some neighborhood and that the intersection of any two neighborhoods of a point contains a neighborhood of that point. The three-dimensional Euclidean space, in which the models discussed here are constructed, is so "topologized".

The **interior** of a set S is the set of points having a neighborhood in S. (Intuitively the interior of a 3-D set is is the whole set except for points on its surface, or more precisely on its boundary, defined later.). A set is **open** if it contains a neighborhood for each one of its points.

The **complement** of a set S in R is the set of points of R that are not in S. The **closure** of S is the complement of the interior of S. (Intuitively, the closure of a set 3-D includes the bounding surfaces, whether they were part of the original set or not.) S is **closed** if its complement is open. (Intuitively, a 3-D set is closed if it includes its surface.)

The **boundary** of S is the difference between its closure and its interior. (Intuitively, for a 3D set, it is the surface. However, if S is the result of subtracting the center point from a ball, then the boundary of S is not only the spherical surface, but also the missing point.)

Two sets are **homeomorphic** if one is the image of the other through a bijective map that is continuous and has a continuous inverse. (Intuitively, we can map each point of any one of these two sets into a unique point of the other set in such a way that they have topologically identical neighborhoods. It does not necessarily mean that we can deform one object in a continuous manner to produce the other object.)

An **open k-ball** of radius r around a point s in a k-dimensional Euclidean space is the set of points at a distance less than r from s, where the distance between two points is defined as the Euclidean norm of the vector separating the two points.

The **dimension** of a set is the minimum dimension of the topological spaces containing the set. A set is **full-dimensional** (with respect to some topological set) if its interior is not empty. An open set is thus always full-dimensional. In a topological space of dimension n, a set of dimension k lower than n is **relatively open** if it is homeomorphic to an open k-ball as a subset of some topological space of dimension k. (A **relative topology** for a set S as a subset of a topological space W may be inherited from W by considering as the open sets of S as the intersections of S with the open sets of W.) For example, a face F has no interior in three-space. However, the **relative interior** of F, defined as F without its bounding edges and vertices is relatively open. This "relativity" concept may be also applied to the boundary: the **relative boundary** of F is its bounding edges and vertices (i.e., the boundary of F in the relative topology of the two-manifold, or surface, supporting it).

A set is **regular** if it is equal to the closure of its interior. A regular set is thus closed and does not contain boundary elements that do not have in their neighborhood any interior point of the set. A set is **s-regular** if it is equal to the interior of its closure. An s-regular set is therefore open and does not contain cracks or lower-dimensional holes. The complement of an s-regular set is regular. S-regular sets were used in [3] for modeling assemblies of sets that share faces.

Two sets are **disjoint** if their intersection is empty, i.e.: if no point belongs to both sets. A set is **connected** if any two of its points may be joined by a continuous curve inside the set. A connected set cannot be divided into two sets, such that the closure of one be disjoint from the other. The (maximally) **connected components** of a set are uniquely defined. A set is **interior-connected** if its interior is connected. Two sets are **quasi-disjoint** if their intersection is not empty, but is not full-dimensional. (For example, two cubes touching at a vertex for a connected set that is not interior-connected. The two cubes are quasi-disjoint.)

A **closed k-ball** of strictly positive radius r around a point s is the set of points at a distance from s less or equal to r. A **k-sphere** is the boundary of the corresponding k-ball. A **k-half-ball** is the intersection of a k-ball with a planar half-space containing s. A **half-space** is a full-dimensional set of points usually

assumed to be connected and regular, and defined by an algebraic or analytic inequality. (A strict inequality defines an open half-space.) The set of points where the first coordinate is positive or null is a good example of closed a planar half-space through the origin.

A **k-manifold** is a set of points whose neighborhoods are homeomorphic to an open k-ball. A **k-manifold with boundary** is a set of points whose neighborhoods are homeomorphic to an open k-ball or to a half-k-ball.

An open set is **simply connected** if it is homeomorphic to an open ball.

A **cavity** in a bounded (i.e. non infinite) set S is a bounded connected component of the complement of S. In two dimensions, cavities correspond to the intuitive notion of holes. In three dimensions, the term **hole** is ill-defined. We prefer to use the term cavity (such as the one found inside a soccer ball) and the term **handle,** which denotes a tunnel or "way through" the set (such as the handle of a tea cup). The number of holes through a set is important for assessing whether two sets are homeomorphic, but does not reflect how they are embedded in in three-space.

The **zero Betti number,** b_0, denotes the number of connected components in a set. The **first Betti number,** b_1, (also called 1-connectivity) specifies the number of handles in a 3D set. It may be defined as the maximum number of "cuts" through the set that may be made without disconnecting it (i.e. producing two separate pieces). A cut through a set may be thought of as the surface swept by drawing a closed curve on the boundary of the solid and contracting it to a single point while maintaining it inside the set. For example the 1-connectivity is 0 for a ball, and 1 for a solid torus, and 2 for the surface of a torus (the zero Betti number for a closed surface is twice the zero Betti number for the solid bounded by the surface). The **second Betti number,** b_2, denotes the number of cavities.

The **genus** of a surface is the maximum number of closed curves (contained in it) that may be subtracted from it without disconnecting it. The genus, also denotes the number of handles, H. One closed surface may be mapped into another by a continuous bijection if they have the same genus. The genus of a closed surface is half its first Betti number and is also equal to the Betti number of the 3D set bounded by the surface.

A **k-simplex** is the convex hull of k+1 linearly independent points in R. An **m-face** of a k-simplex is the convex hull spanned by m of the k points of the k-simplex and is an m-simplex. All k-simplices are closed and homeomorphic to a closed k-ball. The boundary of a k-simplex is homeomorphic to a k-sphere. A **simplicial complex** is a finite union of simplices glued together such that for any pair (A,B) of these simplices: either A and B are disjoint, or A and B share a common m-face, or A is an m-face of B, or B is an m-face of A (for some m). The **polytope** of a simplicial complex is the union of the sets of all of its simplices.

A **CW complex** is a finite union of mutually disjoint relatively open cells, each being homeomorphic to an open ball and having for boundary the union of the sets of other cells in the complex. The intersection of the closure of two cells is either empty or is the union of other cells in the complex. CW complexes generalize the notion of simplicial complexes because their cells are not restricted to simplices (i.e. points, line segments, triangles, and tetrahedra), but may include relatively open sets of arbitrary shape and of an arbitrary finite number of bounding simplices (k-faces), provided that the 2-D cells have no holes and that the 3-D cells have no handles.

Two distinct k-cells of a (simplicial, CW, or geometric) complex are **adjacent** if they share one or more bounding cells. A (k+1)-cell c is **incident** on a k-cell b if b is a bounding cell of c.

For a two-dimensional two-manifold closed surface without boundary made of F faces, E edges, and V vertices, the **Euler characteristic** (or Euler number) is equal to $V - E + F$.

For a 3-D manifold CW complex (a set bounded by a two-manifold surface) made of R 3-D cells, F faces, E edges, V vertices, the Euler characteristic is a topological invariant independent of the subdivision subdivision and is equal to $V - E + F - R$. The **Euler equation** states that the Euler characteristic is equal to $b_0 - b_1 + b_2$. Since $b_0 + b_2$, the number of connected components plus the number of cavities is the number of shells, S, in the surface bounding the 3D set, we have for a 3D set:

$$V - E + F - R = S - H,$$

where H is the number of handles through the entire 3-D set.

The Euler characteristic of a surface in 3-D is twice the Euler characteristic of the solid bounded by the surface. Since b_0, the number of shells is equal to the number of cavities, b_2, and since the maximum number of non-separating cuts in the surface is twice the number of handles ($b_1 = 2H$), the Euler equation for a surface is:

$$V - E + F = 2(S - H).$$

Since V, E, F, R are readily available and S may be easily computed by constructing connected components, the above formulae yield a practical means for computing H! The formulae are restricted to manifold sets, although they can be extended to non-manifold CW complexes by incorporating the counts of various on-manifold situations, such as the additional cones of faces incident upon a vertex.

We can verify the Euler equation for a solid torus represented as a CW complex. We need to introduce a vertex and two curves that will split the surface of the torus into a single face whose relative interior is homeomorphic to an open disk (2-D ball). Furthermore, we need to introduce a cut-face through the interior of the torus, so that the 3-D interior be homeomorphic to an open ball. The Euler equation for the resulting complex has: $V = 1$, $E = 2$, $F = 2$, $e = 0$, $R = 1$, $f = 0$, $S = 1$, $H = 1$.

The popular geometric primitives, such as cylinders or cones, cannot be represented directly as simplicial complexes nor even as CW complexes if their faces, edges, and vertices are not simply connected. Artificial bridge-edges and cut-faces may have to be introduced. **Geometric Complexes** [33] generalize the concept of CW complexes allowing cells to be open sets of arbitrary genus (rather than being restricted to be homeomorphic to open balls). For example, a torus may be represented as a geometric complex by only two cells: its 3-D interior and its 2-D boundary.

Simplicial complexes, CW complexes, and Geometric Complexes are closed, i.e.: they contain the boundaries of all of their cells. A **Selective Geometric Complex** (also called SGC) developed in [33] further extends the notion of a geometric complex by associating with each cell an attribute stating whether the cell is **active** (i.e. contributes to the final set) or not. For example, an open sphere without its center point may be modeled by an SGC with three cells: the 3-D interior without the point, the 2-D bounding sphere, and the central vertex. Only the interior is active.

9.0 References

1. Ala, S. Universal Data Structure: A tool for the Design of Optimal Boundary Data Structures. In J. Rossignac and J. Turner, editors, *ACM/SIGGRAPH Sym. on Solid Modeling Foundations and CAD/CAM Applications ACM Symp. on Solid Modeling Foundations and CAD/CAM Applic.*, 13-24, ACM Press, Order number 429912, Austin, TX, June 5-7 1991.
2. Ansaldi, S., De Floriani, F. and Falcidieno, B. Geometric Modelling of Solid Objects by Using a Face Adjacency Graph Representation. *ACM Computer Graphics*, 19(3):131-139, July 1985.
3. Arbab, F. Set Models and Boolean Operations for Solids and Assemblies. Computer Science Dept., Univ. of S. Calif., Los Angeles, CA. July 1988.

4. Bardis, L. and Patrikalakis, N. Topological Structures for Generalized Boundary Representation. MIT, Design Laboratory Memo 91-18. 1992.
5. Baumgart, B.G. Winged Edge Polyhedron Representation. *AIM-79, Stanford Univ.*, Report STAN-CS-320, 1972.
6. Baumgart, B. A Polyhedron Representation for Computer Vision. *AFIPS Nat. Conf. Proc.*, 44:589-596, 1975.
7. Brisson, E. Representing Geometric Structures in D-Dimensions: Topology and Order. *Fifth ACM Symposium on Computational Geometry, Saarbruchen,*, 218-227, June 1989.
8. Brisson, E. *Representation of d-Dimensional Geometric Objects*, PhD thesis. Dept. of Compt. Sci. and Engr. University of Washington, Seattle, WA, 1990.
9. Cattani, C. and Paoluzzi, A. Solid Modeling in Any Dimension. In Dip. di Mathematica, Univer. "La Sapienza", Rome, Italy, editor, *Report*, Univ. 'La Sapienza, Rome, Italy, 1989.
10. Dobkin, D.P. and Laszlo, M.J. Primitives for the Manipulation of Three-Dimensional Subdivisions. *Third ACM Symp. on Computational Geometry, Waterloo, Canada*, 86-99, June 1987.
11. Eastman, C.M. and Weiler, K. Geometric Modelling Using the Euler Operators. *Proc. 1st Annual Conf. on Computer Graphics in CAD/CAM*, 248-259, 1979.
12. Ellis, J.L., Kedem, G., Lyerly, T.C., Thielman, D.G., Marisa, R.J. and Menon, J.P. The Ray Casting Engine and ray representations. In J. Rossignac and J. Turner, editors, *ACM Symp. on Solid Modeling Foundations and CAD/CAM Applic.*, 255-268, ACM Press, Order number 429912, Austin, TX, June 5-7 1991.
13. Ferrucci, V. and Paoluzzi, A. Extrusion and Boundary Evaluation for Multidimensional Polyhedra. *Computer-Aided Design*, 23(1):40-50, January/February 1991.
14. Floriani, L. and Falcidieno, B. A Hierarchical Boundary Model for Solid Object Representation. *ACM Trans. Graphics*, 7(1):42-60, 1988.
15. Guibas, L. and Stolfi, J. Primitives for the Manipulation of General Subdivisions and the Computation of Voronoi Diagrams. *ACM Trans. on Graphics*, 4(2):74-123, April 1985.
16. Gursoz, E. Levent and Prinz, F.B. Node-based Representation of Non-Manifold Surface Boundaries in Geometric Modeling. In M. Wozny, J. Turner and K. Preiss, editors, *Geometric Modeling for Product Engineering, Proc. of the*, North-Holland, 1989.
17. Gursoz, E., Choi, Y. and Prinz. F. Boolean Set operations on Non-Manifold Boundary Representation Objects. *Computer-Aided Design*, 23(1):33-39, January/February 1991.
18. Henle, M. *A Combinatorial Introdution to Topology*. W.H. Freeman and Co., San Francisco, 1979.
19. Kalay, Y.E. The Hybrid Edge: A Topological Data Structure for Vertically Integrated Geometric Modeling. *Computer-Aided Design*, 21(3): 130-140, 1989.
20. Kaufman, A. *Volume Visualization*. IEEE Computer Society Press, Los Alamitos, CA, 1991.
21. Laszlo, M.J. *A Data Structure for Manipulating Three-Dimensional Subdivisions*, PhD thesis. Princeton Univ., August 1987.
22. Lienhardt, L. Topological Models for Boundary Representation: A Comparison With N-dimensional Generalized Maps. *Computer-Aided Design*, 23(1):59-82, January/February 1991.
23. Lienhardt, P. Subdivision of N-Dimensional Spaces and N-Dimensional Generalized Maps. *ACM Sumposium on Computational Geometry*, 228-236, Saarbruecken, Germany, June 1989.
24. Mäntylä, Martti. *An Introduction to Solid Modeling*. Computer Science Press, Rockville, Maryland, 1988.
25. Mendelson, B. *Introduction to Topology*. Volume 3rd ed. Allyyn and Bacon, Inc,, Boston, MA, 1975.
26. Paoluzzi, A., Ramella, M. and Santarelli, A. Boolean Algebra Over Linear Polyhedra. *CAD*, 21(8):474-484, 1989.
27. Requicha, Aristides A.G and Tilove, Robert B. Mathematical Foundations of Constructive Solid Geometry: General Topology of Regular Closed Sets. In Production Automation Project, editor, *Tech. Memo.*, No. 27a, Univ. of Rochester, June 1978.
28. Requicha, Aristides A.G. and Voelcker, Herbert B. Constructive Solid Geometry. *Production Automation Project, Univ. of Rochester*, Tech. Memo No.25, November 1977.
29. Requicha, A.A.G. Mathematical Models of Rigid Solid Objects. *Technical Memo*, No.28, Univ. of Rochester, November 1977.

30. Requicha, A.A.G. and Voelcker, H.B. Boolean Operations in Solid Modelling: Boundary Evaluation and Merging Algorithms. *Proc. IEEE*, 73(1):30-44, January 1985.
31. Rossignac, J. Representing Solids and Geometric Structures. In S. Kodiyalam, M. Saxena, editor, *Geometry and Optimization Techniques for Structural Design*, 1-44, Computational Mechanics Publications,, Southhampton, 1993.
32. Rossignac, J. Through the cracks of the solid modeling milestone. In S. Coquillart, W. Strasser, P. Stucki, editor, *From object modelling to advanced visualization*, 1-75, Springer Verlag, 1994. (State of the art report, Eurographics'91, Vienna)
33. Rossignac, J.R. and O'Connor, M.A. SGC: A Dimension-independent Model for Pointsets with Internal Structures and Incomplete Boundaries. In M. Wozny, J. Turner, K. Preiss, editor, *Geometric Modeling for Product Engineering*, 145-180, North-Holland, Rensselaerville, NY, September 1989.
34. Rossignac, J.R. and Requicha, A.R. Constructive Non-Regularized Geometry. *Computer-Aided Design, Special Issue: Beyond Solid Modeling*, 23(1):21-32, January/February 1991.
35. I. M. Singer and J. A. Thorpe. *Lecture Notes on Elementary Topology and Geometry*. Scott, Foresman, Glenview, IL, 1967.
36. Tilove, R.B. and Requicha, A.A.G. Closure of Boolean Operations on Geometric Entities. *Computer-Aided Design*, 12(5):219-220, September 1980.
37. Weiler, K. Edge-based Data structures for Solid Modeling in Curved-Surface Modeling Environments. *IEEE Computer Graphics and Applications*, 5(1):21-40, January 1985.
38. Weiler, K.J. The Radial Edge Structure: A Topological Representation for Non-Manifold Geometric Modeling. In M. Wozny, H. McLaughlin and J. Encarnacao, editors, *Geometric Modeling for CAD Applications*, Springer Verlag, May 1986.
39. Woo, T.C. A Combinatorial Analysis of Boundary Data Structure Schemata. *IEEE Computer Graphics and Applications*, 5(3):19-27, March 1985.
40. Woo, T.C. and Wolter, J.D. A Constant Expected Time, Linear Storage Data Structure for Representing Three-Dimensional Objects. *IEEE Trans. Systems, Man and Cybernetics*, SMC-14(3):510-515, May/June 1984.

Specification, representation, and construction of non-manifold geometric structures

Jarek Rossignac
IBM Research

Context

- INPUT
  - Sample surface points
  - Space meshes (FEM, voxels)
  - Slices, ray-reps
  - CAD construction steps
  - Procedural models
- REPRESENTATION
  - Geometric primitives (surfaces, curves, points)
  - Topological relations (adjacency, boundary of)
  - Ordering (next vertex, edge, face, branch)
  - Pointsets and structures (non-manifold, features)

Content

- Linear decomposition
- Hierarchical specification
- Constructive Non-Regular Geometry
- Boundary representations
- Selective Geometric Complexes
- SGC operations
- Curved geometry

Lines decompose space into simplices

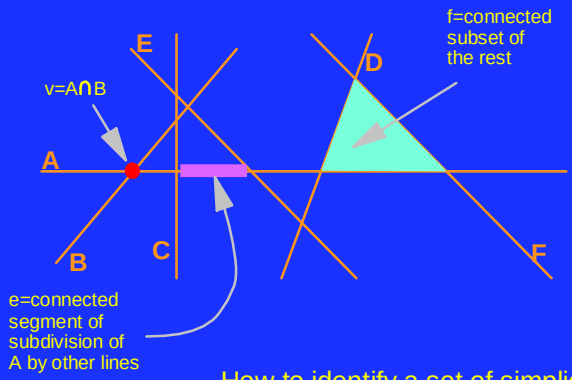

How to identify a set of simplices?

Use Boolean expressions

Half-spaces

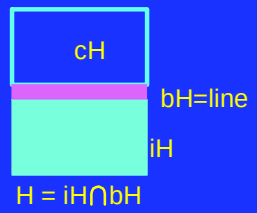

Operators

∪ = union
∩ = intersection
− = difference
b = boundary
i = interior
c = complement
k = closure
0 = zero cells
1 = one cells...

Two operators suffice,∩ and c, but all are convenient

Convention

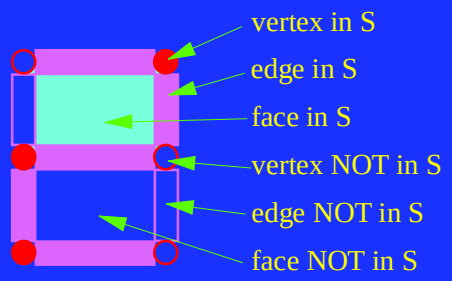

Simplices NOT in S may be omitted

Topological set operators

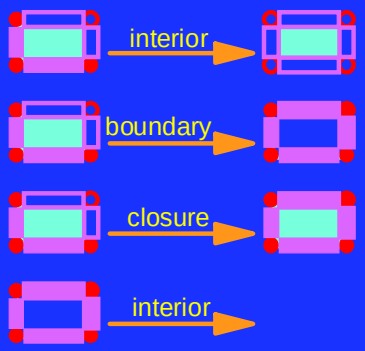

Any collection of simplices

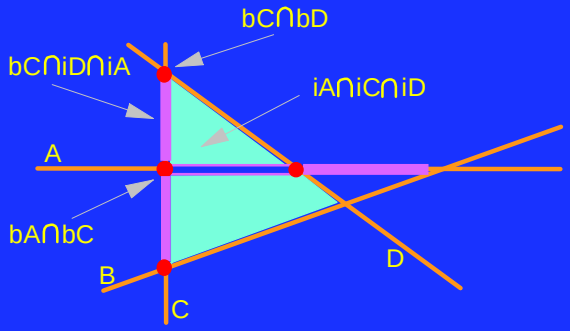

may be expressed using half-space combinations,
which should be computed from higher-level input

Hierarchical construction graph

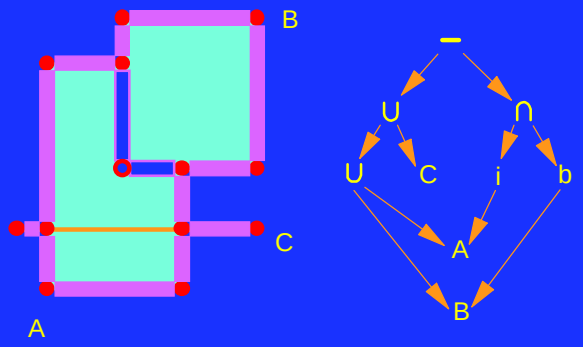

Internal structure

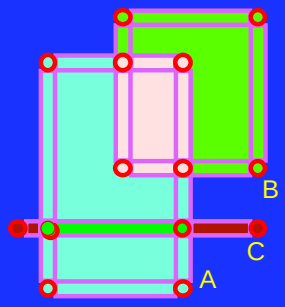

A+B+C

"+" does union of sets but preserves internal structures

Here 5 regions:

B - A - C
A ∩ B - C
A - B - C
A ∩ C - B
C - A - B

out of the 7 possible

Regions are broken into simplices

Boolean CNRG operators

S= (B+C)

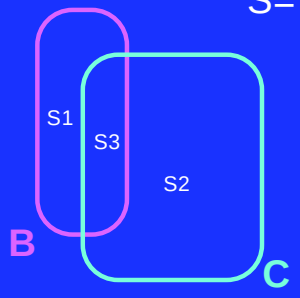

+ yields 3 regions

Boolean CNRG operators

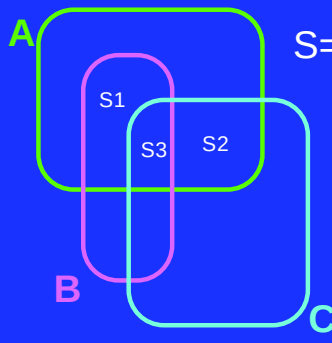

S=(A&(B+C))

& trims down these 3 regions to the interior of A

Boolean CNRG operators

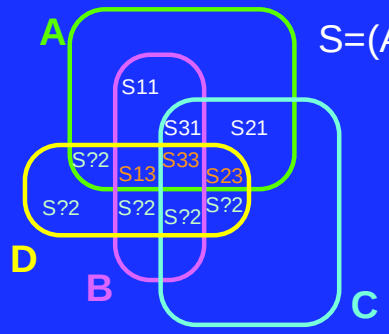

S=(A&(B+C))+D

S23

S?2

don't care for
D - (A&(B+C))

+ splits each one of the 3 regions: iD and cD
+ adds a 7th region: S?2 (the rest of D)

Topological CNRG operators

2 regions

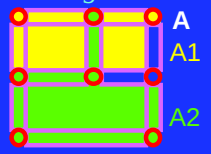

A
A1
A2

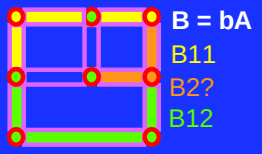

B = bA
B11
B2?
B12

2 regions (trimmed)
+ new 3rd region

2 regions (trimmed)

I = iA
I1
I2

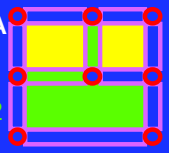

K = kA
K11
K2?
K12

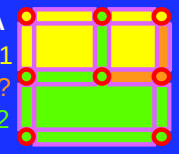

2 original regions
+ new 3rd region

Constructive Non-Regular Geometry

Operators on aggregates of disjoint regions:

- Aggregation — *combines disjoint objects*
- Simplification — *returns single region*
- Complement — *set complement*
- Interior — *restricts each region*
- Exterior — *interior of complement*
- Boundary — *restricted region + one*
- Closure — *old regions + one*
- Intersection — *pairwise combinations*
- Difference — *restricted regions*
- Union — *3 combinations*
- k-cells — *only cells of dimension k*

Features of CNRG objects

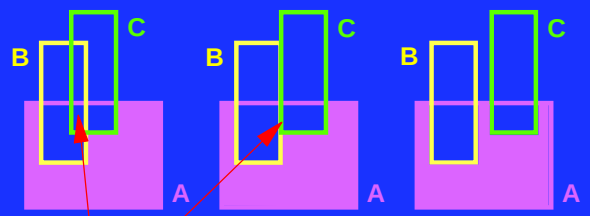

S = (A - B) - C

The feature of interest here is in cS: **S33 = A&B&C**
Extended signature semantics: treat - as a +

CNRG summary

- Compact specification
- Hierarchical (bottom-up) design
- Full topological coverage
- Preserves internal structure
- Signature identifies each region
- Regions have arbitrary topology
- Region existence and connectivity can only be assessed through evaluation

What is a valid polygon?

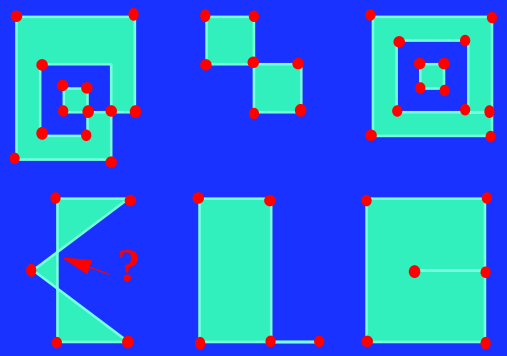

Wrong question! First, ask: "What is a polygon?"
Then select a representation scheme.

A definition

A polygon is a:

- connected
- bounded
- subset of the plane
- equal to the interior of its closure
- having as boundary a finite union of pairwise disjoint cells:
  - crossings
  - vertices
  - edges

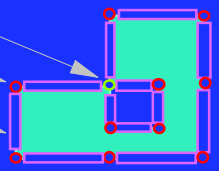

BRep of a polygon

Geometry defines:

- crossings
- vertices
- edges
- loops

crossing = non manifold
vertex = non smooth
edge = connected
orientation = first left
loop = max connected subsets of Bdry

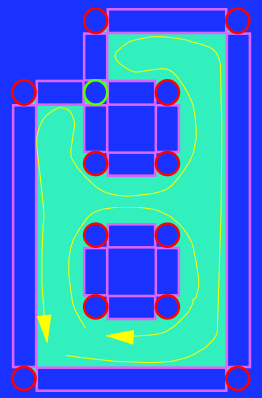

Possible representation of a polygon

- List of points (coordinates)
  - List of loops (external + holes)
    - Each loop = cyclic list of point uses

This representation is completely defined for a given geometry (provided that we choose an ordering scheme for points and uses).

Representation schemes

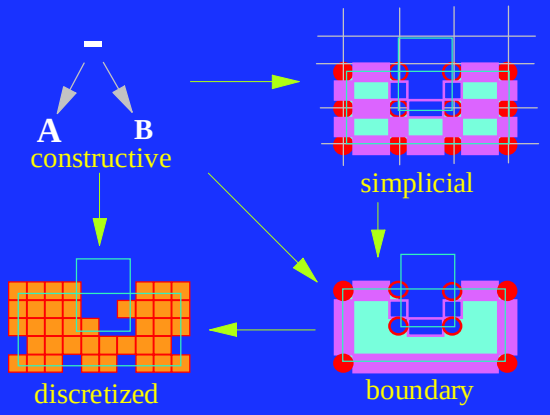

	Recipe	Voxels	Cells	BRep
Data size	Compact	Huge	Big	Medium
Speed	Slow	Very fast	Medium	Fast
Code	Elegant	Simple	Complex	Very hard
Design	Efficient	Tedious	No way!	Tricky

Topological generalization of a polygon

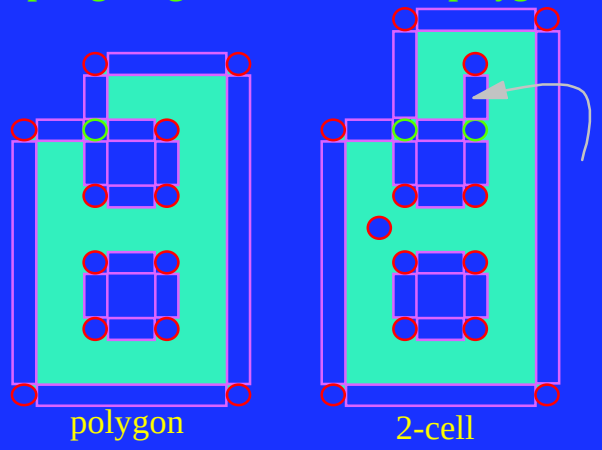

Generalized 2-cell

- connected
- bounded
- relatively open
- subset of manifold
- bounded by a finite union of pairwise disjoint 1-cells and 0-cells

Representation:

- reference to supporting surface
- list of bounding vertices
- list of bounding edges (with nbhd)

Selective Geometric Complex

- Object = list of pairwise disjoint cells
  - Cell = connected, relatively open, bounded, subset of a manifold
  - Boundary of each cell = union of other cells in the object
- Selection of "active" cells
- Features = different selections

Internal structure in SGCs

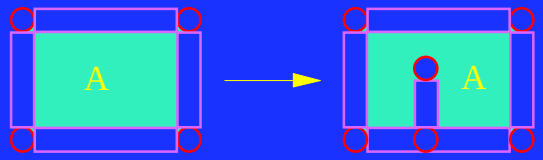

Add the 2 vertices and the edge to the boundary of cell A

This removes them from cell A, but they may still be active in the object or in a feature

Splitting an SGC cell

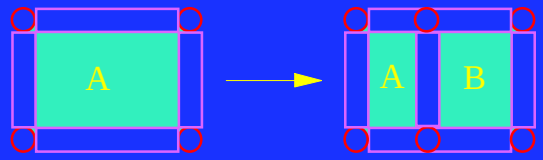

Adding the new edge splits the face

A new 2-cell (B) is created.
Both A and B may retain the attributes of A.

Representation of SGCs

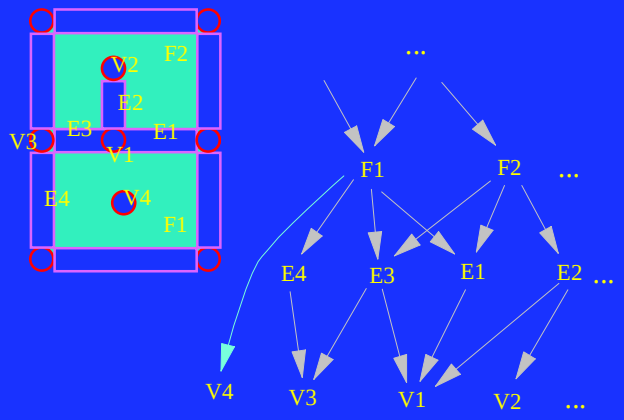

Orientation and neighborhood side

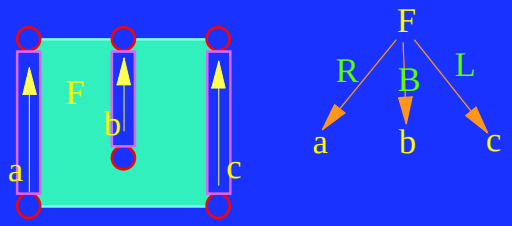

- F is on the right of a
- F is on both sides of b
- F is on the left of c

Orientation and neighborhood side

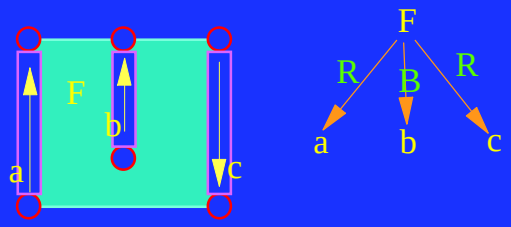

- F is on the right of a
- F is on both sides of b
- F is on the right of c

Neighborhoods in SGCs

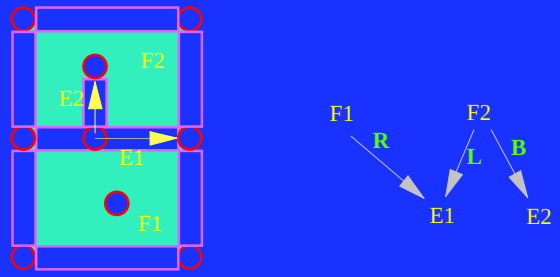

Ordering incidence relations

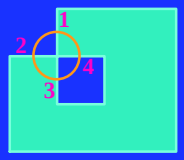

edges around vertices

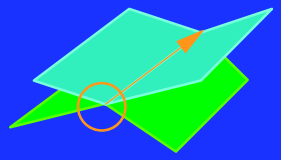

faces/branches around edges

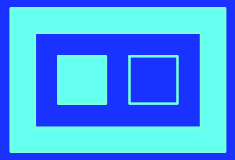

nesting loops and shells

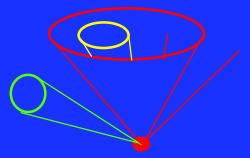

vertex cones

NAILs: Order in SGCs

(Next cell Around cell In cell List)

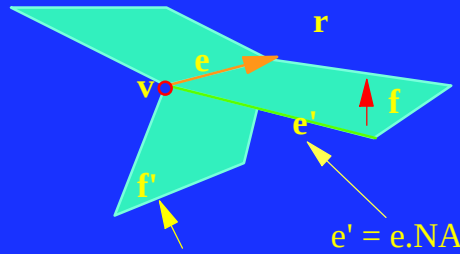

e' = e.NAIL(v,f)

f' = f.NAIL(e,r)

Store NAIL table with each cell of SGC

Putting it all together

Users manipulate CNRG objects

- primitives
- operators
- regions signatures
- features

An SGC model is derived from CNRG

SGC cells are (unions of) connected components of simplices induced by primitives' cells

CNRG regions and features are represented as lists of SGC cells

CNRG-to-SGC conversion

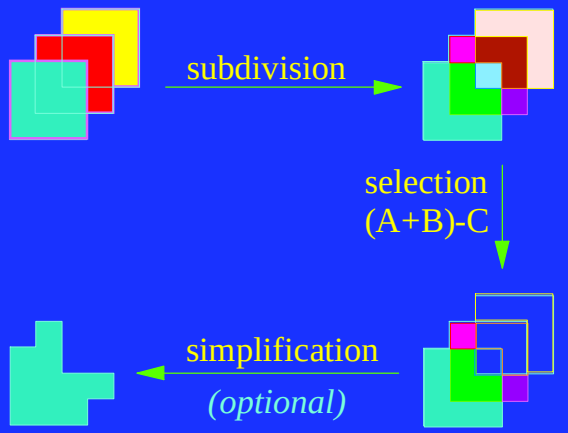

Subdivision

Insert lower-dimensional cells of other primitives into the boundary of each cell

A B

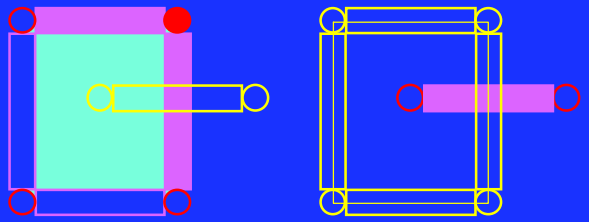

Subdivision

Add vertices of A to boundaries of cells of B and vice versa.

A B

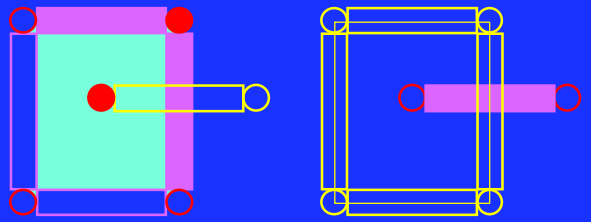

Subdivision

Subdivide edges of both by inserting their pairwise intersections

A B

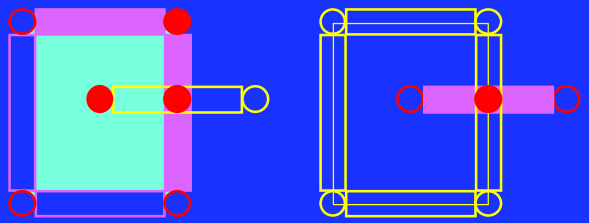

Subdivision

Insert edges of A in the boundaries of the faces of B and vise versa

A\B B\A

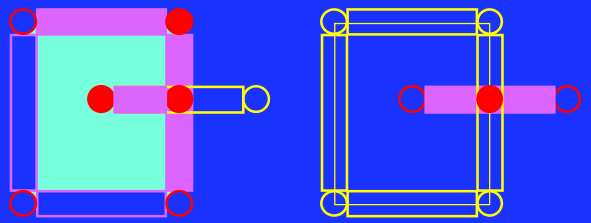

Selection

Combines sells from both and select which cells should be ACTIVE

A-B

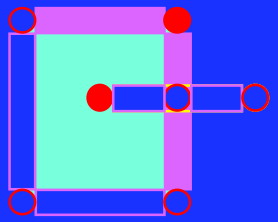

Could apply any filter using CNRG operators and features

A different selection

Combines sells from both and select which cells should be ACTIVE

A+B

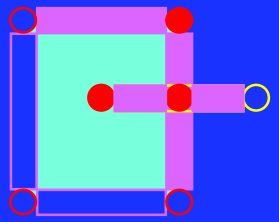

Simplification

Merge cells without changing the pointset nor the structure

s(A+B)

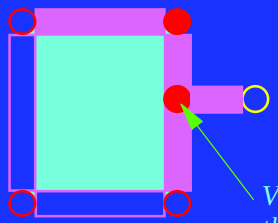

Vertex required to preserve the validity of SGC models

Properties of simplification

One pass algorithm:

For each cell by decreasing dimension

- Delete if non-active and not needed
- Absorb inside a single higher dim cell
- Join with other cells of same dim

sA=ssA

Produces a unique rep for a pointset

Preserves desired structure

Issues for curved geometries

- Cost and reliability of geometric intersections
- Geometric singularities (cusps)
- Identification of branches and components
- Multiple representations (trimmed patch)
- Computing order and inclusion

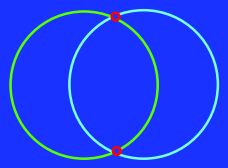

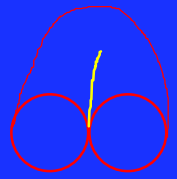

Software architecture issues

- Geometry independent API
- Interface between geometry and topology
  - Intersection returns a complex
  - Bidirectional links
- Robustness (floating point errors)
- Persistent references to user selected cells
- Merge objects from different modellers
- Capture and resolve constraints
- Editing the structure or the creation steps

CONCLUSIONS

- Design/edit in CNRG terms
- Interrogate / mark using features
- Algorithmic conversion to SGCs
- Efficient editing of feature selection
- No topological restrictions
- No geometric or dimension restrictions
- Independent of geometric reps

Modeling with Simplicial Complexes

(Topology, Geometry, and Algorithms)[1]

Herbert Edelsbrunner[2]

Abstract. Geometric modeling often refers to forming and deforming geometric shape. This paper considers the use of simplicial complexes as a general representation of shapes supporting algorithmic solutions to a variety of geometric modeling problems. At this moment, rather little of the potential of simplicial complexes has been exploited algorithmically, and we concentrate on mathematical results that seem most promising to lead to novel algorithmic methods and ideas.

Keywords. Solid modeling, computational geometry, combinatorial topology, grid generation; simplicial complexes, nerves, Voronoi cells, Delaunay simplicial complexes.

[1] This work is partially supported by the National Science Foundation, under grant ASC-9200301 and the Alan T. Waterman award, grant CCR-9118874. Any opinions, findings, conclusions, or recommendations expressed in this publication are those of the authors and do not necessarily reflect the view of the National Science Foundation.

[2] Department of Computer Science, University of Illinois at Urbana-Champaign, Urbana, Illinois 61801, USA.

1 Introduction and Motivation

Unstructured grids in finite element analysis, triangulations in computational geometry, and simplicial complexes in combinatorial topology are one and the same concept. We study this concept from the point of view of using it as a general representation of geometry in solid modeling. The terminology in topology is most advanced and standardized, and it is the one we will mostly use.

Grid generation. In finite element analysis, grids are used to decompose shapes or work-pieces to facilitate the numerical analysis through approximation. The classical approach uses hexahedral elements. Each element has the structure of a cube, with 6 facets, 12 edges, and 8 vertices. These elements are arranged the same way as the cubes in a regular packing, 4 elements around an edge and 8 around a vertex. Indeed, a 3-dimensional array is commonly used as a data structure representing this so-called *structured grid*. This grid implies a homeomorphism between the decomposed shape and a finite portion of a 3-dimensional array. For complicated shapes the construction and maintenance of such a homeomorphism becomes exceedingly difficult [2].

An alternative approach to decomposing shapes uses tetrahedral elements, and the resulting grids are usually referred to a *unstructured* because the number of elements is no longer the same around every interior edge and vertex. In other words, there is no static logical address space that represents the adjacencies between the elements. As a consequence, such a decomposition does not imply any homeomorphism between two possibly very different shapes, and in this respect simplifies the problem. The new challenge is to efficiently handle the less intuitive and less regular structure of a tetrahedral grid. We argue the latter is a challenge that can be met.

Protein structures. Fairly recently, simplicial complexes have been used in the study of proteins and other molecules [5]. The connection between proteins and complexes is less direct than that between shapes and approximating grids. The protein is modeled as a union of balls, one ball per atom, and the complex used is dual to this union [4]. The vertices of the complex are the locations of the atoms in space. Edges, triangles, and tetrahedra are selected on the basis of proximity information. The selection criteria guarantee the dual complex is a subcomplex of the Delaunay simplicial complex of the points, see below. This particular complex plays an important role in our general approach to modeling shapes. It forms a bridge between the globally uniform view of the world using geometry and Euclidean distance and the local view based on decompositions and local neighborhoods.

Dynamical systems. Mechanical systems with several degrees of freedom are commonly mapped to manifolds representing all possible states of the system [1]. Each point of the manifold corresponds to a state. Dynamic change corresponds to a curved traced out on the manifold, which typically lives in a space whose dimension is low but exceeds 3. The intrinsic dimension of the manifold is often much less than that of the embedding space. Such manifolds can be represented by simplicial complexes, which are not restricted to any particular number of dimensions. Simplicial complexes can even model shapes whose intrinsic dimension varies locally.

A particular 3-dimensional modeling problem related to this discussion of dimension is the reconstruction of surfaces. Here the goal is to build a 2-dimensional shape in a 3-dimensional space. With simplicial complexes, there is no principle difference between constructing 3-dimensional grids and 2-dimensional surfaces. In the former problem tetrahedra are fit along triangles, and in the latter triangles are fit along edges. The dimension independent aspect of simplicial complexes makes it possible to generate grids and surfaces with the same tool and format thus bridging the traditional separation between these two problems [8, 14].

Outline. The goal of this paper is to demonstrate the versatility of simplicial complexes as a general representation of geometry. At this moment, limitations of this approach are not well understood and additional research is required to apply this representation to new and old geometric modeling problems.

2 Geometry: Concrete and Abstract

The technical terminology related to decompositions of space and pieces of space is most developed in topology, and in particular in the subarea concerned with combinatorial and algebraic structures within topology [10, 13]. We introduce a few concepts from combinatorial topology relevant to the discussions in this paper. We make an effort to provide intuitive explanations whenever appropriate and possible. The discussion begins with simplices and complexes made up of simplices. Both concepts are geometric in nature, and it is useful to develop abstract counterparts in the form of sets and set systems. The connection between the geometric and the abstract concepts is provided by geometric realizations that map abstract elements to points and sets of elements to simplices.

Simplices. A 2-dimensional simplex is a triangle; it is the simplest 2-dimensional geometric object. A 3-dimensional simplex is a tetrahedron. The author likes to claim the tetrahedron is the simplest 3-dimensional geometric object. It is curious though that a typical high-school curriculum teaches everything about the triangle, and a lot of things about the cube, but little if anything about the tetrahedron. Indeed, mathematical encyclopedia favor a complete treatment of the cube over the discussion of tetrahedra [9]. This is certainly an erroneous path of history.

In general, a k-dimensional simplex, or *k-simplex*, is the convex hull of $k+1$ points in general position. A k-simplex is inherently k-dimensional and requires at least k dimensions to be embedded. We will primarily be concerned with 3-dimensional real space, $\mathbb{R}^3$, though we would like to remind the reader that there are geometric modeling problems beyond 3 dimensions. In $\mathbb{R}^3$ we have four types of proper simplices: *vertices* or 0-simplices, *edges* or 1-simplices, *triangles* or 2-simplices, and *tetrahedra* or 3-simplices. For convenience, the empty set is referred to as a (-1)-simplex. The *dimension* of a simplex σ is denoted by $\dim\sigma$; it is one less than the number of vertices. A subset of the vertices spans a lower-dimensional simplex, τ, called a *face* of σ. For example, a tetrahedron σ is spanned by 4 vertices, there are four subsets of size 3 and thus 4 triangle faces. A tetrahedron has also 6 edges and 4 vertices as faces. We consider σ itself and $\emptyset$ as improper faces of σ.

Simplicial complexes. A collection of simplices forms a proper decomposition of a geometric object or shape if the simplices have no improver overlap. This means if two simplices overlap then they overlap in a face of both. For example, two triangles may share an edge, or a vertex, or they are disjoint. In the latter case we say they share the empty set, which is considered a face of both and also of all other simplices. Technically, such a collection is referred to as a *simplicial complex*, $\mathcal{K}$. The formal requirements are (i) if $\sigma \in \mathcal{K}$ and τ is a face of σ then $\tau \in \mathcal{K}$, and (ii) if $\sigma_1, \sigma_2 \in \mathcal{K}$ then $\sigma_1 \cap \sigma_2$ is a face of both. By condition (i), $\sigma_1 \cap \sigma_2$ is also a simplex in $\mathcal{K}$. A *subcomplex* is a simplicial complex $\mathcal{L} \subseteq \mathcal{K}$. The *underlying space* of $\mathcal{K}$ is $\bigcup \mathcal{K} = \bigcup_{\sigma\in\mathcal{K}} \sigma$. Note that $\bigcup \mathcal{K}$ is a subset of space and thus a geometric object, while $\mathcal{K}$ is a collection of simplices, and thus a combinatorial object. Loose language ignoring the difference between a simplicial complex and its underlying space is however often convenient and frequently used.

Abstract view. There are several reasons why one would want to develop a view that describes simplicial complexes in abstract terms. One is the computational representation of simplices and complexes, which is necessarily symbolic. For example, it is natural to represent a tetrahedron as a set of 4 vertices, or maybe 4 vertex indices. The fact that the tetrahedron is really the convex hull of the 4 points is implicitly understood. This leads to the notions of abstract simplices and abstract simplicial complexes. Let V be a finite set of elements, called *vertices*. The power set or collection of all subsets of V is denoted by 2^V. A subset $\alpha \subseteq V$ is an *abstract simplex*, and its dimension is $\dim\alpha = \operatorname{card}\alpha - 1$. A collection $\mathcal{A} \subseteq 2^V$ of abstract simplices is an *abstract simplicial complex* if $\alpha \in \mathcal{A}$ and $\beta \subseteq \alpha$ implies $\beta \in \mathcal{A}$. The *vertex set* of $\mathcal{A}$ is $\operatorname{vert}\mathcal{A} = \bigcup_{\alpha\in\mathcal{A}} \alpha$.

Abstract simplicial complexes can be constructed directly from finite sets. A particularly important such construction is called the *nerve* of the set, A. It consists of all subcollections of sets in A with non-empty common intersection. Formally,

$$\operatorname{nerve} A = \{U \subseteq A \mid \bigcap_{u\in U} u \neq \emptyset\}.$$

$\operatorname{nerve} A$ is an abstract simplicial complex. To see this note that the sets in $U \in \operatorname{nerve} A$ have a non-empty intersection, by definition. The intersection of the sets in $T \subseteq U$ contains the intersection of the sets in U and is thus also

non-empty. It follows that $T \in \text{nerve } A$, which implies nerve A is indeed an abstract simplicial complex. For example, if A consists of 3 overlapping disks, b_1, b_2, b_3, then nerve $A = \{\emptyset, \{b_1\}, \{b_2\}, \{b_3\}, \{b_1, b_2\}, \{b_2, b_3\}, \{b_3, b_1\}, \{b_1, b_2, b_3\}\}$. This is an abstract representation of a triangle, $\{b_1, b_2, b_3\}$, together with all its faces.

Geometric realization. It is easy to go from a simplicial complex to its abstract counterpart: just replace each simplex by its set of vertices. The other direction is more cumbersome and requires mapping abstract elements to points in some space. Once such a mapping is specified, the other simplices are given as convex hulls of the relevant points. Formally, a map $\varepsilon : \text{vert } \mathcal{A} \to \mathbb{R}^d$ defines a simplicial complex if

$$\text{conv } \varepsilon(\alpha_1) \cap \text{conv } \varepsilon(\alpha_2) = \text{conv } \varepsilon(\alpha_1 \cap \alpha_2)$$

for all abstract simplices $\alpha_1, \alpha_2 \in \mathcal{A}$. Given an abstract simplicial complex, a natural question is how many dimensions are needed for a geometric realization. A special case of this problem is to decide whether or not a graph, which is an abstract simplicial complex consisting of vertices and edges, can be drawn in the plane. A realization of a graph in $\mathbb{R}^3$ is always possible simply by placing the vertices so no 4 are coplanar. This way no two edges can cross. In general, the dimension of the space must be at least the largest dimension of any simplex, k, and a general position argument can be used to show that $2k + 1$ dimensions are always sufficient.

There is little incentive in topology to develop methods that use as few dimensions as possible. Still, this question is essential when computing is involved. The complexity of algorithms typically explodes with increasing dimension. General methods that limit the number of dimensions required for geometric realizations are essential in any effort to make topological ideas and results useful in geometric modeling.

3 Grids from Proximity

We use proximity information to obtain geometric realizations of topological concepts. The emphasis is on discreteness and on limiting the number of dimensions. Simplicial complexes seem like the most obvious candidate for discrete encodings of continuous topological information. To limit the number of dimensions we use Voronoi diagrams [17] and Delaunay simplicial complexes [3]. They are based on point set data and proximity in terms of Euclidean distance. After introducing both concepts, we consider a general method for triangulating possibly complicated shapes.

Voronoi cells. Let $S \subseteq \mathbb{R}^3$ be a finite set of points. We use Euclidean distance to measure proximity. For points $x = (\xi_1, \xi_2, \xi_3) \in \mathbb{R}^3$ and $p = (\phi_1, \phi_2, \phi_3) \in S$,

$$|xp| = (\sum_{i=1}^{3} (\xi_i - \phi_i)^2)^{\frac{1}{2}}$$

is the distance between x and p. For any $x \in \mathbb{R}^3$, we are interested in the point in S nearest to x, or all nearest points in case of a tie. If the points of S are in general position there are at most 4 points of S equidistant from x. Indeed, for any finite set there is an arbitrarily small perturbation so this is the case. Such perturbations can be efficiently simulated, as demonstrated in [6, 18]. For a point $p \in S$, define its *Voronoi cell* as the set of points $x \in \mathbb{R}^3$ so p is nearest to x, that is,

$$V_p = \{x \in \mathbb{R}^3 \mid |xp| \leq |xq|, q \in S\}.$$

The collection of Voronoi cells is $V = V_S = \{V_p \mid p \in S\}$. Clearly, the cells in V_S cover the entire space. Assuming general position, at most 4 Voronoi cells share a common point, namely the point x equidistant from all 4 generators. Two Voronoi cells are either disjoint or they intersect along a 2-dimensional face common to both cells. Similarly, the intersection of three Voronoi cells is either empty or a common edge. The intersection of four Voronoi cells is either empty or a common vertex. Figure 3.1 shows the the Voronoi cells of finitely many points in the plane.

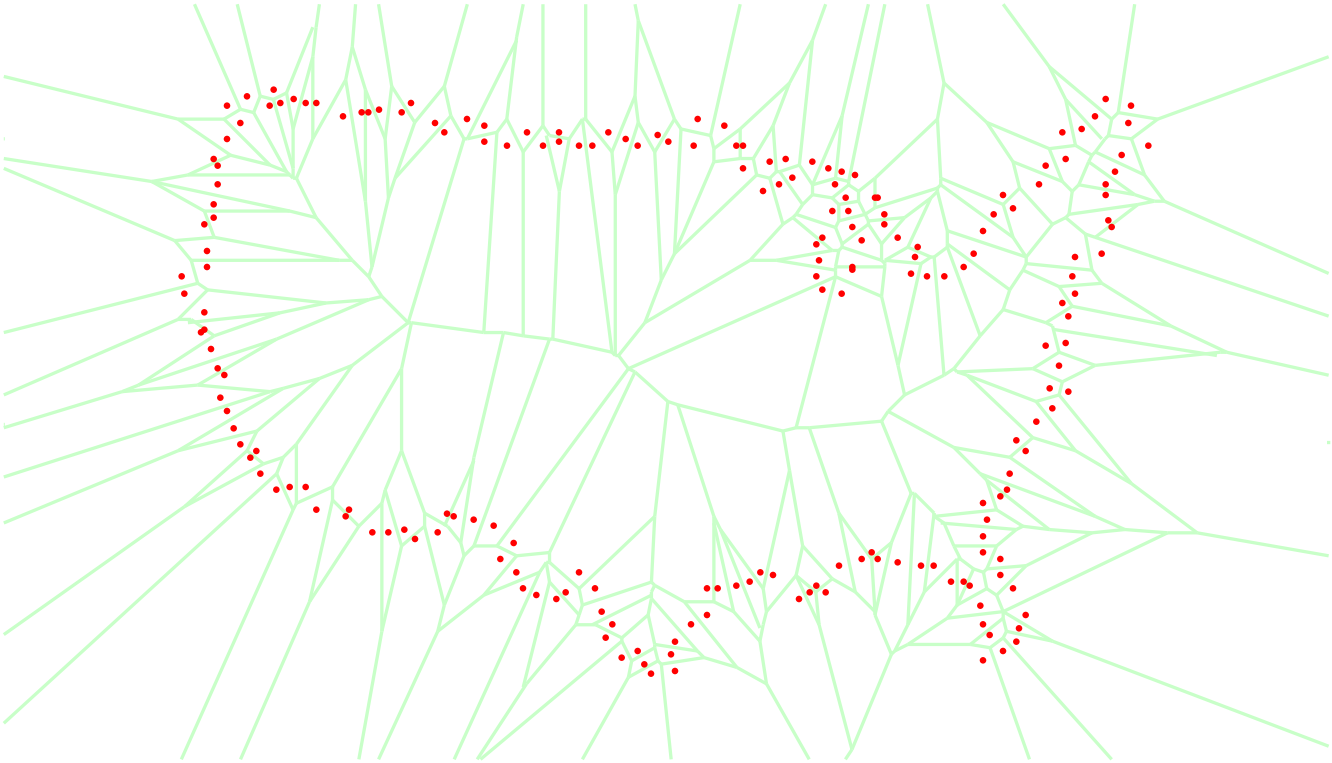

Figure 3.1: The Voronoi cells of a finite set in the plane intersect in pairs and triplets. No higher order intersections occur if general position is assumed.

Delaunay simplicial complexes. Consider the points generating the Voronoi cells, and connect 2 such points by an edge if their cells intersect. Recall that general position implies they intersect along a common 2-dimensional face. Similarly, connect 3 points by a triangle if their cells meet along a common edge, and connect 4 points by a tetrahedron if their cells meet in a common point. The result is a collection of simplices known as the *Delaunay simplicial complex* or *Delaunay triangulation*, $\mathcal{D} = \mathcal{D}_S$, of S, see figure 3.2. A more formal definition can be given using nerves and geometric realizations. The nerve of the set of Voronoi cells, nerve V, contains every subcollection of Voronoi cells with non-empty common intersection. Assuming general position, these subcollections will be of size 1, 2, 3, and 4. nerve V is an abstract simplicial complex. A geometric realization is obtained by mapping each Voronoi cell, V_p, to $p \in S$, see again figure 3.2. This is the Delaunay simplicial complex of S.

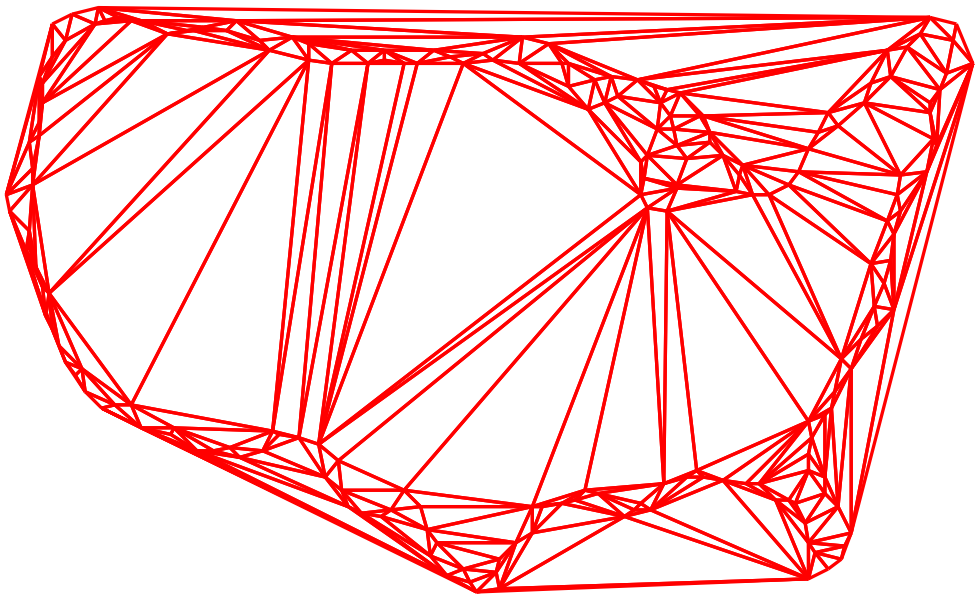

Figure 3.2: The Delaunay simplicial complex of the points generating the Voronoi cells in figure 3.1. The triangles are not shaded although they are genuine elements of the complex.

It is not immediately obvious that the thus realized nerve of V is indeed free of improper intersections and forms a simplicial complex in $\mathbb{R}^3$. To see this is so, one can use the fact that a simplex belongs to $\mathcal{D}$ iff there is a sphere through its vertices so all other points of S lie outside the sphere. There is a long list of nice properties satisfied by Delaunay simplicial complexes, which is the reason they are popular in generating unstructured grids, see e.g. [16].

Restricted cells and complexes. The Delaunay simplicial complex decomposes the entire convex hull of S into tetrahedra. In most applications it is desirable to decompose only a subset $X \subseteq \mathbb{R}^3$, or to find a simplicial complex approximating X. We propose the following mechanism to construct such a simplicial complex.

Let $S \subseteq \mathbb{R}^3$ be a finite point set with Voronoi cells $V = V_S$. S will be the vertex set of the simplicial complex for X, so it makes sense S be a subset of X, but this is not necessary for the construction. Each Voronoi cell, V_p, meets X in a set $V_{p,X} = V_p \cap X$, called the *restricted Voronoi cell* of p and X. The same way unrestricted Voronoi cells define the Delaunay simplicial complex of S, we can use the restricted Voronoi cells to define the *restricted Delaunay simplicial complex*, $\mathcal{D}_X = \mathcal{D}_{X,S}$, of S and X. Let $V_X = \{V_{p,X} \mid p \in S\}$ and consider the nerve,

$$\operatorname{nerve} V_X = \{U \subseteq V_X \mid \bigcap_{V_{p,X} \in U} V_{p,X} \neq \emptyset\}.$$

Again we use the natural geometric realization, which maps a cell $V_{p,X}$ to the generator, $p \in S$. The result is $\mathcal{D}_X$, see figure 3.3.

Homeomorphism theorem. The question arises how well the restricted Delaunay simplicial complex represents or approximates the shape X. Somewhat surprisingly, it is possible to specify local conditions on how the Voronoi

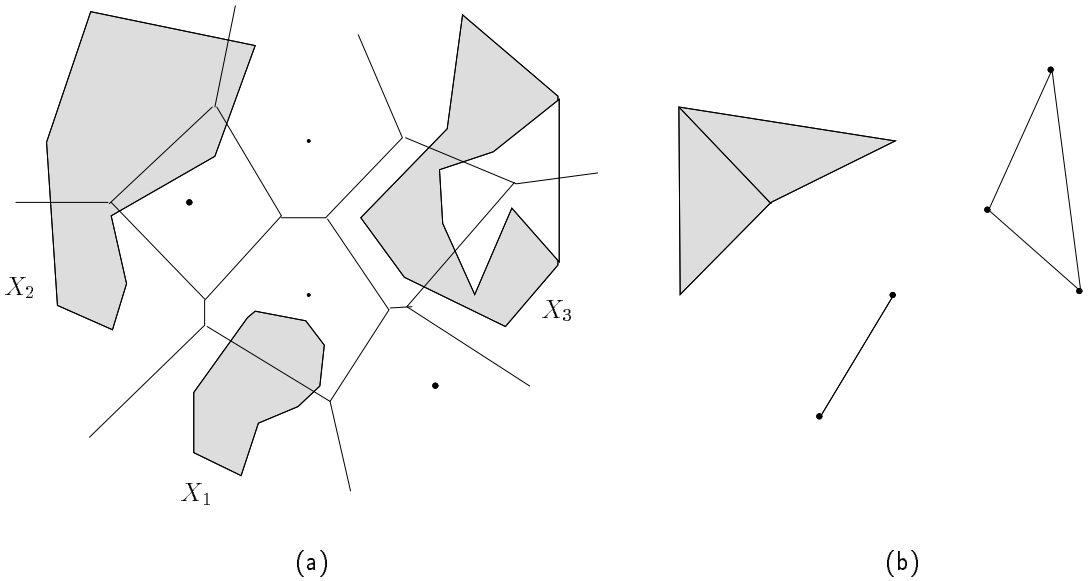

Figure 3.3: By restricting the Voronoi cells to a subset of space, we can specify a subcomplex of the Delaunay simplicial complex suitable to represent the subset. In (a), the Voronoi cells of 10 points decompose 3 shapes, X_1, X_2, X_3. In (b), the corresponding restricted Delaunay simplicial complexes consist of an edge, two triangles sharing an edge, and a cycle of 3 edges, respectively.

cells intersect X that imply that X and $\bigcup \mathcal{D}_X$ are homeomorphic. This means there is a bijective map $\varphi : X \to \bigcup \mathcal{D}_X$ so φ and φ^{-1} are both continuous. The existence of a homeomorphism is about the strongest topological requirement between topological spaces such as X and $\bigcup \mathcal{D}_X$. For example, it implies X and $\bigcup \mathcal{D}_X$ are connected the same way (same number and structure of components, tunnels, and voids) and they are locally of the same dimension.

We state the condition under which X and $\bigcup \mathcal{D}_X$ are homeomorphic only for manifolds X. The extension to more general spaces can be found in [7]. X is a *k-manifold* if the neighborhood of every point $x \in X$ is homeomorphic to an open k-dimensional ball. In case X has boundary, the neighborhood of every point $y \in \operatorname{bd} X$ is homeomorphic to the intersection of an open k-dimensional ball with a closed k-dimensional half-space whose bounding hyperplane passes through the center of the ball. Examples of 2-manifolds are the torus and the sphere, and if open patches with disjoint closures are removed we have 2-manifolds with boundary. An example of a shape $X \subseteq \mathbb{R}^3$ that is not a manifold consists of an edge common to 3 or more triangles. This shape "branches" at the edge, and manifolds are shapes without branching.

We state the condition assuming general position of various kinds. There are arbitrarily small perturbations of S satisfying these assumptions. Intuitively, X and $\bigcup \mathcal{D}_X$ are homeomorphic if all Voronoi cells and common intersections of Voronoi cells meet X and $\operatorname{bd} X$ in closed balls. Formally, if all sets of the form

$$\bigcap_{p \in T} V_p \cap X \quad \text{and} \quad \bigcap_{p \in T} V_p \cap \operatorname{bd} X,$$

$T \subseteq S$, are closed balls of the appropriate dimension then X and $\bigcup \mathcal{D}_X$ are homeomorphic. See figure 3.3 for examples of homeomorphic and non-homeomorphic restricted Delaunay simplicial complexes.

Alpha complexes. In cases where a shape is specified only by a finite set of points, S, sampled from an object, we can get good triangulations by growing a ball around each point. In other words,

$$X_\alpha = \bigcup_{p \in S} b(p, \alpha),$$

plays the role of the shape. $\alpha \geq 0$ is a parameter and $b(p, \alpha)$ is the closed ball with center p and radius α. The Delaunay simplicial complex restricted by X_α is also known as the *α-complex* of S, $\mathcal{K}_\alpha$, see figure 3.4.

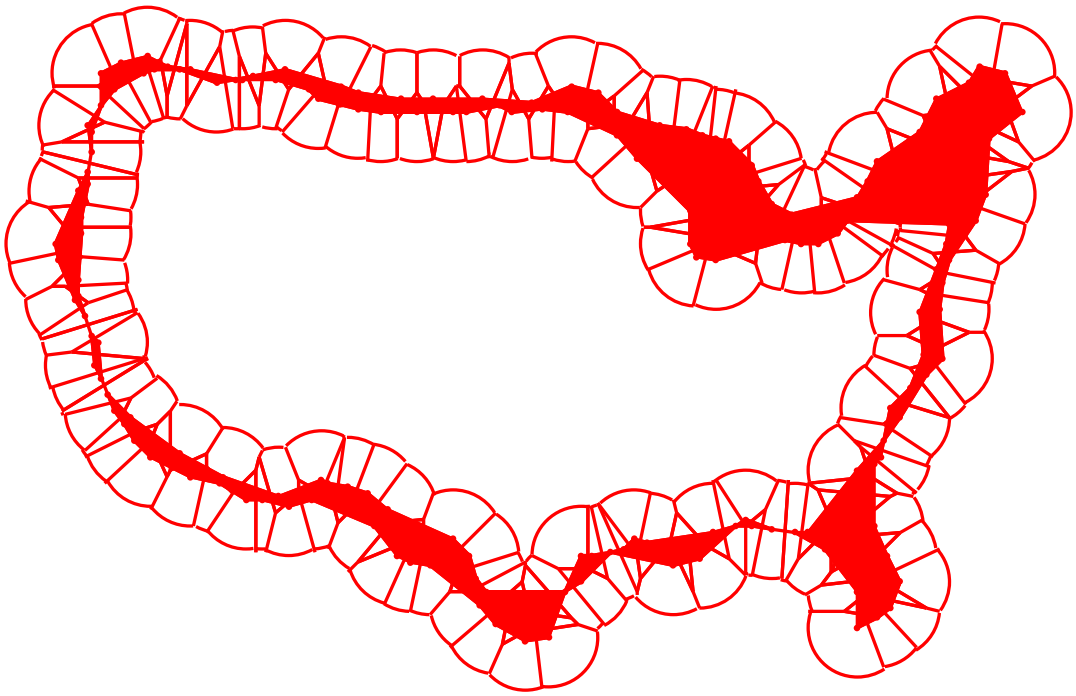

Figure 3.4: The Voronoi cells decompose the union of disks into convex cells. The nerve of the collection of such cells, naturally realized by mapping cells to their generators, is the α-complex. The shaded area in this picture is the underlying space of the α-complex.

Each simplex in the α-complex is also in the Delaunay simplicial complex. In other words, $\mathcal{K}_\alpha$ is a subcomplex of $\mathcal{D}$. More generally, $\mathcal{K}_{\alpha_1} \subseteq \mathcal{K}_{\alpha_2}$ if $\alpha_1 \leq \alpha_2$. By α growing continuously from 0 to $+\infty$, we obtain a nested sequence of complexes, the last one being the Delaunay simplicial complex itself.

An important application of α-complexes is the study of proteins as 3-dimensional structures. Each atom is modeled as a sphere or ball [11, 15]. The size of the sphere depends on the question of interest. For example, the interaction between the protein and a solvent, modeled as a single sphere, can be studied by inflating the atom spheres by the radius of the solvent.

Homotopy equivalence. The decomposition of X_α by Voronoi cells does not always satisfy the closed ball property sufficient for the existence of a homeomorphism. However, all sets of the form

$$\bigcap_{p \in T} V_p \cap X_\alpha ,$$

$T \subseteq S$, are convex. The nerve theorem of algebraic topology [12] implies that X_α and $\bigcup \mathcal{K}_\alpha$ are homotopy equivalent. This is weaker than being homeomorphic. Intuitively, it means X_α and $\bigcup \mathcal{K}_\alpha$ are connected the same way, but locally their intrinsic dimension may not agree. For example, a solid torus is homotopy equivalent to a circle in space. It can be shrunk continuously to the circle, but by doing so it loses its 3-dimensionality and is squeezed to a single dimension.

4 Conclusions

The purpose of this paper is to argue and partially demonstrate that simplicial complexes can serve as a general geometric representation for a broad spectrum of modeling problems. This approach has tradition in combinatorial topology, computational geometry, and grid generation. Indeed, the terms 'triangulation' and 'unstructured grid' are often used as synonyms to 'simplicial complex'. The study of simplicial complexes for modeling problems is relatively recent, which is one of the reasons why this paper concentrates on the geometric and topological fundamentals.

References

[1] D. K. Arrowsmith and C. M. Smith. *Dynamical Systems. Differential Equations, Maps, and Chaotic Behaviour.* Chapman and Hall, London, 1992.

[2] J. E. Castillo (ed.) *Mathematical Aspects of Numerical Grid Generation.* Society for Industrial and Applied Mathematics, Philadelphia, 1991.

[3] B. Delaunay. Sur la sphère vide. *Izv. Akad. Nauk SSSR, Otdelenie Matematicheskii i Estestvennyka Nauk* **7** (1934), 793–800.

[4] H. Edelsbrunner. The union of balls and its dual shape. *In* "Proc. 9th Ann. Sympos. Comput. Geom., 1993", 218–231.

[5] H. Edelsbrunner and P. Fu. Measuring space filling diagrams and voids. Rept. UIUC-BI-MB-94-01, Beckman Institute, Univ. Illinois, Urbana, 1994.

[6] H. Edelsbrunner and E. P. Mücke. Simulation of Simplicity: a technique to cope with degenerate cases in geometric algorithms. *ACM Trans. Comput. Graphics* **9** (1990), 66–104.

[7] H. Edelsbrunner and N. R. Shah. Triangulating topological spaces. *In* "Proc. 10th Ann. Sympos. Comput. Geom. 1994", 285–292.

[8] H. Fuchs, S. M. Kedem and S. P. Uselton. Optimal surface reconstruction from planar contours. *Comm. ACM* **20** (1977), 693–702.

[9] W. Gellert, S. Gottwald, M. Hellwich, H. Kästner and H. Küstner. *The VNR Concise Encyclopedia of Mathematics.* Second edition, van Nostrand Reinhold, New York, 1989.

[10] P. J. Giblin. *Graphs, Surfaces, and Homology.* 2nd edition, Chapman and Hall, London, 1981.

[11] B. Lee and F. M. Richards. The interpretation of protein structure: estimation of static accessibility. *J. Mol. Biol.* **55** (1971), 379–400.

[12] J. Leray. Sur la forme des espaces topologiques et sur les points fixes des représentations. *J. Math. Pure Appl.* **24** (1945), 95–167.

[13] J. R. Munkres. *Elements of Algebraic Topology.* Addison-Wesley, Redwood City, California, 1984.

[14] A. Paoluzzi, B. Bernardini, C. Cattani and V. Ferrucci. Dimension-independent modeling with simplicial complexes. *ACM Trans. Graphics* **12** (1993), 56–102.

[15] F. M. Richards. Areas, volumes, packing, and protein structures. *Ann. Rev. Biophys. Bioeng.* **6** (1977), 151–176.

[16] W. J. Schroeder and M. S. Shephard. A combined octree/Delaunay method for fully automatic 3-d mesh generation. *Internat. J. Numer. Meth. Engin.* **29** (1990), 37–55.

[17] G. F. Voronoi. Nouvelles applications des paramètres continus à la théorie des formes quadratiques. *J. Reine Angew. Math.* **133** (1907), 97–178.

[18] C. K. Yap. Symbolic treatment of geometric degeneracies. *J. Symbolic Comput.* **10** (1990), 349–370.

Polynomial Surface Patch Representations

Chandrajit L. Bajaj*
Department of Computer Science,
Purdue University,
West Lafayette, Indiana 47907

Email: bajaj@cs.purdue.edu

http://www.cs.purdue.edu/people/bajaj

1 INTRODUCTION

Our approach to the design and analysis of geometric algorithms for operations on polynomial (algebraic) curves and surfaces is to take the view of abstract data types, that is, a data representation coupled together with the operations on them [7, 8]. In this framework, the choice of which representation of the polynomial curve or surface patch to use is determined by the desired optimality of the geometric algorithms for the operations.

Polynomial curves and surfaces can be represented in an implicit form, and sometimes also in a parametric form. The implicit form of a real polynomial surface in $\mathbb{R}^3$ is

$$f(x, y, z) = 0 \tag{1}$$

where f is a polynomial with coefficients in $\mathbb{R}$. The parametric form, when it exists, for a real polynomial surface in $\mathbb{R}^3$ is

$$\begin{aligned} x &= \frac{f_1(s,t)}{f_4(s,t)} \\ y &= \frac{f_2(s,t)}{f_4(s,t)} \\ z &= \frac{f_3(s,t)}{f_4(s,t)} \end{aligned} \tag{2}$$

where the f_i are again polynomials with coefficients in $\mathbb{R}$. The above implicit form describes a two dimensional real algebraic variety (a surface) with a single polynomial equation in $\mathbb{R}^3$. The parametric form also describes a real two dimensional algebraic variety (a surface), however with a set of three independent polynomial equations in $\mathbb{R}^5$, with coordinate variables x, y, z, s, t. Alternatively, the parametric form of a real surface may also be interpreted as a rational mapping from $\mathbb{R}^2$ to $\mathbb{R}^3$. We can thus compare the implicit and parametric representations of polynomial surfaces by considering the the parametric form either as a *mapping* or alternatively, an *algebraic variety*.

In these notes, we consider specific geometric operations of display/finite element mesh generation and data fitting, and compare the implicit and parametric polynomial forms for their superiority (or lack thereof) in optimizing algorithms for operations in these categories.

*Supported in part by NSF grant CCR 92-22467, AFOSR grant F49620-94-1-0080 and ONR grant N00014-94-1-0370

Section 2 sets the terminology and introduces some well known facts about polynomial curves and surfaces and their patch representations. Section 3 compares the implicit and parametric surface representations for graphics display and triangular mesh generation operations. Here the rational mapping gives an advantage to the parametric form, though the algorithms to solve this problem in this representation are still non-trivial. Section 4 considers the tradeoff between implicit and parametric surface splines for interactive design and data fitting operations.

2 PRELIMINARIES

2.1 Mathematical Terminology

In this section we review some basic terminology from algebraic geometry that we shall use in subsequent sections. These and additional facts can be found for example in [64, 68].

The set of real and complex solutions (or *zero* set $Z(C)$) of a collection C of polynomial equations

$$\begin{aligned} f_1(x_1, ..., x_d) &= 0 \\ &\vdots \\ f_m(x_1, ..., x_d) &= 0 \end{aligned} \tag{3}$$

with coefficients over the reals $\mathbb{R}$ or complexes $\mathbb{C}$, is referred to as an *algebraic set*. The algebraic set defined by a single equation ($m = 1$) is also known as a hypersurface. A algebraic set that cannot be represented as the union of two other distinct algebraic sets, neither containing the other, is said to be *irreducible*. An irreducible algebraic set $Z(C)$ is also known as an *algebraic variety* V.

A hypersurface in $\mathbb{R}^d$, some d dimensional space, is of *dimension* $d-1$. The *dimension* of an algebraic variety V is k if its points can be put in $(1,1)$ rational correspondence with the points of an irreducible hypersurface in $k+1$ dimensional space. In $\mathbb{R}^d$, a variety V_1 of dimension k intersects a a variety V_2 of dimension h, with $h \geq d-k$, in an algebraic set $Z(S)$ of dimension at least $h+k-d$. The resulting intersection is termed *proper* if all subvarieties of $Z(S)$ are of the same minimum dimension $h+k-n$. Otherwise the intersection is termed *excess* or *improper*. Let the *algebraic degree* of an algebraic variety V be the *maximum* degree of any defining polynomial. A degree 1 hypersurface is also called a *hyperplane* while a degree 1 algebraic variety of dimension k is also called a *k-flat*. The *geometric degree* of a variety V of dimension k in some $\mathbb{R}^d$ is the maximum number of intersections between V and a $(d-k)$-flat, counting both real and complex intersections and intersections at infinity. Hence the geometric degree of an algebraic hypersurface is the maximum number of intersections between the hypersurface and a line, counting both real and complex intersections and at infinity.

The following theorem, perhaps the oldest in algebraic geometry, summarizes the resulting geometric degree of intersections of varieties of different degrees.

[Bezout] A variety of geometric degree p which *properly* intersects a variety of geometric degree q does so in an algebraic set of geometric degree either at most pq or infinity. $\diamond$

The *normal* or *gradient* of a hypersurface $\mathcal{H} : f(x_1, ..., x_n) = 0$ is the vector $\nabla f = (f_{x_1}, f_{x_2}, \ldots, f_{x_n})$. A point $\mathbf{p} = (a_0, a_1, \ldots a_n)$ on a hypersurface is a *regular* point if the gradient at $\mathbf{p}$ is not null; otherwise the point is *singular*. A singular point $\mathbf{q}$ is of multiplicity e for a hypersurface $\mathcal{H}$ of degree d if any line through $\mathbf{q}$ meets $\mathcal{H}$ in at most $d-e$ additional points. Similarly a singular point $\mathbf{q}$ is of multiplicity e for a variety V in $\mathbb{R}^n$ of dimension k and degree d if any sub-space $\mathbb{R}^{n-k}$ through $\mathbf{q}$ meets V in at most $d-e$ additional points. It is important to note that even if two varieties intersect in a *proper* manner, their intersection in general may consist of sub-varieties of various multiplicites. The total degree of the intersection, however is bounded by Bezout's theorem. Finally, one notes that a hypersurface $f(x_1, ..., x_n) = 0$ of degree d has $K = \binom{n+d}{n}$ coefficients, which is one more than the number of independent coefficients. Hypersurfaces $f(x_1, ..., x_n) = 0$ of degree d form $K-1$ dimensional vector spaces over the field of coefficients of the polynomials.

Finally, two hypersurfaces $f(x_1, \ldots, x_n) = 0$ and $g(x_1, \ldots, x_n) = 0$ meet with C^k-continuity along a common subvariety V if and only if there exist functions $\alpha(x_1, \ldots, x_n)$ and $\beta(x_1, \ldots, x_n)$ such that all derivatives upto order k of $\alpha f - \beta g$ equals zero at all points along V, see for e.g., [36].

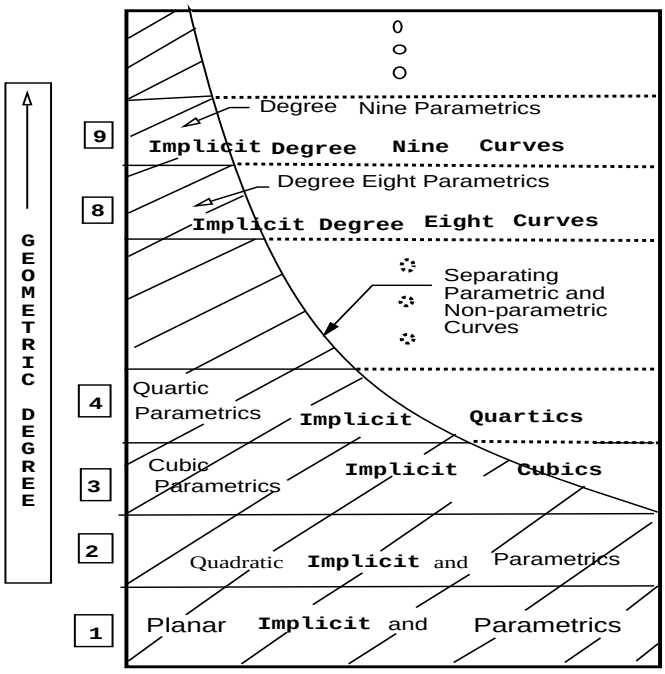

Figure 1: A Classification of Low Degree Algebraic Curves

2.2 Polynomial Curves and Surfaces

We cast our real implicit and parametric curves and surfaces, in the terminology of the previous subsection. A real implicit algebraic plane curve $f(x,y) = 0$ is a hypersurface of dimension 1 in $\mathbb{R}^2$, while a parametric plane curve $[f_3(s)x - f_1(s) = 0, f_3(s)y - f_2(s) = 0]$ is an algebraic variety of dimension 1 in $\mathbb{R}^3$, defined by the two independent algebraic equations in the three variables x, y, s. Similarly, a real implicit algebraic surface $f(x,y,z) = 0$ is a hypersurface of dimension 2 in $\mathbb{R}^3$, while a parametric surface $[f_4(s,t)x - f_1(s,t) = 0, f_4(s,t)y - f_2(s,t) = 0, f_4(s,t)z - f_3(s,t) = 0]$ is an algebraic variety of dimension 2 in $\mathbb{R}^5$, defined by three independent algebraic equations in the five variables x, y, z, s, t.

A plane parametric curve is a very special algebraic variety of dimension 1 in x, y, s space, since the curve lies in the 2-dimensional subspace defined by x, y and furthermore points on the curve can be put in $(1,1)$ rational correspondence with points on the 1-dimensional sub-space defined by s. Parametric curves are thus a special subset of algebraic curves, and are often also called rational algebraic curves. Figure 1 depicts the relationship between the set of parametric curves and non-parametric curves at various degrees.

Example parametric (rational algebraic) curves are degree two algebraic curves (conics) and degree three algebraic curves (cubics) with a singular point. The non-singular cubics are not rational and are also known as elliptic cubics. In general, a necessary and sufficient condition for the rationality of an algebraic curve of arbitrary degree is given by the Cayley-Riemann criterion: a curve is rational iff $g = 0$, where g, the genus of the curve is a measure of the deficiency of the curve's singularities from its maximum allowable limit [66]. Algorithms for computing the genus of an algebraic curve and for symbolically deriving the parametric equations of genus 0 curves, are given for example in [1, 2, 3].

Similarly, a parametric surface is a very special algebraic variety of dimension 2 in x, y, z, s, t space, since the surface lies in the 3-dimensional subspace defined by x, y, z and furthermore points on the surface can be put in $(1,1)$ rational correspondence with points on the 2-dimensional sub-space defined by s, t. Figure 2 depicts the relationship between parametric and non-parametric surfaces.

Example parametric (rational algebraic) surfaces are degree two algebraic surfaces (quadrics) and most degree three algebraic surfaces (cubic surfaces). The cylinders of nonsingular cubic curves and the cubic surface cone

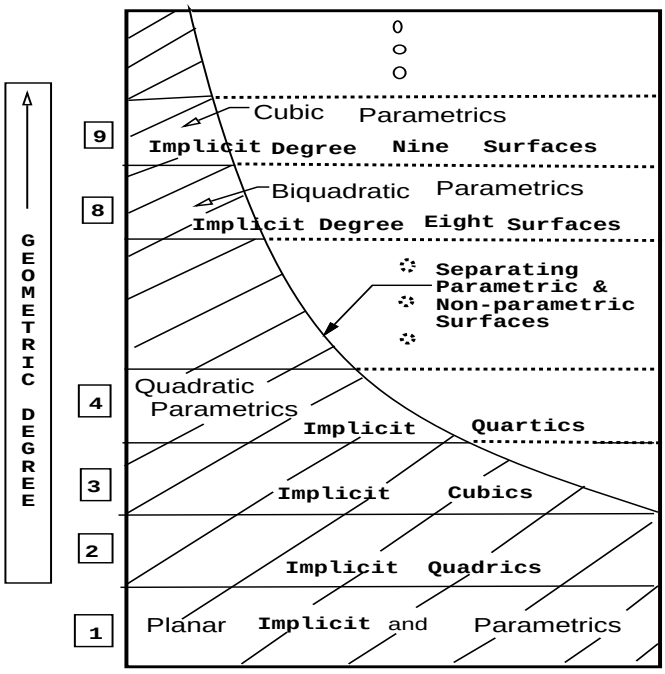

Figure 2: A Classification of Low Degree Algebraic Surfaces

are of not rational. Other examples of rational algebraic surfaces are Steiner surfaces which are degree four surfaces with a triple point, and Plücker surfaces which are degree four surfaces with a double curve. In general, a necessary and sufficient condition for the rationality of an algebraic surface of arbitrary degree is given by Castelnuovo's criterion: $P_a = P_2 = 0$, where P_a is the arithmetic genus and P_2 is the second plurigenus [67]. Algorithms for symbolically deriving the parametric equations of degree two and three rational surfaces are given in [1, 2, 3, 4, 62].

2.3 Degree & Singularities

For implicit algebraic plane curves and surfaces defined by polynomials of degree d, the maximum number of intersections between the curve and a line in the plane or the surface and a line in space, is equal to the maximum number of roots of a polynomial of degree d. Hence, here the geometric degree is the same as the algebraic degree which is equal to d. For parametric curves defined by polynomials of degree d, the maximum number of intersections between the curve and a line in the plane is also equal to the maximum number of roots of a polynomial of degree d. Hence here again the geometric degree is the same as the algebraic degree. For parametric surfaces defined by polynomials of degree d the geometric degree can be as large as d^2, the square of the algebraic degree d. This can be seen as follows. Consider the intersection of a generic line in space $[a_1x + b_1y + c_1z - d_1 = 0, a_2x + b_2y + c_2z - d_2 = 0]$ with the parametric surface. The intersection yields two implicit algebraic curves of degree d which intersect in $O(d^2)$ points (via Bezout's theorem), corresponding to the intersection points of the line and the parametric surface.

A parametric curve of algebraic degree d is an algebraic curve of genus 0 and so have $\frac{(d-1)(d-2)}{2} = O(d^2)$ singular (double) points. This number is the maximum number of singular points an algebraic curve of degree d may have. From Bezout's theorem, we realize that the intersection of two implicit surfaces of algebraic degree d can be a curve of geometric degree $O(d^2)$. Furthermore the same theorem implies that the intersection of two parametric surfaces of algebraic degree d (and geometric degree $O(d^2)$) can be a curve of geometric degree $O(d^4)$. Hence, while the potential singularities of the space curve defined by the intersection of two implicit surfaces

defined by polynomials of degree d can be as many as $O(d^4)$, the potential singularities of the space curve defined by the intersection of two parametric surfaces defined by polynomials of degree d can be as many as $O(d^8)$.

2.4 Polynomial Patch Representations

The popular polynomial bases amongst interactive geometric designers are the Bernstein-Bézier and the B-Spline basis. These bases are defined for restricted subdomains of the deining space as opposed to the power basis which is defined for all points of the space. The example formulations given below are defined for values of each of the variables x, y and z in the unit interval [0,1].

Bernstein-Bézier Basis (BB)

Univariate:

$$P(x) = \sum_{j=0}^{m} w_j B_j^m(x)$$

where

$$B_i^m(x) = \binom{m}{i} x^i (1-x)^{m-i}$$

Bivariate:

(1) Tensor:

$$P(x,y) = \sum_{i=0}^{m}\sum_{j=0}^{n} w_{ij} B_i^n(x) B_j^n(y)$$

(2) Barycentric:

$$P(x,y) = \sum_{i=0}^{m}\sum_{j=0}^{m-i} w_{ij} B_{ij}^n(x,y)$$

where

$$B_{ij}^m(x,y) = \binom{m}{ij} x^i y^j (1-x-y)^{m-i-j}$$

Trivariate:

(1) Tensor:

$$P(x,y,z) = \sum_{i=0}^{m}\sum_{j=0}^{n}\sum_{k=0}^{p} w_{ijk} B_i^n(x) B_j^n(y) B_k^n(z)$$

(2) Mixed:

$$P(x,y,z) = \sum_{i=0}^{m}\sum_{j=0}^{m-i}\sum_{k=0}^{p} \mathbf{b}_{ijk} B_{ij}^n(x,y) B_k^n(z)$$

(3) Barycentric:

$$P(x,y,z) = \sum_{i=0}^{m}\sum_{j=0}^{m-i}\sum_{k=0}^{m-i-j} w_{ijk} B_{ijk}^m(x,y,z)$$

where

$$B_{ijk}^m(x,y,z) = \binom{m}{ijk} x^i y^j z^k (1-x-y-z)^{m-i-j-k}$$

The B-spline basis over the unit interval [0,1] is easily generated by a fractional linear recurrence as given below for the univariate case. The bivariate and trivariate forms can also be similarly generated from this in either tensor product or barycentric form, as given for the BB form above.

B-Spline Basis
Univariate:

$$\mathbf{P}_n = \sum_{l=0}^{m} \mathbf{p}_l N_l^n(x)$$

where

$$N_l^1(x) = \begin{cases} 1 \text{ for } x_l \leq x_{l+1} \\ 0 \text{ otherwise.} \end{cases}$$

and knot sequence $0 = u_0 \leq u_1 < \ldots < u_{m+1} = 1$

$$N_l^n(x) = \frac{x - x_{l-1}}{x_{l+n-1} - x_{l-1}} N_l^{n-1}(x) + \frac{x_{l+n} - x}{x_{l+n} - x_l} N_{l+1}^{n-1}(x)$$

Both the parametric and the implicit representation of algebraic curve segments and algebraic surface patches can be represented in either of the above BB or B-spline bases. Note that the canonical representation of a parametric plane curve segment and surface patch in x, y, z space are given by Curve:

$$\begin{cases} x = P_1(t), \\ y = P_2(t), \\ w = P_3(t). \end{cases}$$

Surface:

$$\begin{cases} x = P_1(s,t), \\ y = P_2(s,t), \\ z = P_3(s,t), \\ w = P_4(s,t). \end{cases}$$

where the P_i are polynomials in any of the above appropriate bases and the variables/parameters s, and t range over the unit interval [0,1].

An implicit curve segment and surface patch can be defined in x, y, z space by Curve:

$$z = P(x,y) \wedge z = 0$$

Surface:

$$w = P(x,y,z) \wedge w = 0$$

where the P is a polynomial in any of the above appropriate basis and the variables x, y, z range over the unit interval [0,1].

The work of characterizing the BB form of polynomials within a tetrahedron such that the zero contour of the polynomial is a single sheeted surface within the tetrahedron, has been attempted in the past. In [60], Sederberg showed that if the coefficients of the BB form of the trivariate polynomial on the lines that parallel one edge, say L, of the tetrahedron, all increase (or decrease) monotonically in the same direction, then any line parallel to L will intersect the zero contour algebraic surface patch at most once. In [39], Guo treats the same problem by enforcing monotonicity conditions on a cubic polynomial along the direction from one vertex to a point of the opposite face of the vertex. From this he derives a condition $a_{\lambda - e_1 + e_4} - a_\lambda \geq 0$ for all $\lambda = (\lambda_1, \lambda_2, \lambda_3, \lambda_4)^T$ with $\lambda_1 \geq 1$, where a_λ are the coefficients of the cubic in BB form and e_i is the i-th unit vector. This condition is difficult to satisfy in general, and even if this condition is satisfied, one still cannot avoid singularities on the zero contour. In[9, 12] sufficient conditions of a smooth, single sheeted zero contour generalizes Sederberg's condition and provides with an efficient way of generating nice implicit surface patches in BB-form (called A-patches for algebraic patches). See Figures 3 and 4.

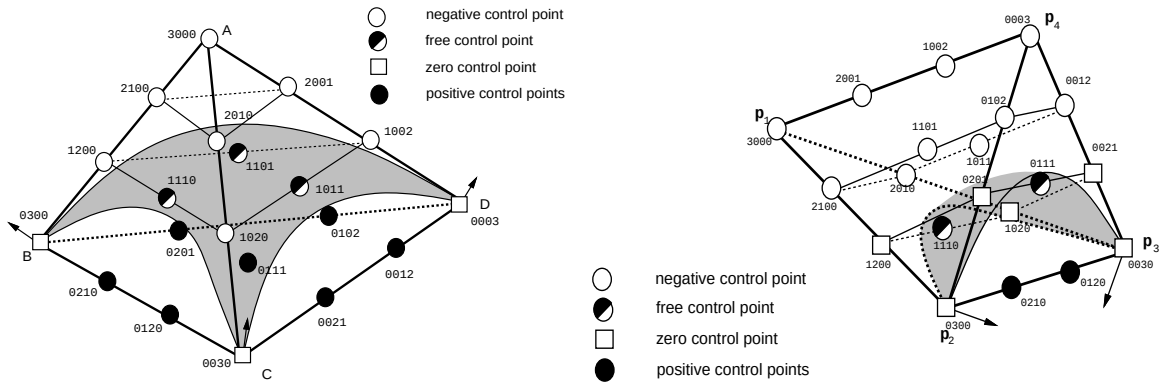

Figure 3: (a) A three sided patch tangent at B, C, D (b) A degenerate four sided patch tangent to face $[p_1 p_2 p_4]$ at p_2 and $[p_1 p_3 p_4]$ at p_3

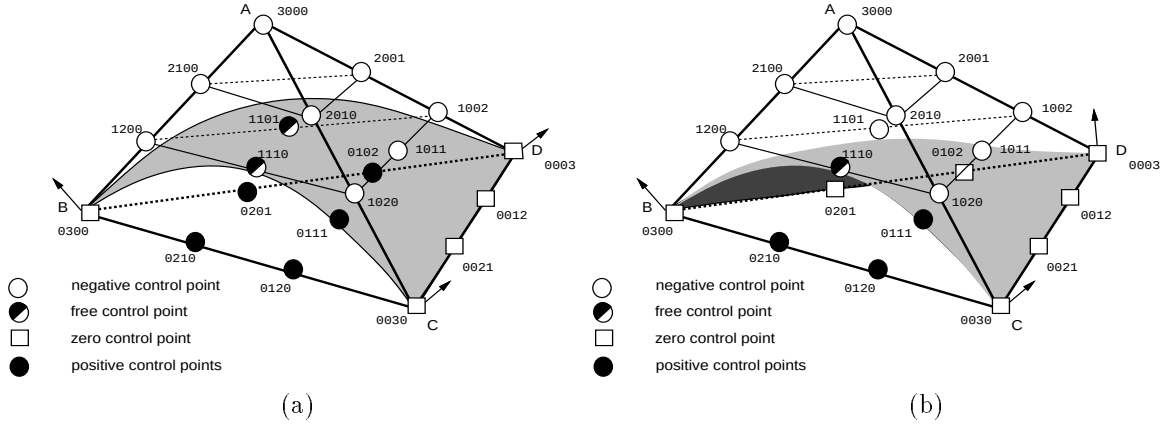

Figure 4: (a) A three sided patch interpolating the edge CD (b) A three sided patch interpolating edges BD and CD

3 DISPLAY & MESH GENERATION

We present two algorithms for computing planar triangular approximations (triangulations) of real algebraic surfaces, one specialized to the implicit representation[19], and the other for the rational parametric[15]. These are easily adaptable to different implicit and parametric surface patch representations. Modern day computer graphics hardware accept such triangulations and accurately render the complicated surfaces with sophisticated lighting and shading models. Similar planar triangular meshes of surfaces are required for finite element methods of solving systems of partial differential equations. See also [17, 20, 19, 21] for higher order, curved finite element approximations of implicit polynomial curves and surfaces with piecewise parametric splines.

3.0.1 Implicit Surfaces

To compute real points on implicit polynomial surfaces requires the solution of polynomial equations. Furthermore, the problem of constructing a polygonal approximation, especially for finite element meshes, is complicated by the need for a correct topology of the mesh even in the presence of singularities and multiple sheets of the real polynomial surface. Direct schemes which work for arbitrary implicit polynomial surfaces are based on the entire enclosing space: either the regular subdivision of the cube [23], a finite subdivision of an enclosing simplex [43], uniform refinement [49] or enclosing simplicial continuation [6] or enclosing cube continuation [25]. However, such spatial sampling methods fail in the presence of point and curve singularities of the polynomial surface, or yield ambiguous topologies in neighborhoods where multiple sheets of the surface come close together. Symbolic methods are necessary to disambiguate or calculate the correct topology for general polynomial curves and surfaces.

Our algorithm uses a triangular surface patch expansion scheme and works directly on the surface instead of a spatial subdivision. It requires a seed point for each real component of the polynomial surface. Compared to the above approaches the patch expansion is centered on points on the surface, and fully uses the polynomial and its derivatives to construct local neighborhoods of convergence. The point selection and hence the final triangulation is adaptive to the k^th order of derivatives (e.g. $k = 2$ implies curvature adaptive) selected for each expansion. By its very nature the triangulation generalizes to arbitrary analytic function surfaces and not just algebraic (polynomial) surfaces.

We begin with a few notational definitions

Expansible edge. During the process of expansion of the triangular mesh, an edge is called expansible if we can go further from this edge to obtain a new triangle on the surface. That is

(a) this edge is on the boundary of the presently constructed mesh

(b) this edge is inside the given boundary box.

The directional expansion, expansion point and the T-plane.

Let $p_0 = (p_0^x, p_0^y, p_0^z)$ be a point on the surface $f(x, y, z) = 0$. If

$$\left|\frac{\partial f(p_0)}{\partial z}\right| \qquad \left(\text{or } \left|\frac{\partial f(p_0)}{\partial x}\right|, \left|\frac{\partial f(p_0)}{\partial y}\right|\right) = ||\nabla f(p_0)||_\infty$$

then the surface $f(x, y, z) = 0$ can be expressed locally as a power (Taylor) series $z = \phi(x, y)$ (or $x = \phi(y, z)$, $y = \phi(x, z)$). We call this a z-*direction expansion.* The point p_0 is referred to as the *expansion point.* The $\frac{\partial f(p_0)}{\partial x}(x - p_o^x) + \frac{\partial f(p_0)}{\partial y}(y - p_o^y) + \frac{\partial f(p_0)}{\partial z}(z - p_o^z) = 0$ the tangent plane of $f = 0$ at p_0, denoted by T-plane. The projection of a space point p onto the T-plane is denoted by $T(p)$.

The following algorithm constructs a triangular mesh on each real component of a real polynomial surface, within a given bounding box. We assume that we have a starting seed point on each real component of the surface in this bounded region. Several numeric and symbolic methods exist to compute such seed points [19, 28]

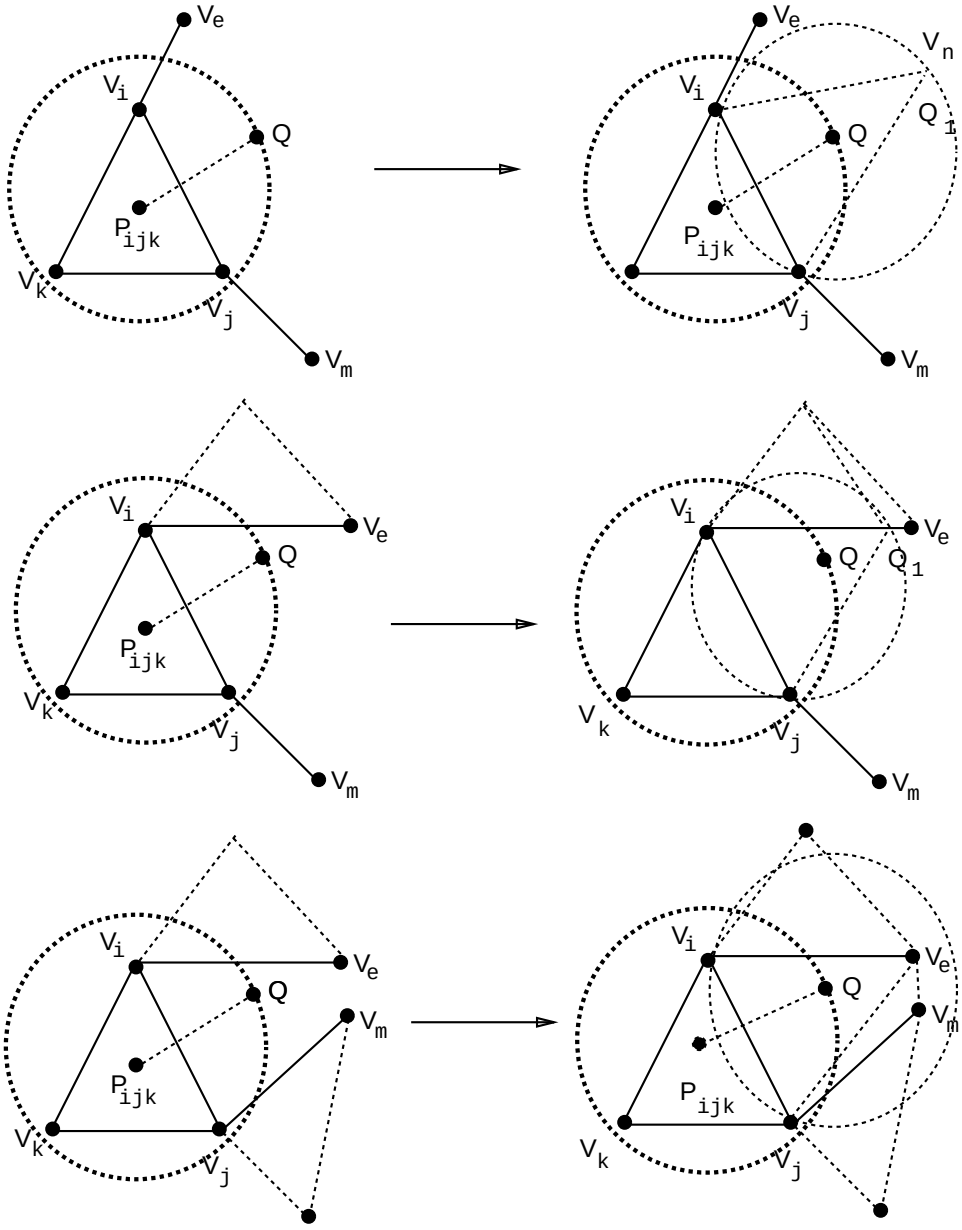

Figure 5: Expansion Steps for the Surface Triangulation

1. *Initial Step*: For a given seed point p_0 on a real component of the surface $f(x,y,z)=0$, we first compute a directional expansion, say $z=\phi(x,y)$. On the T-plane, find a circle with center p_0 such that $\phi(x,y)$ is convergent within the circle. The computation of the radius of convergence, based on the k coefficient terms of a power series expansion are well known and given for example in [44]. Take three points on the circle uniformly, say q_0, q_1, q_2, and refine the points $(q_i, z(q_i))$ by a Newton iteration such that the resulting points V_i are on the surface. The triangle $[V_0, V_1, V_2]$ is the first one we want. Each edge of this triangle is expansible except perhaps if the seed point was chosen such that one edge is on the boundary of the surface with respect to the bounding box.

2. *General Step*: Suppose we have constructed several space triangles that form a connected mesh. Assume at least one edge (V_i, V_j) of a boundary triangle $[V_i, V_j, V_k]$ is expansible. Then the general step is to construct one or more triangles that connects to the edge (V_i, V_j)

   (a) Start from the expansion point P_{ijk} of the triangle $[V_i, V_j, V_k]$ and directional expansion, say $z=\phi(x,y)$. Choose one point Q on the T-plane at P_{ijk} within the convergence radius, such that Q is on the middle-perpendicular line of $[T(V_i), T(V_j)]$ and as far as possible from $T(P_{ijk})$.

   (b) Refine the point $(Q, z(Q))$ to a point on the surface, say Q_1. The point Q_1 becomes a new expansion point. Compute directional expansion at Q_1, say $z=\phi_1(x,y)$, and its circle of convergence. The triangulation around Q_1 is reconstructed as follows.

   - Let $[V_i, V_l]$ and $[V_j, V_m]$ be the neighboring edges of $[V_i, V_j]$. Then on the T-plane at point Q_1, if the angle $< T(V_j)T(V_i)T(V_l) \geq \frac{\pi}{2}$ and $< T(V_i)T(V_j)T(V_m) \geq \frac{\pi}{2}$ or the convergence circle has no intersection points with $[T(V_i), T(V_l)]$ and $[T(V_j), T(V_m)]$, then choose the intersection point Q_2 of the circle and the perpendicular line of $[T(V_i), T(V_j)]$ passing through $T(Q_1)$. If $(T(Q_1), Q_2)$ intersects a previous edge or the bounding box, then Q_2 is chosen to be this intersection point. Refine $(Q_2, \phi_1(Q_2))$ and obtain a new vertex V_n and form the new triangle $[V_i, V_j, V_n]$. Also see top part of Figure 5.
   - If the angle $< T(V_j)T(V_i)T(V_l) < \frac{\pi}{2}$ and $(T(V_i), T(V_j))$ intersect the circle (or, angle $< T(V_i)T(V_j)T(V_m) < \frac{\pi}{2}$ and $(T(V_j), T(V_m))$ intersects the circle), (see middle part of Figure 5, then take Q_1 as this intersection point. Otherwise take $Q_1 = T(V_l)$. In the first case, we add a point on the edge $[V_i, V_l]$ and divide it into two edges, $[V_i, V_]$ and $[V_5, V_4]$. The $[V_2, V_4]$ is expansible and $[V_2, V_5]$ is not. A new expansible edge $[V_1, V_5]$ is produced. In the second case, edge $[V_i, V_j]$ and $[V_i, V_l]$ become non-expansible and a new expansible edge $[V_j, V_l]$ is generated. A related case is shown in the bottom part of Figure 5 and is handled in much the same fashion.

3. *Final Step*. We iterate the General Step, until every edge is non-expansible for that real component.

Figure 6 shows the triangulation of implicitly defined polynomial surfaces.

3.0.2 Rational Parametric Surfaces

A well-known strength of the parametric representation (its mapping from $\mathbb{R}^2$ to $\mathbb{R}^3$) is the ease by which real points can be generated on the parametric curve or surface. However the problem of constructing triangulations with consistent topology is still highly non-trivial. Arbitrary rational parametric surfaces have real *pole curves* in their domain, where the denominators of the parameter functions vanish, domain real *base points* for which all four numerator and denominator polynomials vanish simultaneously, and other features that cause naiive polygonal approximation algorithms to fail. These are ubiquitous problems occurring even among the natural quadrics. See examples shown in Figures 7 and 8.

In geometric design and graphics, where rational Bezier and B-spline surfaces have become popular, the above problems have so far been avoided by a restriction to smooth rational surface patches with denominator polynomials having all positive coefficients [32, 58] (i.e. no real poles or real base points). Sophisticated but unsuspecting triangulation techniques which accept arbitrary rational parametric input (e.g. those implemented

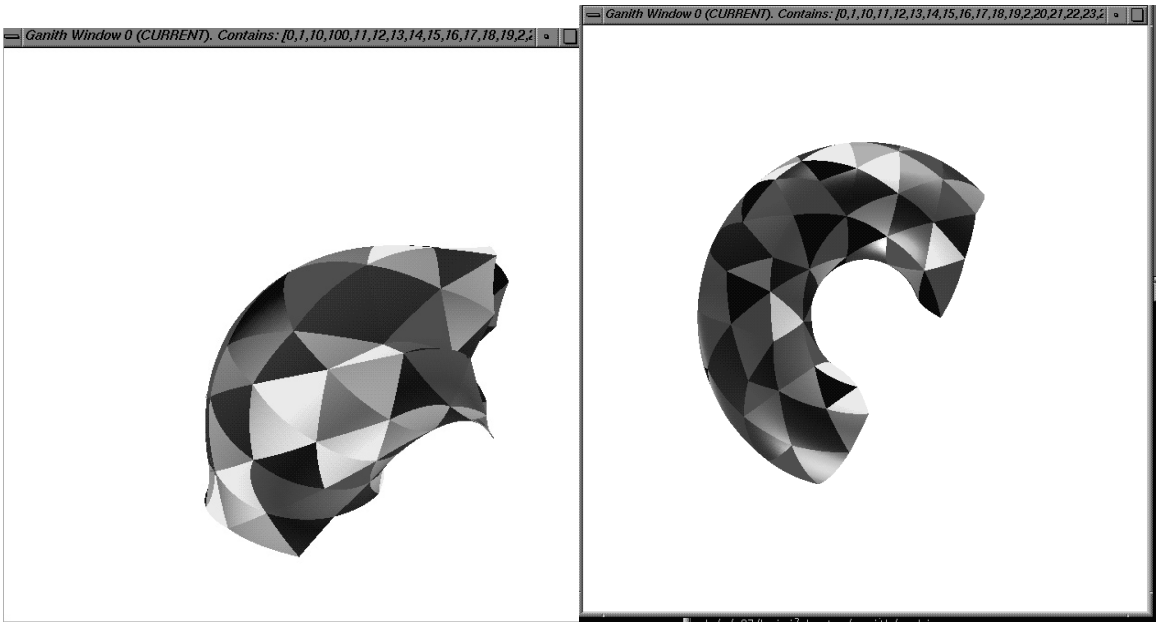

Figure 6: Surface Triangulations of a Cubic Elbow Surface and a Torus

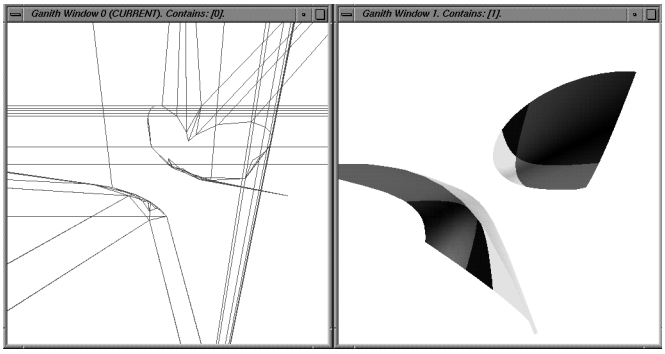

Figure 7: A Quadratic Parametric Surface with Domain Poles

in *MapleV*, *Mathematica*, *Macsyma*) produce completely unintelligible results. Our second algorithm provides a complete and general solution to this problem.

We first illustrate the topological problems that arise if one naively mapped a triangulation from the (s,t) domain to the surface in (x,y,z) space, using the rational parametric equations.

1. [Finite Parameter Range] To fully cover the parametric curve or surface, one must allow the parameters to somehow range over the entire parametric domain, which is infinite. For example, the unit sphere $f(x,y,z) = x^2 + y^2 + z^2 - 1 = 0$ has the standard rational parametric representation $(x = \frac{2s}{1+s^2+t^2}, y = \frac{2t}{1+s^2+t^2}, z = \frac{1-s^2-t^2}{1+s^2+t^2})$ In this parameterization the point $(0,0,-1)$ can only be reached by the parameter values $s = t = \infty$.

2. [Poles] Even when restricting the surface to a bounded real part of the parametric domain, the rational functions describing the surface may have poles over that domain. A hyperboloid of two sheets, with implicit equation $z^2 + yz + xz - y^2 - xy - x^2 - 1 = 0$, has the parametric representation $(x(s,t) =$

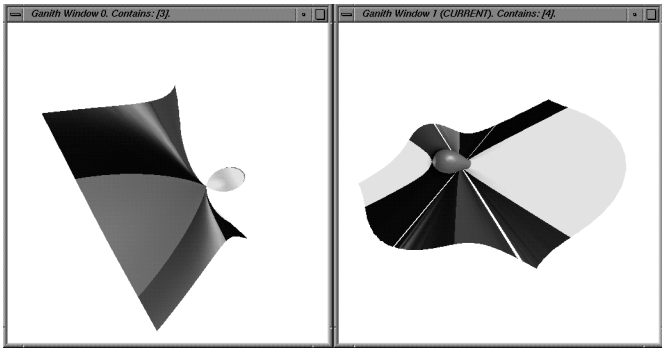

Figure 8: A Cubic Parametric Surface with Seam Curves Due to Base Points

$\frac{4s}{5t^2+6st+5s^2-1}, y(s,t) = \frac{4t}{5t^2+6st+5s^2-1}, z(s,t) = \frac{5t^2+6st-2t+5s^2-2s+1}{5t^2+6st+5s^2-1}$) then problems arise because of the pole curve described by $5t^2 + 6st + 5s^2 - 1 = 0$ in the parameter domain. See Figure 7.

3. [Base Points] The rational parameter functions describing curves and surfaces are generally assumed to be reduced to lowest common denominators, i.e., the numerator and denominator of each rational function are relatively prime. Thus for a curve, there is no parameter value that can cause both numerator and denominator of a rational parameter function to vanish. For surfaces, the situation is different. For the general parametric representation stated earlier, even if f_1, f_2, f_3, f_4 are relatively prime polynomials, it is still possible that there are a finite number of points (a, b) such that $f_1(a,b) = f_2(a,b) = f_3(a,b) = f_4(a,b) = 0$. Each such point is called a *base point* of the parametric surface and is a value for which the parametric mapping is undefined ($\frac{0}{0}$). There may also be base points at infinity in the parameter domain, and the base points can be complex as well as real-valued. Information about base points can be found in books on algebraic geometry such as [64, 67]. Base points are problematic since there is no one surface point for the corresponding domain point. To each base point there actually corresponds a curve on the surface [64], and since there is no parameter value for surface points on such a curve, the entire curve will be missing from the parametric surface. Such a curve is called a *seam curve*. See the right side of Figure 8 which corresponds the cubic parametric surface $x = \frac{t^3-t+s^3-s^2+1}{t^3+s^3+1}, y = \frac{2t^3-t^2-s^2t+2s^3+2}{t^3+s^3+1}, z = \frac{-st-s^3}{t^3+s^3+1}$. Thus for a valid triangulation of a parametric surface, one should also consistently triangulate the gaps caused by the seam curves.

Finite Parameter Range Solution

In [16], the infinite parameter value problem is solved for rational varieties in any dimension using projective linear transformations of the domain. We reproduce without proof the key results, which are necessary for the triangulation algorithm.

Lemma 3.1 *Consider a rational algebraic variety of dimension n in R^m, $n < m$, given by parametric equations*

$$V(\mathbf{s}) = \begin{pmatrix} x_1(s_1, \ldots, s_n) \\ \vdots \\ x_m(s_1, \ldots, s_n) \end{pmatrix}, \qquad s_i \in [-\infty, +\infty]$$

Let the 2^n octant cells in the parameter domain R^n be labelled by the tuples $< \sigma_1, \ldots \sigma_n >$ with $\sigma_i \in \{-1, 1\}$. Then the projective reparameterizations $V(\mathbf{t}_{<\sigma_1,\ldots,\sigma_n>})$ given by

$$s_i = \sigma_i \frac{t_i}{1 - t_1 - t_2 - \ldots - t_n}, \qquad i = 1, \ldots, n \tag{4}$$

together map the entire rational variety using only $t_i \geq 0$ such that $0 \leq t_1 + t_2 + \ldots + t_n \leq 1$.

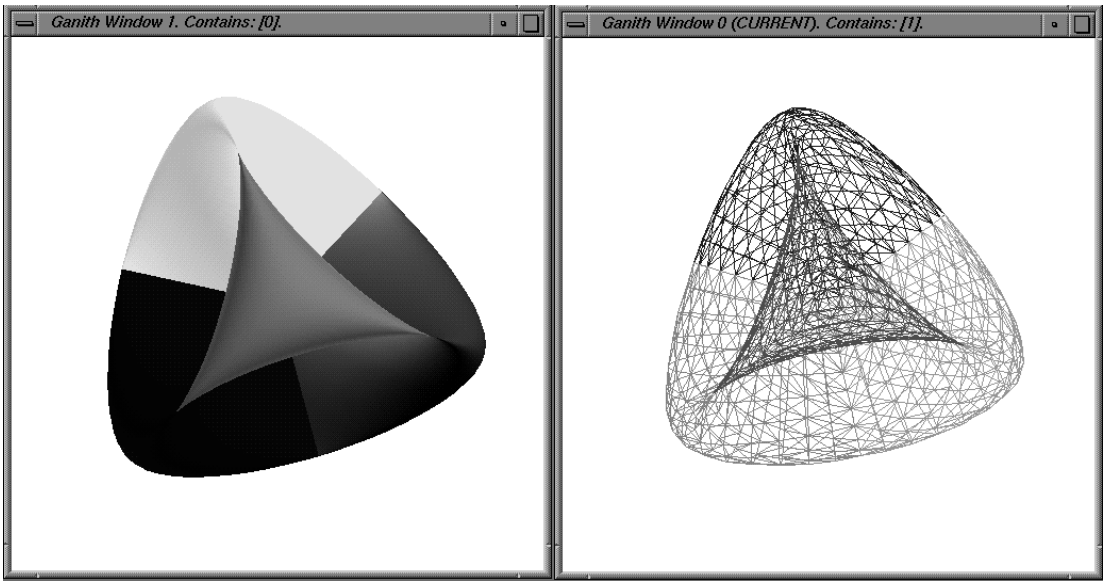

Figure 9: A Complete Triangulation of the Steiner Parametric Surface

Corollary 3.1 *Rational curves* $C(s) = (x_1(s), \ldots, x_m(s))^T$, $s \in [-\infty, +\infty]$ *are covered by* $C(\frac{t}{1-t}), C(\frac{-t}{1-t})$, *using only* $0 \leq t \leq 1$.

Corollary 3.2 *Rational surfaces* $S(s_1, s_2) = (x_1(s_1, s_2), \ldots, x_m(s_1, s_2))^T$, $s_1, s_2 \in [-\infty, +\infty]$ *are covered by*
$S(\frac{t_1}{1-t_1-t_2}, \frac{t_2}{1-t_1-t_2})$, $S(\frac{-t_1}{1-t_1-t_2}, \frac{t_2}{1-t_1-t_2})$,
$S(\frac{-t_1}{1-t_1-t_2}, \frac{-t_2}{1-t_1-t_2})$, $S(\frac{t_1}{1-t_1-t_2}, \frac{-t_2}{1-t_1-t_2})$,
using only $t_i \geq 0 \wedge 0 \leq t_1 + t_2 \leq 1$.

The projective reparameterizations are shown here as fractional affine domain transformations for convenience. In practice, the parametric equations of the rational variety would be homogenized using an additional variable and the numerator and common denominator substituted separately as polynomials, thus avoiding rational function manipulation.

For the Steiner surface ($x = \frac{2st}{1+s^2+t^2}, y = \frac{2s}{1+s^2+t^2}, z = \frac{2t}{1+s^2+t^2}$), and the cubic elbow surface ($x = \frac{4t^2+(s^2+6s+4)t-4s-8}{2t^2-4t+s^2+4s+8}, y = \frac{4t^2+(-s^2-6s-20)t+2s^2+8s+16}{2t^2-4t+s^2+4s+8}, z = \frac{(2s+6)t^2+(-4s-12)t-s^2-4s}{2t^2-4t+s^2+4s+8}$), four different projective reparameterizations yield a complete covering of the rational parametric surface. See Figure 9.

Solution for Domain Poles

The main idea behind the solution is as follows: The (s,t) domain is triangulated in such a way that triangles contain pole points only at their vertices. A domain triangle with a pole at a vertex may map onto an infinite-area surface patch, which may lie partly inside the bounding region. If we determine this to be the case, we binary search on the edges of the surface triangle for points that intersect the bounding box, clip it with respect to the box and re-triangulate the resulting four or five sided convex polygon on the surface.

The algorithm[14] is as follows.

1. Perform the projective reparameterizations so the entire surface is mapped in four pieces. Perform the next steps for each piece.

2. Generate points on the pole curve that lies inside the unit simplex.

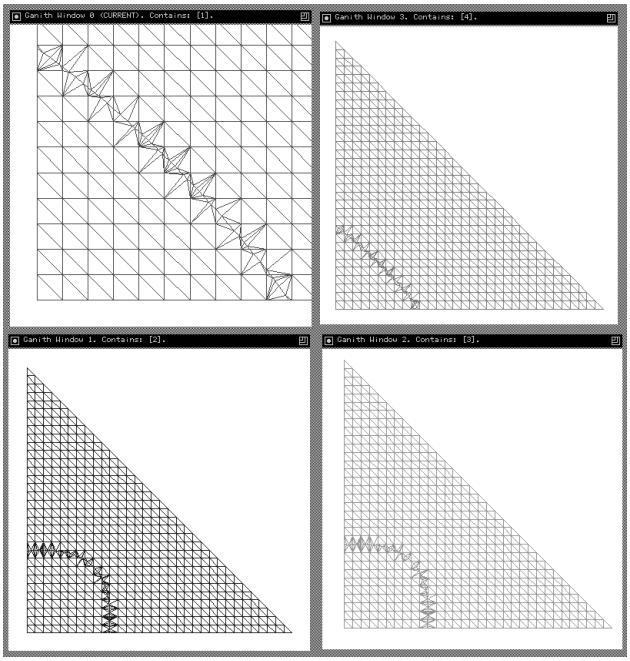

Figure 10: A Domain Triangulation over Unit Simplexes for a Hyperboloid of Two Sheets

3. Generate points in the rest of the unit simplex according to some scheme. The two kinds of points are distinguished from each other.

4. Compute a triangulation of the points thus generated. If an edge of any such triangle intersects the pole curve, insert the intersection point and recompute the triangulation.

5. Every triangle will then have 0, 1, or 2 pole points. A triangle with 3 pole points is split by inserting a simple point in its interior. See also Figure 10. If a triangle has no pole points, it can be mapped immediately to the surface. Suppose it has one pole point and two regular points. Let the pole point be called $\mathbf{p}$ and the regular points $\mathbf{q_1}, \mathbf{q_2}$. We denote the surface point corresponding to a point $\mathbf{x}$ as $S(\mathbf{x})$. We assume that $S(\mathbf{p})$ is a point at infinity, which is likely since $\mathbf{p}$ is a pole. If $S(\mathbf{q_1}), S(\mathbf{q_2})$ both lie outside the bounding region, this triangle will not be mapped. If both lie inside the region, then a binary search is performed along the edges from $\mathbf{p}$ to $\mathbf{q_1}$ and $\mathbf{p}$ to $\mathbf{q_2}$, for the intersection points $S(\hat{\mathbf{q_1}}), S(\hat{\mathbf{q_2}})$ with the bounding box. Then mapped surface triangle is thus replaced by a polygon using the two new vertices. By a similar process a a domain triangle with two pole points, and one simple point is either discarded, or the two pole points in the triangle are replaced by regular points whose images are the intersection of the the bounding box and the mapped triangle. Each resulting four or five sided polygon on th surface is convex and easily triangulated.

Pole curve points with the unit simplex are generated for example by the subdivision method of [37]. In the the second setup, we just generate a constant-size triangular grid on the unit simplex. The grid points are merged with the pole curve points in a special data structure that allows them to be marked as pole or regular points, and an incremental Delaunay triangulation of the entire set of points is constructed [33, 35]. See Figures 10 and ??.

Solution to Base Points

First an important fact about the image of a base point: *Base points blow up to curves on the surface* ([64], Chapter VI, section 2.1, Theorem III, p. 107). Let O be a base point of multiplicity q, and each of the curves

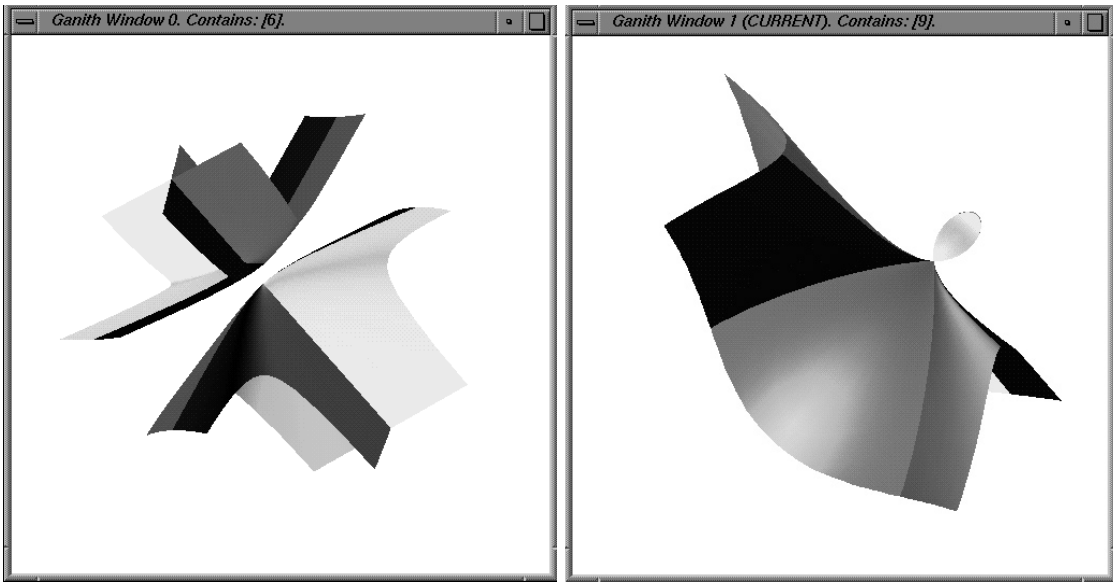

Figure 11: Complete Triangulations and Display of Rational parametric surfaces

$f_1(s,t) = 0, \ldots, f_4(s,t) = 0$ have q distinct tangents at O. Furthermore, let the curves have no common tangents at O. Then the image of the base point O is a curve of degree q on the surface S.

In [15] we show how to compute a parameterization of the seam curve, from the original parameterization and for any base point. For a better correspondence of the surface parameterization to the seam curve parameterization we redefine $X = X(s,t) = f_1(s,t)Y = Y(s,t) = f_2(s,t), Z = Z(s,t) = f_3(s,t), W = W(s,t) = f_4(s,t)$.

Theorem 3.1 *Let (a,b) be an affine base point of multiplicity q. Then for any $m \in \mathcal{R}$, the image of a domain point approaching (a,b) along a line of slope m is given by*

$$(X(m), Y(m), Z(m), W(m)) \quad = \quad \left(\sum_{i=0}^{q} \left(\frac{\partial^q X}{\partial s^{q-i} \partial t^i}(a,b) \right) m^i, \ldots, \sum_{i=0}^{q} \left(\frac{\partial^q W}{\partial s^{q-i} \partial t^i}(a,b) \right) m^i \right) \tag{5}$$

The points $(X(m), Y(m), Z(m), W(m))$ form a one-dimensional family or curve on the surface S, of degree at most q, called the *seam curve* of the base point (a,b).

Corollary 3.3 *If the curves $X(s,t) = 0, \ldots, W(s,t) = 0$ share t tangent lines at (a,b), then the seam curve $(X(m), Y(m), Z(m), W(m))$ has degree $q-t$. In particular, if $X(s,t) = 0, \ldots, W(s,t) = 0$ have identical tangents at (a,b), then for all $m \in R$ the coordinates $(X(m), \ldots, W(m))$ represent a single point.*

Knowing the parameterization $(X(m), Y(m), Z(m), W(m))$, with parameter m of each real seam curve it is quite straightforward to sample this curve at distinct values of m, and stitch the triangulation together.

4 DATA FITTING

Consider the problem of constructing a C^k mesh of smooth surface patches or *splines* that interpolate or approximate scattered data in $\mathbb{R}^3$. Computations which we would like to optimize by our choice of curve and surface representation include:

- solution requiring a small number of surface patches
- reduction of the fitting problem to solving small linear systems

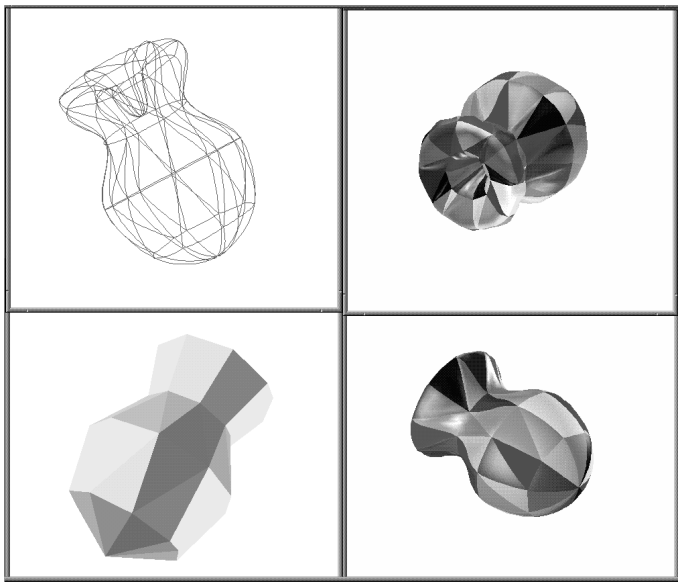

Figure 12: C^1 Implicit Splines over a Spatial Triangulation

- low geometric degree of the solution surfaces

There are several possible variants of the problem depending on the nature of the interpolation problem on hand: local versus non-local patch interpolation, splitting v.s. non-splitting of the surface patches per triangulation face, the convexity versus non-convexity of the given triangulation, etc. In each of these cases, the comparison between the implicit versus parametric representation does not yield a clear winner. While the implicit representation yields lower geometric degree solutions (for reasons relating to degrees of freedom and the number of constraints, the parametric surfaces shows a clear advantage when suitable surfaces need to be selected from an infinite family of interpolatory solutions. Straightforward conditions on the parameter domain can yield parametric surface solutions which are free of poles and base points.

The generation of a C^1 mesh of smooth surface patches or *splines* that interpolate or approximate *triangulated space data* is one of the central topics of geometric design. Alfeld [5], Chui [26], Dahmen and Michelli [31] and Hollig [46] summarize much of the history of scattered data fitting and multivariate splines. Prior work on splines have traditionally worked with a given planar triangulation using a polynomial function basis [5, 57, 63]. More recently surface fitting has been considered over closed triangulations in three dimensions using parametric surface patches [22, 19, 24, 34, 38, 42, 45, 47, 51, 53, 54, 55, 59, 65]. Little work has been done on spline bases using implictly defined algebraic surface patches. Sederberg [60, 61] showed how various smooth implicit algebraic surfaces in trivariate Bernstein basis can be manipulated as functions in Bezier control tetrahedra with finite weights. Patrikalakis and Kriezis [52] extended this by considering implicit algebriac surfaces in a tensor product B-spline basis. However the problem of selecting weights or specifying knot sequences for C^1 meshes of implicit algebraic surface patches which fit given spatial data, was left open. Dahmen [29] presented a scheme for constructing C^1 continuous, piecewise quadric surface patches over a data triangulation in space. In his construction each triangular face is split and replaced by six micro quadric triangular patches, similar to the splitting scheme of Powell-Sabin [56]. More on this later. Moore and Warren [50] extend the marching cubes scheme of [48] and compute a C^1 piecewise quadratic approximation (least-squares) to scattered data. They too use a Powell-Sabin like split, however over subcubes.

In paper [13] the authors consider an arbitrary spatial triangulation $\mathcal{T}$ consisting of vertices $\mathbf{p} = (x_i, y_i, z_i)$ in $\mathbb{R}^3$ (or more generally a simplicial polyhedron $\mathcal{P}$ when the triangulation is closed), with possibly "normal" vectors at the vertex points. An algorithm is given to construct a C^1 continuous mesh of low degree real algebraic surface patches S_i over $\mathcal{T}$ or $\mathcal{P}$. The algorithm first converts the given triangulation $\mathcal{T}$ or simplicial polyhedron

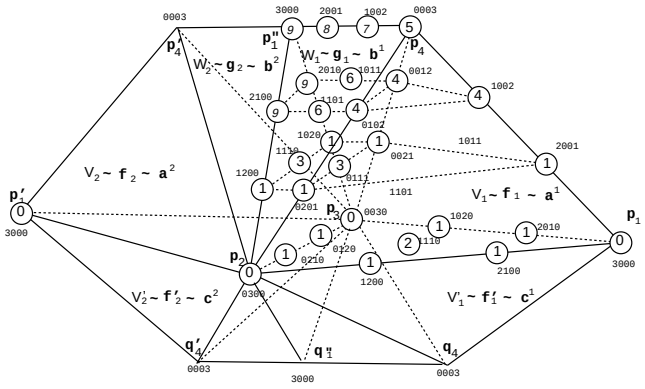

Figure 13: Adjacent Tetrahedra, Cubic Functions and Control Points for two Non-Convex Adjacent Faces

$\mathcal{P}$ into a curvilinear wireframe (with at most cubic parametric curves) which C^1 interpolates all the vertices, followed by a fleshing of the wireframe with low degree algebraic surface patches. See Figure 12. The technique is completely general and uses a single implicit surface patch of degree at most 7, for each triangular face of $\mathcal{T}$ of $\mathcal{P}$, i.e. no local splitting of triangular faces. Furthermore, the C^1 interpolation scheme is local in that each triangular surface patch has independent degrees of freedom which may be used to provide local shape control. Extra free parameters may be adjusted and the shape of the patch controlled by using weighted least squares approximation from additional points and normals, generated locally for each triangular patch. Similar techniques exist for parametrics [24, 34, 38, 54, 59] however the geometric degree of the solution surfaces tend to be prohibitively high.

In papers [9, 12] we show how to join a collection of cubic A-patches of §2 to form a C^1 smooth surface interpolating scattered data points and respecting the topology of a given surface triangulation T of the points. For this problem, prior approaches have been given by [29] using quadric patches, [30, 39, 40] using cubic patches and [13] using quintic for convex triangulations and degree seven patches for arbitrary surface triangulations T. All these papers provide heuristics to overcome the multiple sheeted and singularity problems of implicit patches. In this paper our cubic A-patches are guaranteed to be nonsingular and single sheeted within each tetrahedron.

While the details of the methods of [30] and [40] differ somewhat, they both use the scheme of [29] of building a surrounding simplicial hull (consisting of a series of tetrahedra) of the given triangulation T. Such a simplicial hull is nontrivial to construct for triangulations and neither of the papers [29, 30, 39, 40] enumerate the different exceptional cases (possible even for convex triangulations) nor provide solutions to overcoming them. Paper [9] also uses the same simplicial hull approach but enumerates the exceptional situations and provide strategies for rectifying them. See Figure 15 for an example surface triangulation and its simplicial hull.

In [40], Guo uses a Clough-Tocher split[27] and subdivides each face tetrahedron of the simplicial hull, hence utilizing three patches per face of T. In paper [9], we consider the computed "normals" at the given data points, and distinguish between "convex" and "non-convex" faces and edges of the triangulation. We use a single cubic A-patch per face of T except for the following two special cases. For a non-convex face, if additionally the three inner products of the face normal and its three adjacent face normals have different signs, then in this case one needs to subdivide the face using a single Clough-Tocher split, yielding C^1 continuity with the help of three cubic A-patches for that face. Furthermore for coplanar adjacent faces of T, we show that the C^1 conditions cannot be met using a single cubic A-patch for each face. Hence for this case we again use Clough-Tocher splits for the pair of coplanar faces yielding C^1 continuity with the help of three cubic A-patches per face. See Figures 15,16 for examples of the C^1 interpolation of polyhedra.

The C^1 interpolation schemes of [9, 29, 30, 40, 41] all build an outside simplicial hull (consisting of a series of edge and face tetrahedra) containing the given polyhedron $\mathcal{P}$. As mentioned before, such a simplicial hull is nontrivial to construct for arbitrary $\mathcal{P}$ (even convex $\mathcal{P}$ with sharp corners) and can give rise to several exceptional situations and degeneracies (co-planarity, hull self-intersection, etc). In [10] a new corner-cutting, inner simplicial

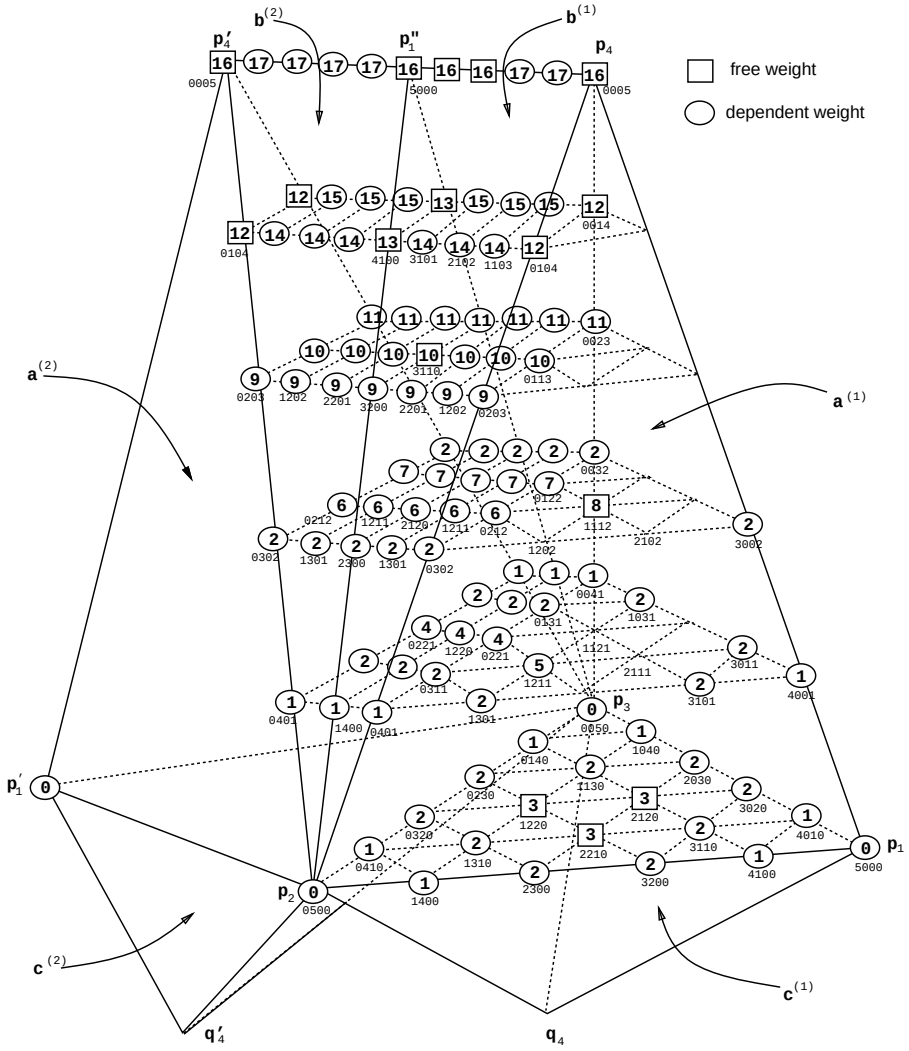

Figure 14: Adjacent Tetrahedra, Quintic Functions and Control Points for two Non-Convex Adjacent Faces

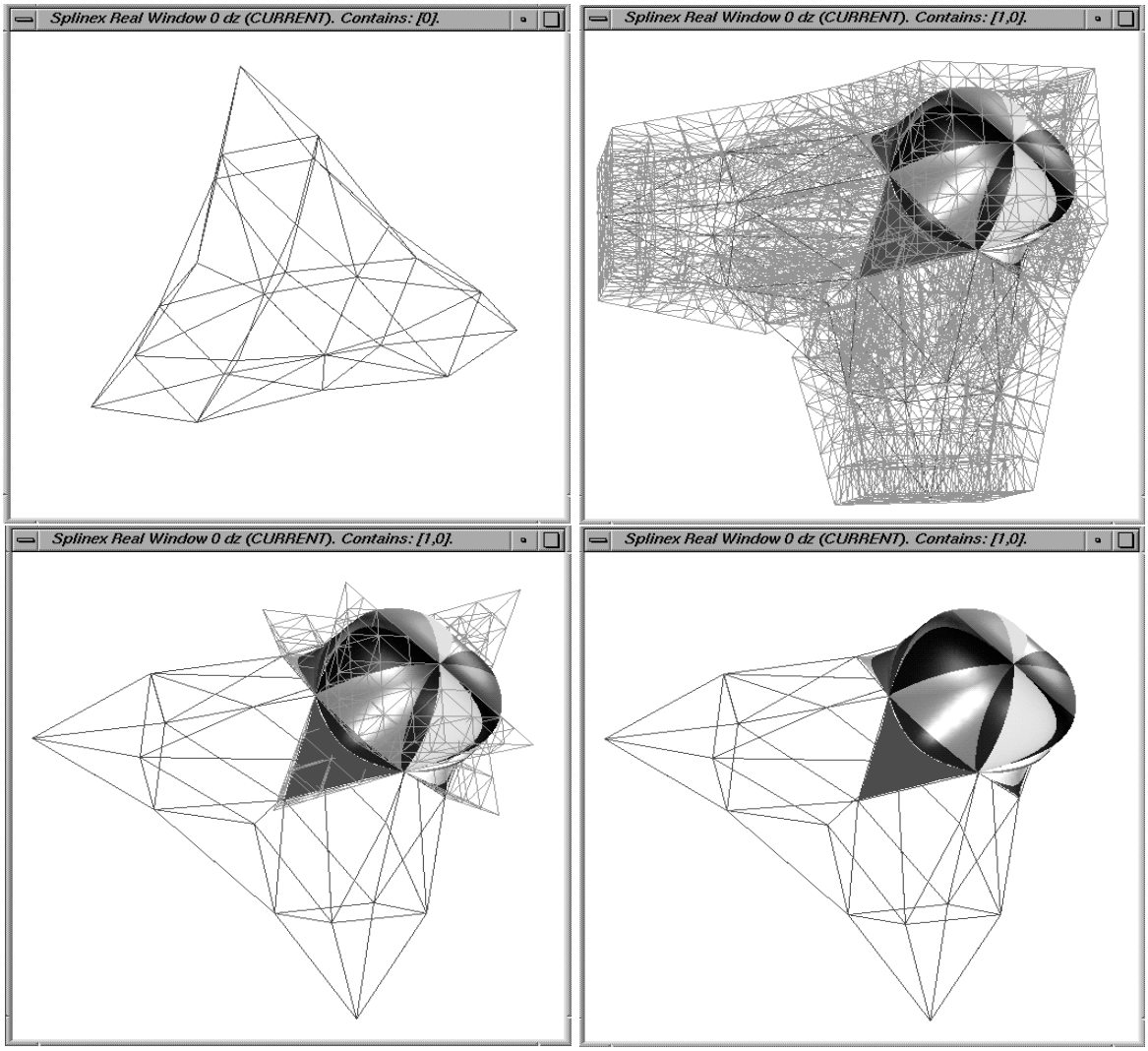

Figure 15: A Surface Triangulation, the Simplicial Hull and some of the interpolatory C^1 Cubic A-Patches

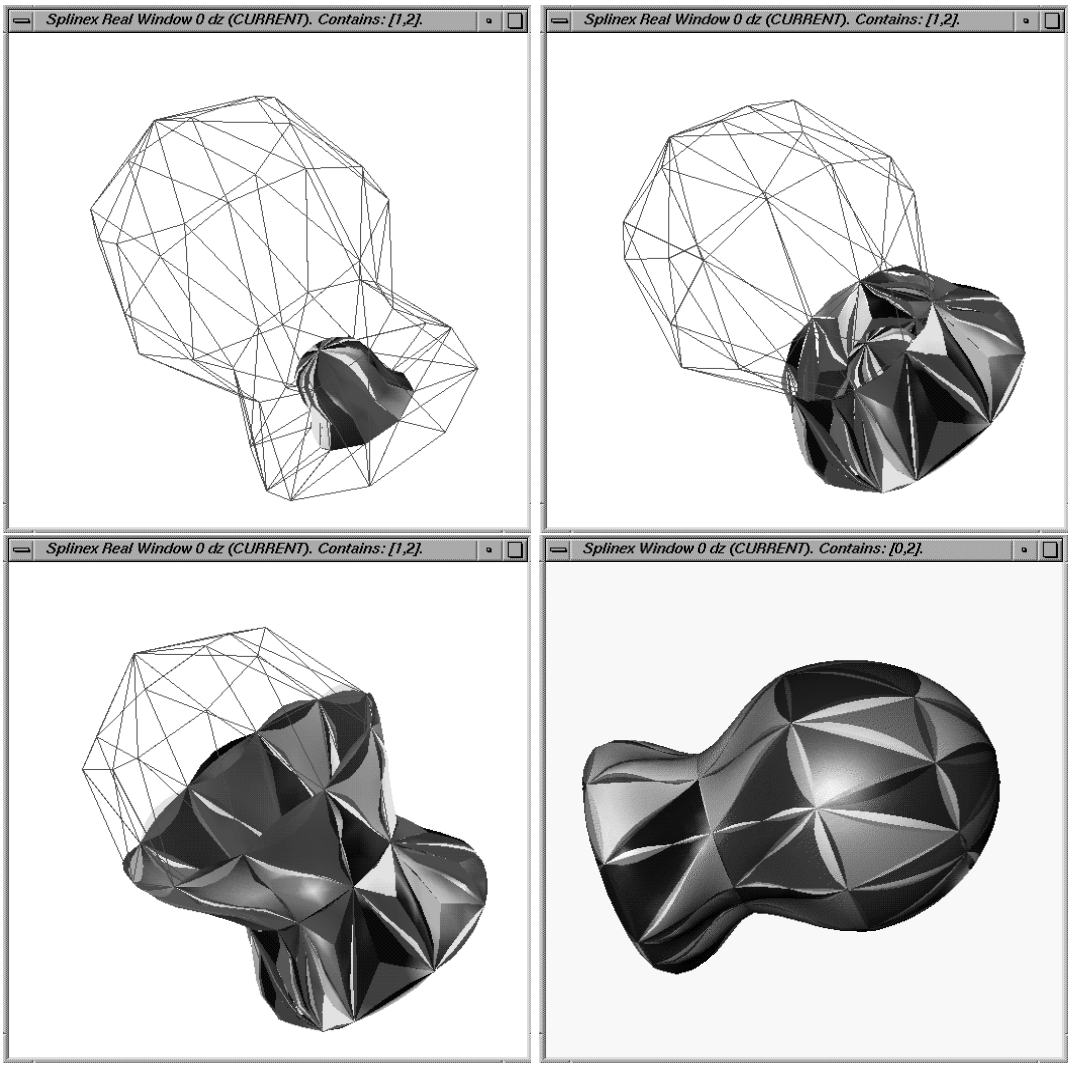

Figure 16: The Complete Smoothing of the Surface Triangulation using C^1 Cubic A-Patches

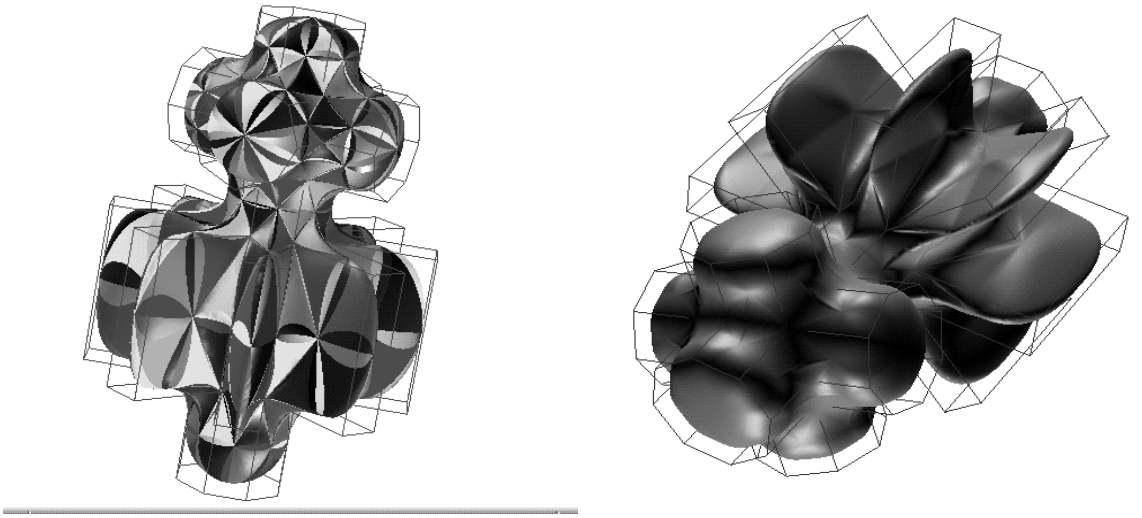

(a) (b)

Figure 17: C^1 and C^2 Smooth Approximations

hull construction is presented and can handle all convex $\mathcal{P}$ and also arbitrary polyhedra with non-convex faces. This new simplicial hull scheme is the three dimensional generalization of the two-dimensional corner-cutting scheme used to construct C^k continuous bivariate A-splines [18]. Using this new hull construction technique paper [10] presents efficient algorithms to construct both a C^1 smooth mesh with cubic A-patches and C^2 smooth mesh with cubic and quintic A-patches to approximate a given polyhedron $\mathcal{P}$ in three dimensions.

For the construction of smooth patch complexes within the simplicial hull built on two adjacent triangles(see Figure 13 for C^1 and Figure 14 for C^2.

See also Figures 17 and 18 for examples of the C^1 and C^2 approximation of polyhedra and their shape modification [11].

Acknowledgement: Implementations of the above algorithms (for parametric and implicit surface patches), were all accomplished in SHASTRA, a distributed and collaborative (multi-user, multi-workstation) free-form geometric design and visualization environment developed by the author at Purdue University. Information on SHASTRA software availability can be obtained from the author or via anonymous ftp from ftp.cs.purdue.edu:pub/shastra/ and via the world wide web from http://www.cs.purdue.edu/research/shastra/shastra.html.

References

[1] S. Abhyankar and C. Bajaj. Automatic Rational Parameterization of Curves and Surfaces I: Conics and Conicoids. *Computer Aided Design*, 19(1):11–14, 1987.

[2] S. Abhyankar and C. Bajaj. Automatic Rational Parameterization of Curves and Surfaces II: Cubics and Cubicoids. *Computer Aided Design*, 19(9):499–502, 1987.

[3] S. Abhyankar and C. Bajaj. Automatic Rational Parameterization of Curves and Surfaces III: Algebraic Plane Curves. *Computer Aided Geometric Design*, 5(1):309–321, 1988.

[4] S. Abhyankar and C. Bajaj. Automatic Rational Parameterization of Curves and Surfaces IV: Algebraic Space Curves. *ACM Transactions on Graphics*, 8(4):324 – 333, 1989.

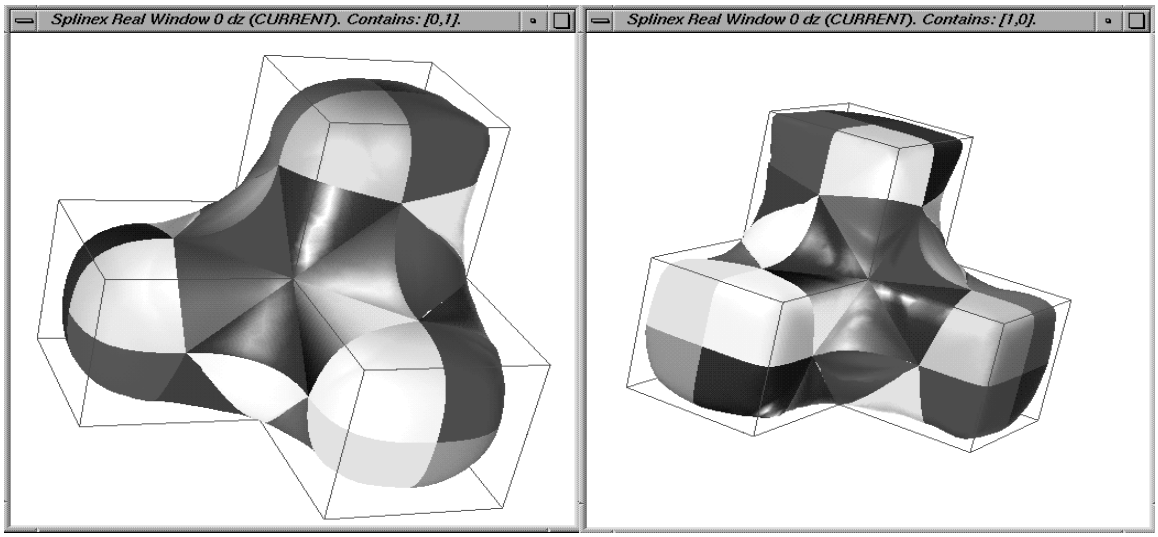

Figure 18: Shape Control of Smooth Approximations of a Polyhedron

[5] P. Alfeld. Scattered Data Interpolation in Three or More Variables. In T. Lyche and L. Schumaker, editors, *Mathematical Methods in Computer Aided Geometric Design*, pages 1–34. Academic Press, 1989.

[6] Allgower, E., and Gnutzmann, S.,. Simplicial Pivoting for Mesh Generation of Implicitly Defined Surfaces. *Computer Aided Geomtric Design*, pages 305–325, 1991.

[7] C. Bajaj. Geometric modeling with algebraic surfaces. In D. Handscomb, editor, *The Mathematics of Surfaces III*, pages 3–48. Oxford Univ. Press, 1988.

[8] C. Bajaj. The Emergence of Algebraic Curves and Surfaces in Geometric Design. In R. Martin, editor, Directions in Geometric Computing, pages 1 – 29. Information Geometers Press, 1993.

[9] C. Bajaj, J. Chen, and G. Xu. Free form Surface Design with A-Patches. In *Proceedings of Graphics Interface'94*, pages 174–181, Banff, Canada., 1994.

[10] C. Bajaj, J. Chen, and G. Xu. *Smooth Low Degree Approximations of Polyhedra.* Computer Science Technical Report, CSD-TR-94-002, Purdue University, 1994.

[11] C. Bajaj, J. Chen, and G. Xu. Interactive Shape Control and Rapid Display of A-Patches. In *Eurographics International Workshop on Implicit Surfaces*, pages 197–215, Grenoble, France., 1995.

[12] C. Bajaj, J. Chen, and G. Xu. *Modeling with Cubic A-Patches. ACM Transactions on Graphics*, 14, 2:103–133, 1995.

[13] C. Bajaj and I. Ihm. C^1 Smoothing of Polyhedra with Implicit Algebraic Splines. *SIGGRAPH'92, Computer Graphics*, 26(2):79–88, 1992.

[14] C. Bajaj and A. Royappa. The Robust Display of Arbitrary Rational Parametric Surfaces. In *Curves and Surfaces in Computer Vision and Graphics III*, pages 70 – 80, Boston, MA, 1992.

[15] C. Bajaj and A. Royappa. *Triangulation and Display of Arbitrary Rational Parametric Surfaces.* In R. Bergeron, A. Kaufman, editor, Proc. of IEEE Visualization '94 Conference, 1994.

[16] C. Bajaj and A. Royappa. *Finite Representation of Real Parametric Curves and Surfaces. Intl. J. of Computational Geometry and Applications*, pages 313–326, 1995.

[17] C. Bajaj and G. Xu. *Piecewise Rational Approximation of Real Algebraic Curves.* Computer Science Technical Report, CAPO-91-19, Purdue University, 1991.

[18] C. Bajaj and G. Xu. *A-Splines: Local Interpolation and Approximation using C^k-Continuous Piecewise Real Algebraic Curves.* Computer Science Technical Report, CAPO-92-44, Purdue University, 1992.

[19] C. Bajaj and G. Xu. *Piecewise Rational Approximation of Real Algebraic Surfaces.* Computer Science Technical Report, CAPO 93-21, Purdue University, 1993.

[20] C. Bajaj and G. Xu. *NURBS Approximation of Surface-Surface Intersection Curves. Advances in Computational Mathematics*, pages 1–21, 1994.

[21] C. Bajaj and G. Xu. Rational spline approximations of real algebraic curves and surfaces. In H.P. Dikshit and C. Michelli, editors, Advances in Computational Mathematics, pages 73 – 85. World Scientific Publishing Co., 1994.

[22] Beeker, E. Smoothing of Shapes Designed with Free Form Surfaces. *Computer Aided Design*, 18(4):224–232, 1986.

[23] Bloomenthal, J. Polygonization of Implicit Surfaces. *Computer Aided Geometric Design*, 5:341–355, 1988.

[24] Chiyokura, H., and Kimura, F. Design of Solids with Free-form Surfaces. *Computer Graphics*, 17(3):289–298, 1983.

[25] Chuang, J.,. *Surface Approximations in Geomtric Modeling.* PhD thesis, Computer Science, Purdue University, 1990.

[26] Chui, C. *Multivariate Splines.* Regional Conference Series in Applied Mathematics, 1988.

[27] R. Clough and J. Tocher. Finite Element Stiffness Matrices for Analysis of Plates In Bending. In Proceedings of Conference on Matric Methods in Structural Analysis, 1965.

[28] G. Collins. Quantifier Elimination for Real Closed Fields: A Guide to the Literature, in *computer algebra, symbolic and algebraic computation*, 1983.

[29] W. Dahmen. Smooth piecewise quadratic surfaces. In T. Lyche and L. Schumaker, editors, *Mathematical Methods in Computer Aided Geometric Design*, pages 181–193. Academic Press, Boston, 1989.

[30] W. Dahmen and T-M. Thamm-Schaar. Cubicoids: modeling and visualization. *Computer Aided Geometric Design*, 10:93–108, 1993.

[31] Dahmen, W. and Micchelli, C. Recent Progress in Multivariate Splines. In L. Schumaker C. Chui and J. Word, editors, *Approximation Theory IV*, pages 27–121. Academic Press, 1983.

[32] DeRose, T. Rational Bezier Curves and Surfaces on Projective Domains. In G. Farin, editor, *NURBS for Curve and Surface Design*, pages 1–14. SIAM, 1991.

[33] H. Edelsbrunner. Algorithms in Combinatorial Geometry. Springer Verlag, 1987.

[34] G. Farin. Triangular Bernstein-Bézier patches. *Computer Aided Geometric Design*, 3:83–127, 1986.

[35] Fortune S.,. Numerical Stability of Algorithms for 2D Delaunay Triangulations. In Proc. of the 8th ACM Symposium on Computational Geometry, pages 83–92, 1989.

[36] Garrity, T., and Warren, J. Geometric continuity. *Computer Aided Geometric Design*, 8:51–65, 1991.

[37] Geisow, A.,. *Surface Interrogations.* PhD thesis, University of Anglia, School of computing Studies and Accountancy, 1983.

[38] Gregory, J., and Charrot, P. A C^1 Triangular Interpolation Patch for Computer Aided Geometric Design. *Computer Graphics and Image Processing*, 13:80–87, 1980.

[39] B. Guo. *Modeling Arbitrary Smooth Objects with Algebraic Surfaces.* PhD thesis, Computer Science, Cornell University, 1991.

[40] B. Guo. Surface generation using implicit cubics. In N.M. Patrikalakis, editor, *Scientific Visualizaton of Physical Phenomena*, pages 485–530. Springer-Verlag,Tokyo, 1991.

[41] B. Guo. Non-splitting Macro Patches for Implicit Cubic Spline Surfaces. *Computer Graphics Forum*, 12(3):434 – 445, 1993.

[42] Hagen, H., and Pottmann, H. Curvature Continuous Triangular Interpolants. *Mathematical Methods in Computer Aided Geometric Design*, pages 373–384, 1989.

[43] Hall, M., and Warren, J. Adaptive Polygonalization of Implicitly Defined Surfaces. *IEEE Computer Graphics and Applications*, pages 33–42, 1990.

[44] P. Henrici. *Applied and Computational Complex Analysis*, 1988.

[45] Herron, G. Smooth Closed Surfaces with Discrete Triangular Interpolants. *Computer Aided Geometric Design*, 2(4):297–306, 1985.

[46] Hollig, K. Multivariate Splines. *SIAM J. on Numerical Analysis*, 19:1013–1031, 1982.

[47] Liu, D., and Hoschek, J. GC^1 Continuity Conditions Between Adjacent Rectangular and Triangular Bezier Surface Patches. *Computer Aided Design*, 21:194–200, 1989.

[48] Lorensen, W., and Cline, H. Marching Cubes: A High Resolution 3D Surface Construction Algorithm. *Computer Graphics*, 21:163–169, 1987.

[49] Micchelli, C., and Prautzsch, H.,. Computing Surfaces Invariant under Subdivision. *Computer Aided Geometric Design*, 4:321–328, 1987.

[50] D. Moore and J. Warren. Approximation of dense scattered data using algebraic surfaces. In *Proc. of the 24th Hawaii Intl. Conference on System Sciences*, pages 681–690, Kauai, Hawaii, 1991.

[51] Nielson, G. A Transfinite Visually Continuous Triangular Interpolant. In G. Farin, editor, *Geometric Modeling Applications and New Trends.* SIAM, 1986.

[52] Patrikalakis, N., and Kriezis, G. Representation of Piecewise Continuous Algebraic Surfaces in Terms of B-splines. *The Visual Computer*, 5(6):360–374, Dec. 1989.

[53] Peters, J. Local Cubic and BiCubic C^1 Surface Interpolation with Linearly Varying Boundary Normal. *Computer Aided Geometric Design*, 7:499–516, 1990.

[54] Peters, J. Smooth Interpolation of a Mesh of Curves. *Constructive Approximation*, 7:221–246, 1991.

[55] Piper, B. Visually Smooth Interpolation with Triangular Bezier Patches. In G. Farin, editor, *Geometric Modeling: Algorithms and New Trends.* SIAM, 1987.

[56] Powell, M., and Sabin, M. Piecewise Quadratic Approximations on Triangles. *ACM Trans. on Math. Software*, 3:316–325, 1977.

[57] Ramshaw, L. Beziers and B-splines as Multiaffine Maps. In *Theoretical Foundations of Computer Graphics and CAD.* Springer Verlag, 1988.

[58] Rockwood, A., Heaton, K., and Davis, T. Real-Time Rendering of Trimmed Surfaces. *Computer Graphics*, 23(3):107–116, 1989.

[59] R. Sarraga. G^1 interpolation of generally unrestricted cubic Bézier curves. *Computer Aided Geometric Design*, 4:23–39, 1987.

[60] T.W. Sederberg. Piecewise algebraic surface patches. *Computer Aided Geometric Design*, 2(1-3):53–59, 1985.

[61] T.W. Sederberg. Techniques for cubic algebraic surfaces, tutorial part ii. *IEEE Computer Graphics and Applications*, 10(5):12–21, Sept. 1990.

[62] Sederberg, T., and J. Snively, J.,. Parameterization of Cubic Algebraic Surfaces. In Oxford University Press R. Martin, editor, *The Mathematics of Surfaces II*, 1987.

[63] Seidel, H-P. A New Multiaffine Approach to B-splines. *Computer Aided Geometric Design*, 6:23–32, 1989.

[64] Semple, J., and Roth, L. *Introduction to Algebraic Geometry*. Oxford University Press, Oxford, U.K., 1949.

[65] Shirman, L., and Sequin, C. Local Surface Interpolation with Bezier Patches. *Computer Aided Geometric Design*, 4:279–295, 1987.

[66] Walker, R. *Algebraic Curves*. Springer Verlag, 1950.

[67] Zariski, O. *Algebraic Surfaces*. Ergebnisse der Mathematik und ihre Grenzgebiete 4, 1935.

[68] Zariski, O., and Samuel, P. *Commutative Algebra (Vol. I, II)*. Springer Verlag, 1958.

A Tutorial on
Binary Space Partitioning Trees

Bruce F. Naylor
Spatial Labs Inc.

I. Introduction

In most applications involving computation with 3D geometric models, manipulating objects and generating images of objects are crucial operations. Performing these operations requires determining for every frame of an animation the spatial relations between objects: how they might intersect each other, and how they may occlude each other. However, the objects, rather than being monolithic, are most often comprised of many pieces, such as by many polygons forming the faces of polyhedra. The number of pieces may be any where from the 100's to the 1,000,000's. To compute spatial relations between n polygons by brute force entails comparing every pair of polygons, and so would require $O(n^2)$. For large scenes comprised of 10^5 polygons, this would mean 10^{10} operations, which is much more than necessary.

The number of operations can be substantially reduced to anywhere from $O(n \log_2 n)$ when the objects interpenetrate (and so in our example reduced to $\sim 10^6$), to as little as constant time, O(1), when they are somewhat separated from each other. This can be accomplished by using Binary Space Partitioning Trees, also called BSP Trees or Partitioning Trees. They provide a computational representation of space that simultaneouly provides a search structure and a representation of geometry. The reduction in number of operations occurs because Partitioning Trees provide a kind of "spatial sorting". In fact, they are a generalization to dimensions > 1 of binary search trees, which have been widely used for representing sorted lists. The figure below gives an introductory example showing how a binary tree of lines, instead of points, can be used to "sort" four geometric objects, as opposed to sorting symbolic objects such as names.

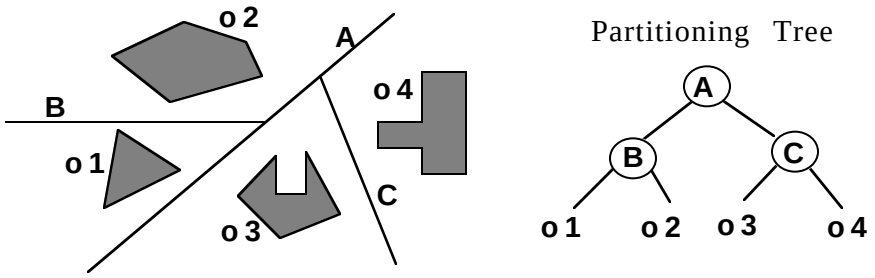

Partitioning Tree representation of inter-object spatial relations

Constructing a Partitioning Tree representation of one or more polyhedral objects involves computing the spatial relations between polygonal faces once and encoding these relations in a binary tree. This tree can then be transformed and merged with other trees to very quickly compute the spatial relations (for visibility and intersections) between the polygons of two moving objects.

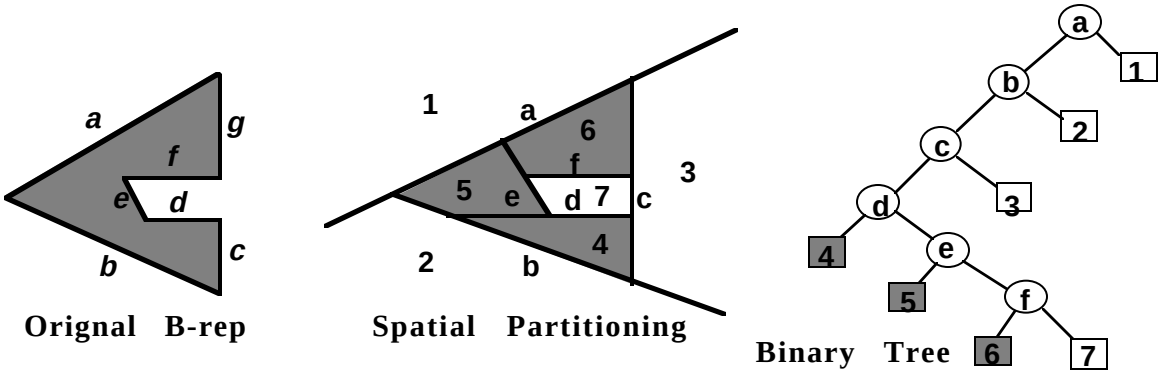

Partitioning Tree representation of intra-object spatial relations

As long as the relations encoded by a tree remain valid, which for a rigid body is forever, one can reap the benefits of having generated this tree structure every time the tree is used in subsequent operations. The return on investment manifests itself as substantially faster algorithms for computing intersections and visibility orderings. And for animation and interactive applications, these saving can accure over hundreds of thousands of frames.

Partitioning Trees achieve an elegant solution to a number of important problems in geometric computation by exploiting two very simple properties occurring whenever a single plane separates (lies between) two or more objects: 1) any object on one side of the plane cannot intersect any object on the other side, 2) given a viewing position, objects on the same side as the viewer can have their images drawn on top of the images of objects on the opposite side (Painter's Algorithm).

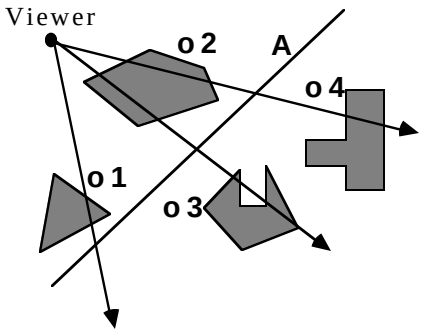

Plane Power: sorting objects w.r.t a hyperplane

These properties can be made dimension independent if we use the term "hyperplane" to refer to planes in 3D, lines in 2D, and in general for d-space, to a (d-1)-dimensional sub-space defined by a single linear equation. The only operation we will need for constructing Partitioning Trees is the partitioning of a convex region by a singe hyperplane into two child regions, both of which are also convex as a result.

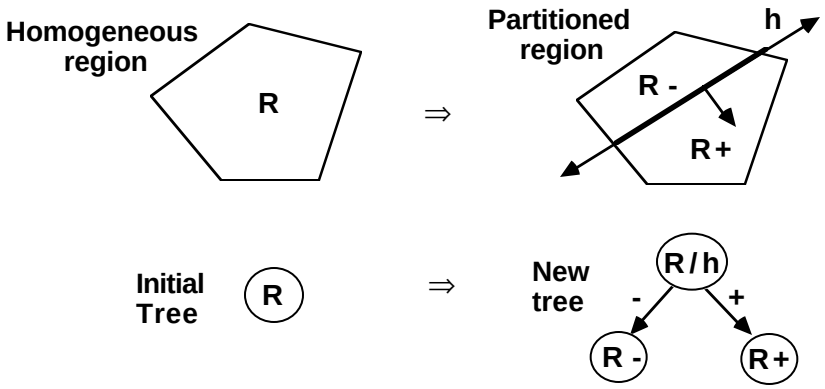

Elementary operation used to construct Partitioning Trees

Partitioning Trees exploit the properties of separating planes by using one very simple but powerful technique to represent any object or collection of objects: recursive subdivison by hyperplanes. A Partitioning Tree is the recording of this process of recursive subdivision in the form of a binary tree of hyperplanes. Since there is no restriction on what hyperplanes are used, polytopes (polyhedra, polygons, etc.) can be represented exactly. Affine and perspective transformations can be applied without having to modify the structure of the tree itself, but rather by modifying the linear equations representing each hyperplane (with a vector-matrix product as one does with points).

A Partitioning Tree is a program for performing intersections between the hyperplane's halfspaces and any other geometric entity. Since subdivsion generates increasingly smaller regions of space, the order of the hyperplanes is chosen so that following a path deeper into the tree corresponds to adding more detail, yielding a multi-resolution representation. This

leads to efficient intersection computations. To determine visibility, all that is required is choosing at each tree node which of the two branches to draw first based solely on which branch contains the viewer. No other single representation of geometry inherently answers questions of intersection and visibility for a scene of 3D moving objects. And this is accomplished in a computationally efficient and parallelizable manner.

II. Partitioning Trees as a Multi-Dimensional Search Structure

Spatial search structures are based on the same ideas that were developed in Computer Science during the 60's and 70's to solve the problem of quickly processing large sets of symbolic data, as opposed to geometric data, such as lists of people's names. It was discovered that by first sorting a list of names alphabetically, and storing the sorted list in an array, one can find out whether some new name is already in the list in $\log_2 n$ operations using a binary search algorithm, instead of n/2 expected operations required by a sequential search. This is a good example of extracting structure (alphabetical order) existing in the list of names and exploiting that structure in subsequent operations (looking up a name) to reduce computation. However, if one wishes to permit additions and deletions of names while maintaining a sorted list, then a dynamic data structure is needed, i.e. one using pointers. One of the most common examples of such a data structure is the binary search tree.

A binary search tree is illustrated in the figure below, where it is being used to represent a set of integers S = { 0, 1, 4, 5, 6, 8 } lying on the real line. We have included both the binary tree and the hierarchy of intervals represented by this tree. To find out whether a number/point is already in the tree, one inserts the point into the tree and follows the path corresponding to the sequence of nested intervals that contain the point. For a balanced tree, this process will take no more than O(log n) steps; for in fact, we have performed a binary search, but one using a tree instead of an array. Indeed, the tree itself encodes a portion of the search algorithm since it prescribes the order in which the search proceeds.

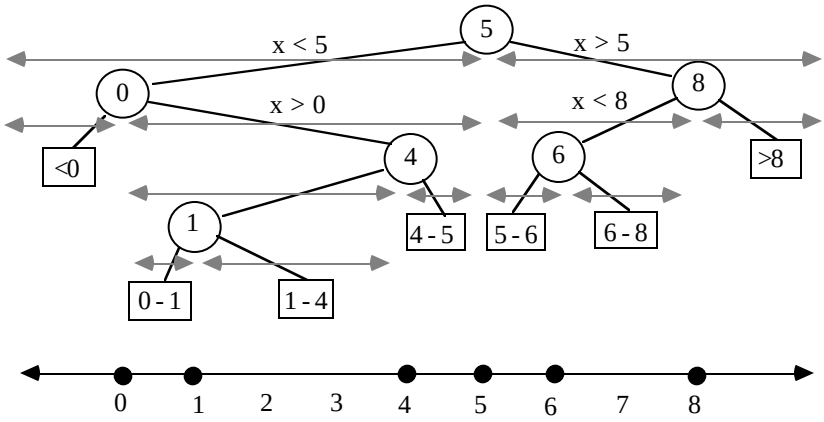

This now bring us back to Partitioning Trees, for as we said earlier, they are a generalization of binary search trees to dimensions > 1 (in 1D, they are essentially identical). In fact, constructing a Partitioning Tree can be thought of as a geometric version of Quick Sort. Modifications (insertions and deletions) are achieve by merging trees, analogous to merging sorted lists in Merge Sort. However, since points do not divide space for any dimension >1, we must use hyperplanes instead of points by which to subdivide. Hyperplanes always partition a region into two halfspaces regardless of the dimension. In 1D, they look like points since they are also 0D sets; the one difference being the addition of a normal denoting the "greater than" side. Below we show a restricted variety of Partitioning Trees that most clearly illustrates the generalization of binary search trees to higher dimensions. (You may want to call this a k-d tree, but the standard semantics of k-d trees does not include representing continuous sets of points, but rather finite sets of points.)

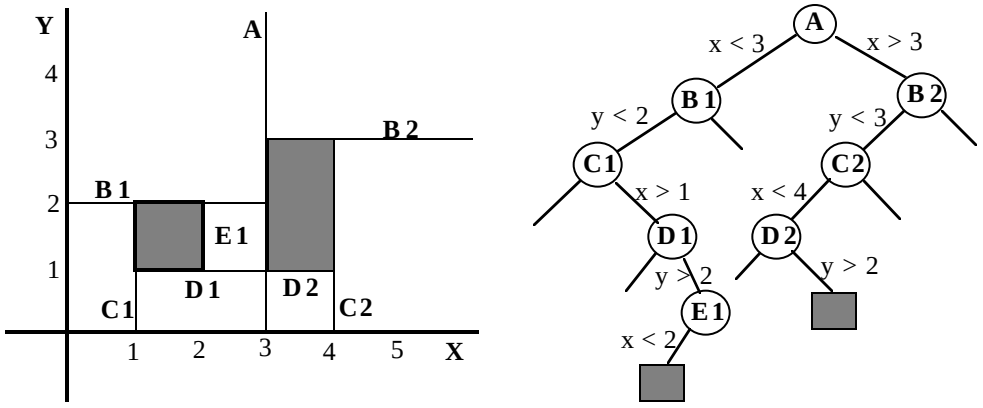

Extension of binary search trees to 2D as a Partitioning Tree

Partitioning Trees are also a geometric variety of Decision Trees, which are commonly used for classification (e.g. biological taxonomies), and are widely used in machine learning. Decision trees have also been used for proving lower bounds, the most famous showing that sorting is Ω(n log n) They are also the model of the popular "20 questions" game (I'm thinking of something and you have 20 yes/no question to guess what it is). For Partitioning Trees, the questions become "what side of a particular hyperplane does some piece of geometry lie".

III. Visibility Orderings

Visibility orderings are used in image synthesis for visible surface determination (hidden surface removal), shadow computations, ray tracing, beam tracing, and radiosity. For a given center of projection, such as the position of a viewer or of a light source, they provide an

ordering of geometric entities, such as objects or faces of objects, consistent with the order in which any ray originating at the center might intersect the entities. Loosely speaking, a visibility ordering assigns a priority to each object or face so that closer objects have priority over objects further away. Any ray emanating from the center or projection that intersects two objects or faces, will always intersect the surface with higher priority first. The simplest use of visibility orderings is with the "Painters Algorithm" for solving the hidden surface problem. Faces are drawn into a frame-buffer in far-to-near order (low-to-high priority), so that the image of nearer objects/polygons over-writes those of more distant ones.

A visibility ordering can be generated using a single hyperplane; however, each geometric entity or "object" (polyhedron, polygon, line, point) must lie completely on one side of the hyperplane, i.e. no objects are allowed to cross the hyperplane. This requirement can always be induced by partitioning objects by the desired hyperplane into two "halves". The objects on the side containing the viewer are said to have visibility priority over objects on the opposite side; that is, any ray emanating from the viewer that intersects two objects on opposite sides of the hyperplane will always intersect the near side object before it intersects the far side object.

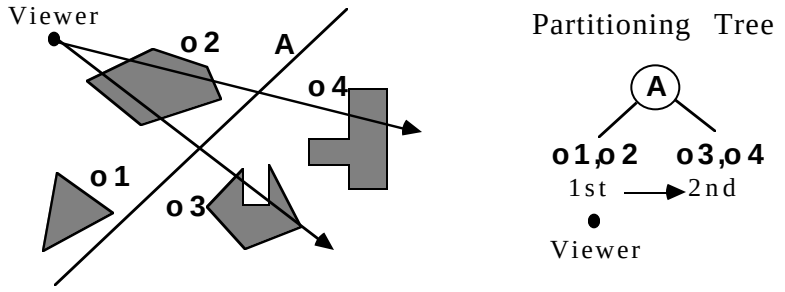

Left side has priority over right side

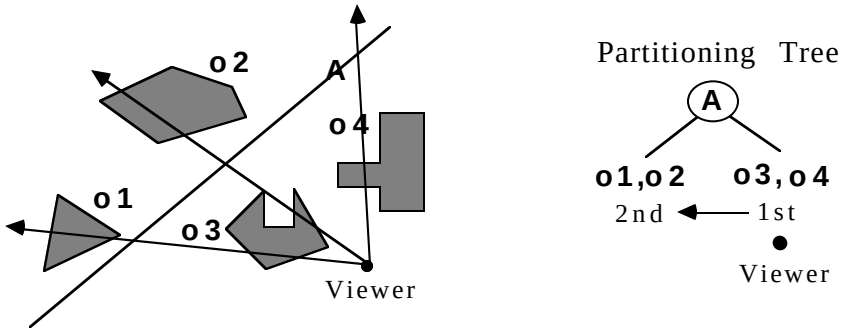

Right side has priority over left side

Total Ordering of a Collection of Objects

A single hyperplane cannot order objects lying on the same side, and so cannot provide a total visibility ordering.

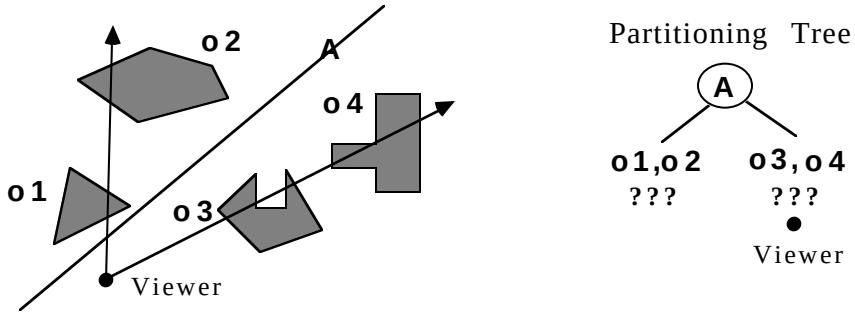

Consequently, in order to exploit this idea, we must extend it somehow so that a visibility ordering for the entire set of objects can be generated. One way to do this would be to create a unique separating hyperplane for evey pair of objects. However, for n objects this would require n^2 hyperplanes, which is too many.

The required number of separating hyperplanes can be reduced to as little as n by using the geometric version of recursive subdivision (divide and conquer). If the subdivsion is performed using hyperplanes whose position and orientation is unrestricted, then the result is a Partitioning Tree. The objects are first separated into two groups by some appropriately choosen hyperplane (as above). Then each of the two groups are <u>independently</u> partitioned into two sub-groups (for a total now of 4 sub-groups). The recursive subdivision continues in a similar fashion until each object, or piece of an object, is in a separate cell of the partitioning. This process of partitioning space by hyperplanes is naturally represented as a binary tree.

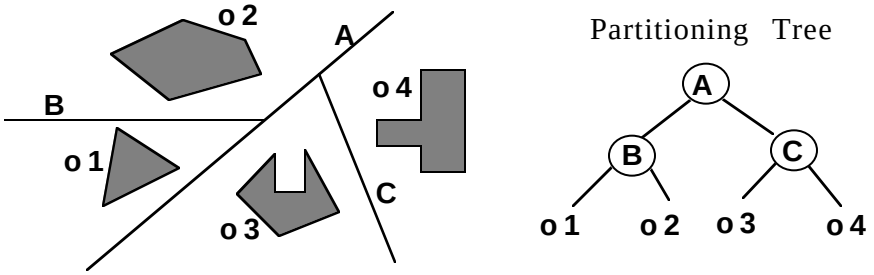

Visibility Ordering as Tree Traveral

How can this tree be used to generate a visibility ordering on the collection of objects? For any given viewing position, we first determine on which side of the root hyperplane the viewer lies. From this we know that all objects in the near-side subtree have higher priority than all objects in the far-side subtree; and we have made this determination with only a constant amount of computation (in fact, only a dot product). We now need to order the

near-side objects, followed by an ordering of the far-side objects. Since we have a recusively defined structure, any subtree has the same form computationally as the whole tree. Therefore, we simply apply this technique for ordering subtrees recursively, going left or right first at each node, depending upon which side of the node's hyperplane the viewer lies. This results in a traversal of the entire tree, in near-to-far order, using only O(n) operations, which is optimal (this analysis is correct only if no objects have been split; otherwise it is > n).

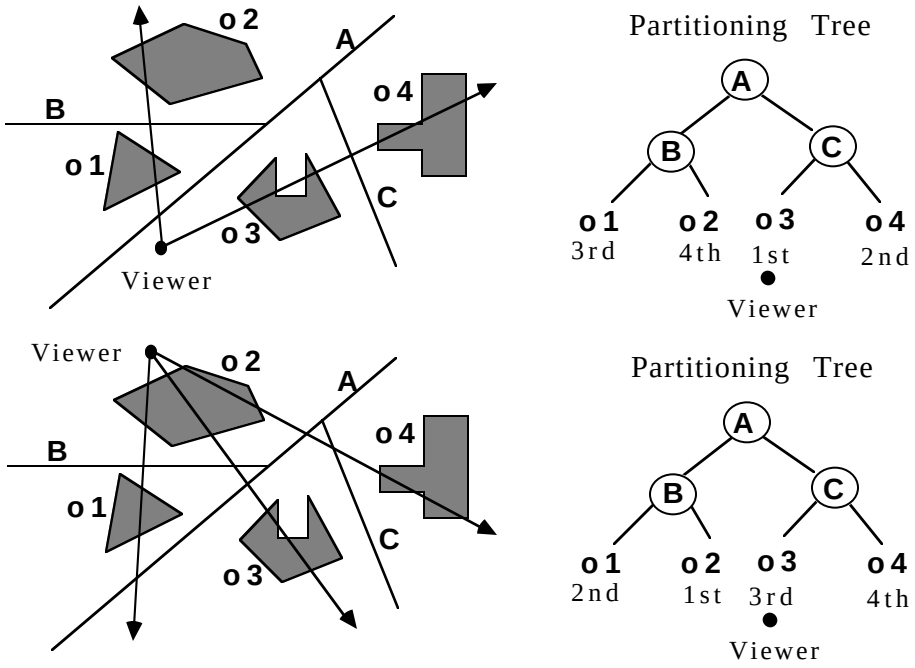

Intra-Object Visibility

The schema we have just described is only for inter-object visibility, i.e. between individual objects. And only when the objects are both convex and separable by a hyperplane is the schema a complete method for determining visibility. To address the general unrestricted case, we need to solve intra-object visibility, i.e. correctly ordering the faces of a single object. Partitioning Trees can solve this problem as well. To accomplish this, we need to change our focus from convex cells containing objects to the idea of hyperplanes containing faces. Let us return to the analysis of visibility w.r.t a hyperplane. If instead of ordering objects, we wish to order faces, we can exploit the fact that not only can faces lie on each side of a hyperplane as objects do, but they can also lie on the hyperplane itself. This gives us a 3-way ordering of: near -> on -> far.

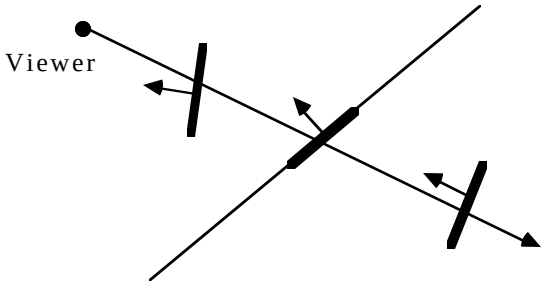

Ordering of polygons: near -> on -> far

If we choose hyperplanes by which to partition space that always contain a face of an object, then we can build a Partitioning Tree by applying this schema recursively as before, until every face lies in some partitioning hyperplane contained in the tree.

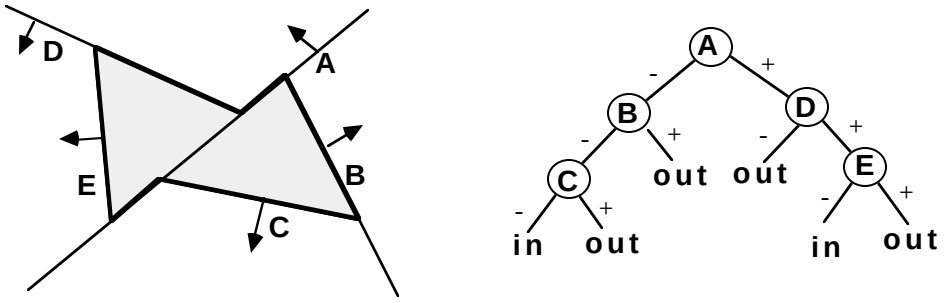

Example intra-object Partitioning Tree

To generate a visibility ordering of the faces in this intra-object tree, we use the method above with one extension: faces lying on hyperplanes are included in the ordering, i.e. at each node, we generate the visibility ordering of near-subtree -> on-faces -> far-subtree.

Using visibility orderings provides an alternative to z-buffer based algorithms. They obviate the need for computing and comparing z-values, which is very suspectible to numerical error because of the perspective projection. In addition, they eliminate the need for z-buffer memory itself, which can be substantial (80Mbytes) if used at a sub-pixel resolution of 4x4 to provide anti-aliasing. More importantly, visibility orderings permit unlimited use of transparency (non-refractive) with no additional computational effort, since the visibility ordering gives the correct order for compositing faces using alpha blending. And in addition, if a near-to-far ordering is used, then rendering completely occluded objects/faces can be eliminated, such as when a wall occludes the rest of a building, using a beam-tracing based algorithm.

Partitioning Tree as a Hierarchy of Regions

Another way to look at Partitioning Trees is to focus on the hierarchy of regions creating by the recursive partitioning, instead of focusing on the hyperplanes themselves. This view helps us to see more easily how intersections are efficiently computed. The key idea is to think of a Partitioning Tree region as serving as a bounding volume: each node **v** corresponds to a convex volume that completely contains all the geometry represented by the subtree rooted at **v**. Therefore, if some other geometric enitity, such as a point, ray, object, etc., is found to not intersect the bounding volume, then no intersection computations need be performed with any geometry within that volume.

Consider as an example a situation in which we are given some test point and we want to find which object if any this point lies in. Initially, we know only that the point lies somewhere in space.

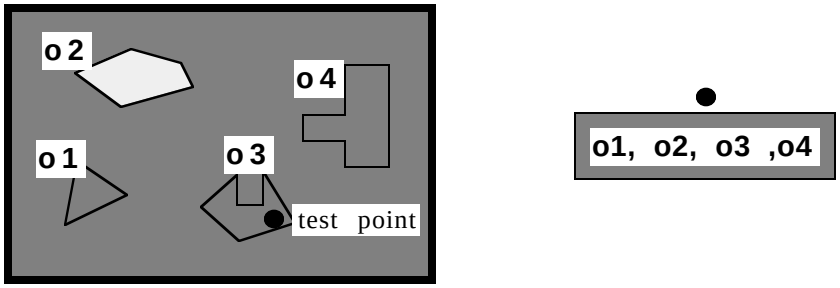

By comparing the location of the point w.r.t. the first partitioning hyperplane, we can find in which of the two regions (a.k.a. bounding volumes) the point lies. This eliminates half of the objects.

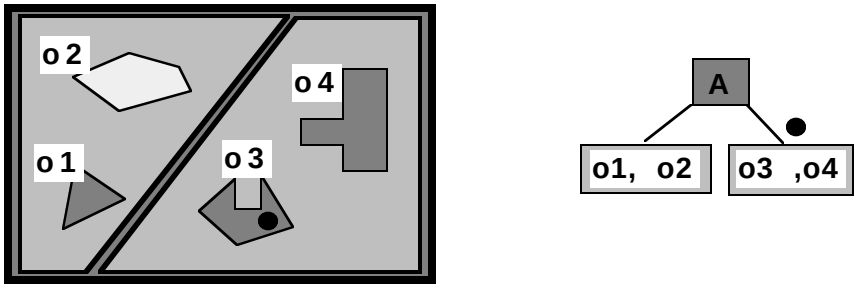

By continuing this process recursively, we are in effect using the regions as a hierarchy of bounding volumes, each bounding volume being a rough approximation of the geometry it bounds, to quickly narrow our search.

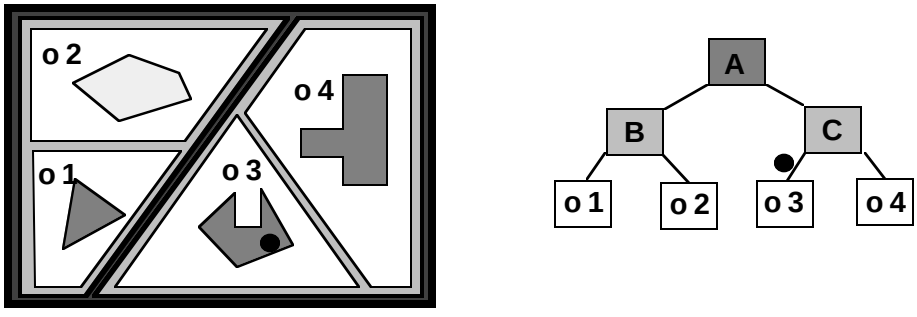

For a Partitioning Tree of a single object, this region-based (volumetric) view reveals how Partitioning Trees can provide a multi-resolution representation. As one decends a path of the tree, the regions decrease in size monotonically. For curved objects, the regions converge in the limit to the curve/surface. Truncating the tree produces an approximation, ala the Taylor series approximations of functions.

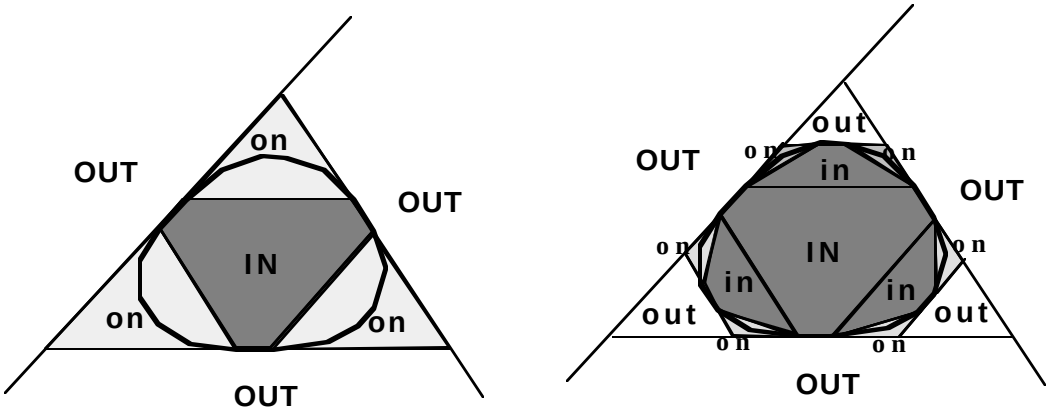

1st level Approximation 2nd level Approximation

Tree Merging

The spatial relations between two objects, each represented by a separate tree, can be determined efficiently by merging two trees. This is a fundemental operation that can be used to solve a number of geometric problems. These include set operations for CSG modeling as well as collision detection for dynamics. For rendering, merging all object-trees into a single model-tree determines inter-object visibility orderings; and the model-tree can be intersected with the view-volume to efficiently cull away off-screen portions of the scene and provide solid cutways with the near clipping plane. In the case where objects are both transparent and interpenetrate, tree merging acts as a view independent geometric sorting of the object faces; each tree is used in a manner analogous to the way Merge Sort merges previously sorted lists to quickly created a new sorted list (in our case, a new tree). The model-tree can be rendered using ray-tracing, radiosity, or polygon-drawing using a far-to-near ordering with alpha blending for transparency. An even better alternative is multi-resolution beam-tracing, since entire occluded subtrees can be elimanted without visiting the contents of the subtree, and distance subtrees can be pruned to the desired resolution. Beam-tracing can also be used to efficiently compute shadows.

All of this requires as a basics operation an algorithm for merging two trees. Tree merging is a recursive process which proceeds down the trees in a multi-resolution fashion, going from low-res to high-res. It is easist to understand in terms of merging a hierarchy of bounding volumes. As the process proceeds, pairs of tree regions, a.k.a. convex bounding volumes, one from each tree, are compared to determine whether they intersect or not. If

they do not, then the contents of the corresponding subtrees are never compared. This has the effect of "zooming in" on those regions of space where the surfaces of the two objects intersect. In the 2D example below, representing two convex polygons, tree merging will require only O(log n) operations.

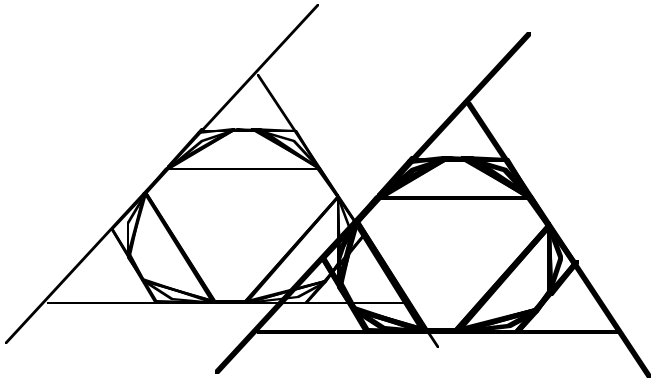

Merging Partitioning Trees

The algorithm for tree merging is quite simple once you have a routine for partitioning a tree by a hyperplane into two trees. The process can be thought of in terms of inserting one tree into the other in a recursive manner. Given trees T1 and T2, at each node of T1 the hyperplane at that node is used to partition T2 into two "halves". Then each half is merged with the subtree of T1 lying on the same side of the hyperplane. (In actuality, the algorithm is symmetric w.r.t. the role of T1 and T2 so that at each recursive call, T1 can split T2 or T2 can split T1.)

```
Merge_Bspts : ( T1, T2 : Bspt ) -> Bspt
 Types
  BinaryPartitioner : { hyperplane, sub-hyperplane }
  PartitionedBspt : ( inNegHs, inPosHs : Bspt )

 Imports
 Merge_Tree_With_Cell : ( T1, T2 : Bspt ) ->  Bspt     User defined semantics.
 Partition_Bspt : ( Bspt, BinaryPartitioner ) ->  PartitionedBspt

 Definition
  IF T1.is_a_cell OR T2.is_a_cell
   THEN
    VAL := Merge_Tree_With_Cell( T1, T2 )
   ELSE
    Partition_Bspt( T2, T1.binary_partitioner ) -> T2_partitioned
    VAL.neg_subtree :=
        Merge_Bspts( T1.neg_subtree, T2_partitioned.inNegHs )
    VAL.pos_subtree:=
        Merge_Bspts( T1.pos_subtree, T2_partitioned.inPosHs )
   END
```

```
    RETURN VAL
END Merge_Bspts
```

While tree merging is easiest to understand in term of comparing bounding volumes, the actual mechanism uses *sub-hyperplanes*, which is more efficient. A sub-hyperplane is created whenever a region is partitioned by a hyperplane, and it is just the subset of the hyperplane lying within that region. In fact, all of the illustrations of trees we have used are drawings of sub-hyperplanes. In 3D, these are convex polygons, and they separate the two child regions of an internal node. Tree merging uses sub-hyperplanes to simulataneously determine the spatial relations of four regions, two from each tree, by comparing the two sub-hyperplanes at the root of each tree. For 3D, this is computed using two applications of convex-polygon clipping to a plane, and there are three possible outcomes: intersecting, non-intersecting and coincident. This is the only overtly geometric computation in tree merging; everything else is data structure manipulation.

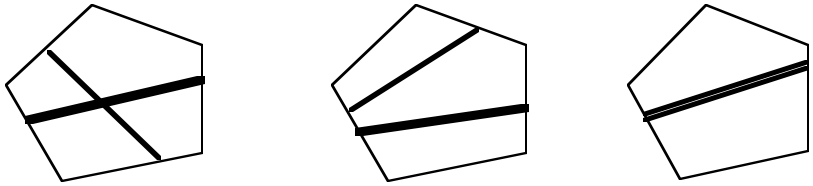

Intersecting Non-intersecting Coincident

Three cases when comparing sub-hyperplanes during tree merging

Good Partitioning Trees

For any given set, there exist an arbitrary number of different Partitioning Trees that can represent that set. This is analogous to there being many different programs for computing the same function, since a Partitioning Tree may in fact be interpreted as a computation graph specifying a particular search of space. Similarly, not all programs/algorithms are equally efficient, and not all searches/trees are equally efficient. Thus the question arises as to what constitutes a good Partitioning Tree. The answer is a tree that represents the set as a sequence of approximations. This provides a multi-resolution representation. By pruning the tree at various depths, different approximations of the set can be created. Each pruned subtree is replaced with a cell containing a low degree polynomial approximation of the set represented by the subtree.

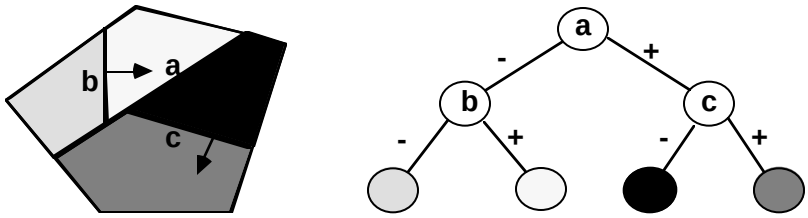

Before pruning

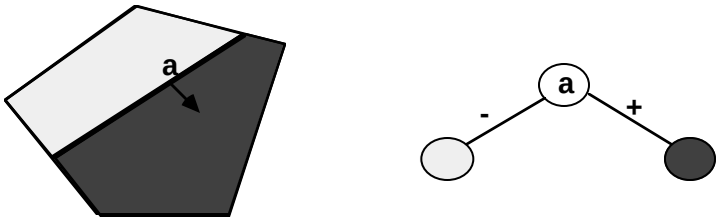

After pruning

Tree Pruning for Multi-Resolution Representations

In figure below, we show two quite different ways to represent a convex polygon, only the second of which employs the sequence of approximations idea. The tree on the left subdivides space using lines radiating from the polygonal center, splitting the number of faces in half at each step of the recursive subdivision. The hyperplanes containing the polygonal edges are chosen only when the number of faces equals one, and so are last along any path. If the number of polygonal edges is n, then the tree is of size O(n) and of depth O(log n). In contrast, the tree on the right uses the idea of a sequence of approximations. The first three partitioning hyperplanes form a first approximation to the exterior while the next three form a first approximation to the interior. This divides the set of edges into three sets. For each of these, we choose the hyperplane of the middle face by which to partition, and by doing so refine our representation of the exterior. Two additional hyperplanes refine the interior and divide the remaining set of edges into two nearly equal sized sets. This process proceeds recursively until all edges are in partitioning hyperplanes. Now, this tree is also of size O(n) and depth O(log n), and thus the worst case, say for point classification, is the same for both trees. Yet they appear to be quite different.

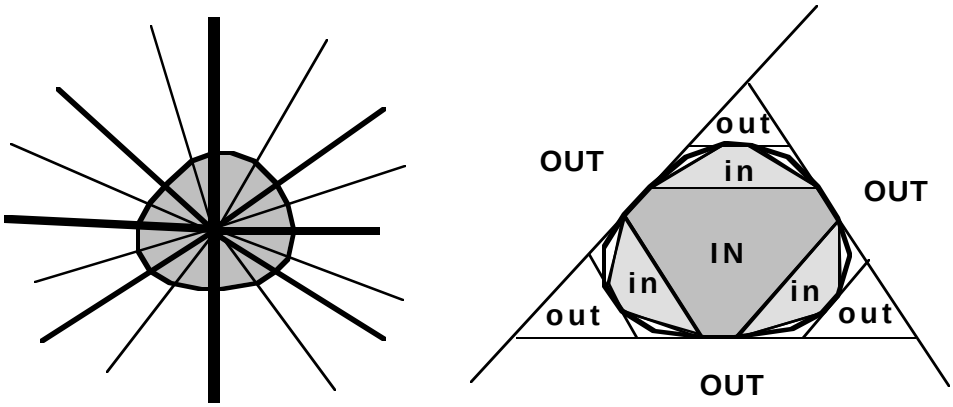

Illustration of bad vs. good trees

This apparent qualitative difference can be made quantitative by, for example, considering the expected case for point classification. With the first tree, all cells are at depth log n, so the expected case is the same as the worst case regardless of the sample space from which a point is chosen. However, with the second tree, the top three out-cells would typically constitute most of the sample space, and so a point would often be classified as OUT by, on average, two point-hyperplane tests. Thus the expected case would converge to O(1) as the ratio of polygon-area/sample-area approaches 0. For line classification, the two trees differ not only in the expected case but also in the worst case: O(n) vs. O(log n). For merging two trees the difference is $O(n^2)$ vs. O(n log n). This reduces even further to O(log n) when the objects are only contacting each other, rather overlapping, as is the case for collision detection.

However, there are worst case "basket weaving" examples that do require $O(n^2)$ operations. These are geometric versions of the Cartesian Product, as for example when a checkerboard is constructed from n horizontal strips and n vertical strips to produce n x n squares. These examples, however, violate the Principle of Locality: that geometric features are local not global features. For almost all geometric models of physical objects, the geometric features are local features. Spatial partitioning schemes can accelerate computations only when the features are in fact local, otherwise there is no significant subset of space that can be eliminated from consideration.

The key to a quantitative evaluation, and also generation, of Partitioning Trees is to use expected case models, instead of worst case analysis. Good trees are ones which have low expected cost for the operations and distributions of input of interest. This means, roughly, that high probability regions can be reached with low cost, i.e. they have short paths from the root the the corresponding node, and similarly low probability regions should have longer paths. This is exactly the same idea used in Huffman codes. For geometric computation, the probability of some geometric entity, such as a point, line segment, plane, etc., lying in some

arbitrary region is typically correlated positively to the size of the region: the larger the region the greater the probability that a randomly chosen geometric entity will intersect that region.

To compute the expected cost of a particular operation for a given tree, we need to know at each branch in the tree the probability of taking the left branch, p^-, and he probability of taking the right branch p^+. If we assign a unit cost to the partitioning operation, then we can compute the expect cost exactly, given the branch probabilities, using the following recurrence relation:

$$E_{cost}[\ T\ ] =$$
$$\quad \text{IF } T \text{ is a cell}$$
$$\quad\ \text{THEN } 0$$
$$\quad\ \text{ELSE } 1 + p^- * E_{cost}[\ T^-\ ] + p^+ * E_{cost}[\ T^+\ ]$$

This formula does not directly express any dependency upon a particular operation; those characteristics are encoded in the two probabilities p^- and p^+. Once a model for these is specified, the expected cost for a particular operation can be computed for any tree.

As an example, consider point classification in which a random point is chosen from a uniform distribution over some initial region **R**. For a tree region of **r** with child regions r^+ and r^- , we need the conditional probability of the point lying in r^+ and r^- given that it lies in **r**. For a uniform distribution, this is determined by the sizes of the two child-regions relative to their parent:

$$p^+ = vol(\ r^+\ ) / vol(\ r\ )$$
$$p^- = vol(\ r^-\ ) / vol(\ r\ )$$

Similar models have been developed for line, ray and plane classification. Below we describe how to use these to build good trees.

Converting B-reps to Trees

Since humans do not see physical objects in terms of binary trees, it is important to know how such a tree be constructed from something which is more intuitive. The most common method is to convert a boundary representation, which corresponds more closely to how humans see the world, into a tree. In order for a Partitioning Tree to represent a solid object, each cell of the tree must be classified as being either entirely inside or outside of the object; thus, each leaf node corresponds to either an in-cell or an out-cell. The boundary of the set then lies between in-cells and out-cells; and since the cells are bounded by the partitioning hyperplanes, it is necessary for all of the boundary to lie in the partitioning hyperplanes.

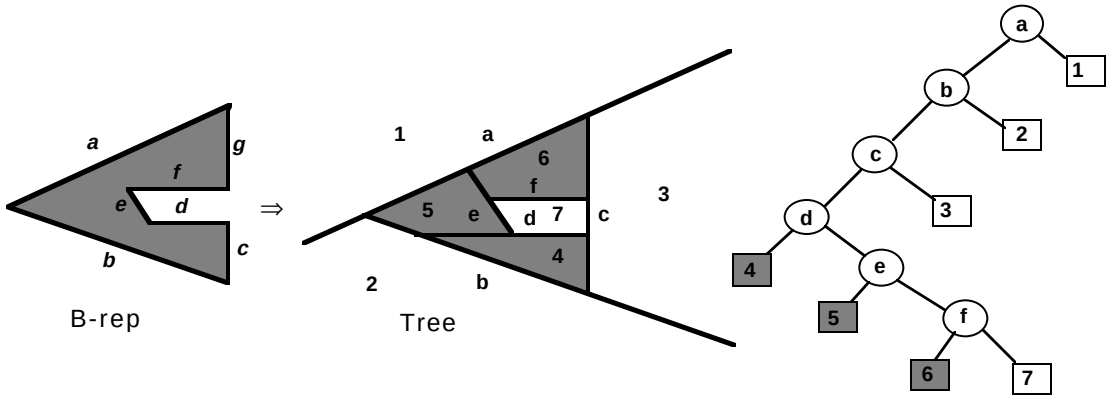

B-rep and Tree representation of a polygon

Therefore, we can convert from a b-rep to a tree simply by using all of the face hyperplanes as partitioning hyperplanes. The face hyperplanes can be chosen in any order and the resulting tree will always generate a convex decomposition of the interior and the exterior. If the hyperplane normals of the b-rep faces are consistently oriented to point to the exterior, then all left leaves will be in-cells and all right leaves will be out-cells. The following algorithm summarizes the process.

```
Brep_to_Bspt:  Brep b -> Bspt T
  IF b == NULL
  THEN
     T = if a left-leaf then an in-cell else an out-cell
  ELSE
     h = Choose_Hyperplane( b )
     { b+, b-, b0 } = Partition_Brep( b, h )
     T.faces = b0
     T.pos_subtree = Brep_to_Bspt( b+ )
     T.neg_subtree = Brep_to_Bspt( b- )
  END
```

However, this does not tell us in what order to choose the hyperplanes so as to produce the best trees. Since the only known method for finding the optimal tree is by exhaustive enumeration, and there are at least n! trees given n unique face hyperplanes, we must employ heuristics. In 3D, we use both the face planes as candidate partitioning hyperplanes, as well as planes that go through face vertices and have predetermined directions, such as aligned with the coordinates axes .

Given any candidate hyperplane, we can try to predict how effective it will be using expected case models; that is, we can estimate the expected cost of a subtree should we choose this candidate to be at its root. We will then choose the least cost candidate. Given a region **r** containing boundary **b** which we are going to partition by a candidate **h**, we can compute

exactly p^+ and p^- for a given operation, as well as the size of b^+ and b^-. However, we can only estimate $E_{cost}[T^+]$ and $E_{cost}[T^-]$. The estimators for these values can depend only upon a few simple properties such as number of faces in each halfspace, how many faces would be split by this hyperplane, and how many faces lie on the hyperplane (or area of such faces). Currently, we use $|b^+|^n$ for $E_{cost}[T^+]$, where n typically varies between .8 and .95, and similarly for $E_{cost}[T^-]$. We also include a small penalty for splitting a face by increasing its contribution to b^+ and b^- from 1.0 to somewhere between 1.25 and 1.75, depending upon the object. We also favor candidates containing larger surface area, both in our heuristic evalution and by first sorting the faces by surface area and considering only the planes of the top k faces as candidates.

One interesting consequence of using expected case models is that choosing the candidate that attempts to balance the tree is usually not the best; instead the model prefers candidates that place small amounts of geometry in large regions, since this will result in high probability and low cost subtrees, and similarly large amounts of geometry in small regions. Balanced is optimal only when the geometry is uniformly distributed, which is rarely the case. More importantly, minimizing expected costs produces trees that represents the object as a sequence of approximations, and so in a multi-resolution fashion.

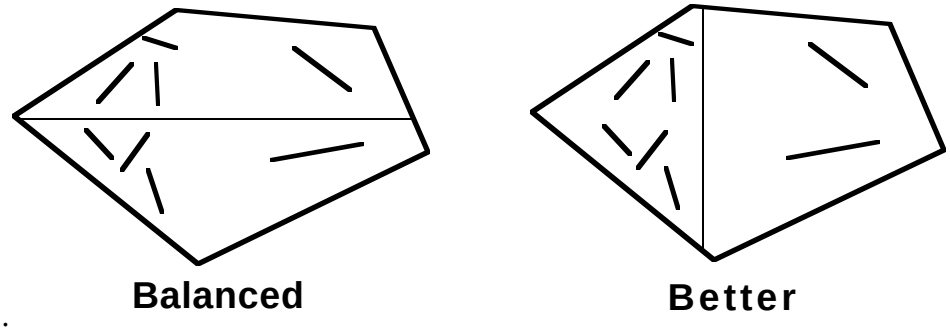

Balanced is not optimal for non-uniform distributions

Boundary Representations vs. Partitioning Trees

Boundary Representations and Partitioning Trees can be thought of as competing alternatives or as complementary representations expressing difference aspects of geometry, the former being topological, the later expressing hierarchical set membership. B-reps are well suited for interactive specification of geometry, expressing topological deformations, and scan-conversion. Partitioning Trees are well suited for intersection and visibility calculations. Their relationship is probably more akin to the capacitor vs. inductor, than the tube vs. transistor.

The most often asked question is what is the size of a Partitioning Tree representation of a polyhedron vs. the size of its boundary representation. This, of course, ignores the fact that expected cost, measured over the suite of operations for which the representation will be used, is the appropriate metric. Also, boundary representations must be supplimented by other devices, such as octrees, bounding volumes hierarchies, and z-buffers, in order to achieve an efficient system; and so the cost of creating and maintaining these structure should be brought into the equation. However, given the instrinsic methodological difficulties in performing a compelling empirical comparision, we will close with a few examples giving the original number of b-rep faces and the resulting tree using our currently implemented tree construction machinery.

Data Set	**brep**	**tree faces**	**ratio**	**nodes**	**ratio**	**E[T]**	**%nodes**
hang glider man	189	406	2.14	390	2.06	1.7, 3.4, 21.4	
space shuttle	575	1,006	1.75	927	1.61	1.2, 2.5, 13.2	
human head 1	927	1,095	1.21	1,156	1.24	1.4, 4.4, 25.0	
human head 2	2,566	5,180	2.01	5,104	1.99	0.2, 0.8, 9.1	
Allosaurous	4,072	9,725	2.38	9,914	2.43	NA	
Lower Manhattan	4,532	5,510	1.22	4,273	0.94	0.3, 0.6, 10.5	
Berkeley CS Bldg.	9,129	9,874	1.08	4,148	0.45	0.4, 1.3, 14.6	
Dungeon	14,061	20,328	1.44	15,732	1.12	0.1, 0.1, 1.7	
Honda Accord	26,033	51,730	1.98	42,965	1.65	NA	
West Point terrain	29,400	9,208	0.31	7636	0.26	0.1, 0.3, 4.2	
US destroyer	45,802	91,928	2.00	65,846	1.43	NA	

The first ratio is number-of-brep-faces/number-of-tree-faces. The second ratio is number-of-brep-faces/number-of-tree-nodes, where number-of-tree-nodes is the number of internal nodes. The last column is the expected cost in terms of point, line and plane classification, respectively, in percentage of the total number of internal nodes, and where the sample space was a bounding box 1.1 times the minimum axis-aligned bounding box. These numbers are pessimistic since typical sample spaces would be much larger than an object's bounding box. Also, the heuristics are controlled by 4 parameters, and these numbers were generate, with some exceptions, without a search of the parameter space but rather using default parameters. There are alos quite a number of ways to improve the conversion process, so it should be possible to do even better.

Binary Space Partitioning Tree Summary

A. Primary operations

1. intersections : between geometric sets (polyhedra, polygons, lines, points).
Interpret tree as a hierarchy of (bounding) volumes

2. visibility orderings : viewer or light source dependent.
Interpret tree as a hierarchy of separating planes

B. Secondary operations

1. set operations : union, intersection and difference between solid objects

2. collision detection

3. view-volume clipping : eliminating objects not within current field of view

a. includes solid cutaways

4. visible surface determination

5. shadows

6. ray-tracing

7. radiosity

8. image segmentation

a. reconstruction of objects from video, MRI, CT, etc.

b. compression

C. Efficiency

1. Utilizing temporally invariant spatial properties

a. knowledge of spatial relations encoded in tree structure exploited over many frames to reduce cost of computation for each frame

b. tree structure is preserved by affine and perspective transformations; and so objects may move without changing the tree structure. Not true of octrees.

2. Multi-resolution representation

Interpret a tree as a hierarchy of convex bounding volumes.

a. intersections

IF no intersection with bounding-volume
THEN there can be no intersections with contents of volume, so stop.
ELSE continue with contents of volume, and so on, recursively.

Reduces $\mathbf{O(n^2)}$ operation to **O(n log n)**, or **O(n)** to **O(log n)**

b. rendering

Tree pruning permits discarding detail too small to see in current view (no manual creation of a levels of detail)

3. Visibility ordering

a. comparison to z-buffer

1. no numerical problems created by perspective projection
2. no z-buffer memory
3. unlimited use of transparency

4 anti-aliasing without subpixel color and z buffers: saves ~16X in this kind of memory (10Mb vs 160Mb), plus reduces computation.

5. for shadows, no quantization errors, which are amplified by the inverse perspective projection, plus all of the above points.

b. visibility culling : do not draw objects occluded by closer objects, e.g. wall occluding rest of a building. Achieved by near-to-far ordering using multi-resolution beam-tracing.

c. transparency: visibility ordering solves this for a single tree. For multiple objects, the required ordering is achieve by merging trees, which can be thought of as merging "pre-sorted lists".

4. Linear equations

Computations involve only linear equations - much cheaper than non-linear. Curved surfaces are approximated as a sequence of piecewise linear approx. which converge to the surface.

5. Parallelization

A partitioning tree is a computation graph (data-flow graph, flow chart), describing all inherent parallelization available. Tree branches indicate independent computation while tree paths indicate pipeline-able computation.

Bibliography (partial)

Solid Modeling

[Bloomberg 86]
Sandra H. Bloomberg, "A Representation of Solid Objects for Performing Boolean Operations", U.N.C. Computer Science Technical Report 86-006 (1986).

[Thibault and Naylor 87]
W. Thibault and B. Naylor, "Set Operations On Polyhedra Using Binary Space Partitioning Trees", **Computer Graphics** Vol. 21(4), pp. 153-162, (July 1987).

[Naylor, Amanatides and Thibault 90]
Bruce F. Naylor, John Amanatides and William C. Thibault, "Merging BSP Trees Yields Polyhedral Set Operations", **Computer Graphics** Vol. 24(4), pp. 115-124, (August 1990).

[Naylor 90a]
Bruce F. Naylor, "Binary Space Partitioning Trees as an Alternative Representation of Polytopes," **Computer Aided Design**, Vol. 22(4), (May 1990).

[Naylor 90b]
Bruce F. Naylor, "SCULPT: an Interactive Solid Modeling Tool," Proceeding of *Graphics Interface* (May 1990).

[Torres 90]
Enric Torres, "Optimization of the Binary Space Partition Algorithm (BSP) for the Visualization of Dynamic Scenes" Eurographics '90 (Sept. 1990).

[Ihm and Naylor 91]
Insung Ihm and Bruce Naylor, "Piecewise Linear Approximations of Curves with Applications," Proceeding of Computer Graphics International '91, Springer-Verlag (June 1991).

[Naylor 92a]
Bruce F. Naylor, "Interactive Solid Modeling Via Partitioning Trees", Proceeding of *Graphics Interface* , pp 11-18, (May 1992).

[Chrysanthou and Slater 92]
Y. Chrysanthou and M. Slater, "Computing Dynamic Changes to BSP Trees", Eurographics '92, 11(3), pp. 321-332.

[Schumacker et al 69]
R. A. Schumacker, R. Brand, M. Gilliland, and W. Sharp, "Study for Applying Computer-Generated Images to Visual Simulation," AFHRL-TR-69-14, U.S. Air Force Human Resources Laboratory (1969).

[Ivan Sutherland 73]
Ivan E. Sutherland, "Polygon Sorting by Subdivision: a Solution to the Hidden-Surface Problem", unpublished manuscript, (October 1973).

[Fuchs, Kedem, and Naylor 80]
H. Fuchs, Z. Kedem, and B. Naylor, "On Visible Surface Generation by a Priori Tree Structures," **Computer Graphics** Vol. 14(3), pp. 124-133, (June 1980).

[Fuchs, Abrams, and Grant 83]
Henry Fuchs, Gregory Abrams and Eric Grant, "Near Real-Time Shaded Display of Rigid Objects", **Computer Graphics** Vol. 17(3), pp. 65-72, (July 1983).

[Naylor and Thibault 86]
Bruce F. Naylor and William C. Thibault, "Application of BSP Trees to Ray-Tracing and CSG Evaluation", Technical Report GIT-ICS 86/03, School of Information and Computer Science, Georgia Institute of Technology, Atlanta, Georgia 30332 (February 1986).

[Chin and Feiner 89]
Norman Chin and Steve Feiner, "Near Real-Time Shadow Generation Using BSP Trees", **Computer Graphics** Vol. 23(3), pp. 99-106, (July 1989).

[Campbell and Fussell 90]
A.T. Campbell and Donald S. Fussell, "Adaptive Mesh Generation for Global Diffuse Illumination", **Computer Graphics** Vol. 24(4), pp. 155-164, (August 1990).

[Campbell 91]
A.T. Campbell "Modeling Global Diffuse for Image Synthesis", Ph.D. Dissertation, Department of Computer Science, University of Texas at Austin, (1991).

[Gordon and Chen 91]
Dan Gordon and Shuhong Chen, "Front-to-Back Display of BSP Trees", **IEEE Computer Graphics & Applications**, pp. 79-85, (September 1991).

[Chin and Feiner 92]

Norman Chin and Steve Feiner, "Fast Object-Precision Shadow Generation for Area Light Sources Using BSP Trees", **Symp. on 3D Interactive Graphics**, (March 1992).

[Naylor 92a]
Bruce F. Naylor, "Partitioning Tree Image Representation and Generation from 3D Geometric Models", Proceeding of *Graphics Interface* (May 1992).

[Lischinski, Tampieri and Greenburg 92]
Dani Lischinski, Filippo Tampieri and Donald Greenburg, "Discountinuity Meshing for Accurate Radiosity", **IEEE Computer Graphics & Applications** 12(6), pp. 25-39, (November 1992).

[Teller and Hanrahan 93]
Seth Teller and Pat Hanrahan, "Global Visibility Algorithms for Illumination Computations", **Computer Graphics** Vol. 27, pp. 239-246, (August 1993).

Image Representation

[Rahda et al 91]
Hayder Rahda, Riccardo Leonardi, Martin Vetterli and Bruce Naylor, "Binary Space Partitioning Tree Representation of Images", **Visual Communications and Image Representation**, Vol. 2(3), pp. 201-221, (Sept. 1991).

[Subramanian and Naylor 92]
K.R. Subramanian and Bruce Naylor, "Representing Medical images with Partitioning Trees", Proceeding of Visualization '92, (Oct. 1992).

[Radha 93]
Hayder M. Sadik Radha, "Efficient Image Representation Using Binary Space Partitioning Trees", Ph.D. dissertation, CU/CTR/TR 343-93-23, Columbia University, (1993).

Theory

[Rabin 72]
Michael O. Rabin, "Proving Simultaneous Positivity of Linear Forms", **Journal of Computer and Systems Science**, v6, pp. 639-650 (1991).

[Reingold 72]
E. M. Reingold, "On the Optimality of some Set Operations", **Journal of the ACM**, Vol. 19, pp. 649-659 (1972).

[Naylor 81]

Bruce F. Naylor, "A Priori Based Techniques for Determining Visibility Priority for 3-D Scenes," Ph.D. Thesis, University of Texas at Dallas (May 1981).

[Paterson and Yao 90]
M.S. Paterson and F.F. Yao, "Efficient Binary Space Partitions for Hidden-Surface Removal and Solid Modeling", **Discrete & Computational Geometry**, v5, pp. 485-503, 1990.

[Paterson and Yao 92]
M.S. Paterson and F.F. Yao, "Optimal Binary Space Partitions for Orthogonal Objects", **Journal of Algorithms**, v5, pp. 99-113, 1992.

[Naylor 93]
Bruce F. Naylor, "Constructing Good Partitioning Trees", Graphics Interface '93, Toronto CA, pp. 181-191, (May 1993).

[Berg, Groot and Overmars 93]
MMark de Berg, Marko M. de Groot and Mark Overmars, "Perfect Binary Space Partitions", Canadian Conference on Computational Geometry, 1993.